P-11-40

Miniature Canister (MiniCan) Corrosion Experiment Progress Report 3 for 2008–2010

N.R Smart, B. Reddy, A.P Rance, Serco

August 2011

Svensk Kärnbränslehantering AB
Swedish Nuclear Fuel
and Waste Management Co

Box 250, SE-101 24 Stockholm
Phone +46 8 459 84 00

ISSN 1651-4416
SKB P-11-40

Miniature Canister (MiniCan) Corrosion Experiment Progress Report 3 for 2008–2010

N.R Smart, B. Reddy, A.P Rance, Serco

August 2011

Executive Summary

To ensure the safe encapsulation of spent nuclear fuel rods for geological disposal, SKB of Sweden are considering using the Copper-Iron Canister, which consists of an outer copper canister and a cast iron insert. Over the years a programme of laboratory work has been carried out to investigate a range of corrosion issues associated with the canister, including the possibility of expansion of the outer copper canister as a result of the anaerobic corrosion of the cast iron insert. Previous experimental work using stacks of test specimens has not shown any evidence of corrosion-induced expansion. However, as a further step in developing an understanding of the likely performance of the canister in a repository environment, Serco has set up a series of experiments in SKB's Äspö Hard Rock Laboratory (HRL) using inactive model canisters, in which leaks were deliberately introduced into the outer copper canister while surrounded by bentonite, with the aim of obtaining information about the internal corrosion evolution of the internal environment. The experiments use five small-scale model canisters (300 mm long · 150 mm diameter) that simulate the main features of the SKB canister design (hence the project name, 'MiniCan'). The main aim of the work is to examine how corrosion of the cast iron insert will evolve if a leak is present in the outer copper canister.

This report describes the progress on the five experiments running at the Äspö Hard Rock Laboratory and the data obtained from the start of the experiments in late 2006 up to Winter 2010. The full details of the design and installation of the experiments are given in a previous report and this report concentrates on summarising and interpreting the data obtained to date. This report follows two earlier progress reports presenting results up to December 2009. The current document (progress report 3) describes work up to December 2010.

The current report presents the results of the water analyses obtained in 2007 and 2008, including gas composition and microbial activity. These data show an increase in the dissolved iron concentration inside the support cage, together with a decrease in the pH. Both these observations may be due to microbial activity, but it is also possible that abiotic processes could have contributed to changes in the local chemistry. Microbial analysis has shown the presence of sulphate reducing bacteria (SRBs) and autotrophic acetogens. The presence of low density bentonite appears to stimulate the growth of SRBs, but recent studies reported in the literature indicate that high density fully compacted bentonite inhibits SRB activity. A further set of water samples was taken for analysis at the end of 2010, but the full set of results from this sampling campaign is not currently available and will be included in a subsequent report.

The electrochemical measurements provide an in situ E_h value which is comparable with published data. The E_h value inside the boreholes decreased with time as oxygen was consumed by microbial activity, reaction with minerals in the surrounding rock and/or corrosion of the MiniCan experiment and its support cage.

Corrosion rates have been obtained using a range of electrochemical methods. The copper corrosion rate was initially measured electrochemically as being <3.5 μm yr^{-1}, but the measured corrosion rates of iron and copper appear to have accelerated to unexpectedly high values. The electrochemically measured corrosion rate of iron was considerably higher (>1 mm yr^{-1} in some cases) than expected on the basis of laboratory experiments in the absence of microbial activity. The increase in corrosion rates appeared to coincide with a minimum value for the E_h being reached and this may correspond to the onset of enhanced anaerobic microbial activity (e.g. SRBs) and hence increased production of sulphide. Based on reports in the literature there is reason to believe that the corrosion rate of iron measured using the LPR and AC Impedance (ACI) techniques may overestimate the corrosion rate by a factor of 10–100 times. The corrosion potentials of the copper and iron electrodes are compared with published Pourbaix diagrams for iron and copper in the presence of chloride and sulphur species and found to be consistent with corrosion by dissolved sulphide to produce metal sulphide films.

The corrosion rates measured using the electrochemical noise technique yielded values that were significantly lower than the values measured using the LPR and ACI techniques. The lowest corrosion rates for copper were measured using the electrical resistance technique using copper wires. This technique gave corrosion rates of less than 1 μm yr^{-1} in Experiment 2 (low density bentonite)

and Experiment 5 (no bentonite). The measured corrosion rates will be corroborated using the weight loss coupons when the experiments are dismantled for examination in due course. It is planned that Experiment 3 will be dismantled first and analysed during 2011 and a plan for this work has been submitted to SKB.

It should be noted that only one experiment (Experiment 4) is a close representation of the proposed SKB disposal concept as it uses compacted bentonite, whereas the other experiments use low density bentonite or no bentonite at all. The results from these experiments (e.g. high levels of microbial activity and high corrosion rates) are therefore only applicable to a fault situation where the density of the bentonite is compromised.

A small scale electrochemical experiment was operated during 2010 consisting of carbon steel and copper electrodes embedded in anoxic compacted bentonite. Electrochemical potential and corrosion rate measurements were carried out on the copper and carbon steel electrodes. The copper corrosion rate passed through a peak due to an oxygen spike during cell manufacture, but the corrosion rate fell to a value of ~3 μm yr^{-1} after the oxygen had been consumed by corrosion reactions.

Contents

1 Introduction

To ensure the safe encapsulation of spent nuclear fuel rods for geological disposal, SKB of Sweden are considering using the Copper-Iron Canister, which consists of an outer copper canister and a cast iron insert. A programme of work has been carried out over a number of years to investigate a range of corrosion issues associated with the canister, including the possibility of expansion of the outer copper canister as a result of the anaerobic corrosion of the cast iron insert. Experimental work using stacks of copper and iron test specimens has not shown any evidence of corrosion-induced expansion [1]. However, as a further step in developing an understanding of the likely performance of the canister in a repository environment, Serco has set up a series of experiments in SKB's Äspö Hard Rock Laboratory (HRL) using inactive model canisters, in which leaks were deliberately introduced into the outer copper canister while surrounded by bentonite, with the aim of obtaining information about the internal corrosion evolution of the internal environment [2].

The experiments use small-scale (300 mm long × 150 mm diameter) model canisters that simulate the main features of the SKB canister design (hence the project name, 'MiniCan'). The main aim of the work is to examine how corrosion of the cast iron insert will develop if a leak is introduced into the outer copper canister, but a number of other issues are also being addressed, such as:

- Does water penetrate into the annulus through a small defect?
- How does corrosion product spread around the annulus from the leak point?
- Does the formation of corrosion product in a constricted annulus cause any expansive damage to the copper canister?
- What is the effect of water penetration on the insert lid seal?
- Is there any detectable corrosion at the copper welds?
- Are there any deleterious galvanic interactions between copper and cast iron?
- Does corrosion lead to failure of the lid on the iron insert?

The experiments were set up between September 2006 and February 2007 and the detailed design, experimental setup and initial results up to May 2008 are reported in reference [3]. The five experiments are automatically monitored and the scheduled experimental data were obtained and analysed. This progress report includes the data obtained up to Winter 2010 and follows two previous progress reports that presented data up to December 2009 [4,5]. Further progress reports will be produced in due course. One of the MiniCan experiments, Experiment 3, will be removed for analysis during 2011.

2 Experimental

The five experiments setup in the boreholes at Äspö HRL are being logged automatically by computer-controlled data logging equipment. The detailed experimental layout and test conditions are given in reference [3] and summarised below.

2.1 Test layout and test conditions

Figure 2-1 shows the layout of the experiments in the boreholes in the Äspö HRL, Figure 2-2 shows the layout of the canisters and the other test pieces inside the support cages and Figure 2-3 shows the insertion of the copper model canisters into the support cages. A summary of the test environments inside the five experiments is given in Table 2-1. In three out of the five experiments a layer of bentonite was mounted inside an annulus between two concentric cylinders around the model canister. The purpose of the bentonite is to condition the chemistry of the incoming groundwater so that it is representative of the repository situation. However, it should be noted that these experiments use a lower bentonite density than is proposed for the SKB repository. The cage prevents direct contact between the bentonite and the surface of the canister in order to avoid blockage of the defect introduced into the copper container. The bentonite holder was filled with compacted bentonite pellets mixed with bentonite powder at a density designed to give a high permeability and low swelling pressure, with the aim of allowing bentonite-conditioned groundwater to reach the model canister rapidly.

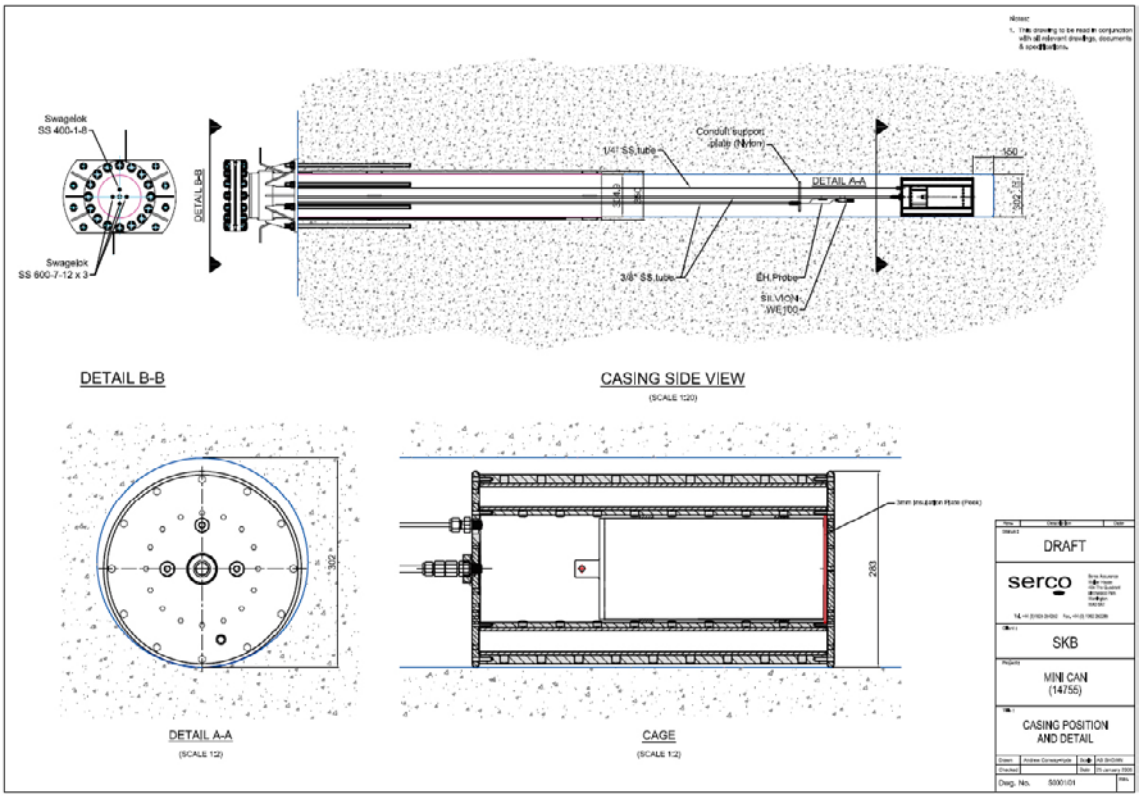

Figure 2-1. *Layout of model canister experiments in borehole.*

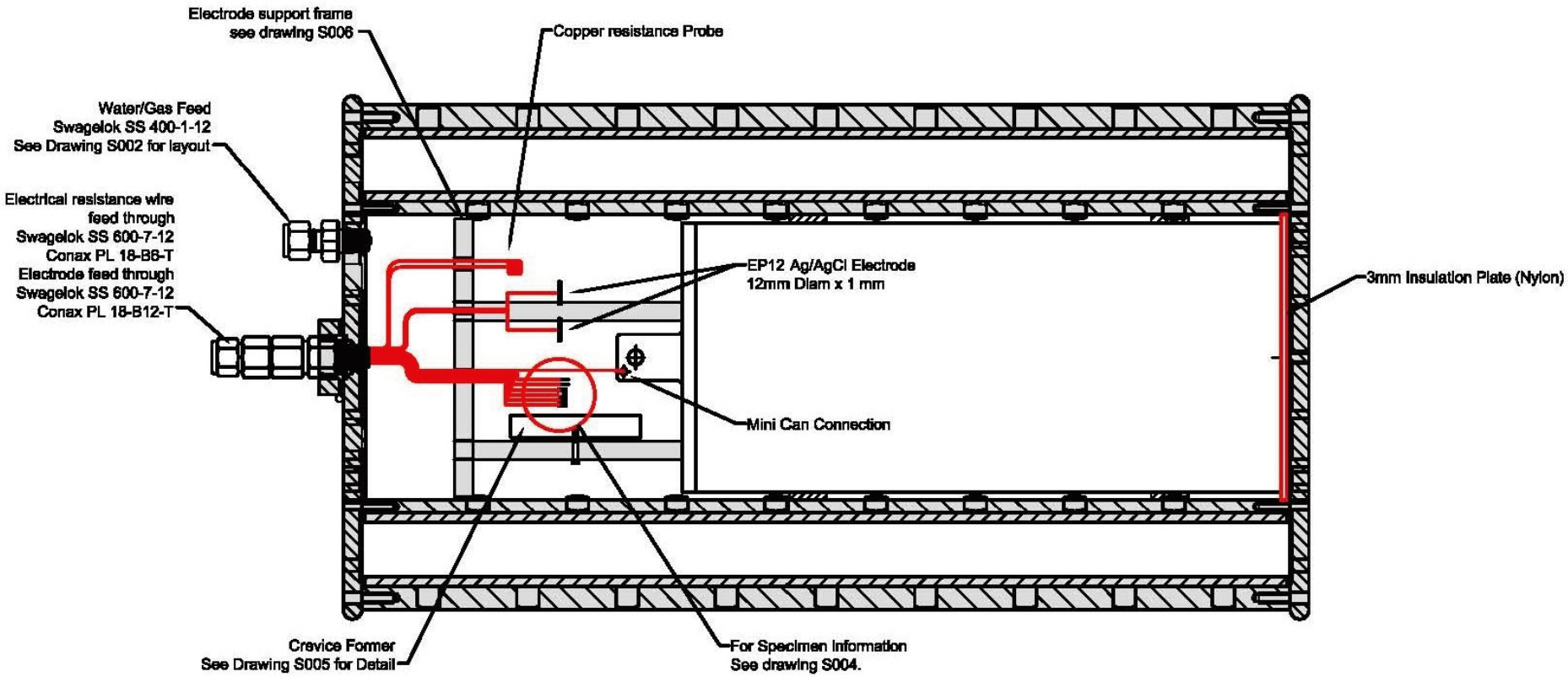

Figure 2-2. *Layout of model canister and sensors inside support cage.*

Figure 2-3. *Left: Strain gauges mounted on model canister; Centre: Positioning of bentonite pellets inside annulus of support cage; Right: insertion of model canister assembly into support cage.*

Table 2-1. Summary of test conditions for model canister experiments.

Experiment number (Borehole number)	Environment and defect details
1 (KA3386A02)	Low density, high permeability bentonite in annulus around model canister. Single defect near top weld, pointing vertically upwards.
2 (KA3386A03)	Low density, high permeability bentonite in annulus around model canister. Single defect near top weld, pointing vertically downwards.
3 (KA3386A04)	Low density, high permeability bentonite in annulus around model canister. Two defects, one near top weld, pointing vertically upwards, one near bottom weld, pointing vertically downwards.
4 (KA3386A05)	Compacted bentonite. Single defect near top weld, pointing vertically downwards.
5 (KA3386A06)	No bentonite, direct contact of groundwater on model canister. Two defects, both near top weld, one pointing vertically upwards, the other vertically downwards.

In the fourth experiment the model canister was surrounded by compacted bentonite, to simulate as exactly as possible the real exposure conditions in the repository, although in this situation it is expected that the extent of corrosion will be limited by the supply of water and diffusion of sulphide through the compacted, low permeability bentonite [6]. In this experiment, where the model canister was in direct contact with the compacted bentonite, there was no inner cylinder and hence no annulus of bentonite, but rings of saturated compacted bentonite were machined to slide over the model canister, inside the outer cylinder. Clay Technology (Lund, Sweden) machined the rings to size. The use of fully saturated bentonite should minimise the time required to achieve full saturation and hence to achieve the full swelling pressure of the bentonite. The thicknesses of the outer cylinder of the support cage and the outer filter cylinder were selected to withstand the swelling pressure exerted by the compacted bentonite (7 MPa). Small holes or slots were machined in the compact bentonite rings to accommodate electrodes and corrosion coupons in the compacted bentonite, and strain gauges on the surface of the model canister.

The fifth experiment was set up without any bentonite around the model canister so that the model canister is exposed directly to raw groundwater without any conditioning by bentonite, this experiment was included to provide a comparison with the experiments with bentonite present and to examine whether any biofilm develops on the surface of the canister and to examine its effect on corrosion behaviour. For this experiment, where the canister is directly exposed to groundwater, the perforated steel cage was used to hold the model canister, but no bentonite was placed inside it. Consequently the groundwater enters directly into the vicinity of the model canister.

3 Monitoring performance of model canisters

A number of parameters have been measured and monitored over the period since the experiments were set up in late 2006 to Winter 2010, as follows:

- electrochemical potential of gold and platinum, and the redox potential, E_h
- corrosion potential of cast iron, copper and the miniature canister itself
- response of strain gauges on two experiments
- in situ corrosion rate measurements for copper and cast iron
- water composition (including gas analysis and microbial measurements).

The reference electrodes used were:

- two small silver-silver chloride reference disc electrodes inside each support cage (World precision instruments EP series)
- long-life reference electrodes for cathodic protection (CP) purposes (Silvion silver-silver chloride reference electrodes), which were mounted outside the support cage but immersed in the borehole water.

The redox potential of the environment was measured by means of a gold wire and a platinum flag located near to the model canister inside the support cage and an E_h sensor located outside the supporting cage (Cumberland Electrochemical Ltd Pt/Ir mixed metal oxide, MOx, probe, which has been successfully used embedded in cementitious grout to monitor fluctuations in redox conditions).

The sensors were supported from a nylon support rack inside the void above the model canister (see Figure 2-2). All reference electrodes were calibrated before installation.

3.1 Water analysis

After installation, water samples were taken for analysis at periodic intervals. Äspö staff carried out the required water analysis. Water samples were extracted through stainless steel tubes that passed out through the borehole flange. For each borehole it was possible to extract samples from both within the support cage itself and from the borehole surrounding the model canister experiment. There was a continuous bleed of gas from each borehole flange to prevent the development of a gas-filled space within the borehole. This gas is assumed to be nitrogen (see Section 4.1.1). The concentration of dissolved gases was determined by Microbial Analytics Sweden AB. The methods used are summarised in Appendix 1 of reference [5]. The concentrations of the following gases were analysed: H_2, He, O_2, N_2, Ar, CH_4, CO_2, CO, C_2H_6, C_2H_4, C_2H_2, C_3H_8, C_3H_6. The microbial analysis was also carried out by Microbial Analytics (see Appendix 1 of reference [5] for details) and was used to measure the following:

1. The total number of microorganisms.
2. The number of aerobic cultivable bacteria.
3. Biomass measured as adenosine triphosphate.
4. The most probable number of the following types of bacteria were determined: sulphate reducing bacteria (SRBs) and autotrophic acetogens.

A programme of water analysis was carried out regularly in the period February to August 2007 and then no more water samples were taken until October 2008, in order to allow the water chemistry to stabilise without any perturbations. The results from the 2007 and 2008 analyses are included in the current report. Additional water samples were taken at the end of 2010 but the full set of results from this sampling campaign is not currently available.

3.2 Pressure

The water pressure in the boreholes was initially measured by means of an analogue pressure gauge that was attached to the flanges on each borehole. Later an electrical pressure gauge was attached to the outlet pipe on the flange and the output was recorded on the datalogging equipment.

3.3 Strain

Strain gauges were applied to measure changes in the strain on the outer surface of two of the copper canisters (Tests 1 and 4). The aim of these measurements was to provide an indication of whether expansion caused by internal corrosion has caused any dimensional changes. Standard strain gauge monitoring technology using bi-axial strain gauges was applied (e.g. Techni-Measure Ltd) using cyanoacrylate adhesives and protected with waterproof coatings.

3.4 Corrosion coupons

A number of types of corrosion coupons were mounted within the cage used for the model canister experiments, as follows:

- *Plain corrosion coupons of copper and cast iron.* The corrosion rate of the materials will be determined from weight loss measurements at the end of experiments. One weight loss sample for each material was installed in each experiment. These coupons were suspended from the nylon mounting rack using polypropylene thread.
- *Coupons of copper and cast iron that are electrically connected to the exterior of the borehole.* These were designed to allow the corrosion potential of the electrodes to be measured. It was also possible to carry out electrochemical measurements of the corrosion rate of these coupons using; linear polarisation resistance, LPR, AC impedance, ACI, and electrochemical noise, ECN. Platinised titanium gauze was used as the counter electrode in a conventional 3-electrode electrochemical cell. Electrical connections were made to the coupons using copper wire for the copper coupons and carbon steel wire for the cast iron coupons.
- *Copper electrical resistance wire probes*. These were set up to measure the corrosion rate of copper using the technique proposed previously by VTT (e.g. [7]). Each coil consisted of a total length of 112.5 cm of 1 mm diameter copper wire (99.9% purity, Advent Cu513918). The length of wire was divided into three regions each of 37.5 cm length by applying heat shrinkable, adhesive-lined polymer tubing to the end sections, leaving the middle section exposed to the test environment. The complete wire was formed into a spiral with a diameter of ~1 cm. The two screened lengths were used as reference resistances and the change in the resistance of the exposed length was used to calculate the corrosion rate. This information was processed by the ACM Field Machine electrochemical unit.
- *Stress corrosion test specimens.* Four Wedge Opening-loaded (WOL) specimens were mounted in the boreholes. They were machined from a scrap copper lid provided by SKB and they were pre-cracked to give a range of stress intensity factors. In addition four U-bend specimens were manufactured from the same lid material, with dimensions of 2.5 × 80 × 20 mm. Two U-bend specimens and two WOL specimens were mounted in each of experiment boreholes 3 and 4, by loosely suspending them from the stainless steel push rod using plastic connectors. They were thus exposed directly to the groundwater. They will be examined for any indications of Stress Corrosion Cracking (SCC) at the end of the experiments.
- *Copper-cast iron-copper sandwich specimens to investigate jacking effects.* These specimens were based on the multi-crevice assembly specimen used in previous galvanic corrosion experiments [8], in which cast iron castellated nuts were tightened against sheets of copper. The aim of these specimens was to investigate a number of possible corrosion mechanisms, including crevice corrosion, galvanic corrosion and expansive corrosion. They consisted of a sheet of copper which was clamped against a block of cast iron using a ring of nylon bolts. To investigate the effect of separation distance between mating surfaces a series of steps was machined into the surface of the cast iron to give separation

distances between the mating surfaces ranging from direct contact around the edges of the specimens, increasing in steps of 10 μm to 30 μm. The materials used for the sandwich specimens were prepared from copper sheet and the same type of cast iron used for the insert in the model canisters. The specimens will be removed and examined at the end of the exposure period.

3.5 Mounting system for sensors and corrosion test pieces

The corrosion coupons and environmental sensors were supported in a nylon rack which was placed inside the stainless steel support cage above the model canisters before the support cage was sealed. It rested on the top of the model canisters by means of support legs. Electrical connections were taken out through Conax compression fittings in the support cage lid. For Test 4, where the model canister was embedded in compacted bentonite, the corrosion coupons and sensors were placed in slots that were machined into the compacted bentonite before it was loaded into the supporting cage.

3.6 Electrical connections

A summary of the sensors in each of the experiments and the conduits required for the connecting cables and details of output from each experiment is reported in reference [3]. Connecting wires from metal samples inside the canister cage (i.e. corrosion coupons and the model canister itself) were passed through compression glands (316L stainless steel Conax fittings) and connected to cables that were taken out to the external environment through stainless steel tubes which were attached to the supporting cages using Swagelok-type pressure fittings. All connections were made using soldered joints which were then sheathed in heat shrink. It should be noted that the electrochemical measurements rely on the integrity of the sheathing system throughout the experiments and the success of the sheathing will only be confirmed when the experiments are dismantled and the sheathing can be examined. The tubes were passed through the stainless steel flange at the entrance to the boreholes using bulkhead compression fittings.

3.7 Monitoring equipment

The electrochemical monitoring is being performed using an ACM Ltd Field Machine and an Agilent datalogger. The ACM equipment is being used to carry out the electrochemical measurements of corrosion rate (10 channels) and measurements of electrical resistance of the copper wire electrodes (2 channels), and the Agilent datalogger is used to monitor the potentials of the various electrodes, together with monitoring the strain gauges. The datalogging equipment is located in a control room near the boreholes and data is then transmitted via the Internet to Serco for analysis.

3.8 Electrochemical cell

In order to obtain experimental measurements of the electrochemical behaviour of carbon steel embedded in compacted bentonite an electrochemical cell had previously been set up to measure the redox potential, E_h, and the corrosion potential of a steel electrode in compacted bentonite. This work was carried out as part of the NF-PRO project on near-field processes in a repository [9]. In the current MiniCan programme a second cell was set up using a similar technique, but a copper working electrode and an additional sliver-sliver chloride electrode were added to the set of electrodes tested previously. The design of the cell was as follows. A compacted bentonite holder of the design used for gas generation experiments [9] was modified by inserting a Conax pressure fitting in the top lid. This allowed electrical connections to be made to a gold wire, a steel wire and a copper wire which were embedded in compacted bentonite. The compacted bentonite was inserted into the sample holder in three sections consisting only of compacted bentonite. Holes were then drilled into the compacted bentonite and the test electrodes, a 1 mm diameter gold wire, a 1 mm carbon steel wire, which had been pickled, and a 1 mm copper wire, were then inserted into the holes in the compacted

bentonite. The Conax fitting was then tightened around the wires to give a pressure tight seal. Electrical connection was also made to the stainless steel holder, which acted as a counter electrode. The sample holder was placed in a polythene beaker and the assembly was mounted inside a glass cell, which had a glass-to-metal seal in the lid to allow electrical connections to be made to the test assembly. The whole assembly was placed in a nitrogen-purged glovebox to ensure that when the experiment was started the oxygen concentration was under 5 ppm. It was found that it was possible to measure a potential between the electrodes even before the test solution was placed around the sample holder, due to the residual water in the bentonite. The test solution was placed around the sample holder and a silver-silver chloride reference electrode was placed in the test solution. The potential of the gold, steel, copper and stainless steel were monitored with respect to the silver-silver chloride electrode as the artificial groundwater penetrated into the bentonite. The test solution used for the experiment was 1M NaCl solution at pH 8.4. After a few days the lid of the glass cell was fixed to the body using epoxy adhesive, allowed to cure then withdrawn from the nitrogen-purged glovebox and placed in an oil bath at a temperature of 30°C. On removing the cell from the glovebox after preparation of the cell was complete, the electrode potentials increased to more positive values, indicating possible oxygen ingress. Because of this concern, the cell was returned to the glovebox where continued monitoring of the electrode potentials was conducted. After a week the potentials had reduced to values comparable to the original potentials (i.e. prior to possible oxygen ingress). The cell has since been resealed and monitoring is continuing outside the glovebox, with no indications of further oxygen ingress.

Corrosion rate measurements were carried out periodically (i.e. every 2–3 months) using two standard electrochemical techniques, Linear Polarisation Resistance, (LPR) and Electrochemical Impedance Spectroscopy (EIS, also known as AC Impedance, ACI). Both of these techniques were conducted in accordance with the relevant ASTM standards for electrochemical corrosion rate measurements.

4 Results

4.1 Water analysis

4.1.1 Inorganic analysis

The results from the water analyses (SO_4^{2-}, HCO_3^-, sulphide and Fe^{2+}) taken from both within the support cage and external to the support cage in the borehole for the five experiments for samples taken in October 2008 are given in Table 4-1, together with the May 2007 results. In October 2008, data from outside the support cages was only obtained in Experiment 2. The previous data obtained up to October 2007 [3] (Figure 4-1–Figure 4-8) showed a slight variation in the internal and external compositions. The sulphide concentrations were in the range 0.02 to 0.03 mg/L. The values measured in 2008 were lower than the values measured in 2007, in some experiments by a factor of two. The overall sulphide concentrations are generally low (at least three orders of magnitude less than the sulphate concentration). The greatest variation between the internal and external ion concentrations was found in the dissolved iron analyses with 0.15 mg/L of Fe^{2+} external to the support cage compared to values up to 19.2 mg/L inside the support cage, in experiments with low density bentonite (Experiments 1 to 3) or no bentonite at all (Experiment 5). Similar variation was noted previously in 2007. The pH values of the water samples taken from inside and outside the support cages are also shown in Table 4-1. These data show a slight decrease in the pH of water inside the support cages compared to the water in the boreholes. Table 4-2 gives the measured concentrations of a range of metallic elements and anions, including those present in trace quantities, together with the total organic content (TOC) and conductivity of the water. It is noticeable that chloride, sodium, calcium, bromide, silicon, total sulphur, manganese, lithium, strontium, barium, cobalt, chromium, nickel and conductivity were all significantly higher in Experiment 5 than in other experiments or in the borehole of Experiment 2. The concentrations of nickel and chromium were at least two orders of magnitude greater than in borehole water, suggesting that in Experiment 5 (no bentonite) corrosion of the stainless steel support cage was occurring, as well corrosion of the cast iron insert. Low concentrations of nickel and chromium were observed in Experiments 1, 2 and 3, indicating that most of the increased concentration of iron in these experiments was due to corrosion of the cast iron insert rather than the stainless steel support cage (unless any nickel and chromium released had precipitated as an insoluble corrosion product). The higher concentrations of chloride, sodium, calcium, bromide, silicon, total sulphur, manganese, lithium, strontium, barium, in Experiment 5 indicate that there are local variations in water chemistry, which are presumably due to different water flow patterns through the rock fractures.

Table 4-1. Chemical composition in the water from inside and the outside (2G) of the Model Canister experiments sampled in 05-2007 and 10-2008.

Experiment	SO_4^{2-} (mgL^{-1})		HCO_3^- (mgL^{-1})		sulphide (mgL^{-1})		Fe^{2+} (mgL^{-1})		pH	
	05-2007	10-2008	05-2007	10-2008	05-2007	10-2008	05-2007	10-2008	05-2007	10-2008
1	486	417	28	19	0.036	0.021	11.1	19.2	7.4	7.3
2	506	413	27	20	0.057	0.020	2.33	4.15	7.6	7.4
2G	354	481	28	23	0.062	0.023	0.16	0.15	7.6	7.6
3	439	410	51	38	0.037	0.022	0.82	15.7	7.6	7.2
5	605	567	14	8	0.051	0.030	6.30	11.1	7.6	6.8

Note: It is not possible to extract any water for analysis from inside the support cage of Experiment 4, because of the presence of compacted bentonite.

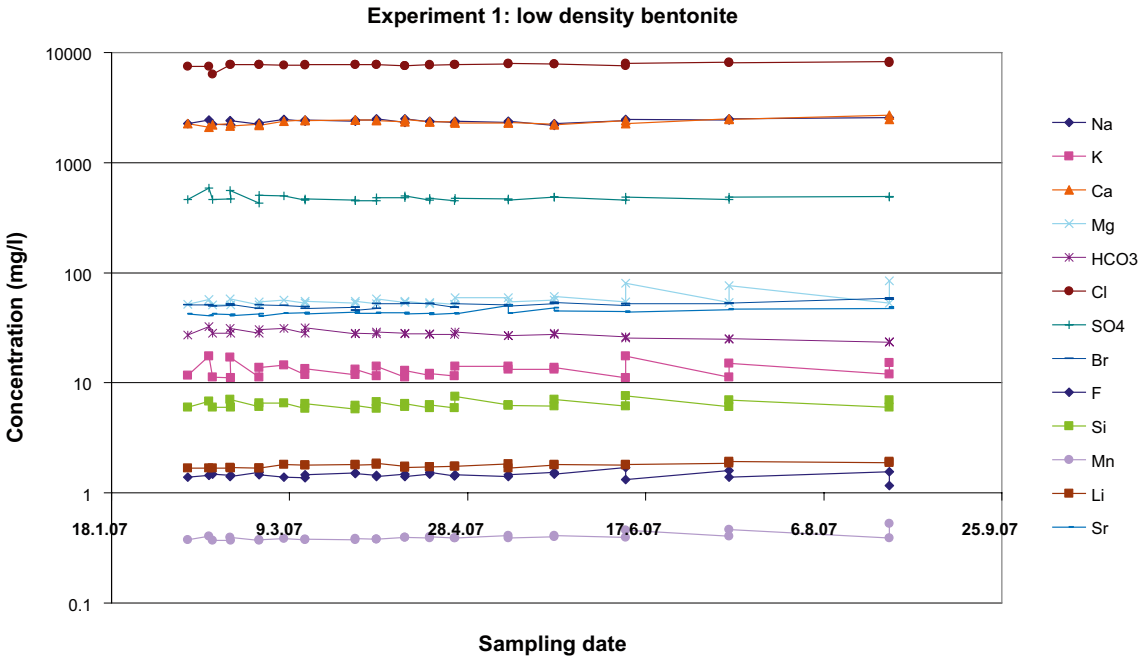

Figure 4-1. *Summary of water analyses: Experiment 1. For any given sampling date the first concentration shown when approaching along the line from the left hand side of the diagram refers to the analysis in the borehole, but outside the support cage, and the point on the right hand side, but on the same date, refers to the concentration on the inside of the support cage. The results of the iron analyses are shown in Figure 4-7.*

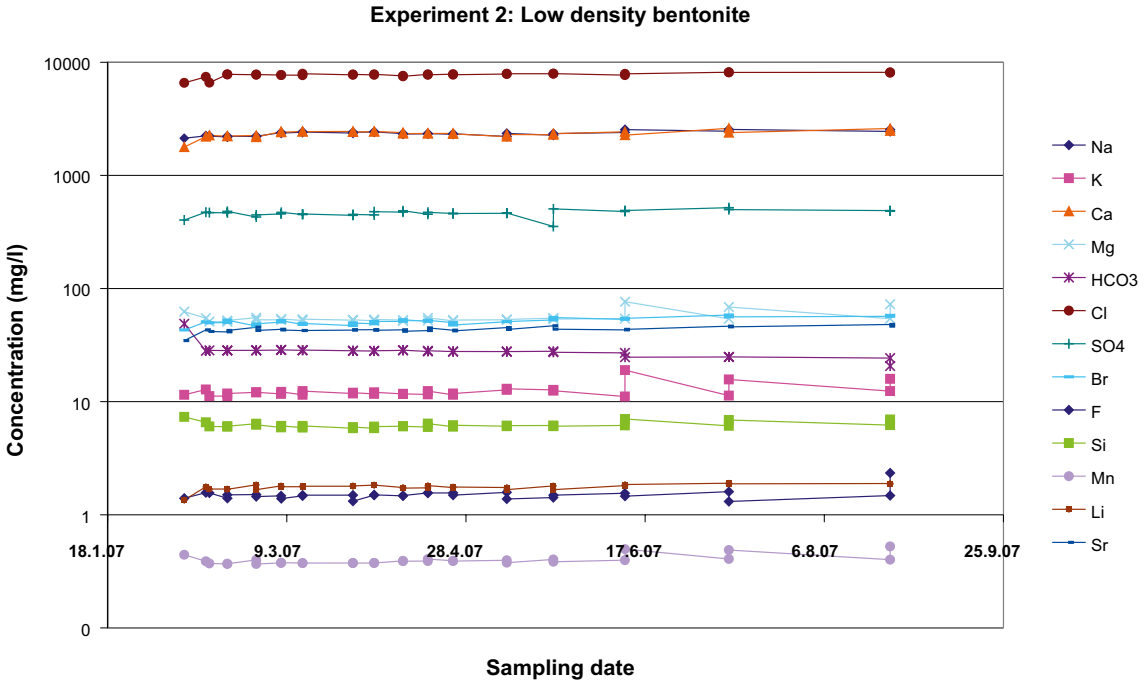

Figure 4-2. *Summary of water analyses: Experiment 2. For any given sampling date the first concentration shown when approaching along the line from the left hand side of the diagram refers to the analysis in the borehole, but outside the support cage, and the point on the right hand side, but on the same date, refers to the concentration on the inside of the support cage. The results of the iron analyses are shown in Figure 4-7.*

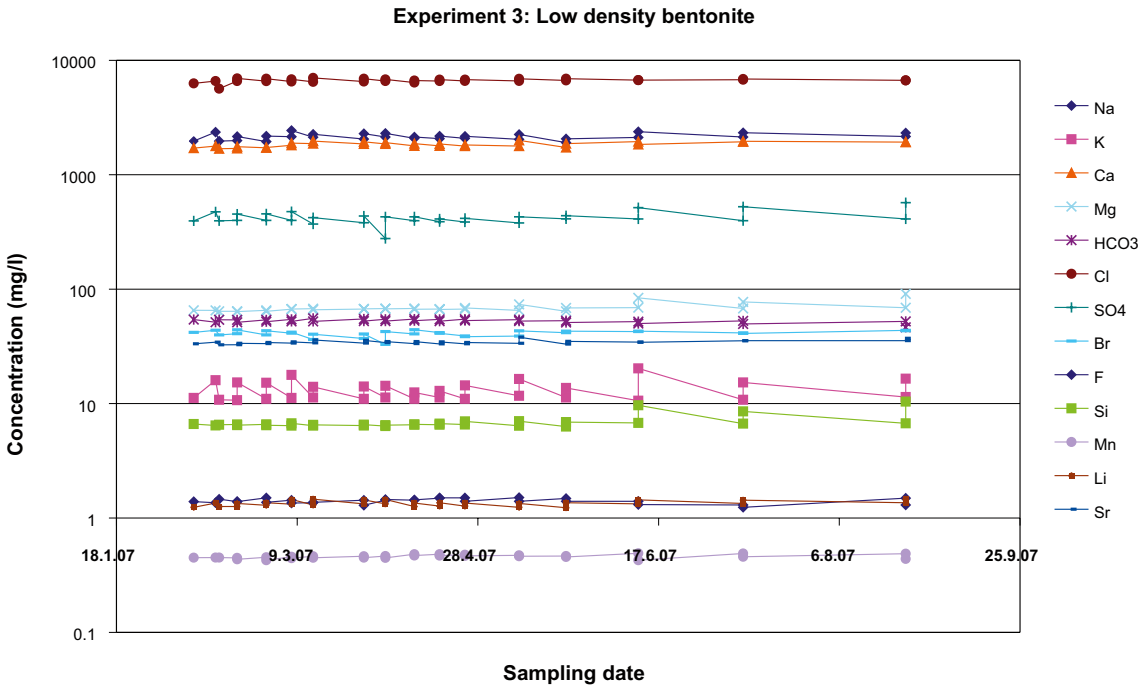

Figure 4-3. *Summary of water analyses: Experiment 3. For any given sampling date the first concentration shown when approaching along the line from the left hand side of the diagram refers to the analysis in the borehole, but outside the support cage, and the point on the right hand side, but on the same date, refers to the concentration on the inside of the support cage. The results of the iron analyses are shown in Figure 4-7.*

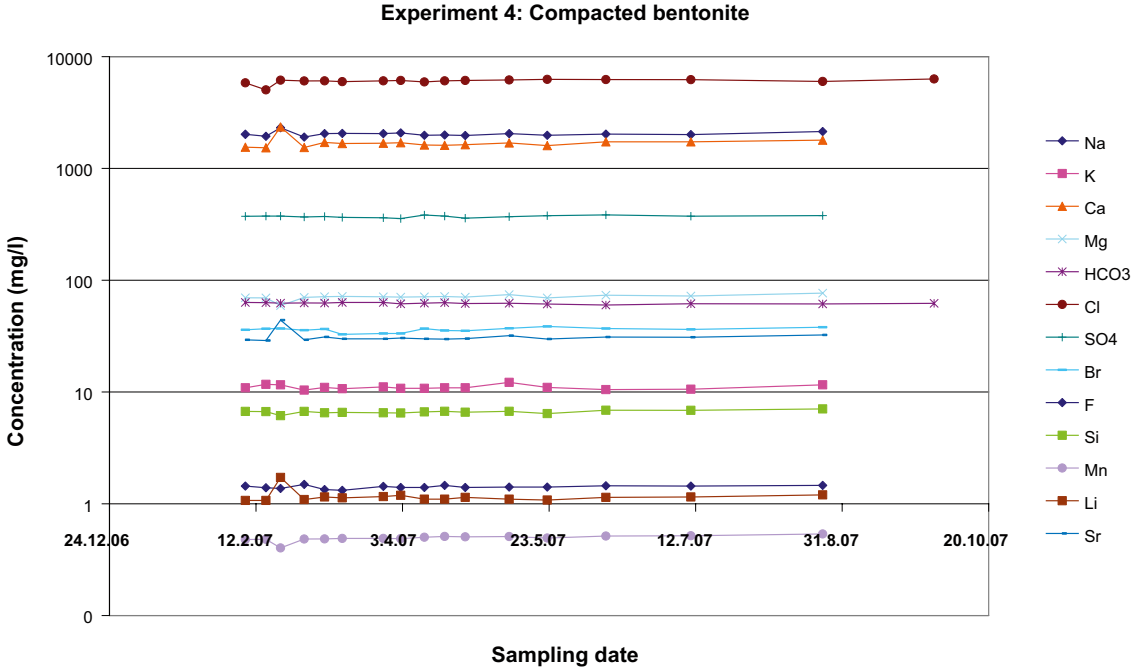

Figure 4-4. *Summary of water analyses: Experiment 4. It was not possible to remove any water from inside the support cage for analysis, so all data refer to a water sample taken from the borehole outside the support cage. The results of the iron analyses are shown in Figure 4-7.*

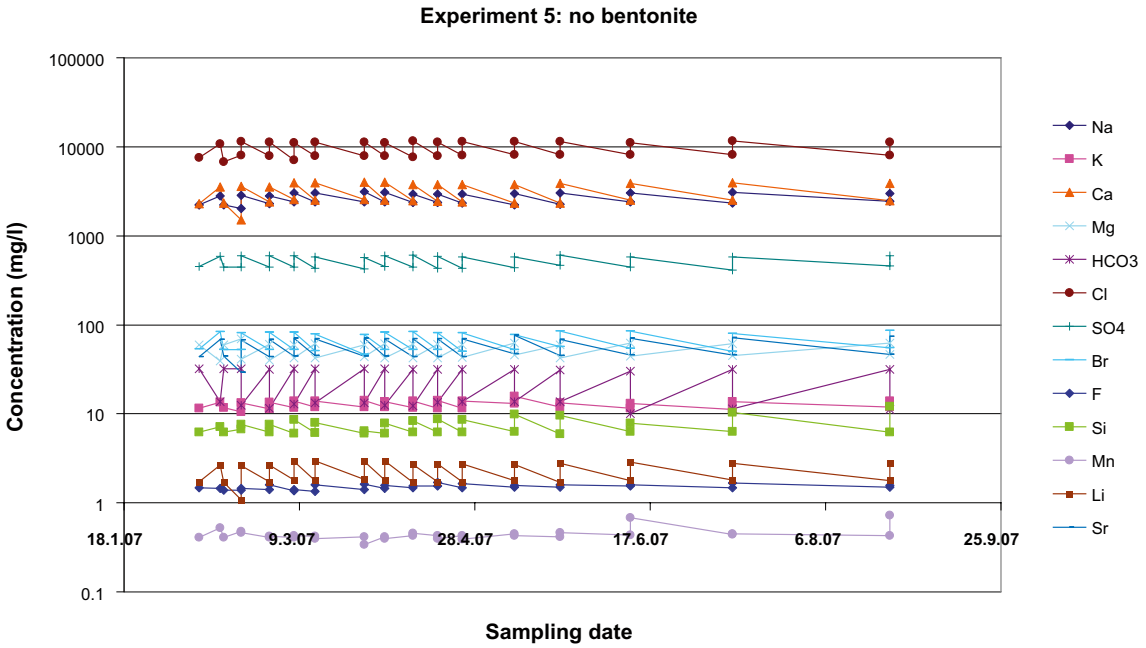

Figure 4-5. *Summary of water analyses: Experiment 5. For any given sampling date the first concentration shown when approaching along the line from the left hand side of the diagram refers to the analysis in the borehole, but outside the support cage, and the point on the right hand side, but on the same date, refers to the concentration on the inside of the support cage. The results of the iron analyses are shown in Figure 4-7.*

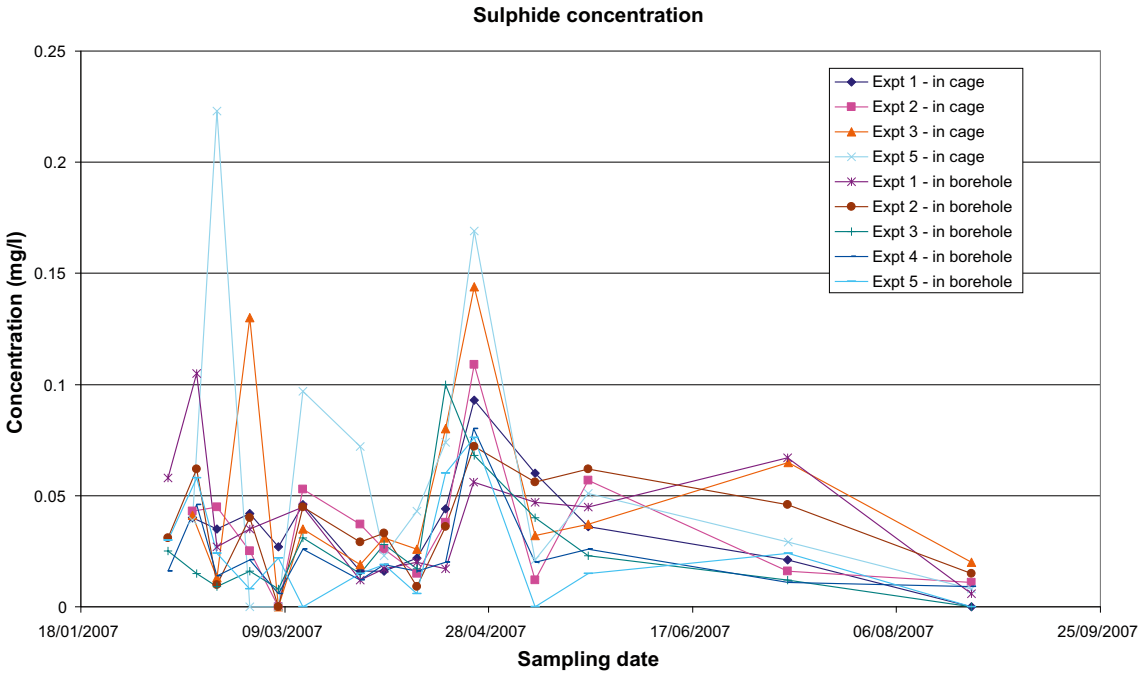

Figure 4-6. *Summary of sulphide concentration in water samples.*

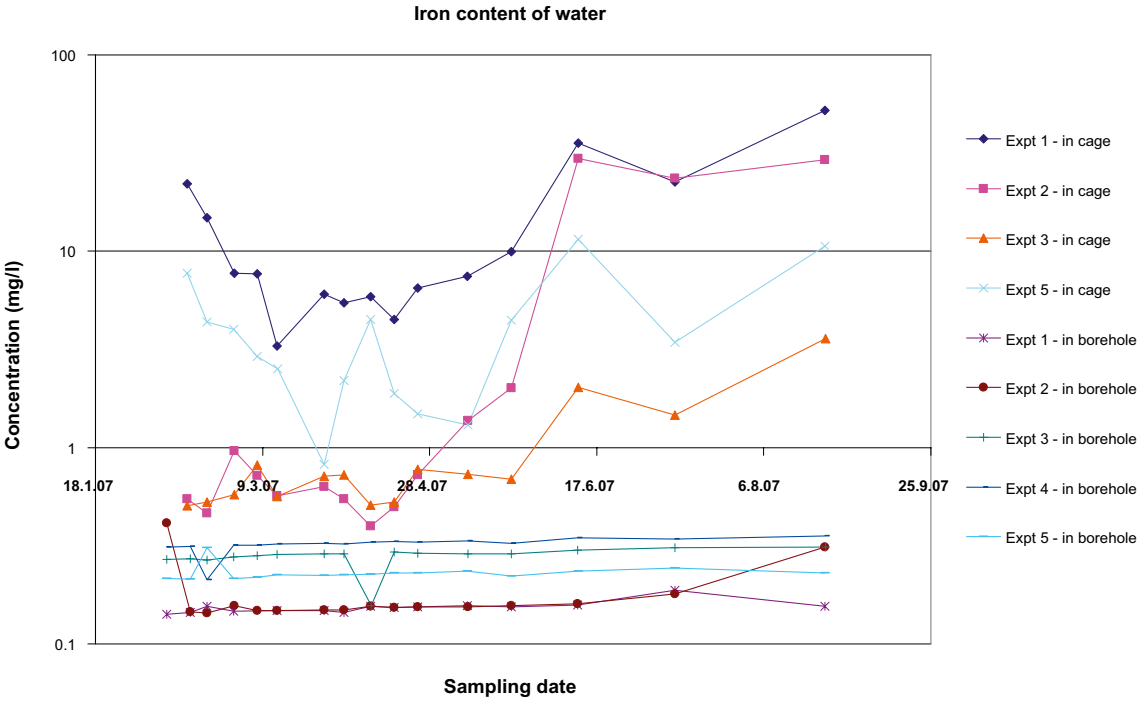

Figure 4-7. *Summary of iron analysis in water samples.*

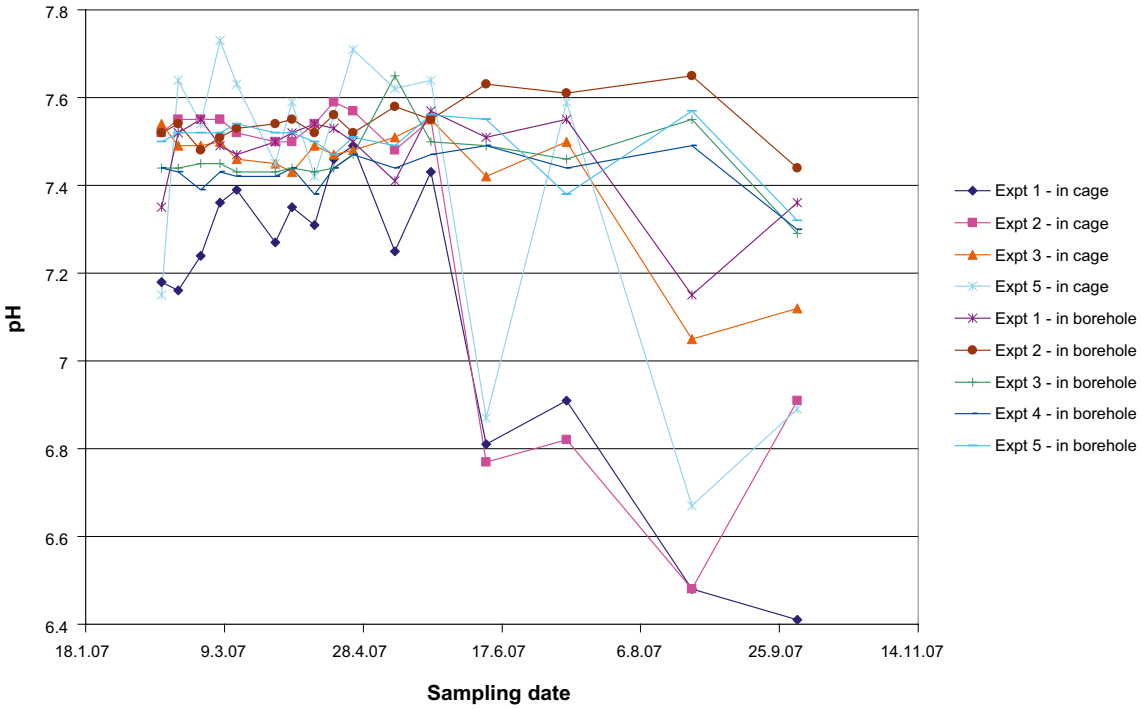

Figure 4-8. *pH of water samples taken from model canister experiments.*

Table 4-2. Chemical composition of the water from inside and outside (Experiment 2 only) the support cage around the model canister experiments, as sampled in October 2008 (measurement uncertainty ~±12%).

	Experiment 1	Experiment 2	Experiment 2 (borehole)	Experiment 3	Experiment 5
Cl (mg/l)	7,887	7,674	7,926	6,895	11,362
Na (mg/l)	2,350	2,350	2,330	2,130	2,930
Ca (mg/l)	1,910	2,470	2,460	1,930	3,840
Total S (mg/l)	129	186	188	157	233
Br (mg/l)	49.8	44.7	48.3	35.7	71.3
Mg (mg/l)	47.9	51.9	51.3	76.0	42.9
Sr (mg/l)	36.7	46.6	46.6	37.8	73.2
K (mg/l)	9.01	11.6	11.4	11.0	13.5
Si (mg/l)	4.01	6.00	6.04	5.91	9.28
F (mg/l)	1.83	1.83	1.75	1.23	1.87
Li (µg/l)	1,410	1,820	1,750	1,360	2,670
Mn (µg/l)	362	387	370	490	678
Ba (µg/l)	89.0	80.3	78.3	89.8	101
Mo (µg/l)	54.0	60.1	57.4	60.5	53.4
Zn (µg/l)	1.08	4.03	1.19	<0.8	4.33
Ni (µg/l)	0.866	2.87	<0.2	0.971	322
Al (µg/l)	0.745	4.42	3.20	1.37	1.17
Cu (µg/l)	0.251	0.767	<0.2	<0.2	0.283
V (µg/l)	0.199	0.275	0.291	0.215	0.0455
Pb (µg/l)	0.179	0.383	0.152	0.174	0.220
Cr (µg/l)	0.169	1.80	0.159	0.191	248
Co (µg/l)	0.0391	0.152	0.0526	0.022	8.12
NO_2^- (mg/l)	0.0013	0.0006	<0.0002	0.0008	0.0012
NO_3^- (mg/l)	0.0010	<0.0003	0.0015	0.0021	0.0006
PO_4^{3+} (mg/l)	<0.0005	<0.0005	<0.0005	<0.0005	<0.0005
TOC (mg/l)	3.2	1.9	1.3	3.6	1.2
Conductivity, mS/m	2,230	2,178	2,197	1,975	2,960

The results of the dissolved gas analyses are shown in Table 4-3. The dissolved oxygen concentration in the groundwater was essentially zero [3]. The dominant dissolved gas is nitrogen, with significant quantities of helium, argon, carbon dioxide and methane also present. The concentration of hydrogen was particularly high in Experiment 5 compared to data obtained in 2007; however the high concentration of hydrogen (215 µL L^{-1}) previously observed in Experiment 1 was much lower (7.3 µL L^{-1}) in 2008. Also the levels of both carbon dioxide and the alkalinity were lower in 2008.

Table 4-3. Dissolved gas in the water from the model canister experiments sampled in September 2007 and October 2008 (bd = below detection level).

Gases	Date	Experiments				
		1	2	2 G	3	5
Gas/water (mL L^{-1})	09-07	68	128	76	69	112
	10-08	90	109	103	53	86
H_2 (µL L^{-1})	09-07	0.22	0.52	0.22	0.10	215
	10-08	90.1	0.57	0.52	0.55	7.3
CO (µL L^{-1})	09-07	0.58	1.08	3.39	0.72	1.14
	10-08	0.52	0.53	0.70	0.69	6.8
CH_4 (µL L^{-1})	09-07	326	317	210	245	117
	10-08	500	593	344	215	216
CO_2 (µL L^{-1})	09-07	913	786	186	1,850	843
	10-08	338	284	338	568	394
C_2H_6 (µL L^{-1})	09-07	0.33	0.20	0.09	0.12	0.65
	10-08	bd	018	bd[a]	0.28	1.08
C_2H_{2-4} (µL L^{-1})	09-07	0.14	0.17	bd	0.02	bd
	10-08	bd	bd	bd	bd	bd
C_3H_8 (µL L^{-1})	09-07	bd	bd	bd	bd	bd
	10-08	bd	bd	bd	0.05	0.05
C_3H_6 (µL L^{-1})	09-07	bd	bd	bd	bd	bd
	10-08	bd	bd	bd	bd	bd
Ar (µL L^{-1})	09-07	838	1,060	649	849	710
	10-08	1,110	1,190	740	185	bd
He (µL L^{-1})	09-07	7,980	8,420	8,110	4,920	14,200
	10-08	9,990	9,100	9,070	6,600	14,900
N_2 (µL L^{-1})	09-07	57,800	118,000	67,100	61,100	95,600
	10-08	77,400	91,900	98,200	44,900	71,200
O_2(µL L^{-1})	09-07	0.00	0.00	0.00	0.00	0.00
	10-08	0.00	0.00	0.00	0.00	0.00

4.1.2 Microbial analysis

The results of the microbial analyses for sulphate reducing bacteria and autotrophic acetogens are summarised in Table 4-4 and Table 4-5. The details of the experimental measurement and the analyses, which were provided by Microbial Analytics AB, are given in Appendix 1 of the previous progress report [5], but are not repeated here. The data from the sample taken in October 2008 show that the autotrophic acetogens were the dominant species, but that sulphate reducing bacteria were also present in significant numbers. No other types of microbes were analysed in detail, because these two varieties were believed to be significant in relation to corrosion, but the possibility that other species could be present cannot be excluded. The results of the following measurements are included in Table 4-4 and Table 4-5:

- most probable numbers (MPN) and metabolites produced by sulphate-reducing bacteria (SRB) and autotrophic acetogens (AA)
- biomass measured as adenosine-tri-phosphate (ATP) content
- total number of cells
- number of cultivable heterotrophic aerobic bacteria (CHAB) and
- molecular biology analyses which investigate the RNA and DNA pools in the samples.

The total number of cell levels remained unchanged in 2008 but the ATP level increased by almost 10-fold inside the model canister, where the water was in contact with cast iron. Further details and discussion of the results are given in Appendix 1 of reference [5].

Table 4-4. The microbial composition inside and the outside (2G) the model canister experiments sampled in 05-2007.

Experiment	ATP (amol mL^{-1}) a	TNC (mL^{-1}) a	Q-PCR 16S DNA (mL^{-1})	CHAB (mL^{-1}) a	MPN SRB (mL^{-1}) c	Q-PCR active SRB (relative activity)	Q-PCR total SRB (mL^{-1})	MPN AA (mL^{-1}) c	Q-PCR AA (relative activity)	Acetate (mg L^{-1})
1	2,400 ± 450	130,000 ± 16,000	na [b]	227 ± 42	5,000 (2,000–17,000)	10	na [b]	30,000 (2,000–17,000)	631	8.5
2	2,800 ± 240	95,000 ± 39,000	na [b]	200 ± 57	1,400 (600–3,600)	2	na [b]	50,000 (20,000–200,000)	10	8
2 G	3,300 ± 710	31,000 ± 11,000	na [b]	20 ± 35	3 (1–12)	3	na [b]	3 (1–12)	3	6.9
3	15,500 ± 810	150,000 ± 61,000	na [b]	530 ± 28	230 (90–860)	2	na [b]	7,000 (3,000–21,000)	336	6.9
5	3,000 ± 680	13,000 ± 4,900	na [b]	17 ± 12	300 (100–1,100)	1	na [b]	bd	1	11

[a] ± standard deviation [b] not analysed [c] 95% confidence interval).

Key

ATP adenosine triphosphate.
TNC total number of cells.
CHAB number of cultivable heterotrophic aerobic bacteria.
MPN most probable numbers.
AA autotrophic acetogens.
SRB sulphate-reducing bacteria.
Q-PCR quantitative real time polymerase chain reaction.
DNA deoxyribonucleic acid.

Table 4-5. The microbial composition inside and outside (2G) the model canister experiments sampled in October 2008.

Experiment	ATP (amol mL^{-1}) a	TNC (mL^{-1}) a	Q-PCR 16S DNA (mL^{-1})	CHAB (mL^{-1}) a	MPN SRB (mL^{-1}) c	Q-PCR active SRB (mL^{-1})	Q-PCR total SRB (mL^{-1})	MPN AA (mL^{-1}) c	Q-PCR active AA (mL^{-1})	Acetate (mg L^{-1})
1	17,400 ± 2,500	180,000 ± 4,600	6,700,000	bd [b]	5,000 (2,000–17,000)	5,500	540,000	1.7 (0.7–4)	bd [b]	1.7
2	10,400 ± 690	180,000 ± 18,000	4,500,000	3 ± 6	800 (300–2,500)	31	37,000	17 (7–48)	bd [b]	1.6
2 G	4,400 ± 570	2,500 ± 880	8,000,000	3 ± 6	2.3 (0.9–8.6)	bd [b]	bd [b]	0.4 (0.1–1.7)	bd [b]	2.9
3	27,400 ± 1,820	200,000 ± 22,000	5,000,000	20 ± 17	70 (30–210)	350	74,000	90 (30–290)	bd [b]	1.8
5	18,600 ± 1,270	71,000 ± 11,000	14,000,000	bd [b]	110 (40–300)	bd [b]	11,000	2,700 (1,200–6,700)	bd [b]	2.3

[a] ± standard deviation [b] below detection limit [c] 95% confidence interval).

Key

ATP	adenosine triphosphate.
TNC	total number of cells.
CHAB	number of cultivable heterotrophic aerobic bacteria.
MPN	most probable numbers.
AA	autotrophic acetogens.
SRB	sulphate-reducing bacteria.
Q-PCR	quantitative real time polymerase chain reaction.
DNA	deoxyribonucleic acid.

4.1.3 Pressure readings

The results from the pressure gauges in the boreholes are shown in Figure 4-9. Unfortunately there was a loss of data due to a fault with the datalogging system during the Winter of 2007/8. The data show that there is a general tendency for the pressure to fall with time, although the rate of decrease has fallen and the pressures have stabilised and increased slightly in recent months. The low pressure is mainly due to water loss through the rock face surrounding the boreholes.

4.2 Electrochemical potential measurements

This section presents the electrochemical potential measurements for each of the model canister experiments. Some of the figures also include the results of corrosion rate measurements (see Section 4.3). The exposure period for all experiments up to the end of the data shown in this report was ~33,000 hours (i.e. ~3.8 years).

4.2.1 Experiment 1: Low density bentonite

In this experiment the defect in the outer copper shell (located near the top cap weld), is pointing vertically upwards. Figure 4-10 shows the results from the potential measurements for gold, platinum, E_h probe and the miniature canister. These data show the E_h values using gold and platinum, which are inside the support cage, and the E_h measured using the mixed-metal oxide electrode outside the support cage. Initially the internal silver-silver chloride reference electrodes were used for the Au and Pt electrodes, but these failed and it was necessary to switch to the Silvion reference electrode, which was mounted in the borehole outside the support cage (see change at 4,000 hours). The Au, Pt and Minican potential data up to 4,000 hours should be discounted. It is not clear why the Ag-AgCl disc electrodes failed in these experiments, since they had behaved satisfactorily during the laboratory autoclave tests [3]. To date, the Silvion reference electrodes have performed satisfactorily.

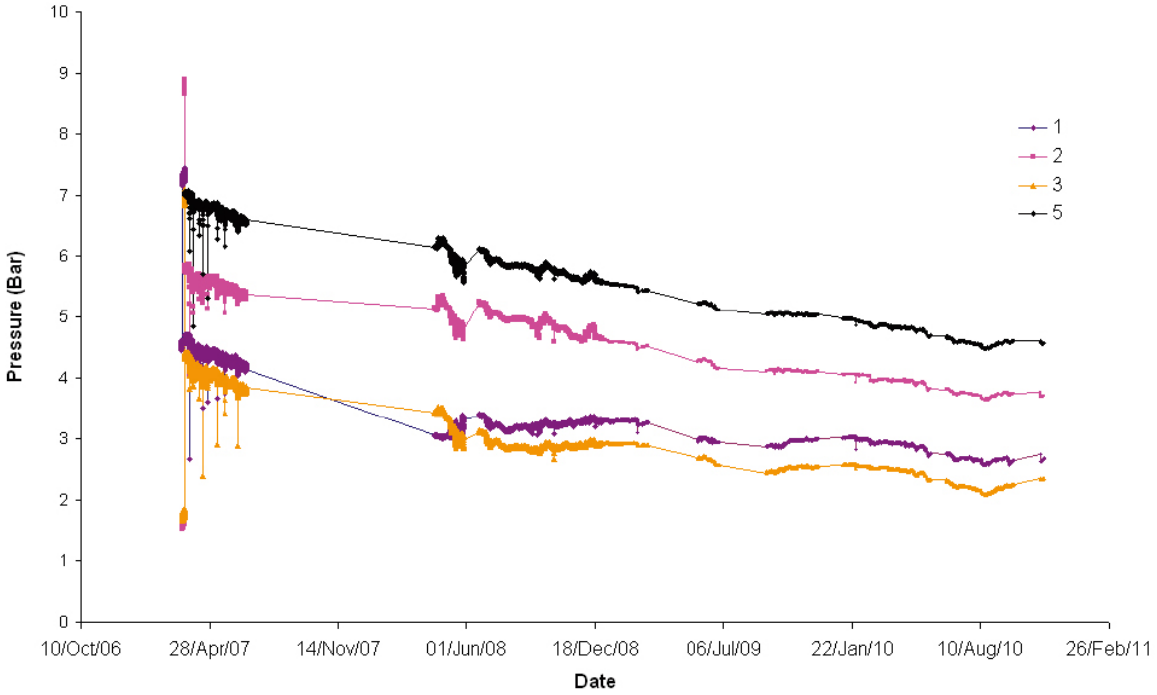

Figure 4-9. *Pressure reading for borehole 1 to 5 (pressure inside support cage, no measurements possible for Experiment 4 because of presence of compacted bentonite).*

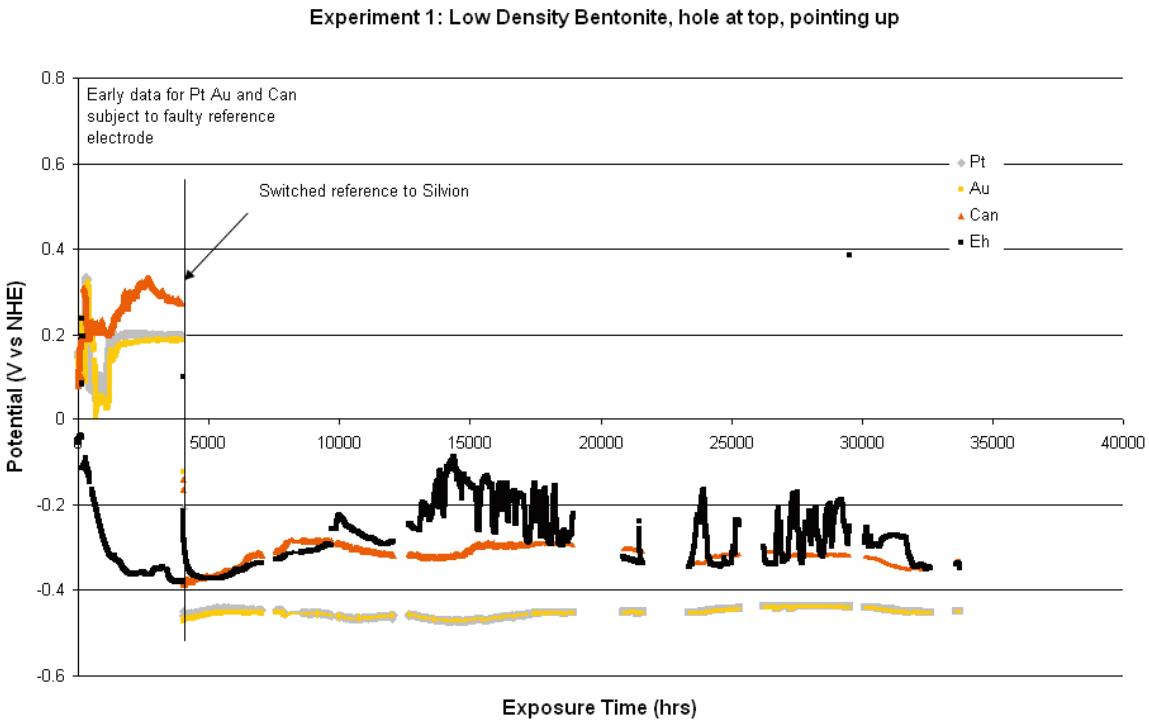

Figure 4-10. *Results of E_h and canister potential measurements from Experiment 1 (low density bentonite).*

The mixed metal oxide E_h values are reliable and show a decrease in the E_h with time. This is expected, since oxygen is consumed by microbial activity, mineral reactions and corrosion. The E_h value is lower inside the cage than outside, indicating more reducing conditions, possibly due to the ongoing corrosion reactions. Recently there have been some fluctuations in the E_h values; the reasons for these are not clear at present.

The electrochemical potential for the model canister represents a mixed potential for the copper canister itself and the inner cast iron insert, which would probably have been partially wetted by water passing through the 1 mm defect in the outer copper canister.

Figure 4-11 shows the potentials for the iron and copper coupons inside Experiment 1, up to October 2010. Again there was a problem with the reference electrodes up to 27 June 2007, but after that date the measurements were changed to be with respect to the Silvion reference electrode, at which point reasonable values of about –450 mV vs NHE were obtained, for both iron and copper. The iron and copper potentials are consistent with anoxic conditions existing in the boreholes.

4.2.2 Experiment 2: Low density bentonite

In this experiment the defect in the outer copper shell is at the top end of the canister (i.e. near the lid) but pointing downwards. Figure 4-12 shows the results from the potential measurements for gold, platinum, E_h probe and the model canister.

With Experiment 2, as for Experiment 1, there was a problem with the small Ag-AgCl reference electrodes mounted inside the support cages, but when the measurements were carried out against the external Silvion reference electrode reasonable values were obtained. The E_h value is again slightly more reducing inside the support cage than outside.

The electrochemical potential values for iron and copper are shown in Figure 4-13. As for Experiment 1 it was necessary to measure the values against the Silvion reference electrode because the internal silver-silver chloride electrodes failed. This correction was made after June 2007. The potentials have been stable since the reference electrode system was changed; they are consistent with anoxic reducing conditions.

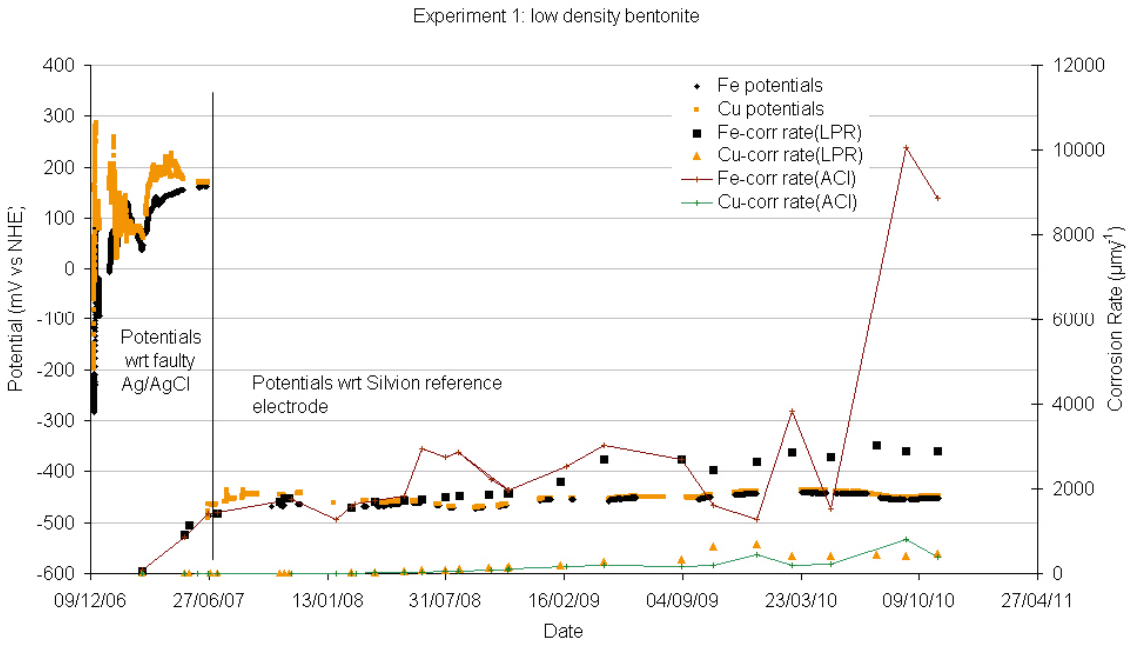

Figure 4-11. *Results of corrosion potential and corrosion rate measurements for cast iron and copper electrodes in Experiment 1 (low density bentonite).*

Figure 4-12. *Results of E_h and canister potential measurements from Experiment 2 (low density bentonite).*

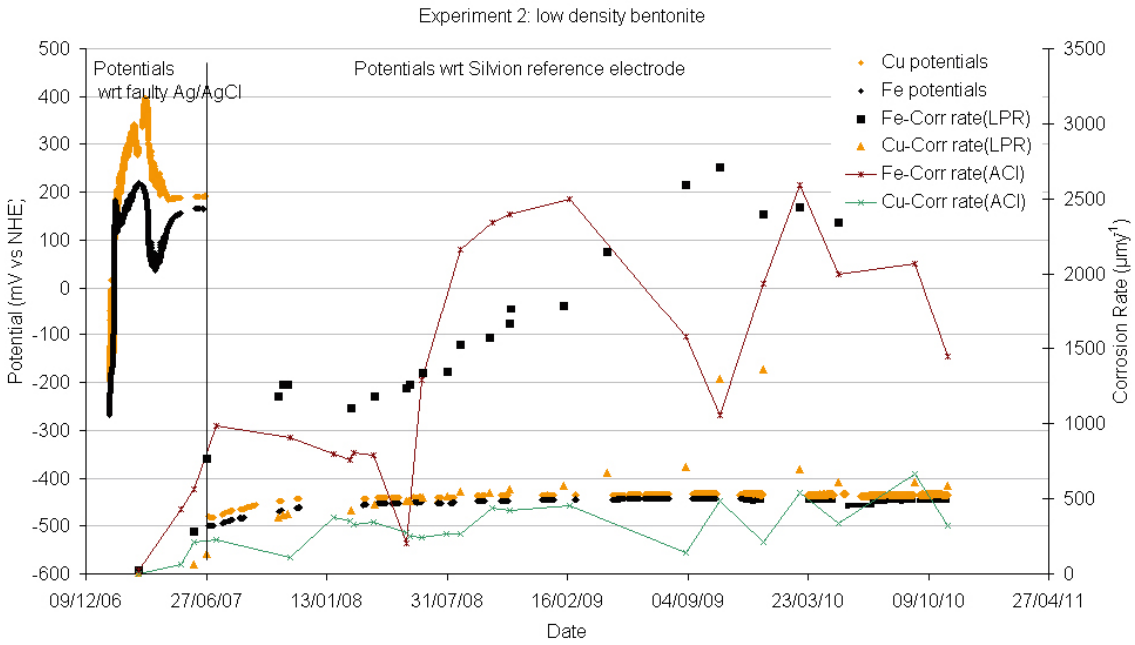

Figure 4-13. *Results of corrosion potential and corrosion rate measurements for cast iron and copper electrodes in Experiment 2 (low density bentonite).*

4.2.3 Experiment 3: Low density bentonite

In this experiment there are two defects present in the outer copper shell; the defect near the top lid is pointing upwards, while the defect near the bottom cap is pointing downwards. Figure 4-14 shows the results from the potential measurements for gold, platinum, E_h probe and the model canister. In Experiment 3 the internal Ag-AgCl electrodes worked properly until approximately 8,000 hours had elapsed, when it was necessary to change to the Silvion reference electrode outside the support cage. The early fluctuations in E_h inside the support cage appear to be genuine. The E_h value external to the support cage stabilised at ~–300 mV after 3,500 hours.

The electrochemical potential values for iron and copper in Experiment 3 are shown in Figure 4-15. These data show a decrease in the corrosion potential of the copper initially, stabilising at highly negative values. The potentials were subsequently measured against Silvion after failure of the internal silver-silver chloride reference electrodes after approximately 7,500 hours. The potentials have been stable for the last 18 months but have attained more positive values than initially (~-430 mV NHE).

4.2.4 Experiment 4: Compacted bentonite

In Experiment 4 the defect in the outer copper shell is near the top lid but pointing downwards. The whole model canister is surrounded by compacted bentonite, with the test electrodes placed in slots cut into the compacted bentonite. Figure 4-16 shows the results from the potential measurements for gold, platinum, E_h probe and the model canister. The potentials for the platinum exhibited a considerable amount of noise. It was necessary to use the external Silvion reference electrodes to measure the potentials after about 3,500 hours. It is noticeable that the E_h values are not as negative as in the fully saturated bentonite tests.

The electrochemical potential values for copper and iron in Experiment 4 are shown in Figure 4-17 and Figure 4-18 respectively. Contact has now been lost with the iron electrode in this experiment (it appears to be in contact with the stainless steel flange). This may have been caused by expansion of the compact bentonite leading to crushing of the electrical connections.

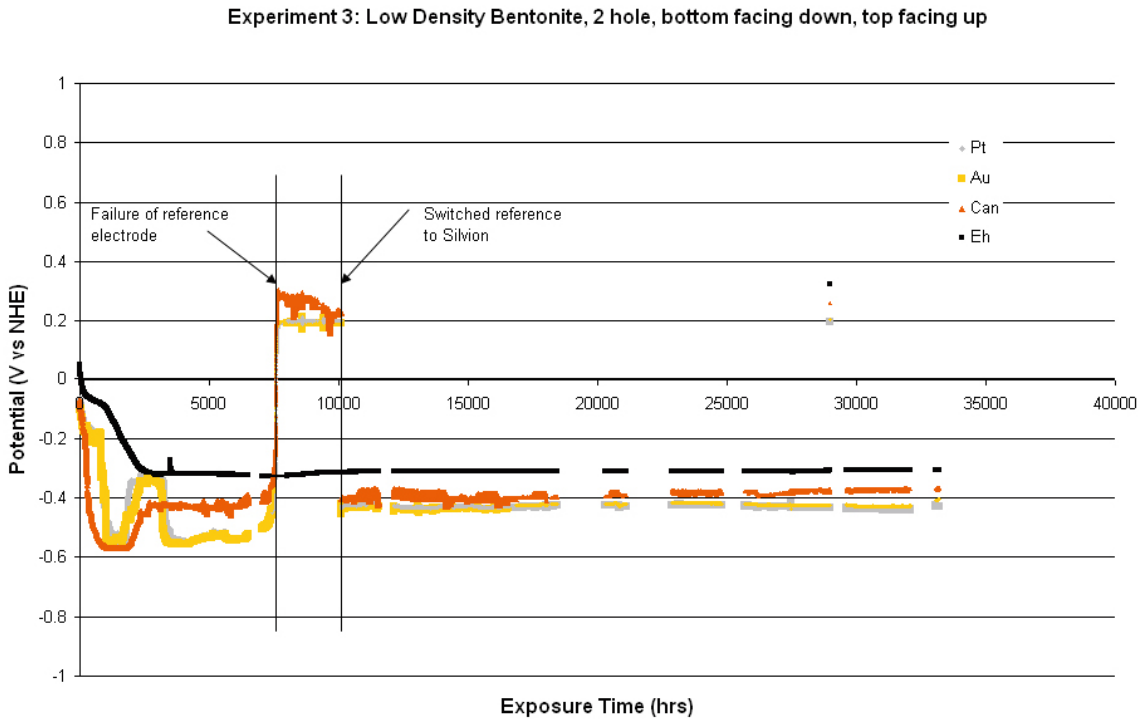

Figure 4-14. *Results of E_h and canister potential measurements from Experiment 3 (low density bentonite).*

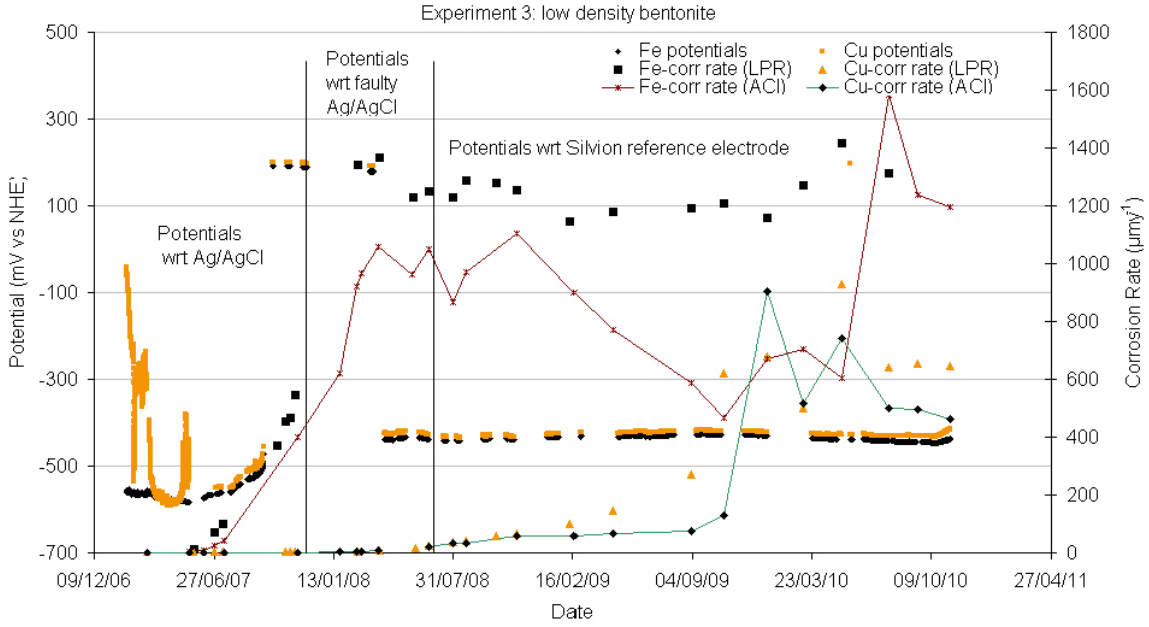

Figure 4-15. *Results of corrosion potential and corrosion rate measurements for cast iron and copper electrodes in Experiment 3 (low density bentonite).*

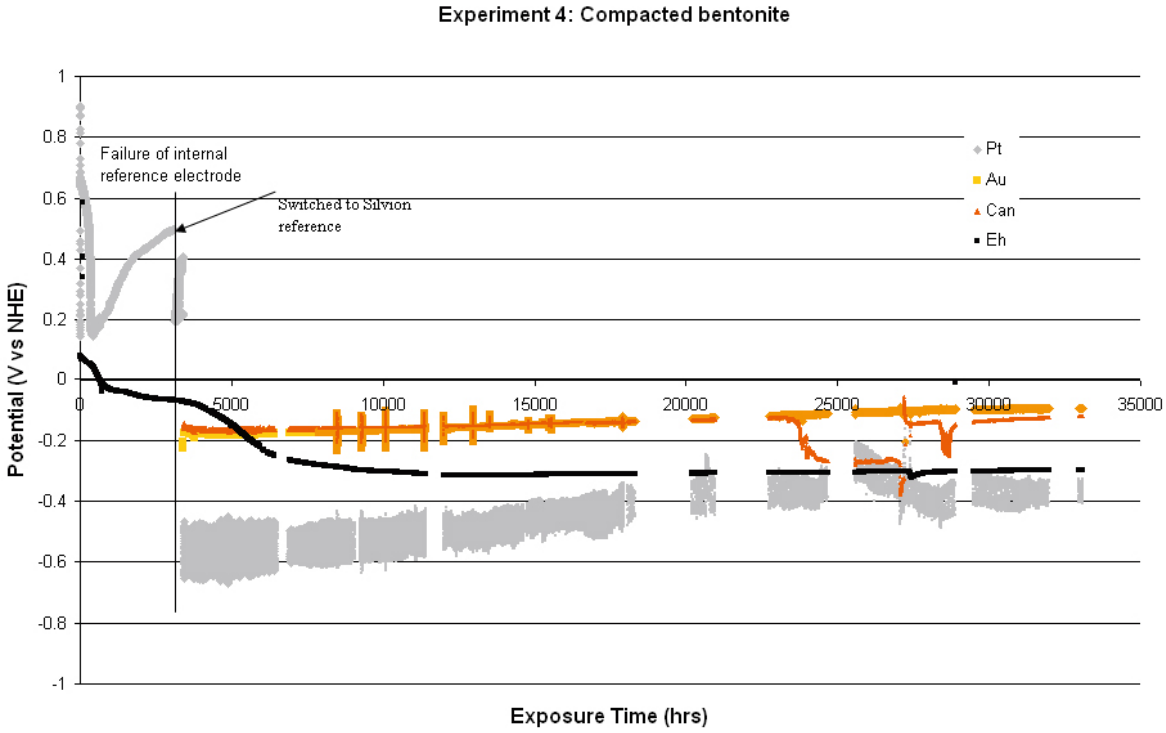

Figure 4-16. *Results of E_h and canister potential measurements from Experiment 4 (compact bentonite).*

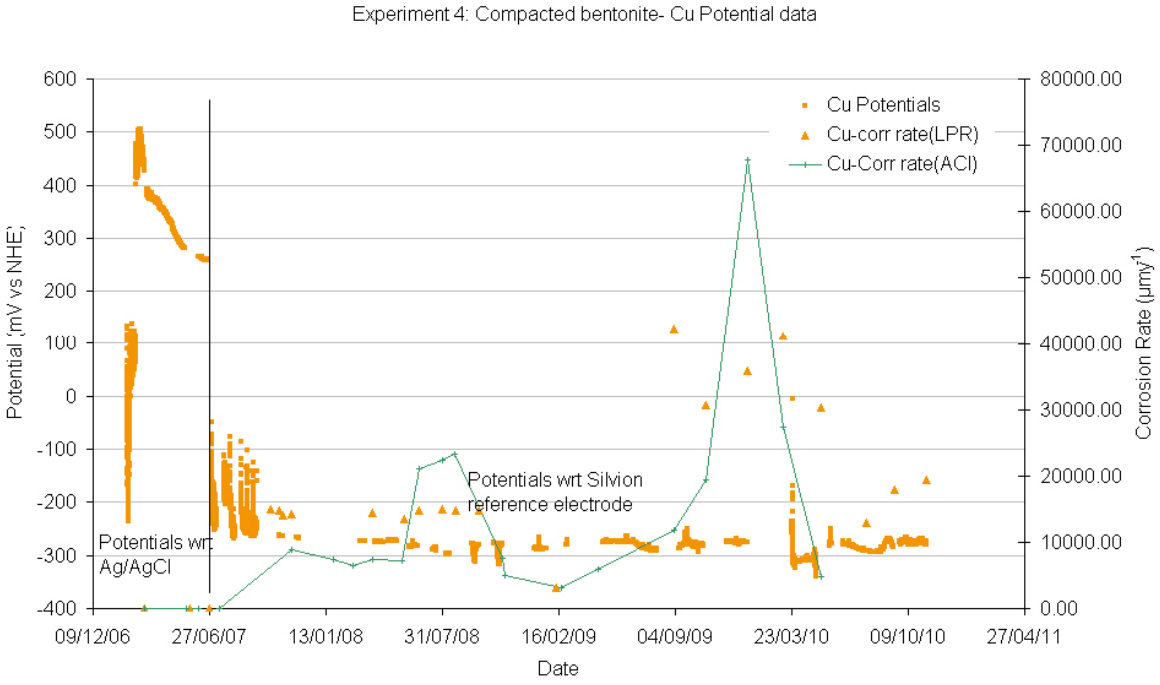

Figure 4-17. *Results of corrosion potential and corrosion rate measurements for copper electrodes in Experiment 4 (compacted bentonite).*

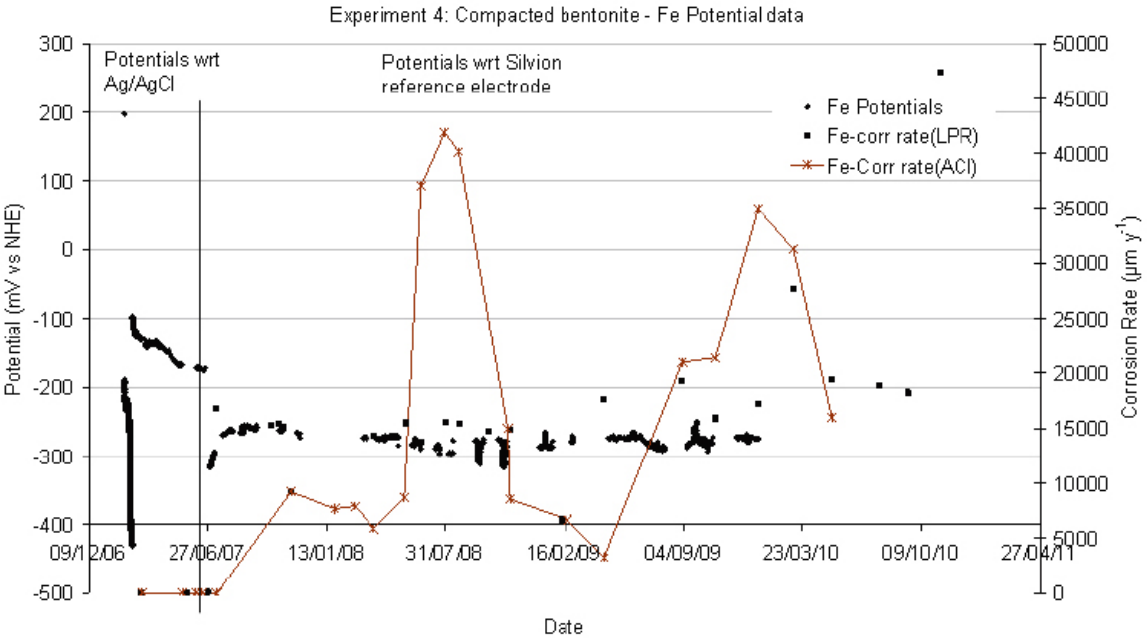

Figure 4-18. *Results of corrosion potential and corrosion rate measurements for cast iron electrodes in Experiment 4 (compacted bentonite).*

4.2.5 Experiment 5: No bentonite

In this experiment there are two defects in the outer copper shell, both of which are near the top lid. One defect is pointing vertically upwards, the other is pointing downwards. In this experiment there is no bentonite around the model canister (i.e. it is in direct contact with the Äspö groundwater). Figure 4-19 shows the results from the potential measurements for gold, platinum, E_h probe and the model canister. In this experiment there was a problem with both the internal silver-silver chloride reference electrodes and the external E_h probe and the Silvion electrode and so it was necessary to set up an external reference electrode and E_h probe, mounted on the borehole flange. The iron and copper potentials in this experiment are shown in Figure 4-20. Again there were problems with the small internal Ag-AgCl reference electrodes up to June 2007, after which it was necessary to switch to using the stainless steel flange as a pseudo reference electrode and then to an external reference electrode. The E_h probe data and the recent iron and copper potentials are unusually high and there was some doubt about the reliability of this reference electrode system, using a Clarke's silver-silver chloride reference electrode system. In May 2010 the external reference electrode was replaced with a Silvion external reference electrode and this appears to be operating satisfactorily (see Figure 4-19).

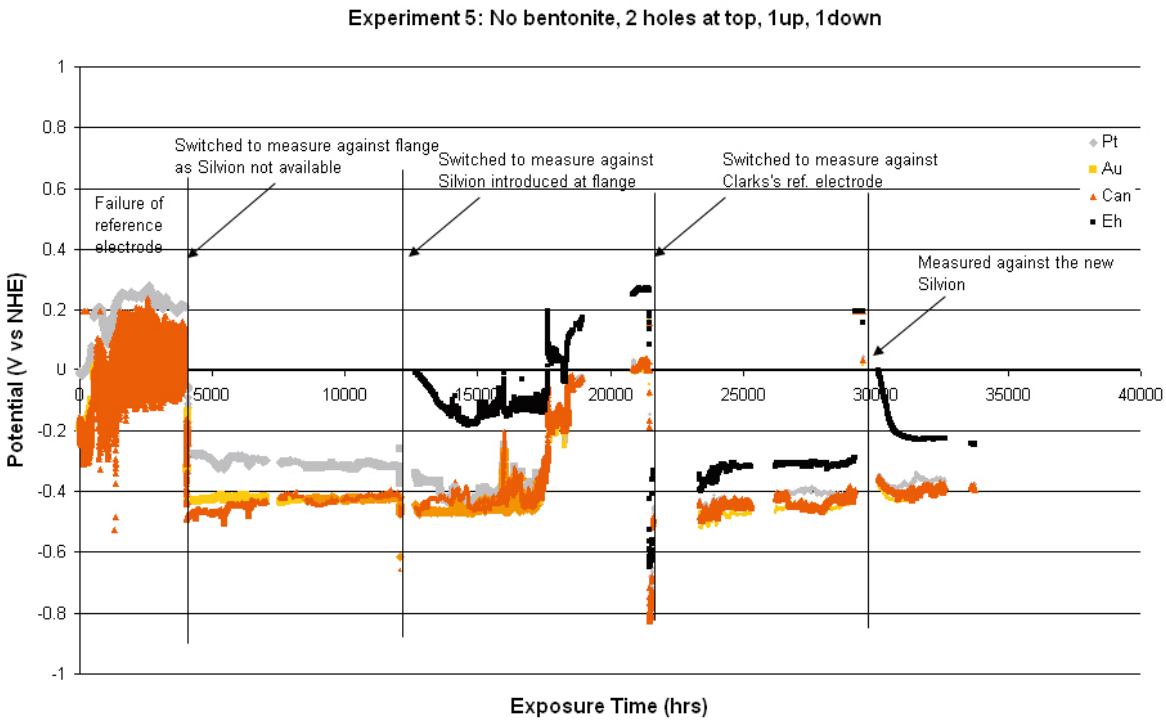

Figure 4-19. *Results of E_h and canister potential measurements from Experiment 5 (no bentonite).*

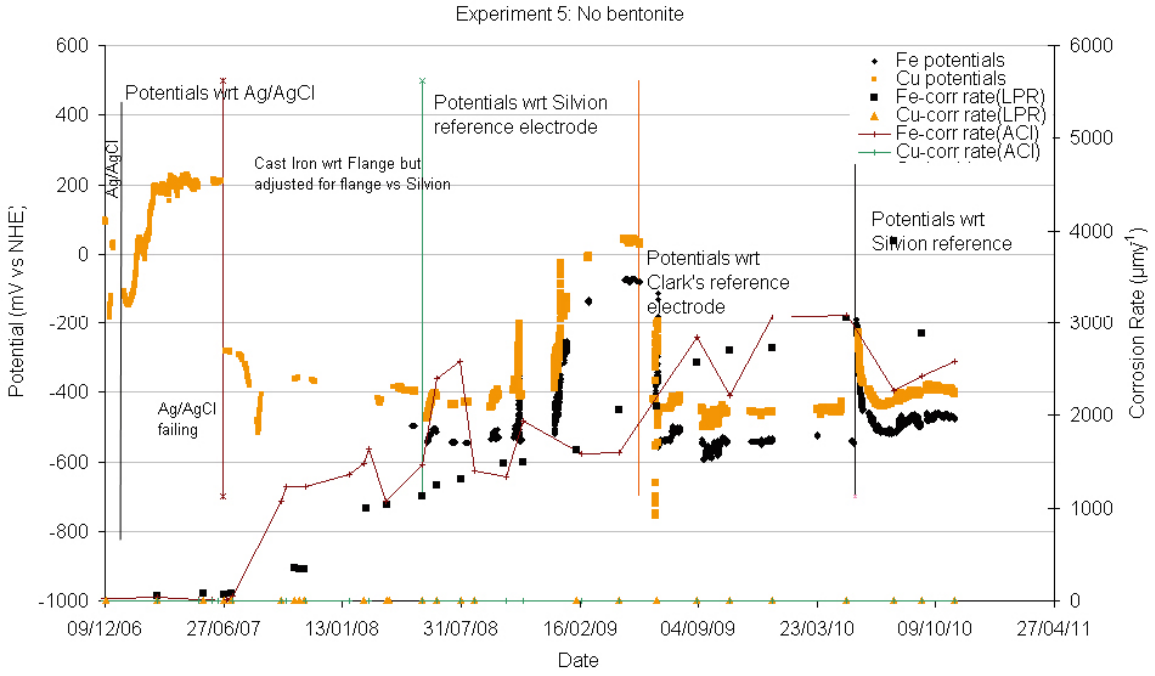

Figure 4-20. *Results of corrosion potential and corrosion rate measurements for cast iron and copper electrodes in Experiment 5 (no bentonite).*

4.3 Electrochemical corrosion rate measurements

Corrosion rate measurements were carried out using the following electrochemical techniques: linear polarisation resistance, LPR, AC impedance, ACI, and electrochemical noise, ECN. The LPR measurements were carried out over a potential range of ±10 mV with respect to the corrosion potential at a scan rate of 10 mV min^{-1} (starting with the electrode polarised to -10 mV). The corrosion rate is obtained by measuring the slopes of the plots and applying the Stern-Geary approximation [10], with a Stern-Geary constant of 26 mV. The AC impedance measurements were carried out using a perturbation of ±10 mV, starting at an initial frequency of 10 kHz start and a final frequency of 10 mHz finish, with 100 readings taken per test. The electrochemical noise measurements were carried out at a sampling rate of ten readings per second for a period of one hour. Examples of typical LPR and AC impedance measurements for copper and iron electrodes in Experiment 1 are shown in Figure 4-21 and Figure 4-22. All the raw data obtained during 2010 are given in Appendix 1 and the raw data acquired during previous reporting periods are shown in Appendix 2. The plots in these two appendices show how the LPR data and the AC impedance data in Nyquist and Bode format have evolved with exposure time. An increasing slope in the LPR plots corresponds to an increasing corrosion rate. Similarly a decrease in the diameter of the AC impedance Nyquist plots corresponds to an increase in corrosion rate. It is possible to see some fine structure in the Nyquist plots at the high frequency end of the scans, which probably represent the development of features in the surface films rather than instrumental artefacts.

Summaries of the measured corrosion rate data for copper and cast iron are presented in Figure 4-23 to Figure 4-26. The measured corrosion rates are also shown on the plots of corrosion potential against time for each of the five experiments (i.e. Figure 4-11, 13, 15, 17, 18 and 20). Generally speaking, good agreement was obtained between the corrosion rates derived from the two techniques, although it should be noted that they essentially measure the same parameter (i.e. charge transfer resistance) so that agreement does not necessarily mean that the corrosion rates are accurate. There is a peculiarity about the corrosion rate data for cast iron from Experiment 4 because it appears that the electrode is currently in contact with the stainless steel flange. Figure 4-26 shows that up to June 2006 the corrosion rate was less than 100 μm yr^{-1} but thereafter there was a sudden change in behaviour. This seems unlikely to be a genuine change in corrosion rate and the most likely explanation is that swelling of the bentonite clay caused damage to the electrical connections and forced the electrodes up into contact with the stainless steel flange. This would have had the effect of producing a much larger electrode surface area and hence the measured currents would have increased sharply.

The corrosion rate values obtained for copper in Experiments 1, 2, 3 and 5 are summarised in Figure 4-23 and the values from electrochemical measurements on cast iron in Experiments 1, 2, 3 and 5 are shown in Figure 4-25. The corrosion rate data for copper in Experiment 4 are plotted separately for copper in Figure 4-24 because it yielded considerably higher corrosion rate values. The corrosion rates measured for copper in Experiment 4 (Figure 4-24) are impossibly high because if such corrosion rates had actually occurred there would not be any electrode material left to measure. This suggests that, at least for Experiment 4, the corrosion rates after November 2007 were not being measured accurately and that there must be some kind of experimental artefact affecting them. It is possible that there has been some disruption of the electrodes and the connections due to the swelling pressure exerted by the compacted bentonite. The most recent AC Impedance data for copper in Experiment 4 (e.g. Figure A1-17) are clearly not correct and should be discounted. Prior to the step change in the corrosion rate at the end of 2007 the measured corrosion rate of the copper in compacted bentonite was of the order of 1 μm yr^{-1} (Figure 4-24). Data obtained after this date are not credible. There is also an unresolved question about whether the high pressure exerted by the swelling bentonite in Experiment 4 could affect the electrochemical response of any corrosion product films.

The data in Figure 4-23 show that initially the measured corrosion rate of copper in Experiments 1 to 3, with low density bentonite was <10 μm yr^{-1}, but after an incubation period, which varied in duration between the experiments, the electrochemically measured corrosion rate increased by several orders of magnitude. The measured corrosion rate of copper in Experiment 5, where no bentonite was present, has remained at <6 μm yr^{-1} based on LPR measurements and <3 μm yr^{-1}, based on AC impedance measurements for the duration of the experiment. This indicates that the presence of low density bentonite has either (i) increased the corrosion rate of the copper, or (ii) changed the surface of the copper electrode so that the electrochemical properties indicated an increased, but inaccurate, corrosion rate.

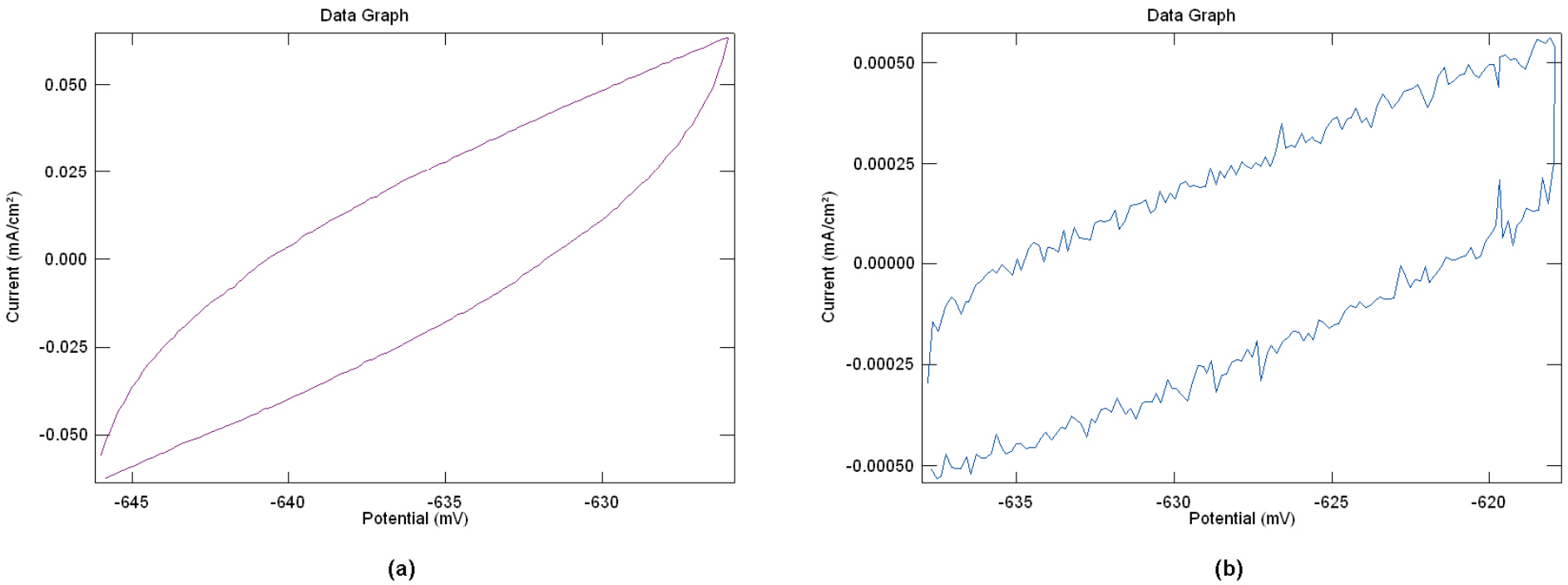

Figure 4-21. *Typical examples of linear polarisation resistance (LPR) measurements on Experiment 1: (a) cast iron, (b) copper.*

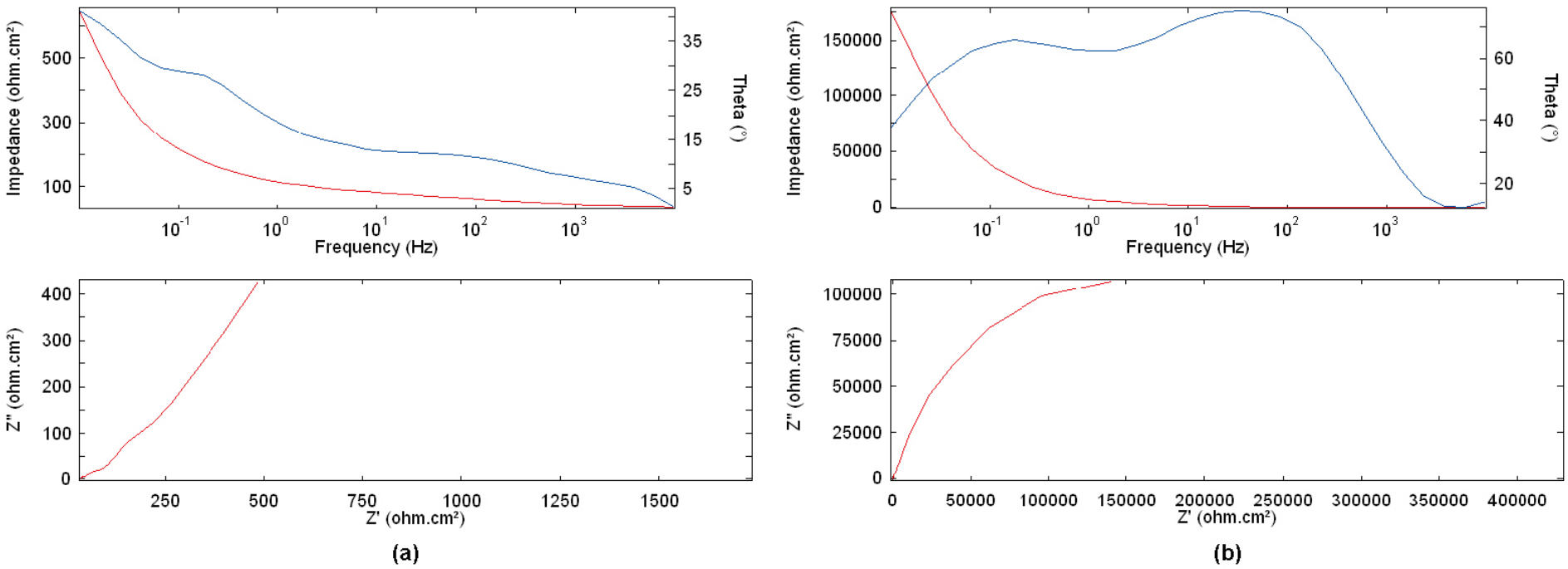

Figure 4-22. *Typical examples of AC impedance measurements (ACI) on Experiment 1: (a) cast iron, (b) copper. Top figure: blue line = theta plot; red line = impedance plot.*

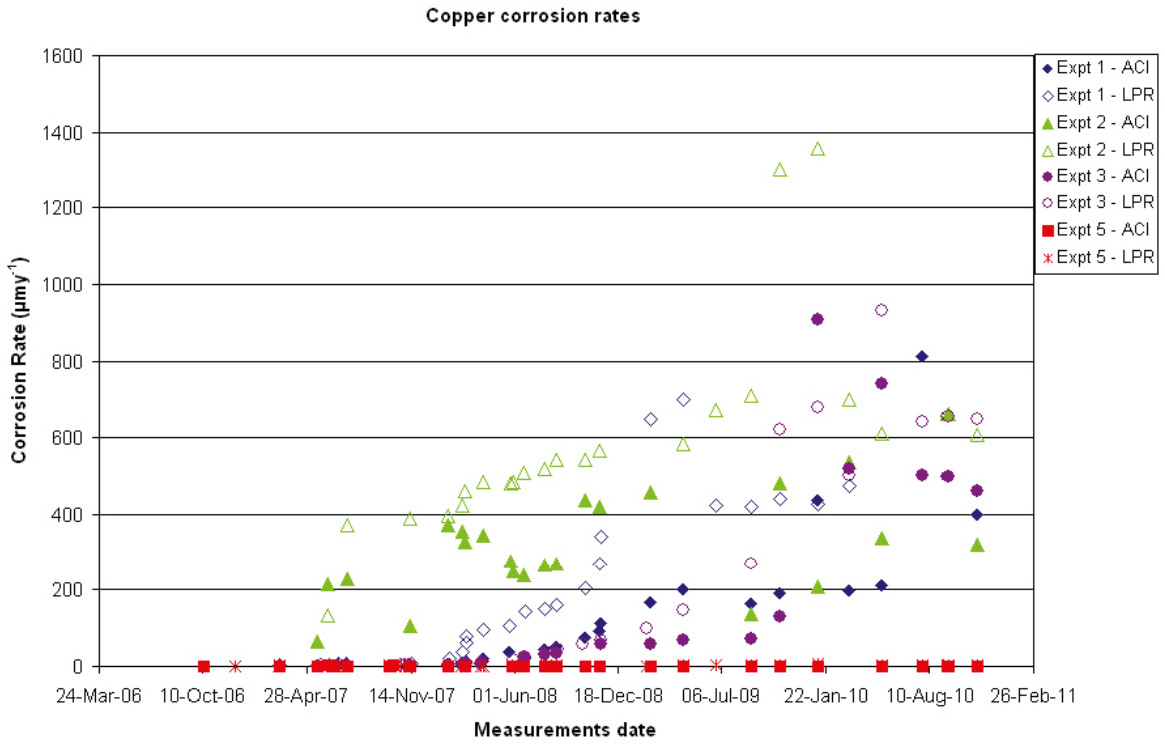

Figure 4-23. *Summary of copper corrosion rates obtained by AC impedance and LPR measurements.*

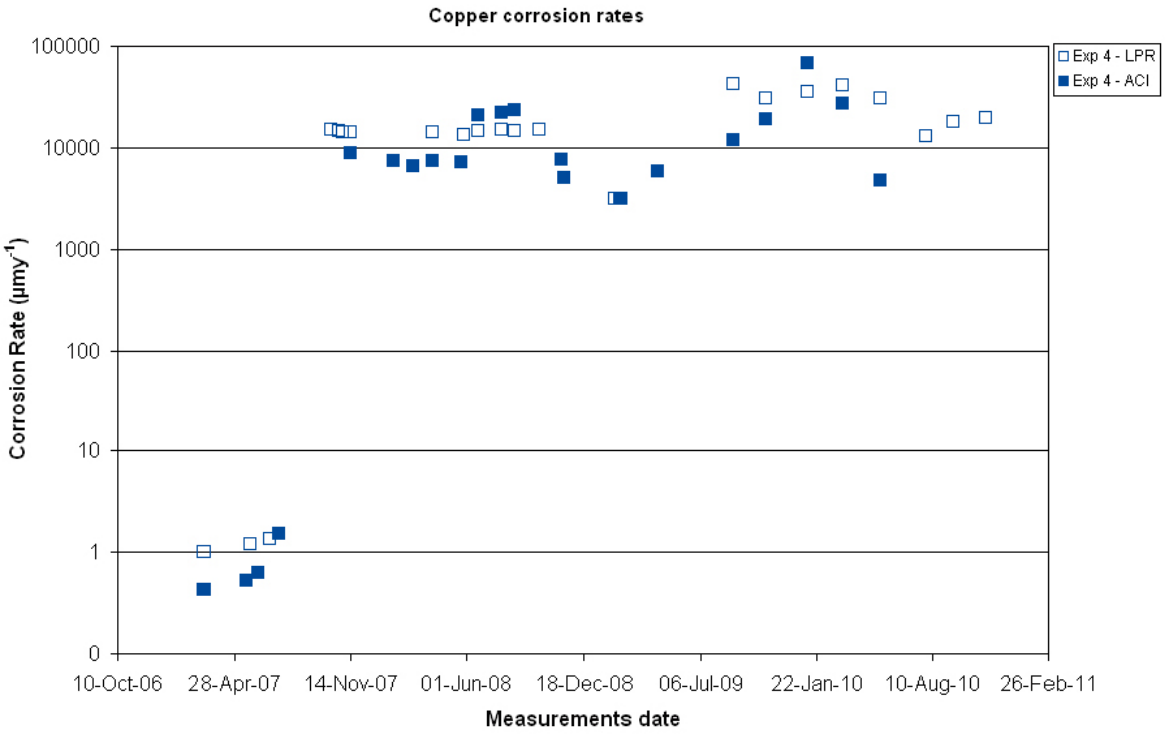

Figure 4-24. *Summary of copper corrosion rates obtained by AC impedance and LPR measurements (Experiment 4).*

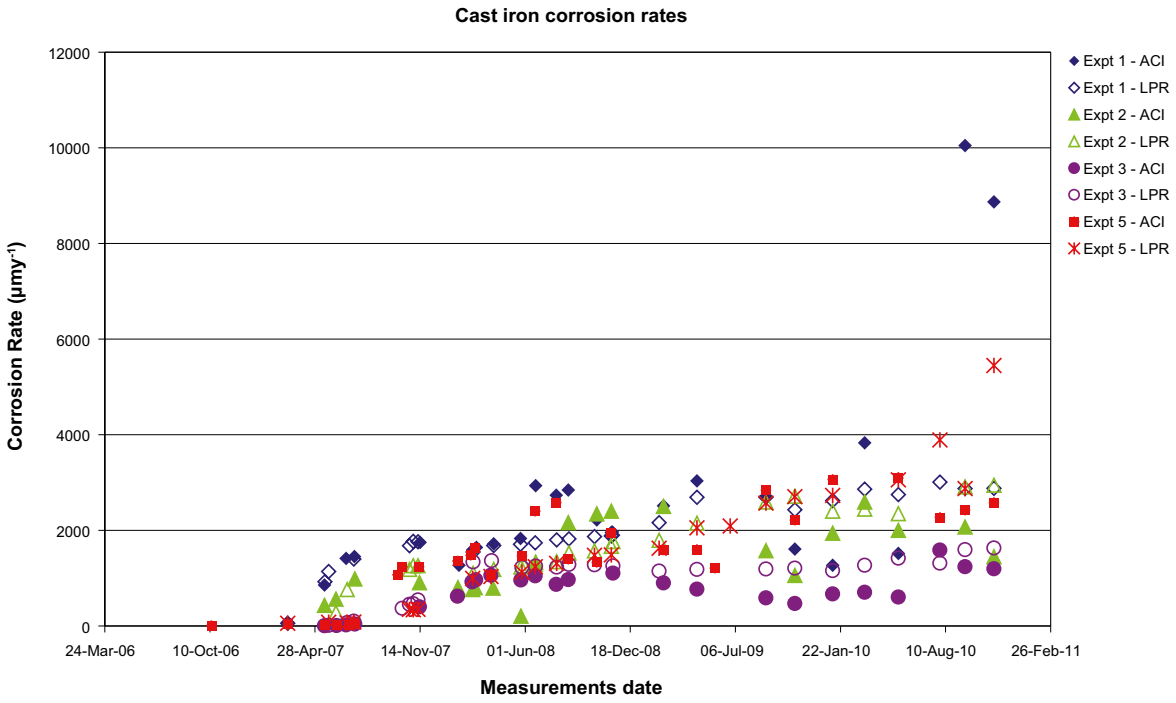

Figure 4-25. *Summary of cast iron corrosion rates obtained by AC impedance and LPR measurements.*

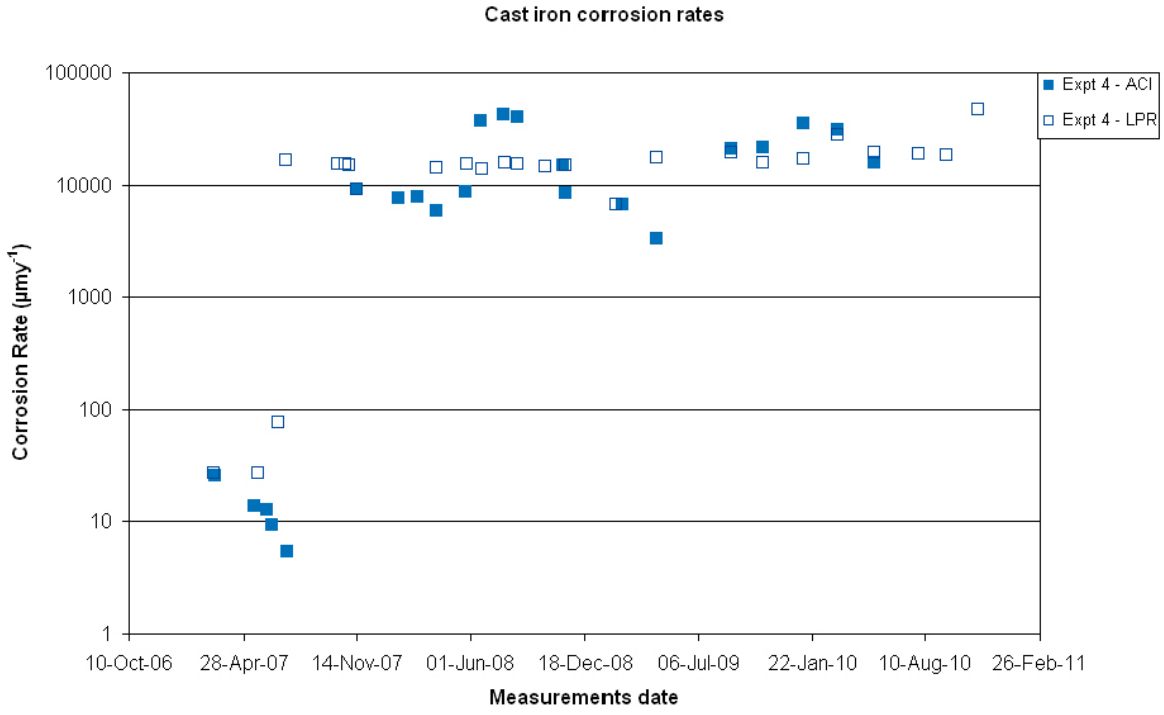

Figure 4-26. *Summary of cast iron corrosion rates obtained by AC impedance and LPR measurements (Experiment 4).*

One possible explanation is that the microbial activity is enhanced in the presence of low density bentonite, leading to a greater production of sulphide by SRB activity, which is known to increase the corrosion rate of copper [16]. It is interesting to note that the lowest corrosion rates for both iron and copper, corresponded to the time when water samples were being extracted most frequently (e.g. see Figure 4-1 for dates of water sampling) and it is possible that the increase in corrosion rate corresponded to the time when microbial activity was least disturbed by drawing water out of the support cage. In situ studies by Hallbeck and Pedersen at a location near to the MiniCan experiment in the Äspö laboratory have shown that closure of a groundwater test loop can lead to an increase in the concentration of sulphide in the groundwater [11] due to SRB activity, which produced sulphide at a rate of 0.08 mg sulphide L^{-1}. It should be noted that these experiments did not contain any bentonite in the test loop, showing that the SRB activity can be sustained even in the absence of an additional source of nutrients such as the organic material in bentonite.

The data in Figure 4-25 indicate that the measured corrosion rate of the cast iron in experiments 1, 2, 3 and 5 has increased but then stabilised at values of several thousand μm yr^{-1}. However, based on values published in the literature there is reason to believe that the corrosion rate measured using electrochemical methods may overestimate the true value because of the nature of the iron sulphide film formed in the presence of SRB activity; this is discussed further in Section 5.3.

During 2010 the possibility that changes in the reference electrode configuration might have affected the corrosion rate measurements was investigated. Normally, in an electrochemical cell, the reference electrode would be placed near to the working electrode to minimise any potential drop effects (known as IR drop effects) caused by the resistance of the solution to the current passing through it during the electrochemical measurement. However, because of the failure of the internal; Ag-AgCl electrodes it was necessary to use an external Silvion reference electrode which was further from the working electrode and so the IR drop would have been greater. The groundwater has a high conductivity and so this effect is unlikely to be large, but in order to be able to eliminate the possibility a series of experiments was carried out in which the gold electrode was used as a pseudo-reference electrode. The gold electrode was close to the working electrode and so this would have reduced any IR drop effects. The results from this set of measurements are given in Table 4-6. The results indicate that the measured corrosion rates were not significantly affected by the choice of reference electrode. This view is supported by the fact that the measured corrosion rates did not exhibit a step change when the reference electrode was changed (e.g. see Figure 4-15). Other possible reasons for the measured increased corrosion rates are that localised attack is occurring on the electrodes, or that crevice corrosion has occurred around the polymeric sheathing on the electrodes. It is anticipated that these questions will be resolved when Experiment 3 is removed and analysed during 2011.

Table 4-6. Comparison of the LPR corrosion rate data obtained on the copper and cast iron coupons using different reference electrodes: Reference electrode A (external Silvion electrode) and Reference electrode B (gold as pseudo-reference electrode inside compacted bentonite).

Experiment	Corrosion rates (μmyr^{-1})			
	Reference electrode A		Reference Electrode B	
	Cast Iron	Copper	Cast Iron	Copper
1 (low density bentonite)	1,519	211	2,800	407
2 (low density bentonite)	2,000	337	2,960	586
3 (low density bentonite)	604	741	1,500	1,009
4 (compacted bentonite)	16,000	4,742	8,900	7,005
5 (no bentonite)	3,097	1.5	2,400	1.3

4.4 Copper wire resistance measurements

The results from the electrical resistance measurements on coils of copper wire are shown in Figure 4-27 (Experiment 2) and Figure 4-28 (Experiment 5). The resolution of these measurements is expected to increase with increasing measurement duration. It appears that the long-term corrosion rate for copper is close to zero in these measurements, but the signal is rather noisy. The manufacturers of the measuring equipment (ACM instruments) advised that an average value for the corrosion rate from the electrical resistance data should be taken. It is also possible to smooth the data, as shown in Figure 4-29. The averaged values based on the electrical resistance data for copper are 0.25 µm yr^{-1} for Experiment 2 (low density bentonite) and 0.39 µm yr^{-1} for Experiment 5 (no bentonite).

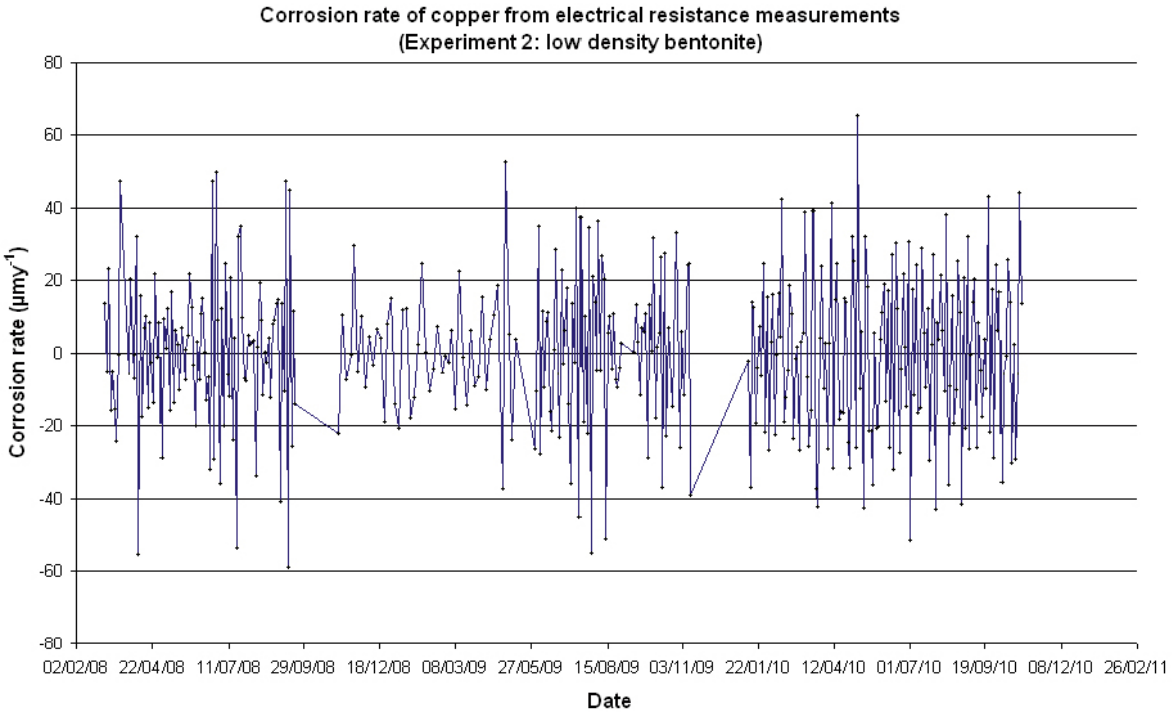

Figure 4-27. *Results of corrosion measurement from copper wire electrical resistance measurement (Experiment 2: low density bentonite).*

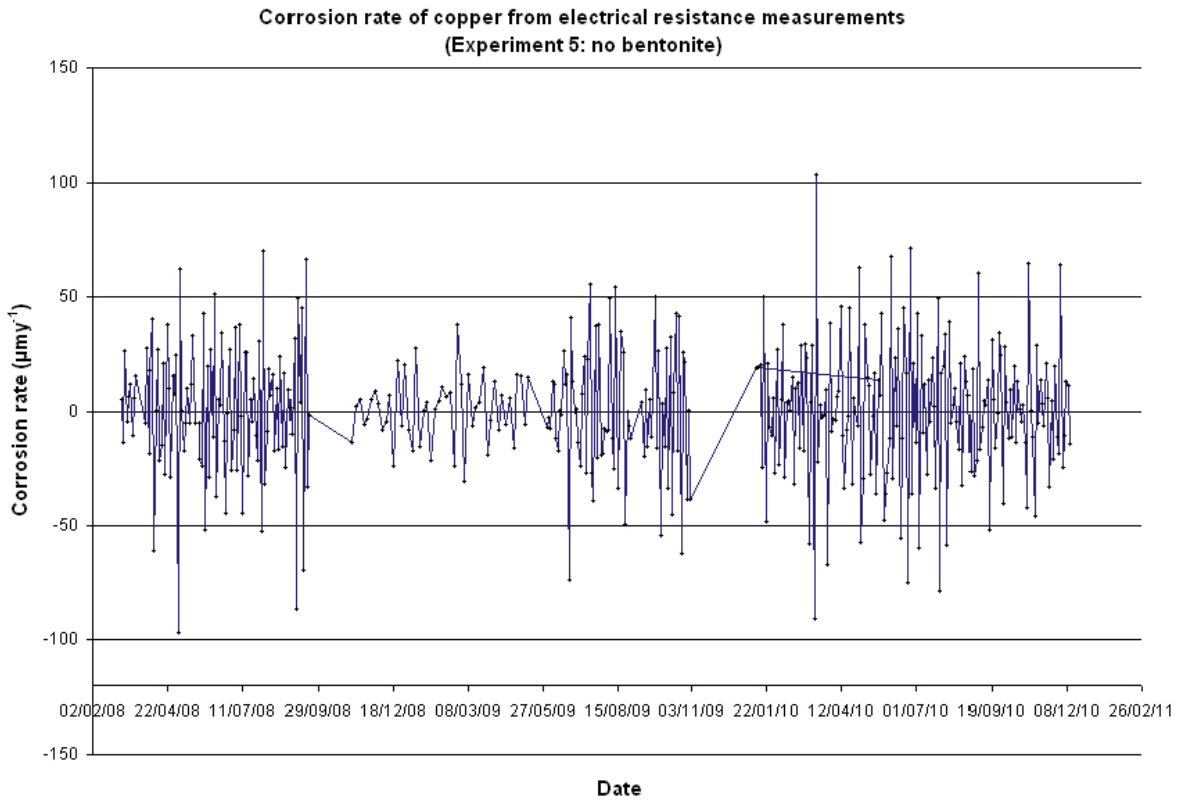

Figure 4-28. *Results of corrosion measurement from copper wire electrical resistance measurement (Experiment 5: no bentonite).*

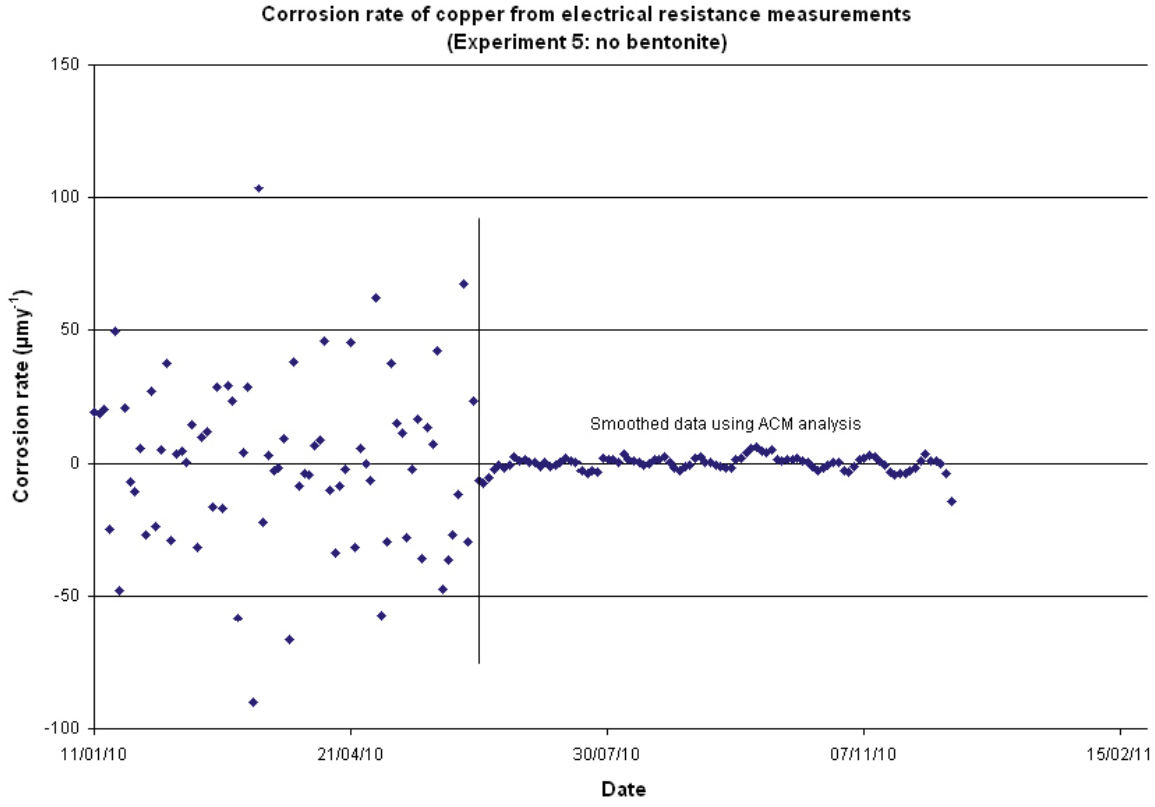

Figure 4-29. *Example of smoothed corrosion rate data obtained from copper wire electrical resistance measurement.*

4.5 Pressure and strain gauge data

The strain gauge results for Experiments 1 and 4 are shown in Figure 4-30. Gauges 1a and 1b showed an initial increase in tensile strain and we are not clear about the explanation for this behaviour. It seems to be too early to be due to expansion caused by a corrosion process. It is possible that the variation is caused by small local temperature fluctuations, particularly as all the strain gauges show small synchronised changes which are probably due to temperature fluctuations affecting the measuring equipment, as it is unlikely that there would be any significant temperature fluctuations inside the boreholes.

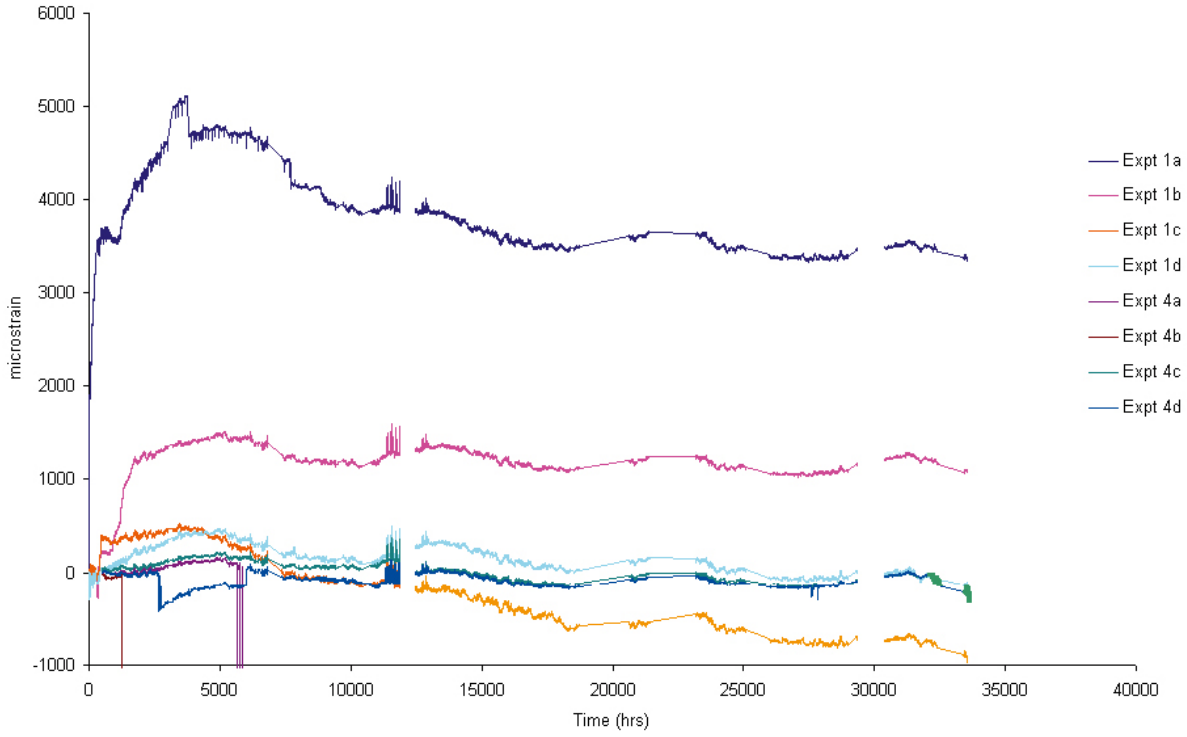

Figure 4-30. *Strain gauge results from Experiments 1 and 4.*

4.6 Evolution of electrochemical noise data

Electrochemical noise is a technique used to look for indications of localised corrosion; an example of the data acquired to date is shown in Figure 4-31 and Figure 4-32. These data were obtained by coupling two copper electrodes together and measuring the current and potential noise between them. If localised corrosion were occurring transients would be expected in the results. To date, there are no indications of localised corrosion occurring on the MiniCan corrosion coupons (e.g. sharp transients lasting 10 s of seconds), for either cast iron or copper. It is also possible to calculate the corrosion rate of the coupled electrodes by applying the software provided by ACM instruments Ltd. This software calculates the charge transfer resistance by dividing the root mean square of the potential noise by the root mean square of the current noise. These results will be checked by exporting the raw data to a spreadsheet and carrying out further analysis. The results of the corrosion rates derived from the electrochemical noise measurements are shown graphically in Figure 4-33. It can be seen that the measured corrosion rate values are significantly lower than those measured by the LPR and AC impedance techniques.

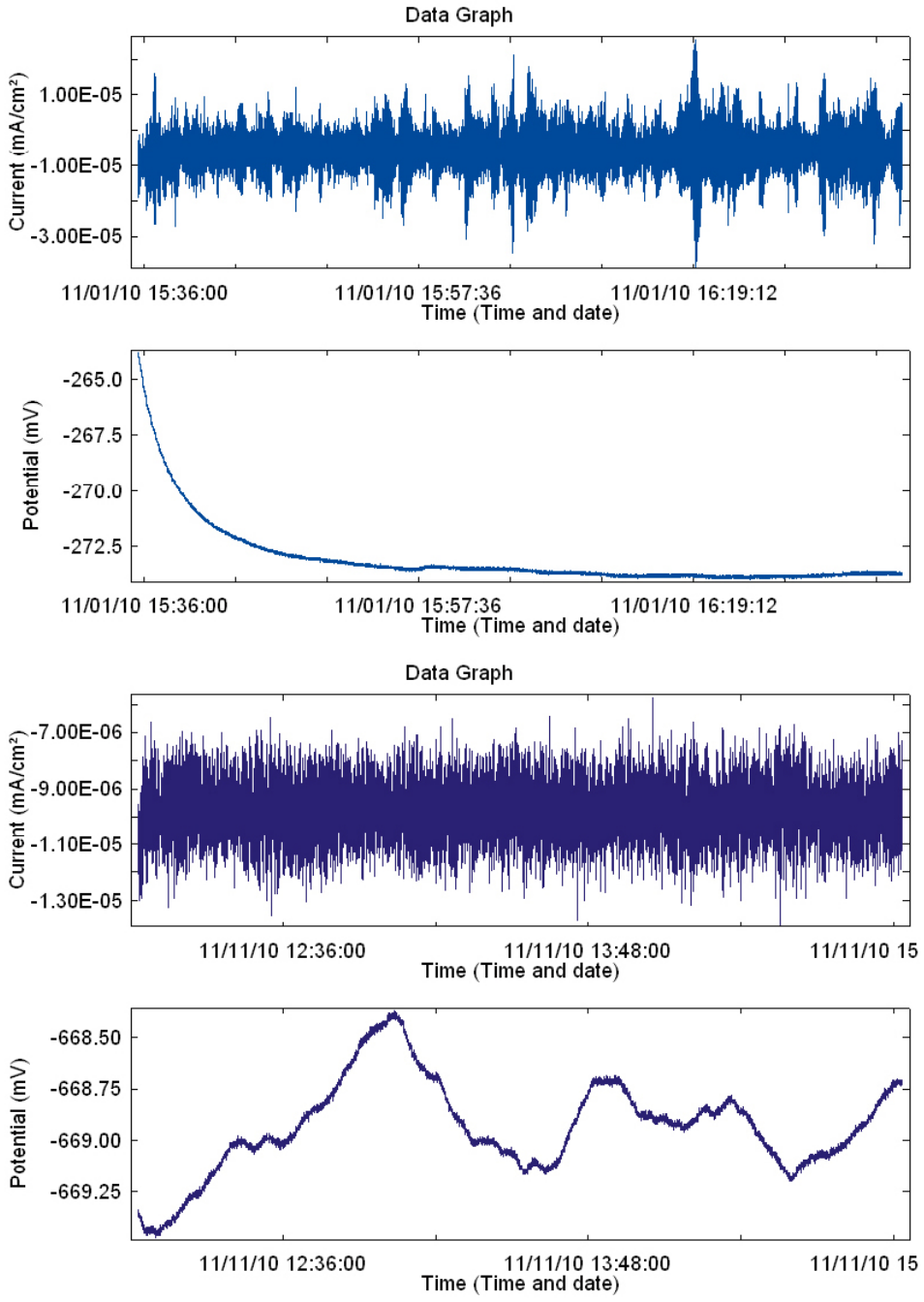

Figure 4-31. *Results from electrochemical noise measurements for cast iron electrode in Experiment 5 (no bentonite).*

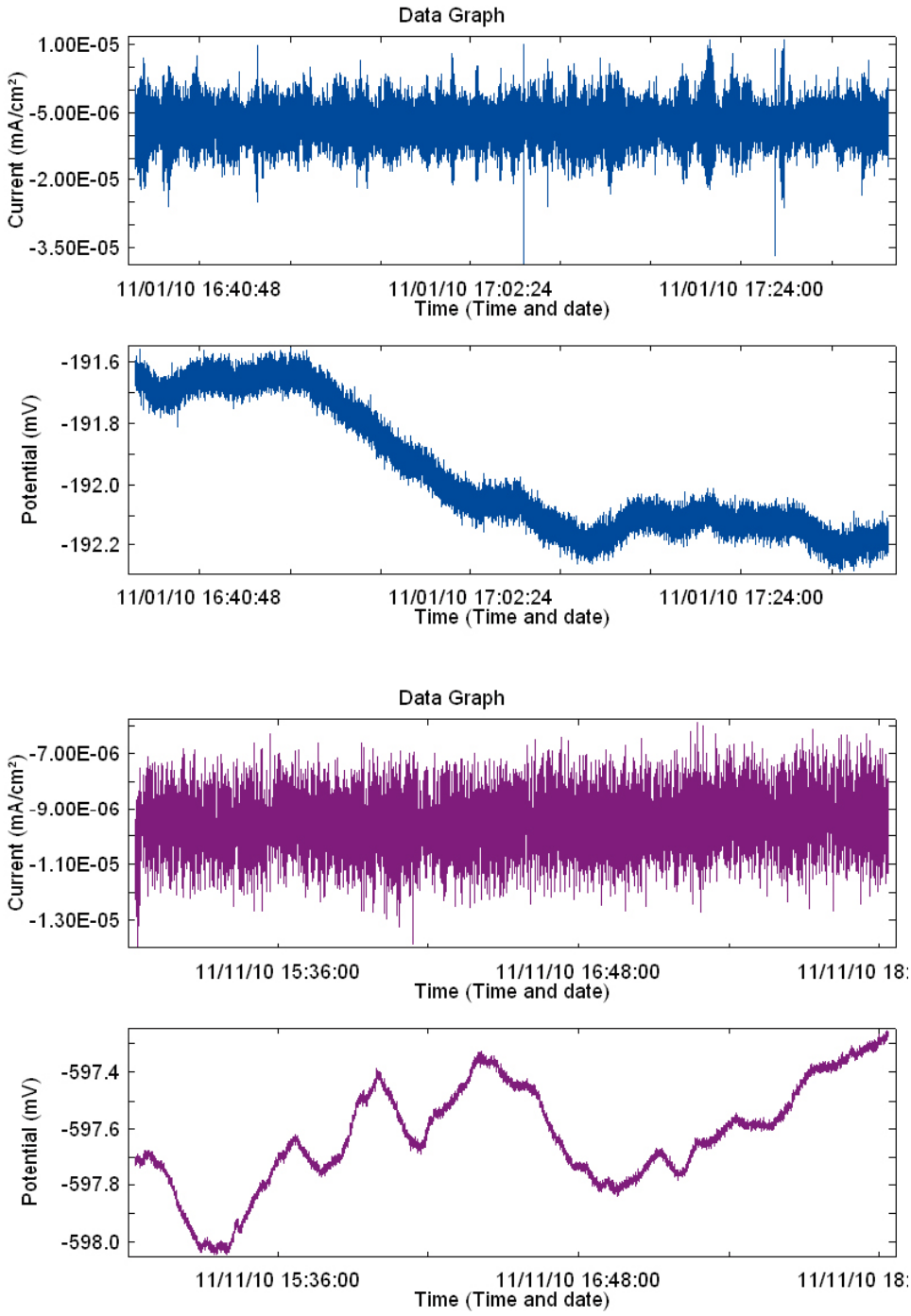

Figure 4-32. *Example of electrochemical noise data from for copper electrode in Experiment 5 (no bentonite).*

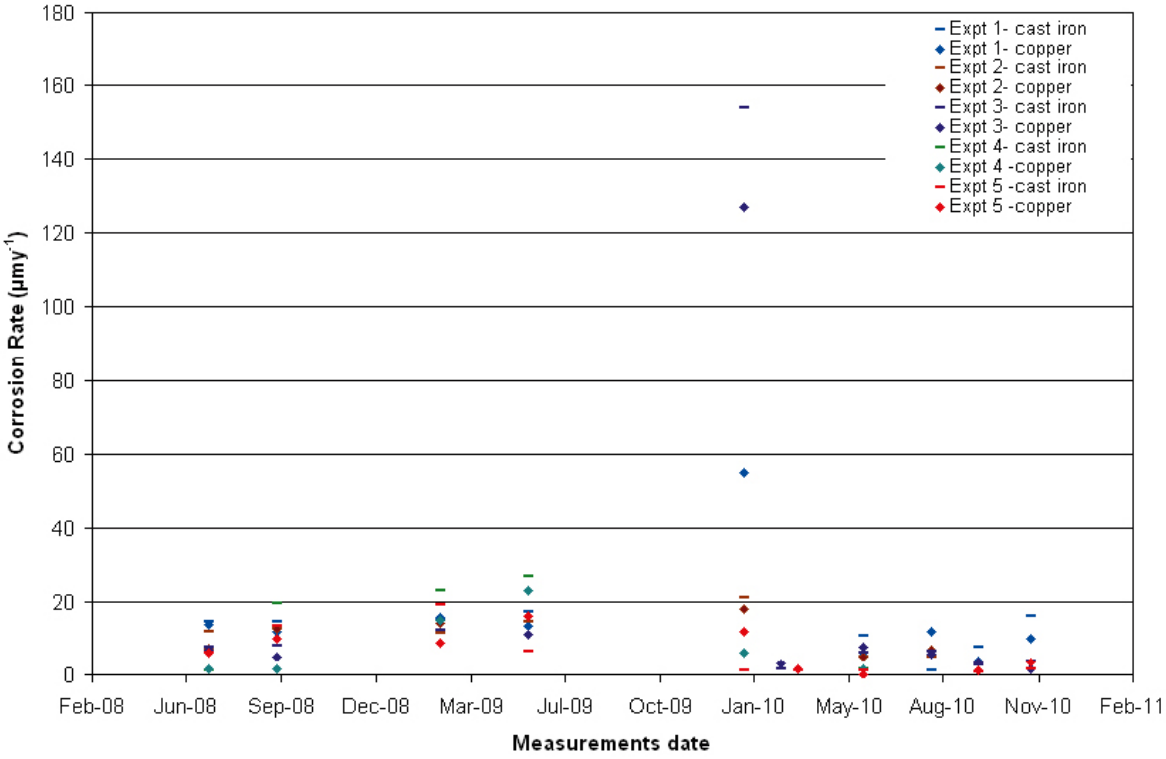

Figure 4-33. *Corrosion rates for copper and cast iron calculated from electrochemical noise data using ACM analysis software.*

4.7 Electrochemical cell

The electrochemical potential results obtained from the electrochemical cell with carbon steel, copper and gold electrodes mounted in compacted bentonite in the laboratory are shown in Figure 4-34 and the corresponding corrosion rate data for carbon steel and copper are given in Figure 4-35 and Figure 4-36 respectively. The initial high potentials in Figure 4-34 correspond to air ingress into the cell but when the air leaks were fixed the potentials of the copper and gold fell to values similar to those measured in the MiniCan experiments. The corrosion rate of carbon steel was measured as several tens of µm yr^{-1} and the corrosion rate is increasing. These values are higher than those measured by gas generation experiments but are consistent with previous electrochemical measurements in compacted bentonite [9]. The corrosion rate of copper appeared to pass through a peak before attaining a corrosion rate of ~3 µm yr^{-1}, which is a similar value measured for copper in compacted bentonite at the start of Experiment 4 (Figure 4-24). This peak in corrosion rate may correspond to the oxygen spike at the start of the experiment, but when the oxygen was consumed by corrosion of the carbon steel or copper wires the corrosion rate decreased again.

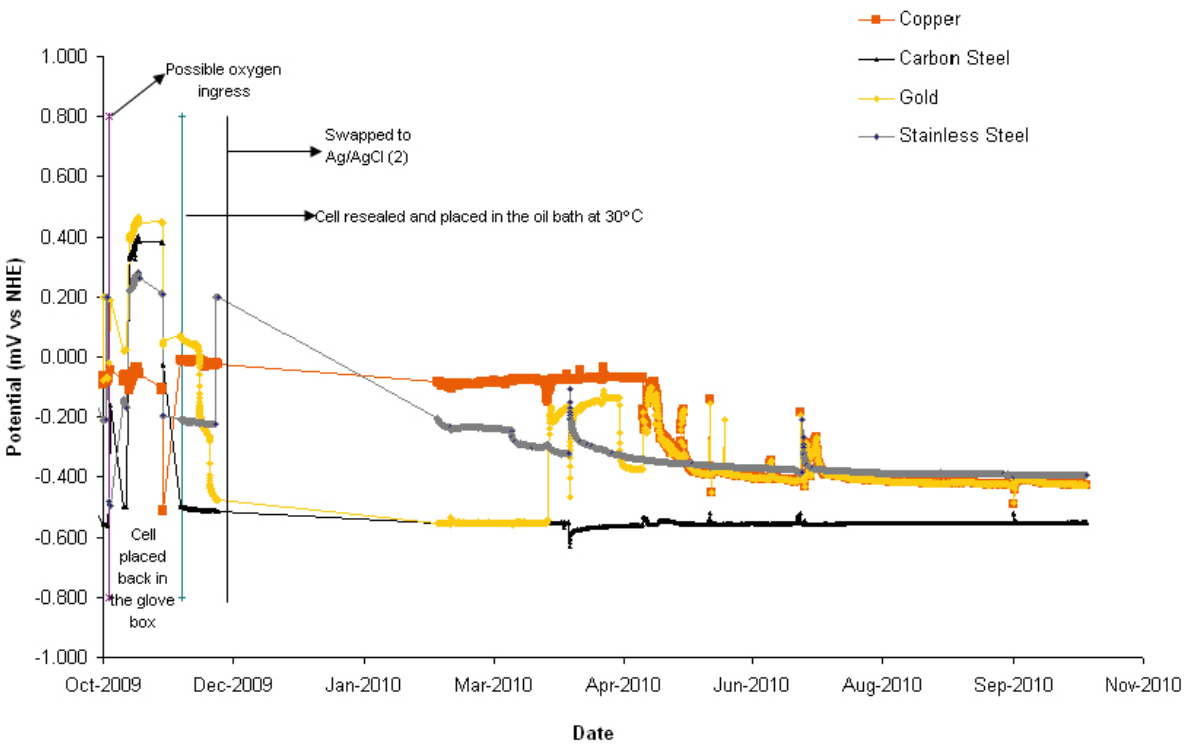

Figure 4-34. *Summary of corrosion potential data for carbon steel and copper electrodes in compacted bentonite (Cell BE2).*

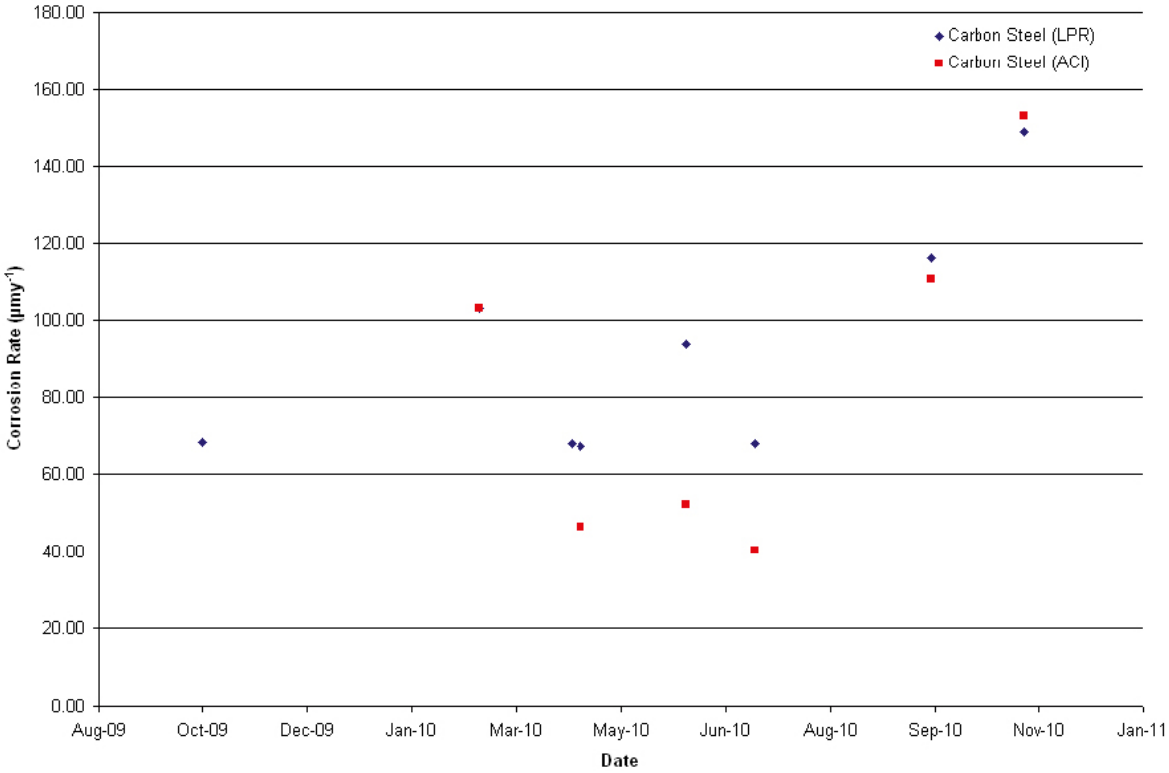

Figure 4-35. *Summary of carbon steel corrosion rates obtained by AC impedance and LPR measurements in compacted bentonite (Cell BE2).*

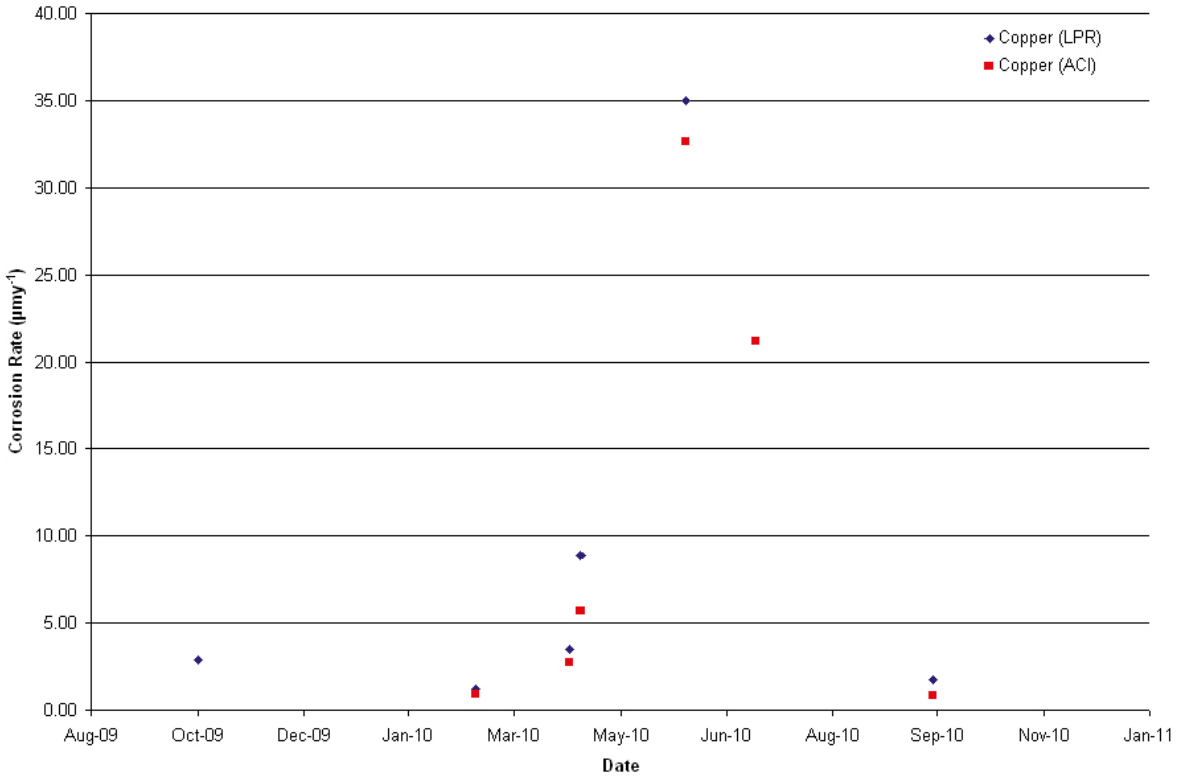

Figure 4-36. *Summary of copper corrosion rates obtained by AC impedance and LPR measurements for copper electrode in compacted bentonite (Cell BE2).*

5 Discussion

5.1 Water analysis and microbial activity

There are a number of interesting features regarding the results of the water analysis from the model canister experiments. In general, the groundwater composition outside the support cages does not vary significantly between boreholes. Firstly, there is a marked increase in the iron concentration inside the model canister support cage compared to the surrounding water in the borehole. This is accompanied by an increase in the concentration of nickel and chromium. This increase in dissolved metal concentration could be due to corrosion of the stainless steel support vessel, the cast iron coupons, and/or the cast iron insert itself, which will be in contact with groundwater as a result of the defect in the outer copper canister. The concentration of chromium and nickel is much lower than the concentration of iron, suggesting that most of the iron results from corrosion of the cast iron, rather than stainless steel, unless there is some kind of selective dissolution of the stainless steel occurring. In addition, the solubilities of chromium and nickel oxides are significantly lower than that of iron (II) oxides at the pH values measured inside the support cages (see Figure 4-8) [12].

Table 4-1 shows that there has been a decrease in the pH inside the support cage compared to outside the support cage. This could be a result of the microbial activity inside the support cage, as shown in Table 4-5, or it could be due to hydrolysis reactions involving dissolved metal ions. The gas analysis data (Table 4-3) show the very low oxygen content of the groundwater and the presence of helium and methane from geological sources.

The enhanced corrosion of the iron and/or stainless steel, as shown by the high concentrations of dissolved metals, would not be expected in anoxic near-neutral water at low temperature, even with the high concentrations of chloride present, based on the results of laboratory experiments in the absence of microbial activity. This result suggests that the corrosion is enhanced by microbial activity. This may also account for the high corrosion rates for iron and copper measured electrochemically. It should be noted that the concentration of dissolved copper was very low.

The microbial analysis indicates that autotrophic acetogens and sulphate reducing bacteria (SRBs) are active in the vicinity of the model canisters. The key metabolic reactions for these species are:

Autotrophic acetogens: $4H_2 + 2CO_2 \Rightarrow CH_3COO– + H^+ + 2H_2O$

Sulphate reducing bacteria: $CH_3COOH + SO_4^{2–} \Rightarrow H_2S$ and $Fe^{2+} + H_2S \Rightarrow FeS + 2H^+$

The acetogens produce acetate, which can cause stress corrosion cracking (SCC) of copper and sulphur from SRB activity is detrimental to copper. In principle, hydrogen produced by the anaerobic corrosion of iron could drive the activity of the acetogens and hence there is a possibility of autocatalytic behaviour (see Appendix 1 of reference [5] for further discussion). The processes summarised above are consistent with the measured fall in pH and the increase in corrosion rate and release of iron observed during these experiments.

5.2 Electrochemical measurements

5.2.1 E_h measurements

The potential values for the gold and platinum inside the support cages, and the E_h probe outside the support cages in the borehole, show that after sealing the boreholes the E_h fell from initial values of the order of 0 mV vs NHE, which correspond to aerated conditions in the groundwater, to values of the order of –300 mV, as any residual oxygen was consumed by reaction with rock minerals, microbial activity and/or corrosion processes. It is notable that the E_h values inside the support cages (e.g. Experiment 3 in Figure 4-14) fell more rapidly than outside the support cage, suggesting that residual oxygen was consumed more rapidly due to the increased surface area on which corrosion reactions could take place.

The long-term electrochemical potentials of the gold, platinum and the miniature canisters are indicative of very low oxygen concentrations. The electrochemical potential values obtained for the gold in the MiniCan experiments are comparable to the electrochemical potential values obtained

during laboratory investigations of galvanic corrosion of iron-copper couples in anoxic conditions [8,13], and the anaerobic corrosion of iron [14,15]. They are also comparable to E_h values reported in the literature for deep Swedish groundwaters [16,17]. The data show that for Experiments 1 to 3, with low density bentonite, the long-term E_h outside the cage is slightly higher than inside the cage, whereas for Experiment 4, with compacted bentonite the situation is reversed.

It should be noted that the increase in corrosion rate for both copper and iron (for example see Figure 4-12 and Figure 4-13 for Experiment 3), began when the E_h had reached its minimum value. Since SRBs are organisms that only proliferate under anoxic conditions it is possible that the increase in corrosion rate corresponded to the time when SRBs became active and started to generate sulphide, which then caused an increase in the corrosion rate of both the copper and the iron electrodes.

5.2.2 Corrosion potential of copper and iron

The corrosion potential of the copper and the model canisters can be compared with other measurements and modelling activities [16]; for example the predicted long-term corrosion potential of a copper canister in aerated compacted bentonite reported previously [16]. The modelling calculations showed that the predicted short-term corrosion potential for a copper canister is of the order of -300 mV vs SCE (i.e. ~–50 mV vs NHE). This is more positive by approximately 100 mV than the value measured in Experiment 4 for the model canister embedded in compact bentonite under anoxic conditions (Figure 4-16). However, it should be noted that the corrosion potential of copper is a strong function of chloride concentration, oxygen concentration and mass-transport conditions [16] and direct comparisons with the results from the MiniCan experiment are not therefore possible because the environmental conditions considered in the modelling were not necessarily the same as those in the MiniCan experiment. The rest potential of the canister became more negative towards the end of 2009. The potential of the copper electrode in the same experiment was similar to that of the copper canister (Figure 4-17).

The long-term corrosion potentials of the copper electrodes in Experiments 1–3 (low density bentonite) generally fell in the range –400 to –500 mV vs NHE, the corrosion potential for copper in Experiment 4 (compact bentonite) was ~–300 mV vs NHE and the potential for Experiment 5 (no bentonite) was approximately –500 mV vs NHE. The corrosion potentials of the model canisters themselves in Experiments 1–5 were generally approximately 100 mV more positive than the potentials of the copper electrodes, but it should be noted that the potential of the copper canisters represents a mixed potential of the copper-cast iron couple, assuming that wetting of the cast iron insert had occurred by water penetration through the 1 mm defect in the copper shell. These corrosion potential values can be compared to published Pourbaix diagrams [18] for copper in pure water (Figure 5-1), in the presence of carbonate and high concentrations of chloride (Figure 5-2) and in the presence of sulphide (Figure 5-3). In pure water, copper is thermodynamically immune to corrosion at the temperature of the MiniCan experiment and the measured corrosion potentials (Figure 5-1). In high concentrations of chloride, the measured corrosion potentials for the MiniCan experiments also show that copper is immune to corrosion by the formation of copper chlorides (Figure 5-2). However, in the presence of sulphide, Figure 5-3 indicates that for Experiments 1–4 the potential of the copper is in the domain of stability of copper sulphide. This would account for the higher corrosion rates measured in these experiments. Experiment 5 exhibited a more negative copper corrosion potential which was nearer the region of thermodynamic stability of copper and this may account for the lower corrosion rate measured in this experiment. In addition the concentration of sulphide produced by SRB activity would probably have been lower in Experiment 5 because there was no low density bentonite to support the growth of SRBs. The Pourbaix diagrams in Figure 5-1 to Figure 5-3 should only be used as a guide for interpreting the MiniCan experiments, because they were calculated for a specific set of conditions (i.e. concentrations of dissolved species such as chloride, sulphur, carbonate and copper at 25°C) that were not exactly the same as those in the MiniCan experiment, which was at an ambient temperature of 15°C. The calculations of thermodynamic stability for copper could be extended to take account of the measured chemical conditions for inside the support cages of the MiniCan experiments.

The potentials of the iron electrodes are below the hydrogen evolution potential at pH 7 and are consistent with the occurrence of anaerobic corrosion, with the resulting formation of hydrogen. The measured corrosion potentials for the cast iron electrodes are also consistent with the domain of stability of iron sulphide (Figure 5-4) [19,20].

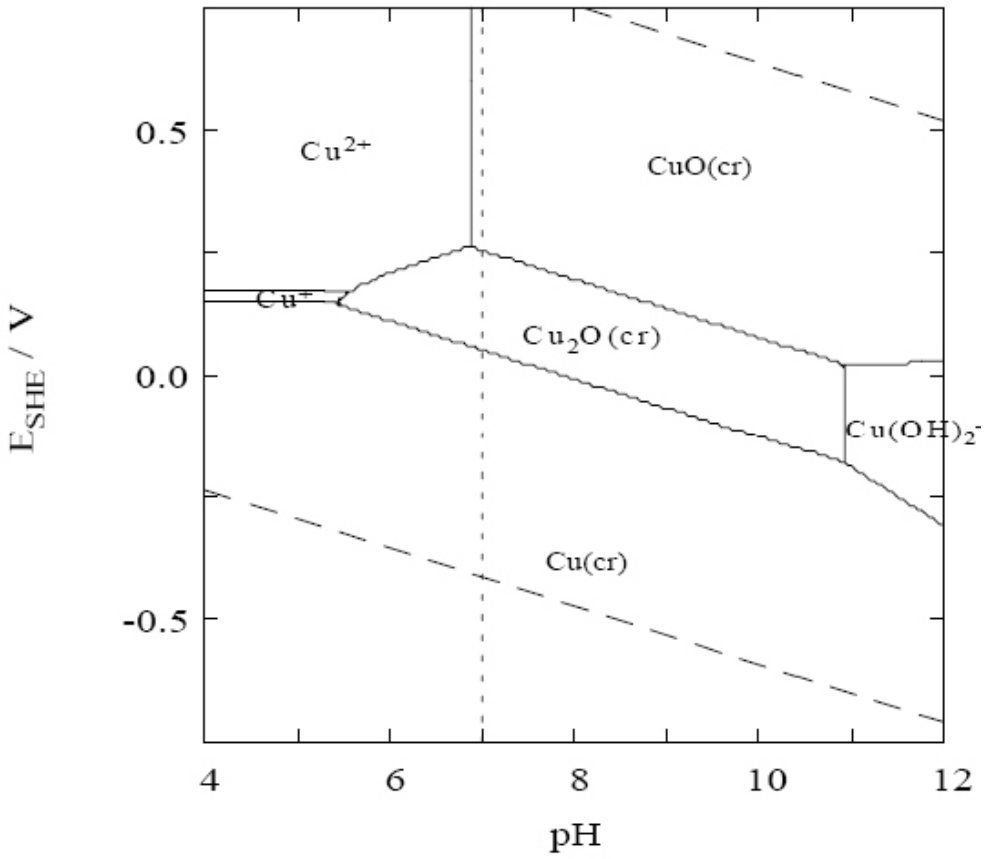

Figure 5-1. *Pourbaix diagram for copper in pure water $[Cu]_{TOT} = 10^{-6}$ mol/kg at 25°C [18].*

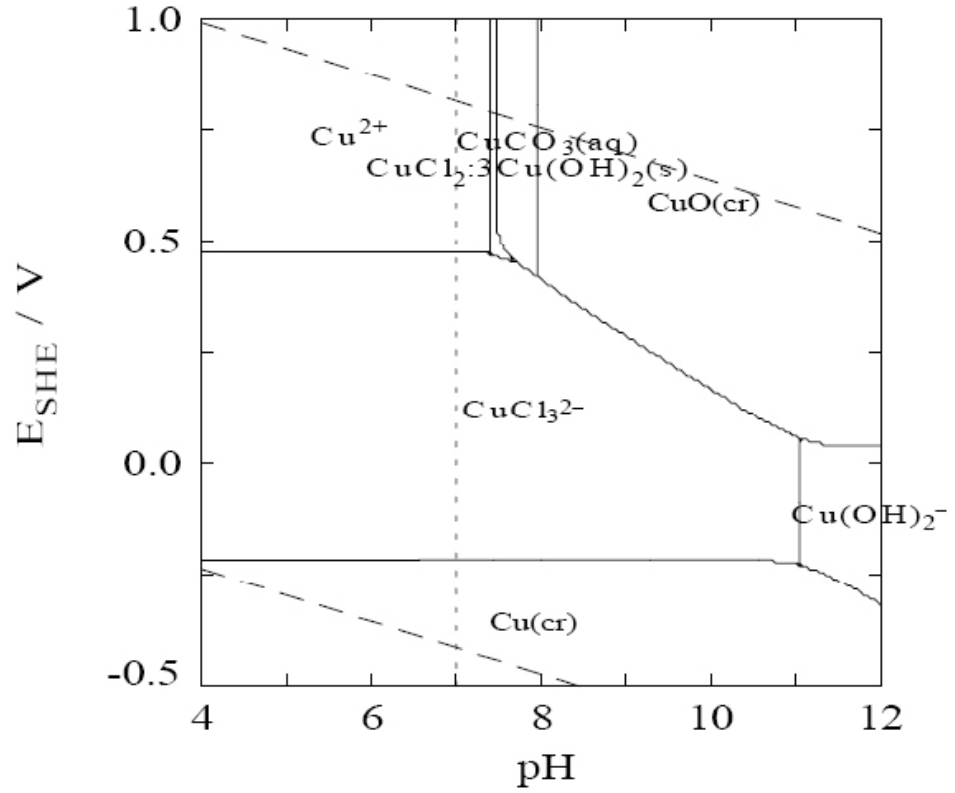

Figure 5-2. *Pourbaix diagram for copper at $[Cu]_{TOT} = 10^{-6}$ mol/kg at 25°C in solution containing $[CO_3^{2-}]_{TOT} = 2$ mmol/kg and $[Cl]_{TOT} = 1.7$ mol/kg [18].*

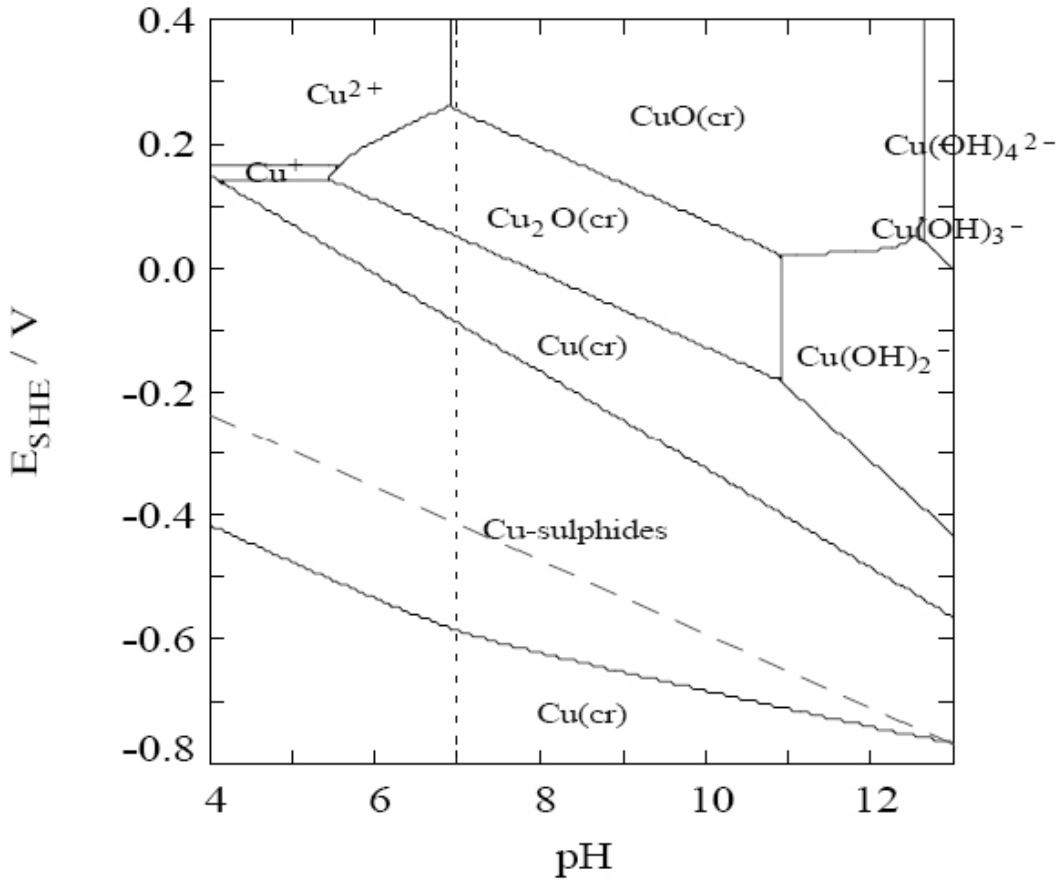

Figure 5-3. *Pourbaix diagram for copper in solutions containing $[HS^-]_{TOT}$ = 0.2 mmol/kg and $[Cu]_{TOT}$ = 10^{-6} mol/kg at 25°C [18].*

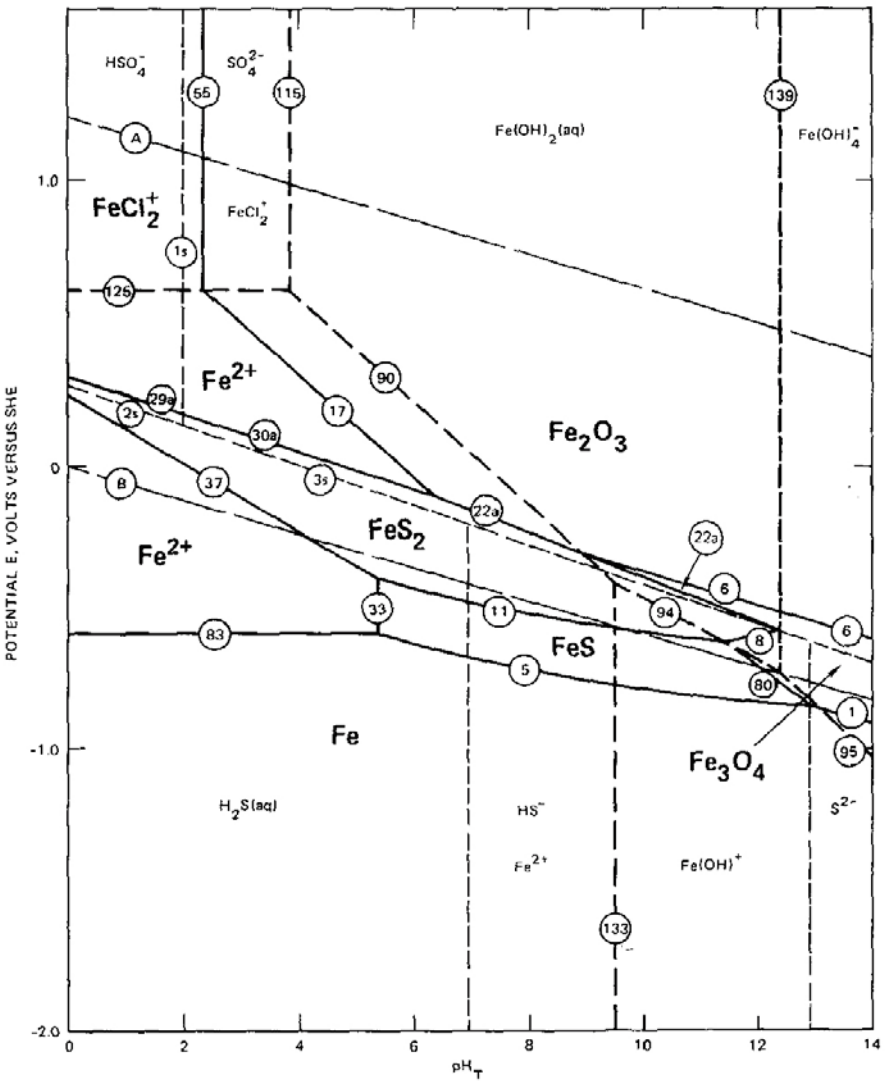

Figure 5-4. *Potential-pH diagram for iron in high salinity brine at 25°C in the presence of 10 ppm total dissolved sulphide (H_2S + HS^- + S^{2-}). Activities of HSO_4^- and SO_4^{2-} = 10^{-6} molal. Activities of dissolved iron species = 10^{-4} molal [19].*

5.3 Corrosion rate measurements

5.3.1 Iron corrosion rates

The corrosion rates for iron are high but in Experiments 1, 2, 3 and 5 they appear to have stabilised (Figure 4-25). They are considerably higher than would be expected from laboratory experiments on the anaerobic corrosion on iron [21,22]. They have to be treated with some caution as electrochemical measurements tend to overestimate the true values, since they only provide an instantaneous measure of corrosion rate, which is based on a number of assumptions about the nature of the electrochemical interface. The overall corrosion rates will be checked against weight loss measurements at the end of the experiments (i.e. a long-term integrated measurement of corrosion rate). There is also a possibility that crevice corrosion might be occurring if the environmental conditions are correct, although it is normally believed that crevice corrosion is not possible in anoxic conditions. The high rates reported here may support the observation of increased iron concentrations in the water analyses. It is possible that the high rates may be a result of microbial activity inside the support cage (see Section 4.1.2 and Appendix 1 of reference [5]).

Hilbert et al. [23] investigated the use of the LPR and ACI techniques to measure corrosion rates of steel in anoxic environments containing sulphide produced by SRB activity. Their conclusion was that under these conditions the formation of porous reactive sulphide films dominates the electrochemical response, leading to misleadingly high values of corrosion rate by a factor of 10–100 times. It is therefore possible, in fact probable, that the high corrosion rates measured for cast iron in the MiniCan experiment by LPR and ACI are an overestimate of the true corrosion rate. Nevertheless, even if a factor of ×100 is assumed, the cast iron corrosion rate would be of the order of 10s of μm yr^{-1} in Experiments 1–3 and 5. The cast iron corrosion rate for Experiment 4 (Figure 4-26) is not clear because of the probable difficulties with the connections and electrodes damaged by the swelling of the compacted bentonite. The extent of the overestimate will be evaluated when Experiment 3 is dismantled and it is possible to carry out a weight loss experiment. This investigation will also enable a more detailed analysis of the corrosion product film to be made so that its morphology and composition can be evaluated in more detail and this in turn will enable a better analysis of the electrochemical response to be conducted. The corrosion rates derived from the electrochemical noise experiments are considerably lower than the measurements from the LPR and ACI measurements, by a factor of ×100 for the cast iron and ×10 for the copper.

5.3.2 Copper corrosion rates

The electrochemical measurements of the initial corrosion rate gave values for copper below 5 μm yr^{-1} [3]. This is based on a Stern-Geary constant of 26 mV, whereas other authors (e.g. [24]) have used lower values. Thus the figures reported here are conservative values (i.e. they may exaggerate the corrosion rate). The derived corrosion rate values can be compared with values given in the literature for experiments on copper in compacted bentonite; for example values of up to 2.5 μm yr^{-1} have been reported by Rosborg et al. [24] for measurements during the LOT experiment and 4.7 μm yr^{-1} by Saario et al. [25] for weight loss measurements on copper in compacted bentonite in laboratory tests.

However more recent measurements (e.g. Figure 4-23) suggest that higher corrosion rates of copper may be occurring. The electrochemically measured corrosion rate for copper in Experiment 2 is much higher than that measured using the copper coil electrical resistance method (see Figure 4-23 and Figure 4-27), which suggests that there may be some experimental difficulties associated with the electrochemical corrosion rate measurements. Nevertheless this cannot be confirmed until one of the experiments is dismantled. The possible effect of enhanced microbial activity on the corrosion rates should be considered.

5.3.3 Application of corrosion rate results to SKB repository

It should be recognised that the environmental conditions within Experiments 1, 2, 3 and 5 are not fully representative of the conditions that will be experienced in a repository because the containers are in contact with low density bentonite (Experiments 1 to 3) or raw groundwater (Experiment 5), rather than fully compacted bentonite. In both these environments it is likely that microbial activity would be different to that expected in the fully compacted bentonite that would be used in the repository situation, since fully compacted bentonite is expected to inhibit microbial activity [26]. Experiment 4 therefore represents the closest analogy to the proposed SKB design since it uses fully compacted bentonite. Unfortunately, the corrosion rates measured electrochemically in Experiment 4 appear to be unreliable, probably because the swelling of the bentonite has led to deformation or damage to the electrical connections. It should also be noted that in the repository situation the temperatures would be higher than in the MiniCan experiments. This could have the effect of increasing the corrosion rate, if it is due to abiotic corrosion processes, or it may affect the viability of microbial populations and hence reduce the rate of any microbially influenced corrosion processes. Conversely, the rate of corrosion may be controlled by the supply of sulphide external to the compacted bentonite so that the corrosion rate will be controlled by the rate of transport of sulphide through the bentonite layer, as discussed by King et al. [16] and the rate of production of sulphide by sulphate reducing bacteria in the vicinity of the external surfaces of the bentonite buffer. Recent work [27] by Masurat et al. suggests that the rate of production of sulphide by microbial activity within compacted bentonite is very limited and that the amount of sulphide that can be produced by microbial activity is insufficient to sustain significant degrees of corrosion of the copper canister. This work also showed that

the rate of growth of SRBs is two orders of magnitude higher in lower density bentonite (1.5 g cm^{-3}) compared to that in compacted bentonite with a density of 2 g cm^{-3}. For comparison, the density of the bentonite used in Experiments 1 to 3 of the MiniCan project was 1.16 to 1.36 g cm^{-3}, whereas the density of the compacted bentonite in Experiment 4 was ~2 g cm^{-3}.

Experiments 1, 2 and 3 demonstrate that if the integrity of the compacted bentonite were to be compromised for any reason and the density of the bentonite decreased, for example due to erosion by glacial freshwater, then there is a high probability that the corrosion rate would be affected by the increased levels of microbial activity that are supported by low density bentonite. The extent of this increase in activity has not been fully determined yet from the MiniCan experiments, because there are some uncertainties about the measured corrosion rates. It is anticipated that these questions will be resolved when Experiment 3 is dismantled and examined later in 2011. Experiments 1 to 3 also raise the question, could microbial activity be increased on the outer surface layers of the bentonite surrounding the canisters, if there is a band of reduced bentonite density at the bentonite-geosphere interface? If this was the case there could be an acceleration in the rate of production of sulphide, which would diffuse towards the surface of the copper canister and could lead to enhanced corrosion rates.

The results from Experiment 5 (no bentonite) indicate that the corrosion rate of copper in raw groundwater is significantly lower than in the experiments with low density bentonite present and this is probably due to the lower concentration of sulphide present in a system with less organic material present in bentonite to support microbial activity and the lower corrosion potential, which may indicate that the copper is within its thermodynamic domain of stability in this experiment. The corrosion rate of the iron in Experiment 5 is similar to the values recorded in the presence of low density bentonite and significantly higher than those values measured in laboratory experiments under anoxic conditions, in the absence of sulphur. This suggests that even if the available sulphide concentration is lower than in Experiments 1 to 3 there is still sufficient sulphide present in Experiment 5 for iron sulphide production to occur. This could be as a result of SRB activity supported by the metabolism of hydrogen produced by the anaerobic corrosion of the cast iron components of the experiment [27].

6 Future work

The following suggestions are made for future activities on the MiniCan experiment:

- Carry out thermodynamic calculations to define Pourbaix diagrams for copper and iron in the environments measured for the interior of the support cages in the MiniCan experiments.
- Carry out hydrogen evolution measurements for copper in the environments determined for the interior of the support cages in the MiniCan experiments, to obtain instantaneous values for the corrosion rate of copper by an independent measuring technique. This could be done using the techniques used previously for characterising the anaerobic corrosion of iron in anoxic conditions [22]. It should be conducted in pure water, to establish whether hydrogen is generated by anaerobic corrosion of copper, as suggested by Hundquist et al. [28-32], and also in Äspö groundwater, with and without the presence of additional sulphide to simulate SRB activity.
- Continue with the electrochemical laboratory measurements in compacted bentonite, but add sulphide to the water surrounding the compacted bentonite to simulate the activity of SRBs on the surface of the bentonite buffer.
- Dismantle Experiment 3 and carry out a full detailed analysis of the extent of any corrosion or corrosion product films. A separate plan for this activity has been submitted to SKB [33].

7 Conclusions

The main conclusions from the project to date are as follows:

1. Water analysis has shown that there are compositional differences between the water inside the support cages compared to the external borehole water. These can be explained on the basis of enhanced corrosion of the iron and microbial activity inside the support cages.
2. Microbial analysis has demonstrated that SRBs are active in the experimental boreholes.
3. E_h measurements have shown that the test conditions within the support cages around the MiniCan experiments became reducing over a period of a few thousand hours at the start of the experiments.
4. The corrosion potentials of the copper and iron electrodes in the experiments with low density bentonite (Experiments 1 to 3) are consistent with the formation of copper sulphide and iron sulphide corrosion products.
5. The electrochemically measured corrosion rates have accelerated for both copper and iron. These data need to be confirmed by weight loss measurements, when the experiments are dismantled. It is possible that the corrosion rates measured for iron by LPR and ACI are overestimated due to the electrochemical properties of the sulphide films formed on the surface by SRB activity.
6. The corrosion rate of copper in compacted bentonite (Experiment 4) was initially of the order of 1 $\mu m\ yr^{-1}$ but it appears that later measurements are not valid, possibly because the swelling pressure exerted by the bentonite has disrupted the electrical connections.
7. High corrosion rates have been measured for copper in low density bentonite but it should be recognised that these test conditions are not directly comparable with the proposed repository conditions. It appears that the low density bentonite is conducive to microbial activity, particularly that of SRBs, and this has led to an increase in the measured corrosion rate. However, the corrosion rates measured by the electrical resistance method in low density bentonite and raw groundwater are considerably lower ($<1\ \mu m\ yr^{-1}$). In fully compacted bentonite microbial activity will be limited by the low activity of water and the corrosion rate is likely to be determined by the rate of diffusion of sulphide through the bentonite buffer.
8. It is necessary to remove Experiment 3 for analysis to confirm the corrosion rate measurements made remotely to date using electrochemical methods by comparison with direct weight loss measurements on corrosion coupons.

8 Acknowledgments

The authors gratefully acknowledge assistance provided by the following during the reporting period:

- SKB: Christina Lilja, Lars Werme, Richard Bäck, Mats Lundqvist, Teresita Morales, Stefan Grandin Svärdh, Siren Bortelid Moen, SKB chemistry laboratory staff at Äspö.
- Microbial Analytics: Karsten Pedersen and Sara Eriksson.

The authors also gratefully acknowledge financial support provided by SKB for conducting this project.

9 References

SKB's (Svensk Kärnbränslehantering AB) publications can be found at www.skb.se/publications.

1 **Smart N R, Rance A P, Fennell P A H, 2005.** Expansion due to anaerobic corrosion of iron. Report SA/EIG/15031/C001, Serco Assurance.

2 **Smart N R, Bäck R, Fennell P A H, Knowles G, Lundqvist M, Rance A P, Reddy B, Spencer D, Werme L O, 2007.** In situ corrosion testing of miniature copper-cast iron radioactive waste canisters. In: Corrosion 2007, Extended abstract, Research in progress Symposium, Nashville, March 2007.

3 **Smart N R, Rance A P, 2009.** Miniature canister corrosion experiment – results of operations to May 2008. SKB TR-09-20, Svensk Kärnbränslehantering AB.

4 **Smart N R, Rance A P, Reddy B, 2010.** Miniature canister (MiniCan) corrosion experiment progress report 1 for 2008–9. SERCO/TAS/E.003110.01/Issue 01, Serco Assurance.

5 **Smart N R, Rance A P, Reddy B, 2010.** Miniature canister (MiniCan) corrosion experiment progress report 2 for 2008–9. SERCO/TAS/E.003110.02/Issue 01, Serco Assurance.

6 **Bond A E, Hoch A R, Andrew R, Jones G D, Tomczyk A J, Wiggin R M, Worraker W J, 1997.** Assessment of a Spent Fuel Disposal Canister. Assessment Studies for a Copper Canister with Cast Steel Inner Component. SKB TR 97-19, Svensk Kärnbränslehantering AB.

7 **Saario T, 2004.** Effect of the degree of compaction of bentonite on the general corrosion rate of copper, presented at EuroCorr 2004, Nice, 12–16 August 2004. Published in a separate volume: Prediction of Long Term Corrosion Behaviour in Nuclear Waste Systems. Proceedings of 2nd International Workshop, Nice, September 2004, EuroCorr 2004, published by Andra in Science and Technology Series.

8 **Smart N R, Rance A P, Fennell P A H, 2004.** Galvanic corrosion of copper-cast iron couples. Report SA/EIG/13974/C001, Serco Assurance.

9 **Reddy B, Smart N R, Rance A P, 2009.** Continuation of NF-PRO experiments on iron-bentonite interactions, progress report 2009. SERCO/TAS/E.002918/01 Draft Issue 1, Serco Assurance.

10 **ASTM, 2003.** Standard test method for conducting potentiodynamic polarization resistance measurements. ASTM G59-97e1, ASTM International.

11 **Hallbeck L, Pedersen K, 2008.** Characterization of microbial processes in deep aquifers of the Fennoscandian Shield. Applied Geochemistry, 23, pp 1796–1819.

12 **Pourbaix M (ed), 1974.** Atlas of electrochemical equilibria in aqueous solutions. Houston, TX: NACE.

13 **Smart N R, Fennell P A H, Rance A P, Werme L O, 2004.** Galvanic corrosion of copper-cast iron couples in relation to the swedish radioactive waste canister concept. Published in a separate volume: Prediction of Long Term Corrosion Behaviour in Nuclear Waste Systems, Proceedings of the 2nd International Workshop, Nice, France, September 2004, EuroCorr 2004, published by Andra in Science and Technology Series.

14 **Peat R, Brabon S, Fennell P A H, Rance A P, Smart N R, 2001.** Investigation of Eh, pH and corrosion potential of steel in anoxic groundwater. SKB TR-01-01, Svensk Kärnbränslehantering AB.

15 **Smart N R, Fennell P A H, Peat R, Spahiu K, Werme L, 2001.** Electrochemical measurements during the anaerobic corrosion of steel. In: Hart K P, Lumpkin G R (eds). Scientific basis for nuclear waste management XXIV: symposium held in Sydney, Australia, 27–31 August 2000. Warrendale, PA: Materials Research Society. (Materials Research Society Symposium Proceedings 663), pp 487–495.

16 **King F, Ahonen L, Taxen C, Vuorinen U, Werme L, 2001.** Copper corrosion under expected conditions in a deep geological repository. SKB TR-01-23, Svensk Kärnbränslehantering AB.

17 **Puigdomenech I, Ambrosi J-P, Eisenlohr L, Lartigue J-E, Banwart S A, Bateman K, Milodowski A E, West J M, Griffault L, Gustafsson E, Hama K, Yoshida H, Kotelnikova S, Pedersen K, Michaud V, Trotignon L, Rivas Perez J, Tullborg E-L, 2001.** O_2 Depletion in granitic media. The REX project. SKB TR-01-05, Svensk Kärnbränslehantering AB.

18 **Puigdomenech I, Taxén C, 2000.** Thermodynamic data for copper. Implications for the corrosion of copper under repository conditions. SKB TR-00-13, Svensk Kärnbränslehantering AB.

19 **MacDonald D D, Syrett B C, 1979.** Potential-pH diagrams for iron and nickel in high salinity geothermal brine containing low concentrations of hydrogen sulphide. Corrosion, 35, pp 471–474.

20 **Smart N R, 2011.** The anaerobic corrosion of carbon steel and the potential influence of sulphur species, presented at the SACNUC workshop, Brussels, 2008. In: Kursten B, Féron D, Druyts F (eds). Sulphur-assisted corrosion in nuclear waste disposal systems (EFC 59). Leeds: Maney Publishing, Chapter 5.

21 **Smart N R, Blackwood D J, Werme L, 2002a.** Anaerobic Corrosion of carbon steel and cast iron in artificial groundwaters: Part 1–Electrochemical aspects. Corrosion, 58, pp 547–560.

22 **Smart N R, Blackwood D J, Werme L, 2002b.** Anaerobic corrosion of carbon steel and cast iron in artificial groundwaters: Part 2-Gas generation. Corrosion, 58, pp 627–637.

23 **Hilbert L R, Hemmingsen T, Nielsen L V, Richter S, 2005.** When can electrochemical techniques give reliable corrosion rates on carbon steel in sulfide media. Corrosion/05, NACE International, Houston, Texas, Paper 436.

24 **Rosborg B, Eden D, Karnland O, Pan J, Werme L, 2004.** Real-time monitoring of copper corrosion at the Äspö laboratory. Published in a separate volume: Prediction of Long Term Corrosion Behaviour in Nuclear Waste Systems. Proceedings of 2nd International Workshop, Nice, September 2004, EuroCorr 2004, published by Andra in Science and Technology Series.

25 **Saario T, Betova I, Heinonen J, Kinnunen P, Lilja C, 2004.** Effect of the degree of compaction of bentonite on the general corrosion rate of copper. Published in a separate volume: Prediction of Long Term Corrosion Behaviour in Nuclear Waste Systems. Proceedings of 2nd International Workshop, Nice, September 2004, EuroCorr 2004, published by Andra in Science and Technology Series.

26 **Motamedi M, Karnland O, Pedersen K, 1996.** Survival of sulfate reducing bacteria at different water activities in compacted bentonite. FEMS Microbiology Letters, 141, pp 83–87.

27 **Masurat P, Eriksson S, Pedersen K, 2010.** Microbial sulphide production in compacted Wyoming bentonite MX-80 under in situ conditions relevant to a repository for high-level radioactive waste. Applied Clay Science, 47, pp 58–64.

28 **Szakalos P, Hultqvist G, Wikmark G, 2007.** Corrosion of copper by water, Electrochemical and Solid State Letters 10(11), 2007.

29 **Hultqvist G, Szakalos P, Graham M J, Belonoshko A B, Sproule G I, Grasjo L, Dorogokupets P, Danilov B, AAstrup T, Wikmark G, Chuah G-K, Eriksson J-C, Rosengren A, 2009.** Water corrodes copper. Catalysis Letters, 132, pp 311–316.

30 **Apted M J, Bennett D G, Saario T, 2009.** A review of the evidence for copper corrosion by water. Stockholm: Strålsäkerhetsmyndigheten (Swedish Radiation Safety Authority). (SSM 2009:30).

31 **Hultquist G , Graham M J, Szakalos P, Sproule G I, Rosengren A, Gråsjö L, 2011.** Hydrogen gas production during corrosion of copper by water. Corrosion Science, 53, pp 310–319.

32 **Seo M, Hultquist G, Grasjo L, Sato N, 1987.** Hydrogen evolution kinetics in corrosion of copper, iron and zinc in water. In: Proceedings of the10th International Congress on Metallic Corrosion, Madras, India, November 1987.

33 **Smart N R, Rance A P, Reddy B, Winsley R J, 2010.** Plan for the proposed removal of MiniCan experiment 3 from borehole KA3386A04. SERCO/TCS/004427.02/001 Issue 1, Serco Assurance.

Appendix 1

Electrochemical corrosion rate measurements January to October 2010

Please note that all potentials shown in the electrochemical measurements are with respect to the reference electrode (i.e. Ag/AgCl), not NHE.

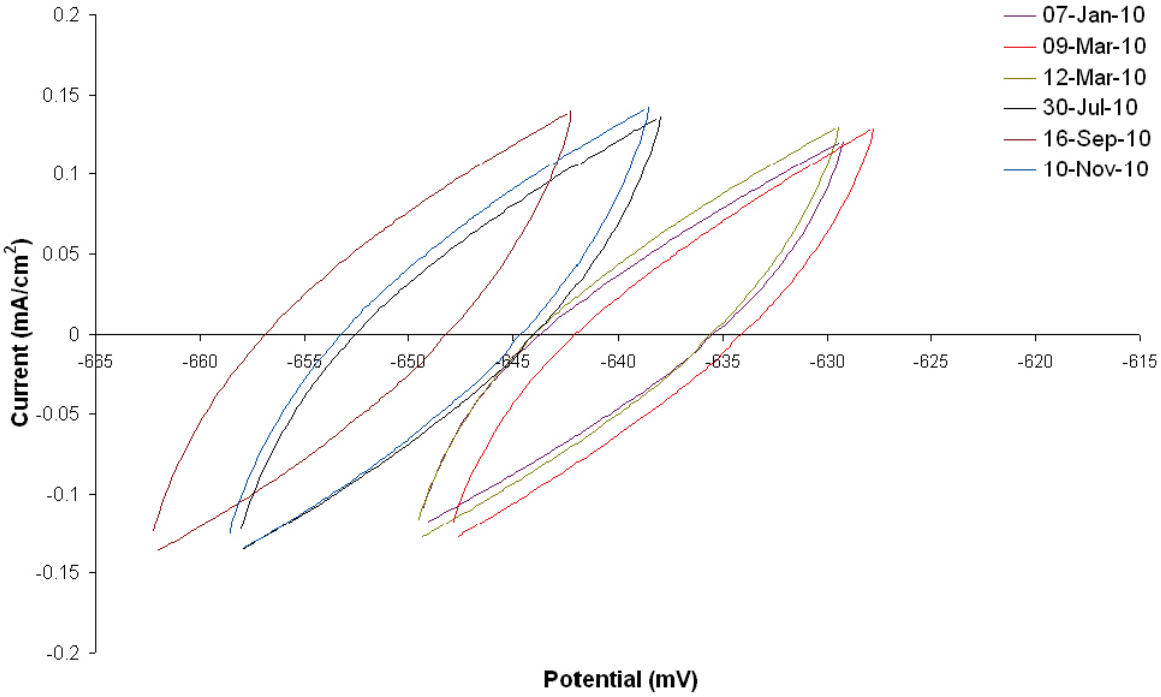

Figure A1-1. *LPR plots of cast iron in Experiment 1 (low density bentonite).*

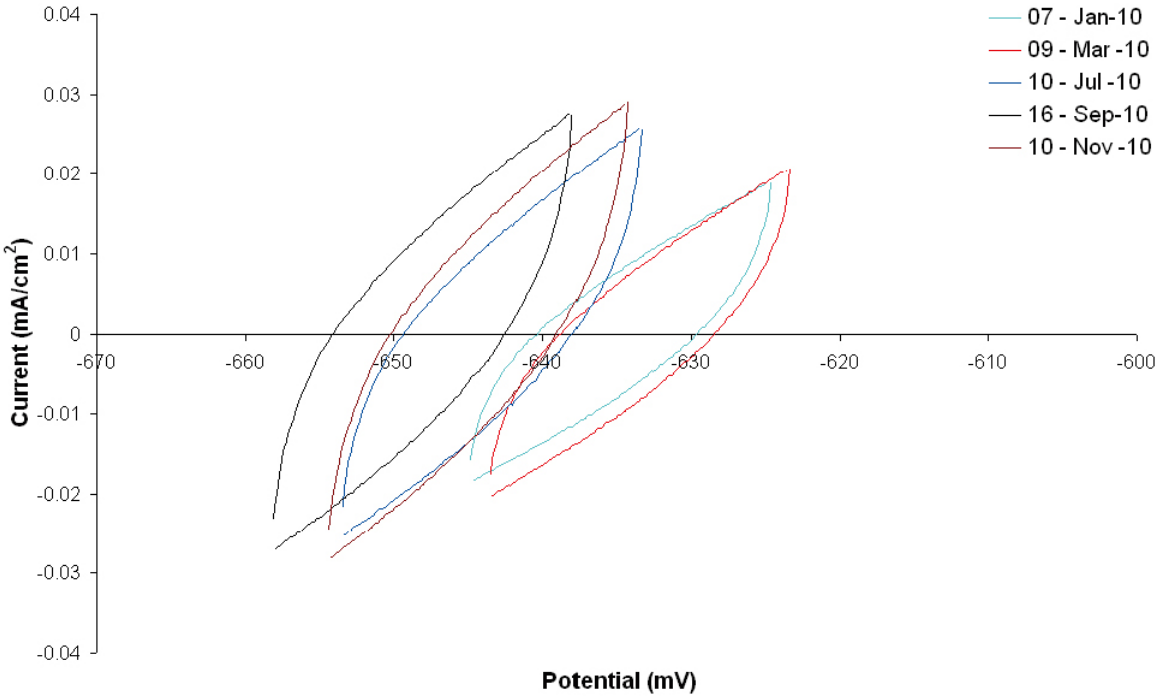

Figure A1-2. *LPR plots of copper in Experiment 1 (low density bentonite).*

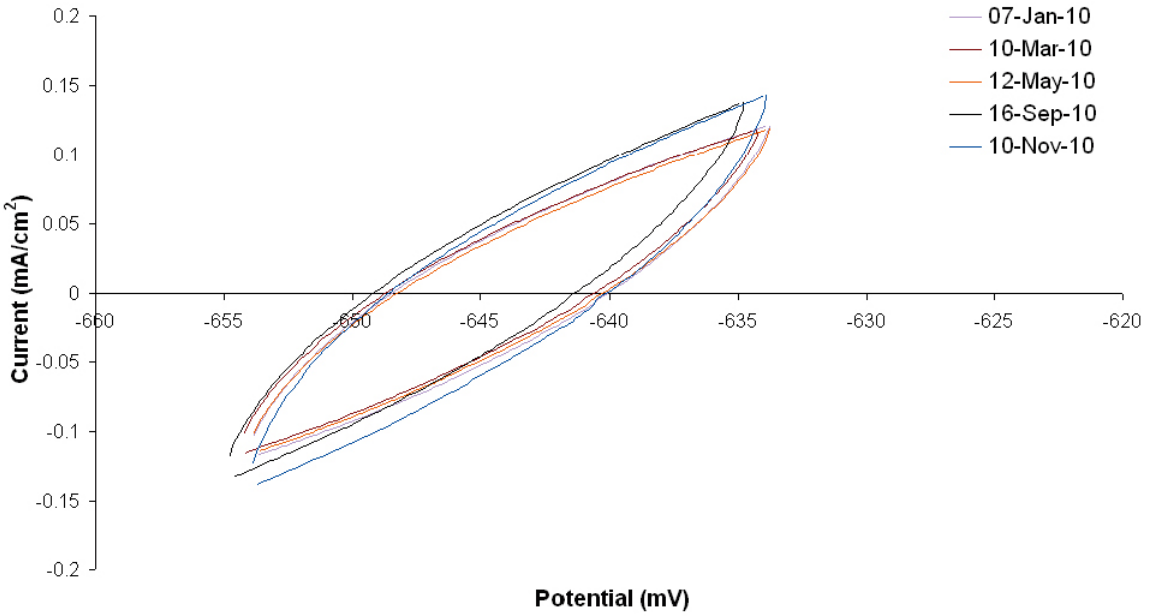

Figure A1-3. *LPR plots of cast iron in Experiment 2 (low density bentonite).*

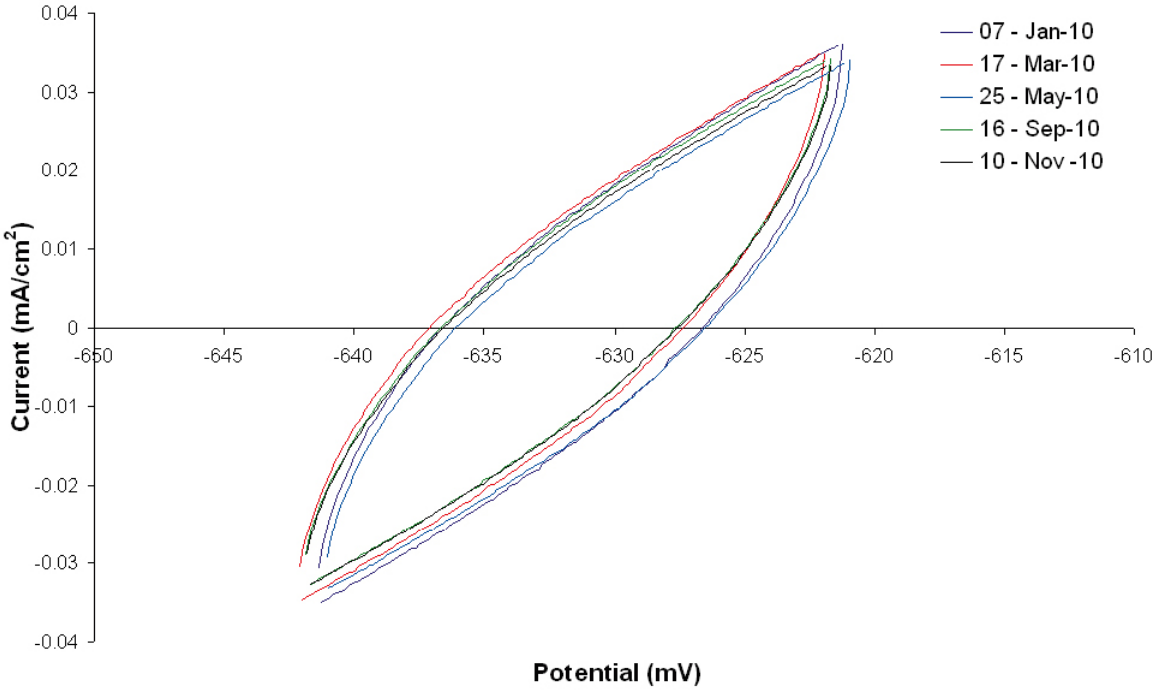

Figure A1-4. *LPR plots of copper in Experiment 2 (low density bentonite).*

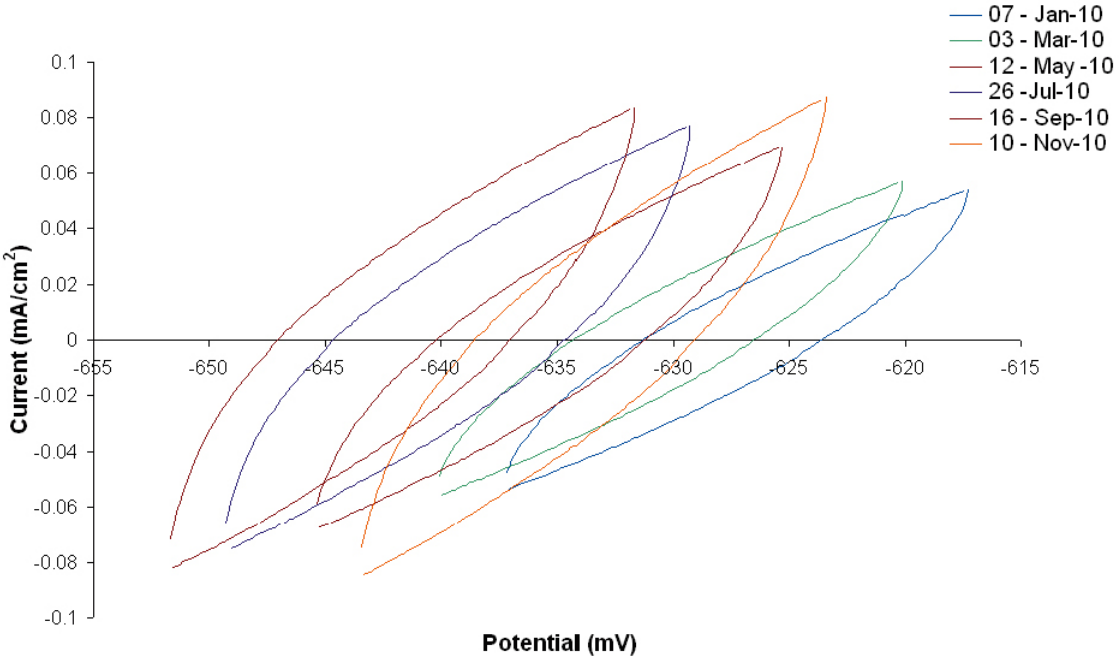

Figure A1-5. *LPR plots of cast iron in Experiment 3 (low density bentonite).*

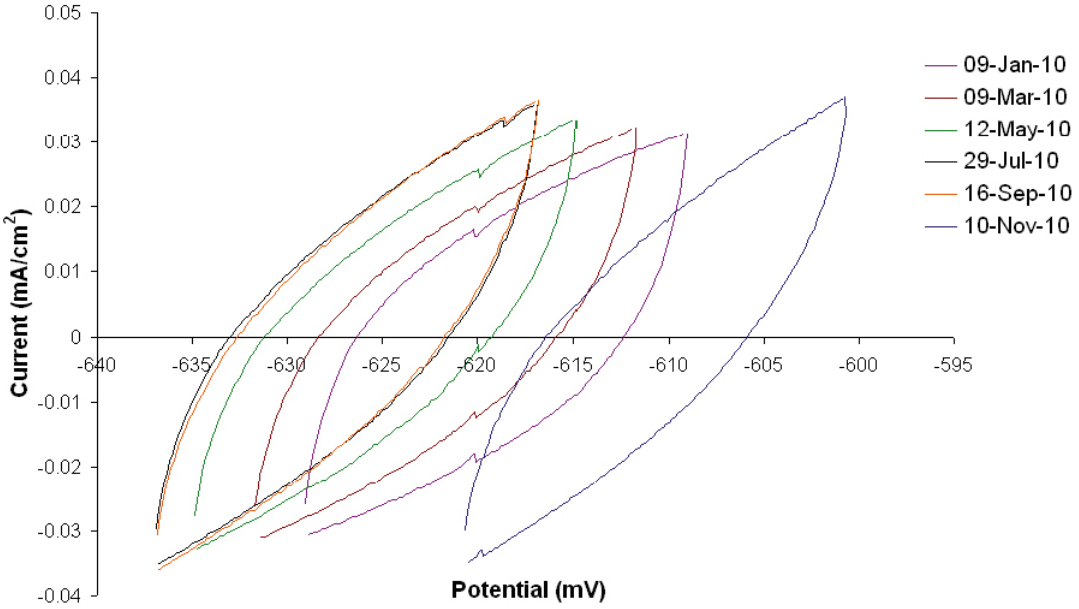

Figure A1-6. *LPR plots of copper in Experiment 3 (low density bentonite).*

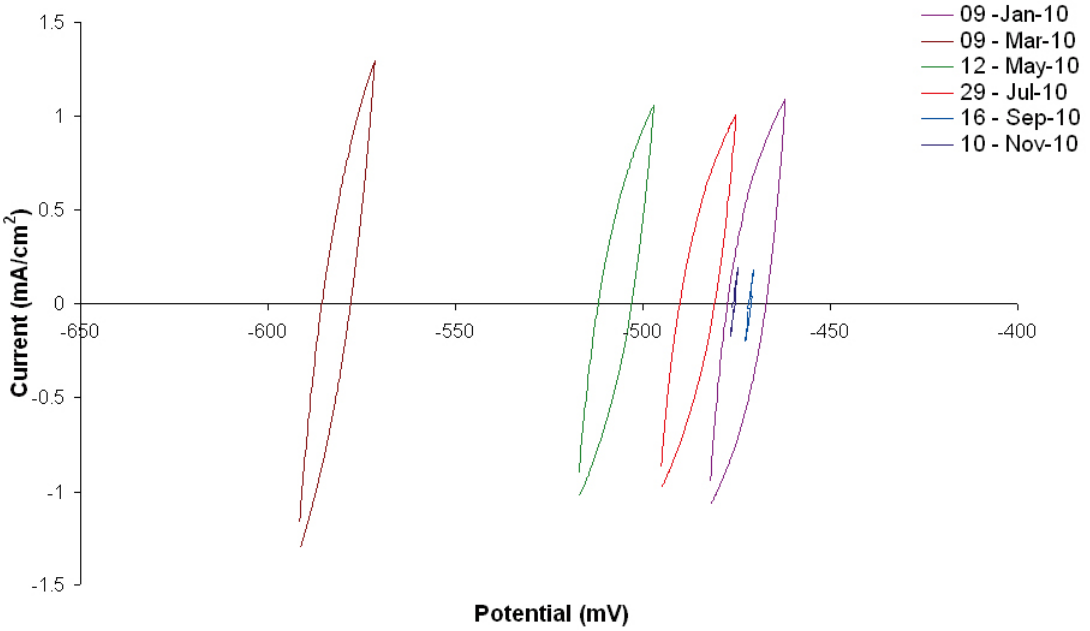

Figure A1-7. *LPR plots of iron in Experiment 4 (compacted bentonite) Note: It is likely that the iron electrode was in contact with the stainless steel flange of the support cage for these measurements).*

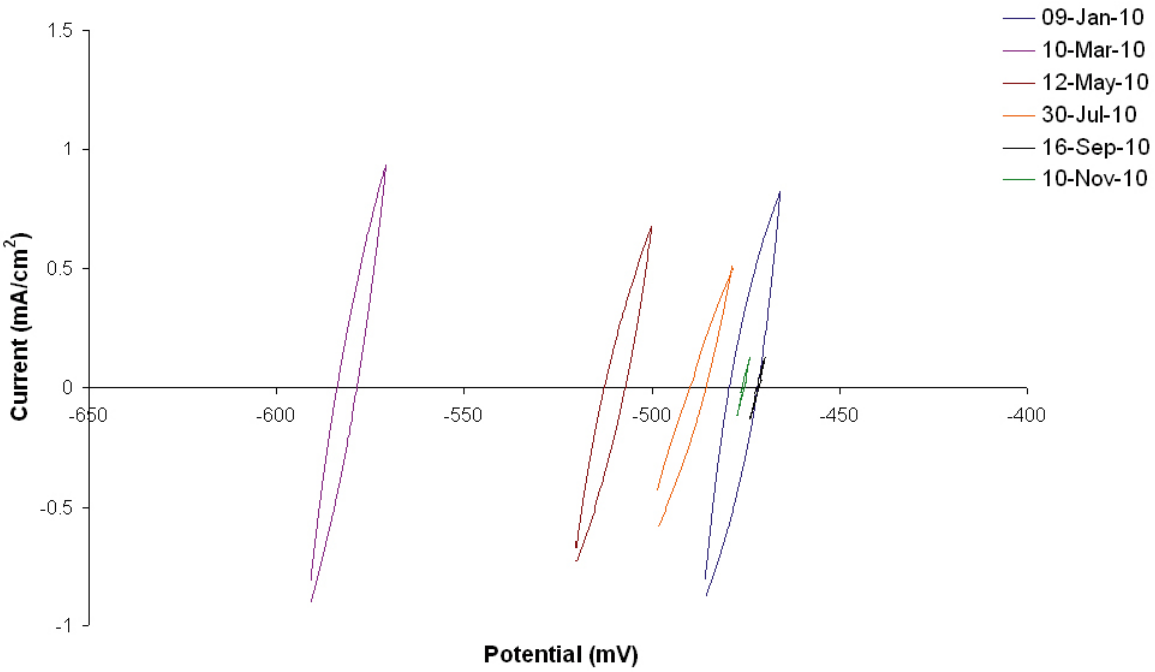

Figure A1-8. *LPR plots of copper in Experiment 4 (compacted bentonite).*

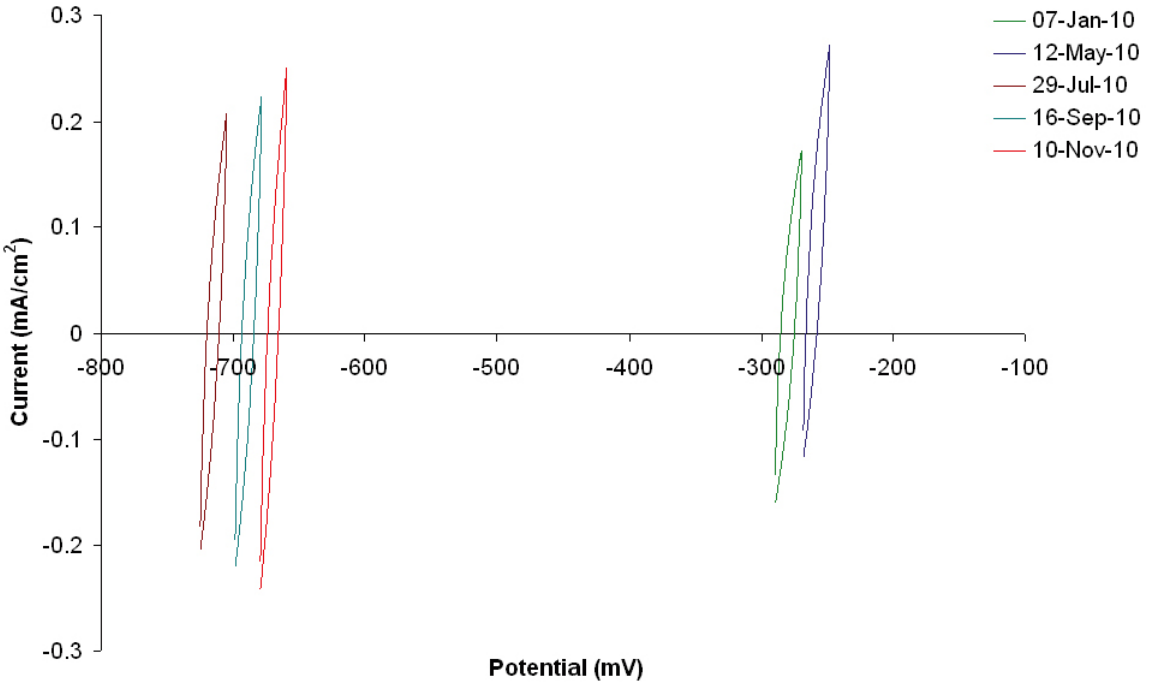

Figure A1-9. *LPR plots of cast iron in Experiment 5 (no bentonite).*

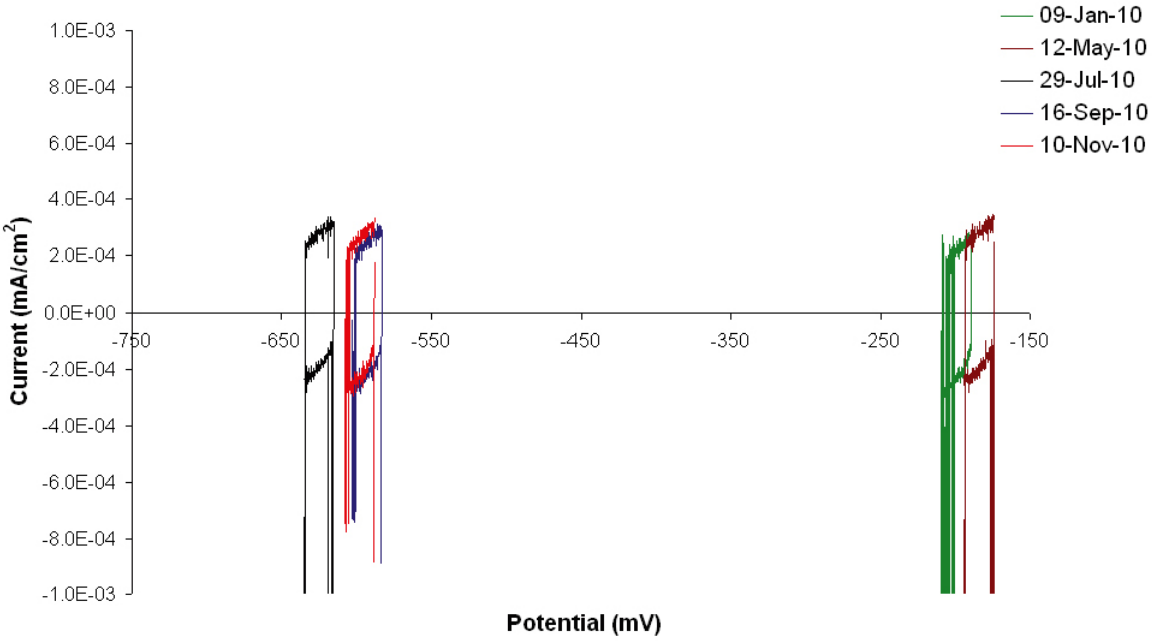

Figure A1-10. *LPR plots of copper in Experiment 5 (no bentonite).*

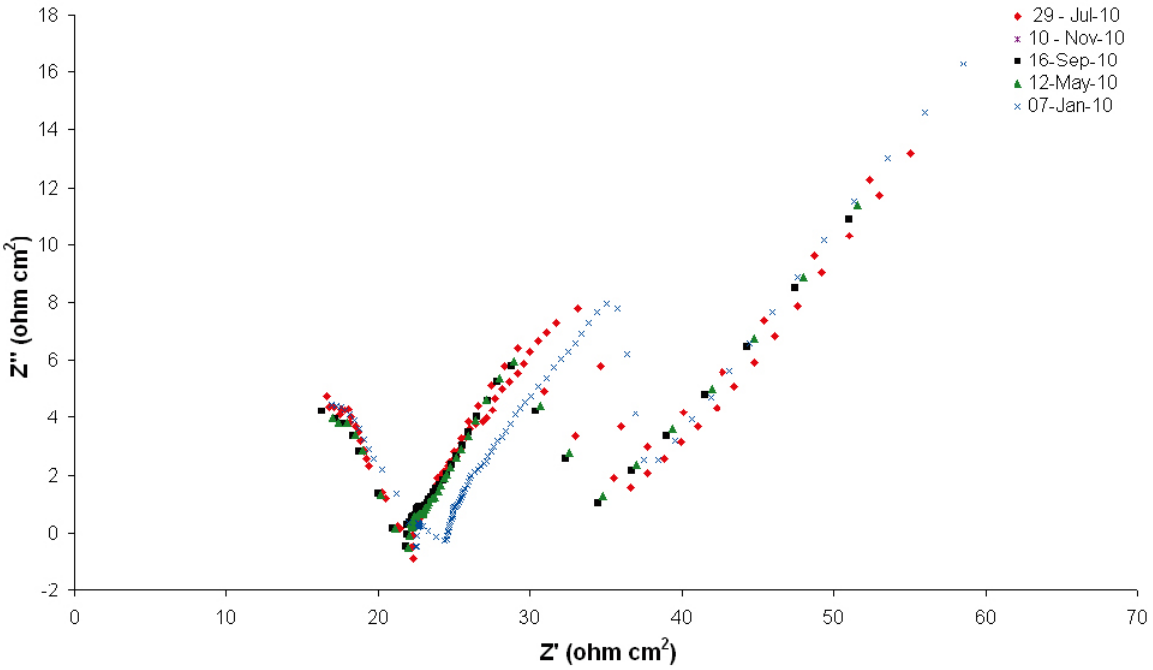

Figure A1-11. *ACI plots of cast iron in Experiment 1 (low density bentonite).*

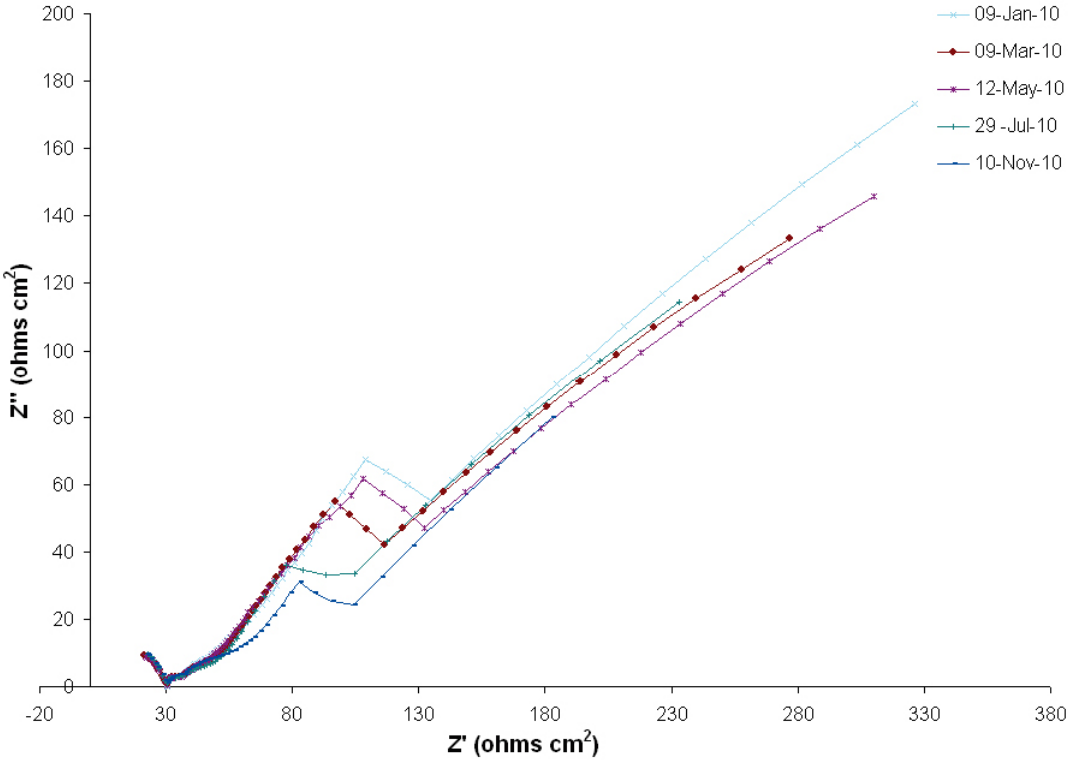

Figure A1-12. *ACI plots of copper in Experiment 1 (low density bentonite).*

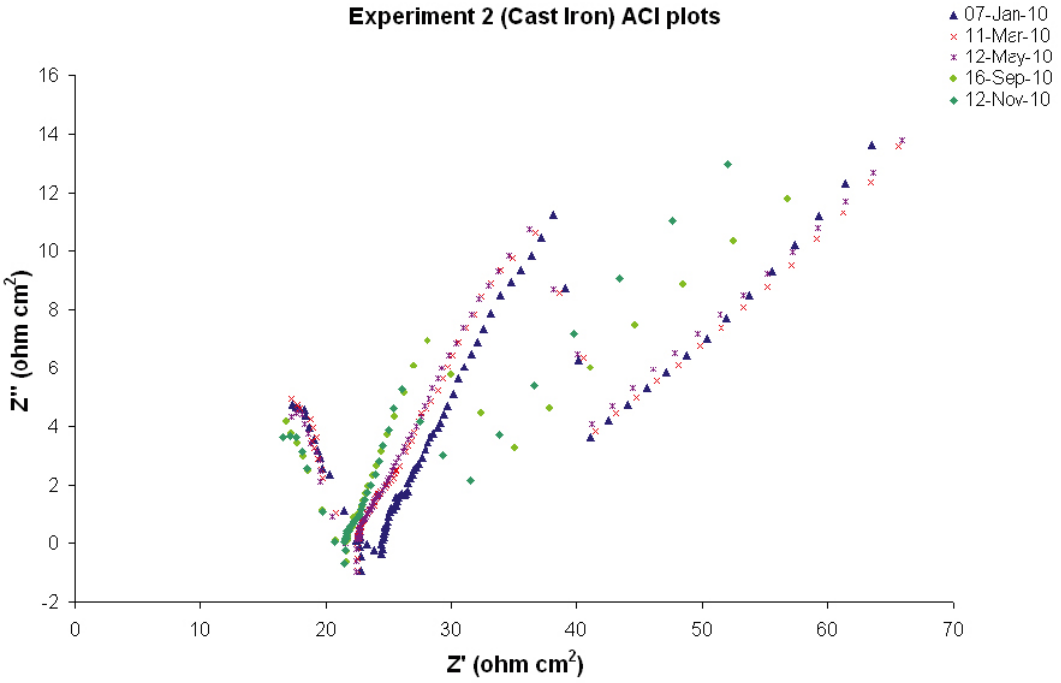

Figure A1-13. *ACI plots of cast iron in Experiment 2 (low density bentonite).*

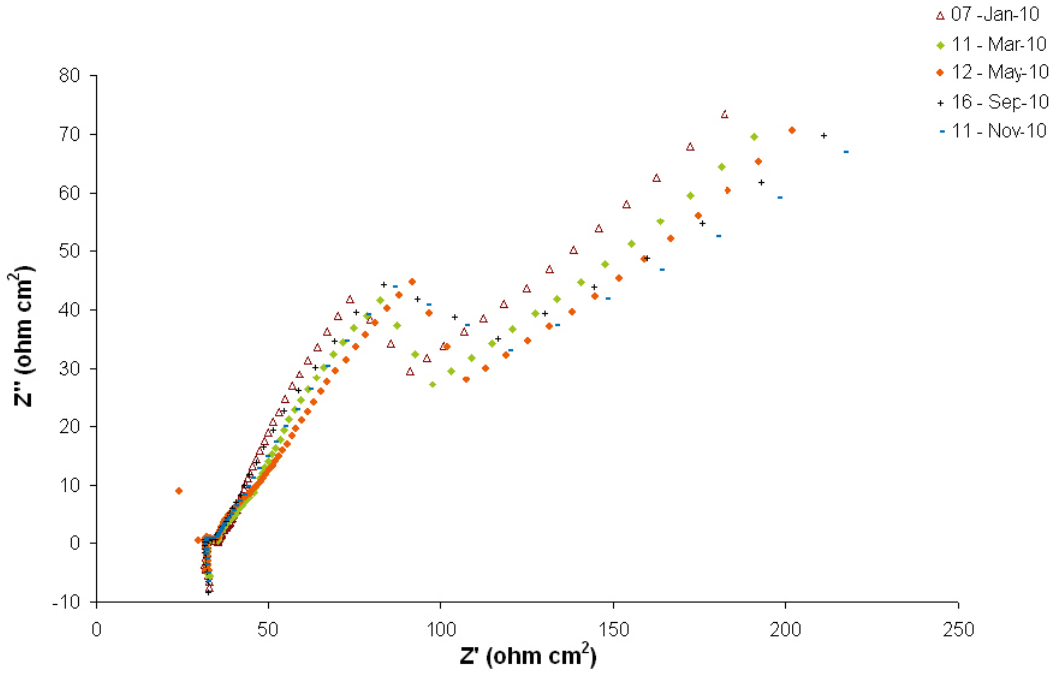

Figure A1-14. *ACI plots of copper in Experiment 2 (low density bentonite).*

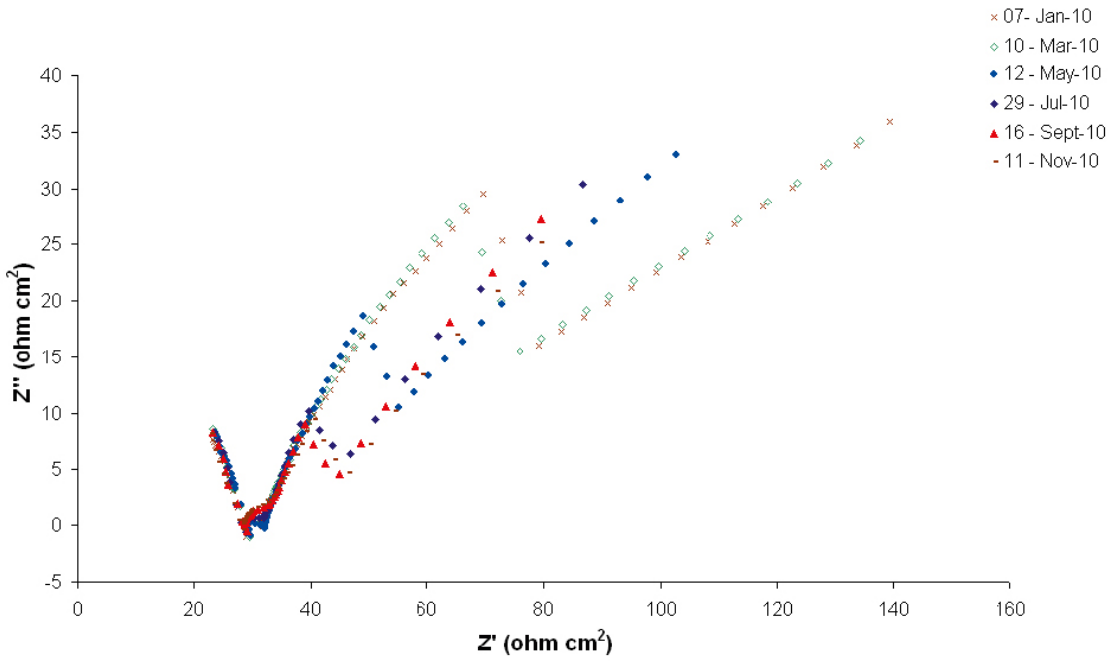

Figure A1-15. *ACI plots of cast iron in Experiment 3 (low density bentonite).*

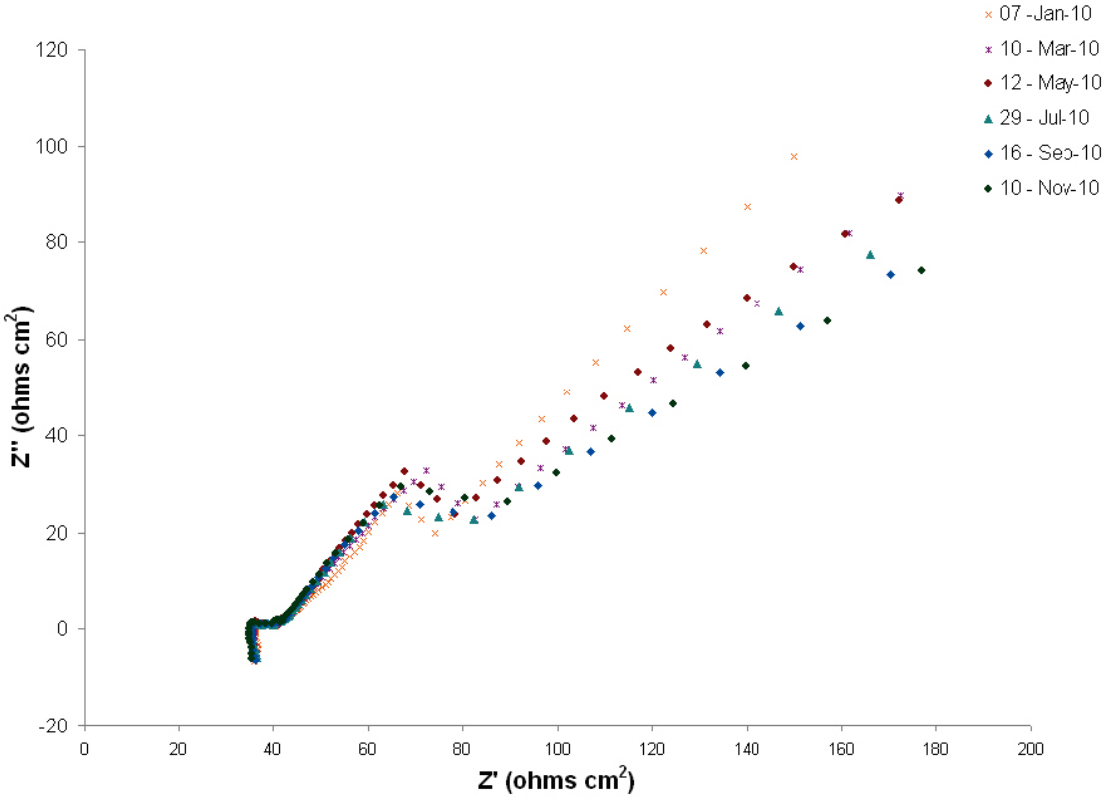

Figure A1-16. *ACI plots of copper in Experiment 3 (low density bentonite).*

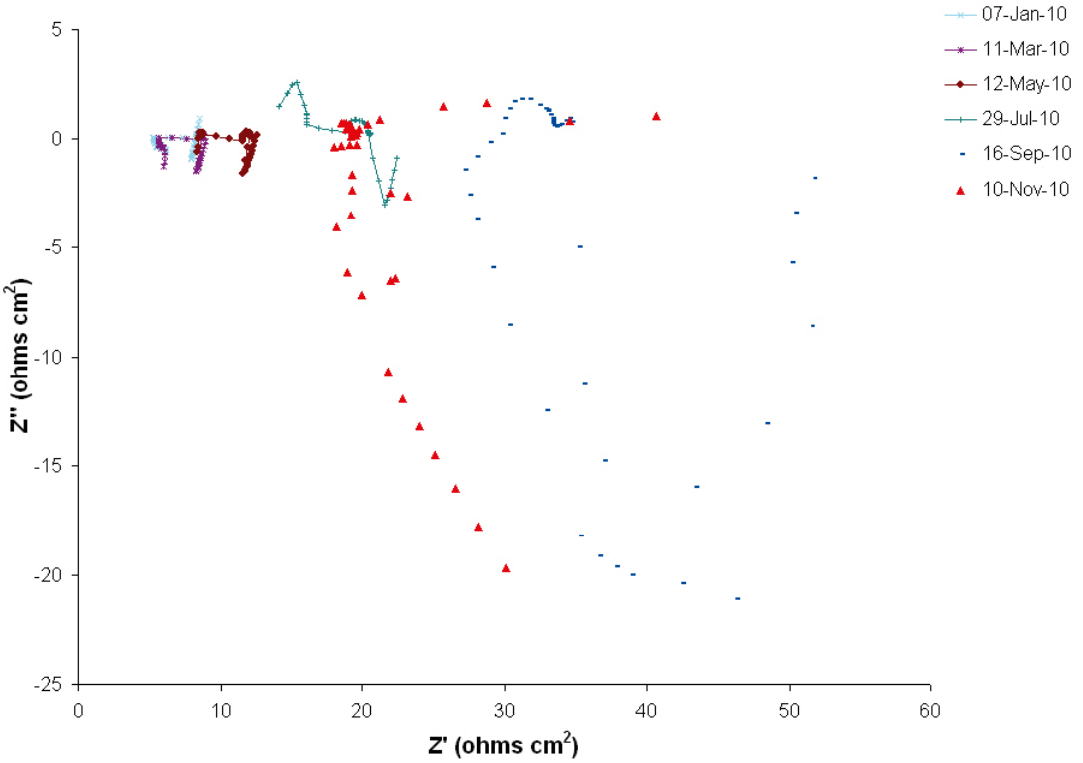

Figure A1-17. *ACI plots of copper in Experiment 4 (compacted bentonite).*

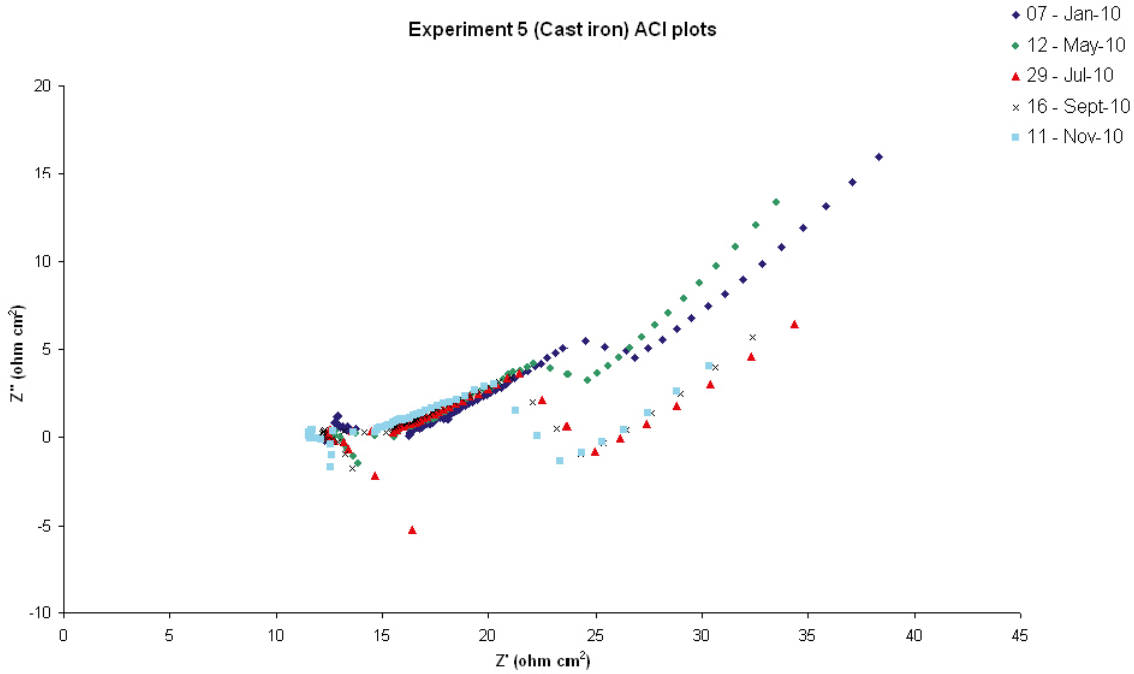

Figure A1-18. *ACI plots of cast iron in Experiment 5 (no bentonite).*

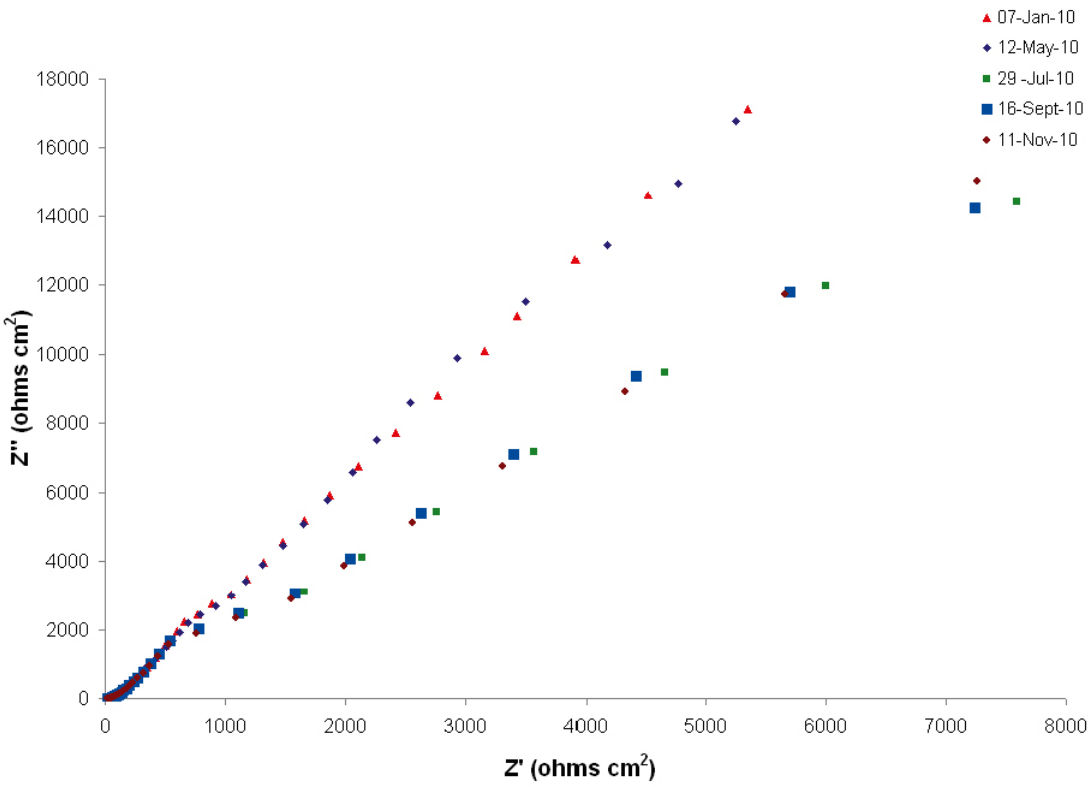

Figure A1-19. *ACI plots of copper in Experiment 5 (no bentonite).*

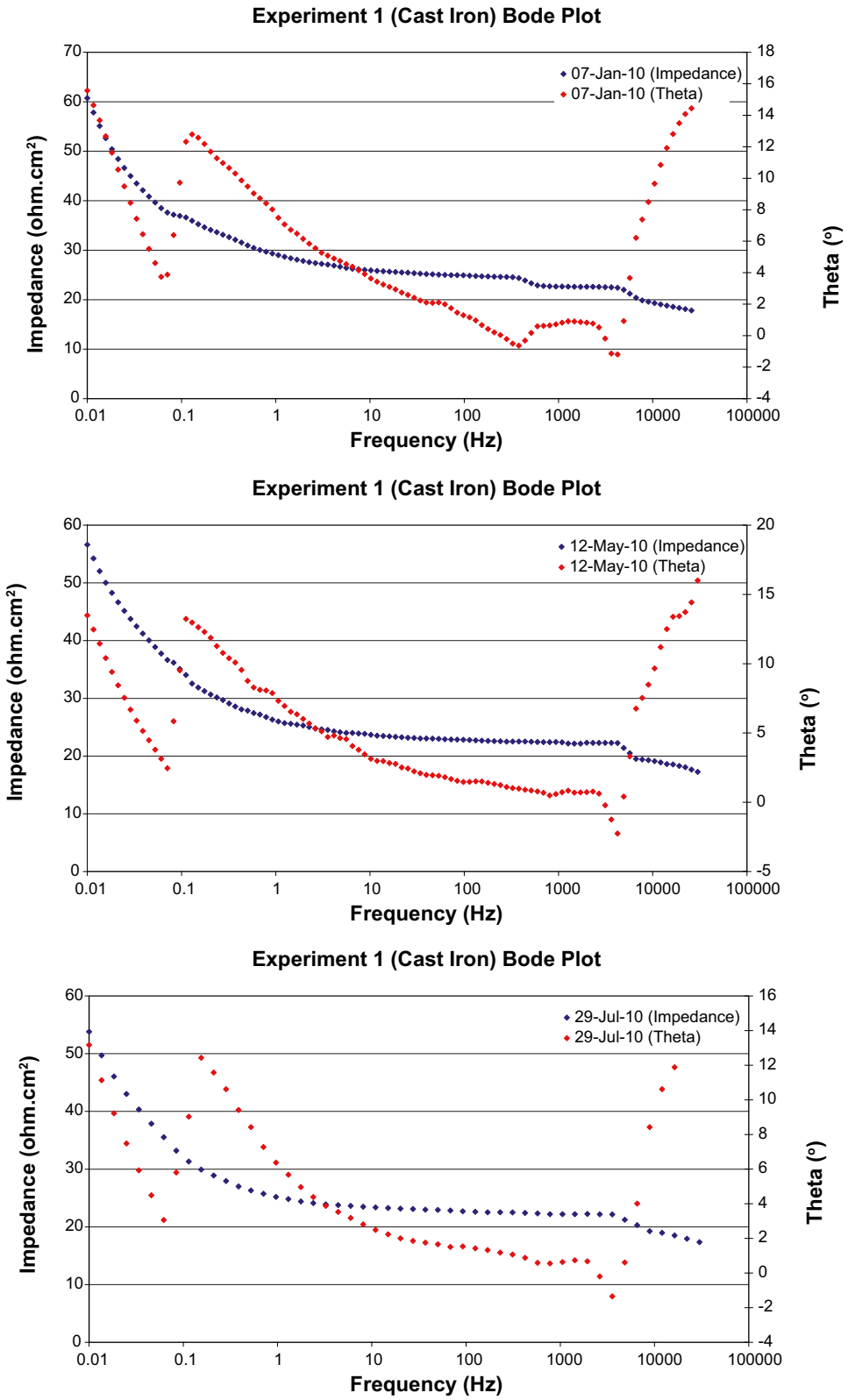

Figure A1-20. *Bode plots of cast iron in Experiment 1 (low density bentonite).*

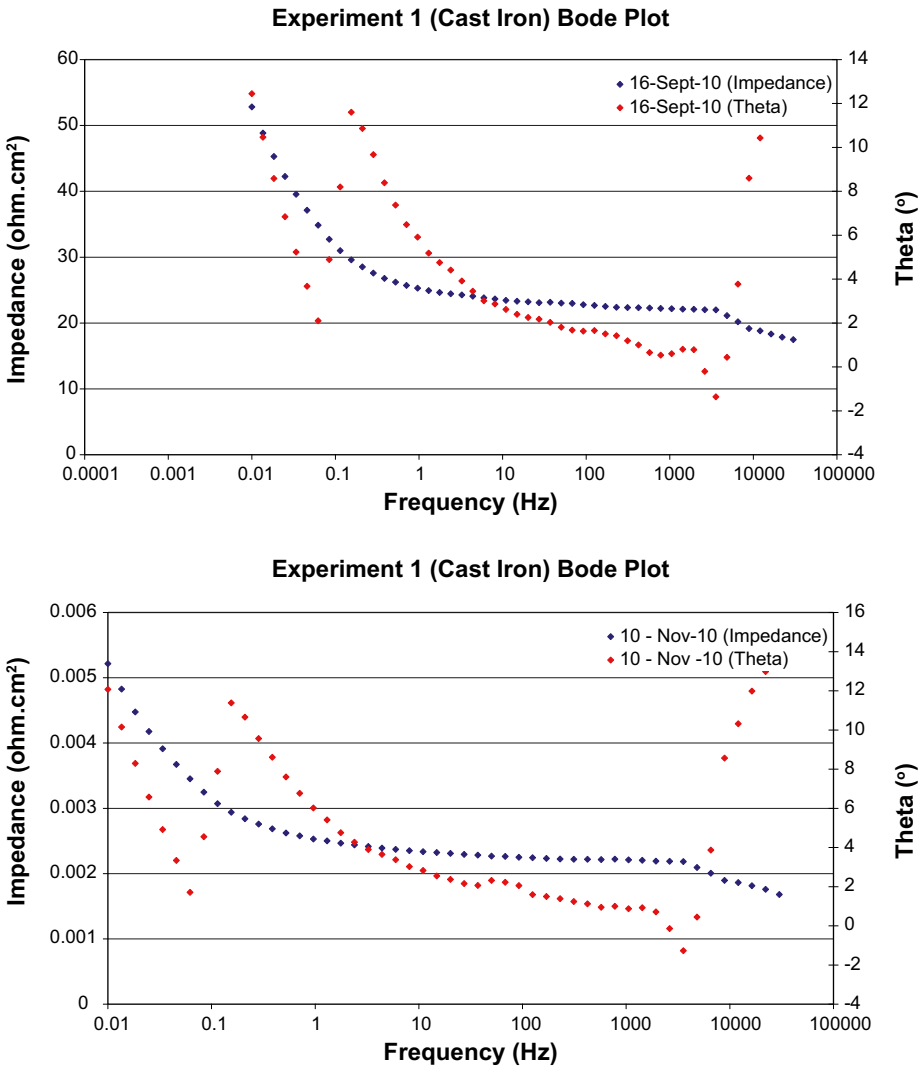

Figure A1-21. *Bode plots of cast iron in Experiment 1 (low density bentonite).*

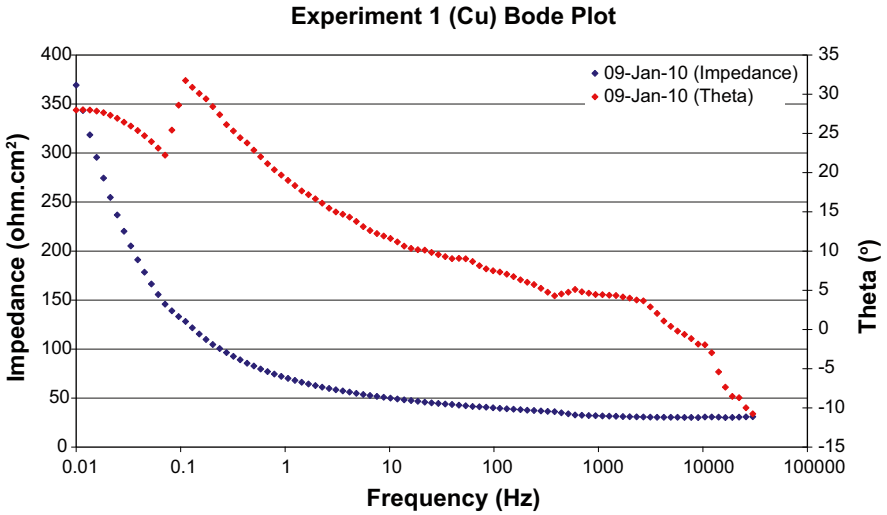

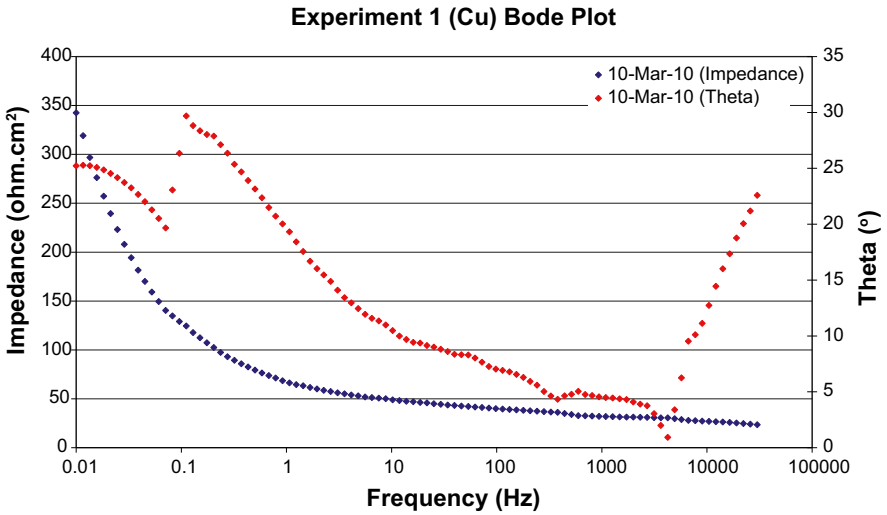

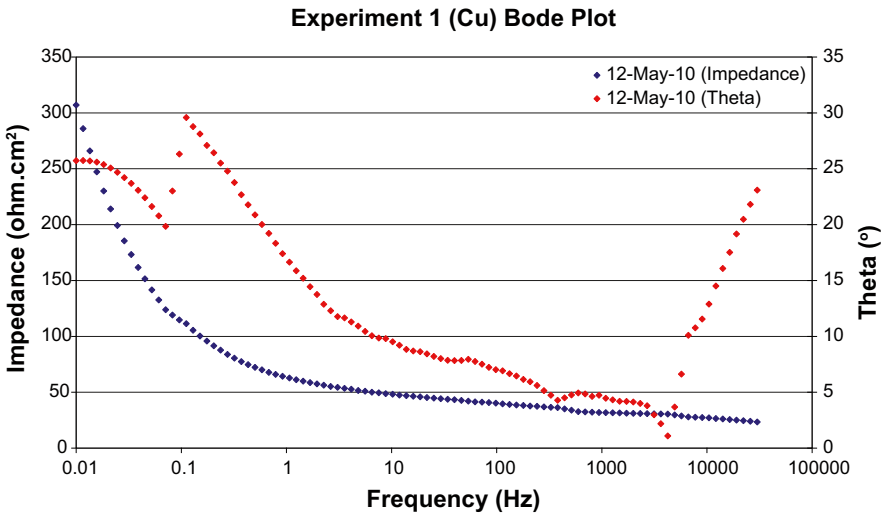

Figure A1-22. *Bode plots of copper in Experiment 1 (low density bentonite).*

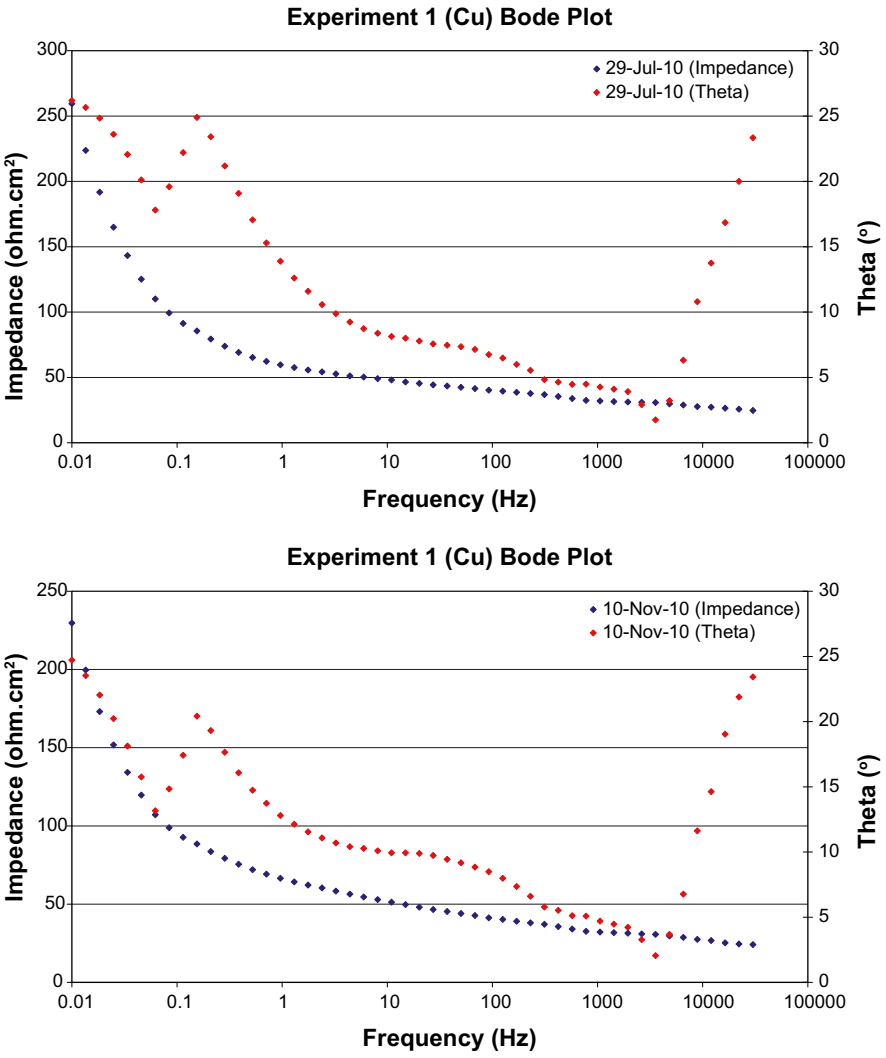

Figure A1-23. *Bode plots of copper in Experiment 1 (low density bentonite).*

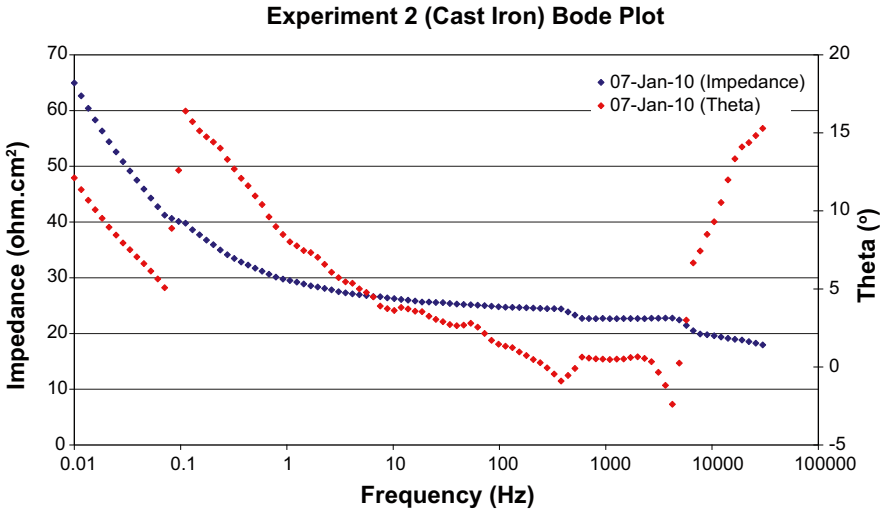

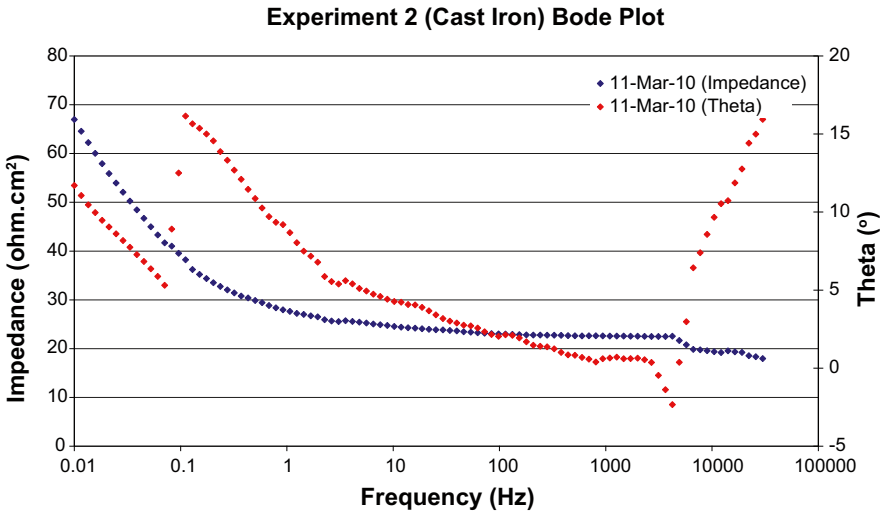

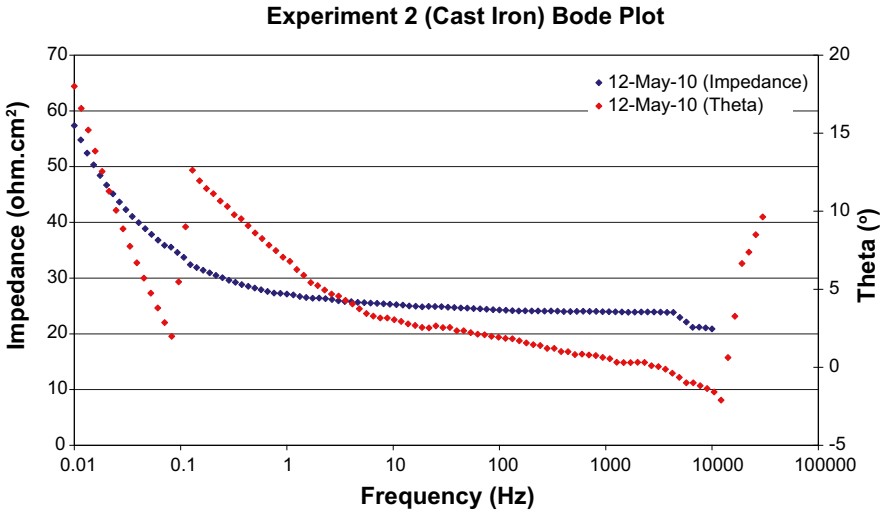

Figure A1-24. *Bode plots of cast iron in Experiment 2 (low density bentonite).*

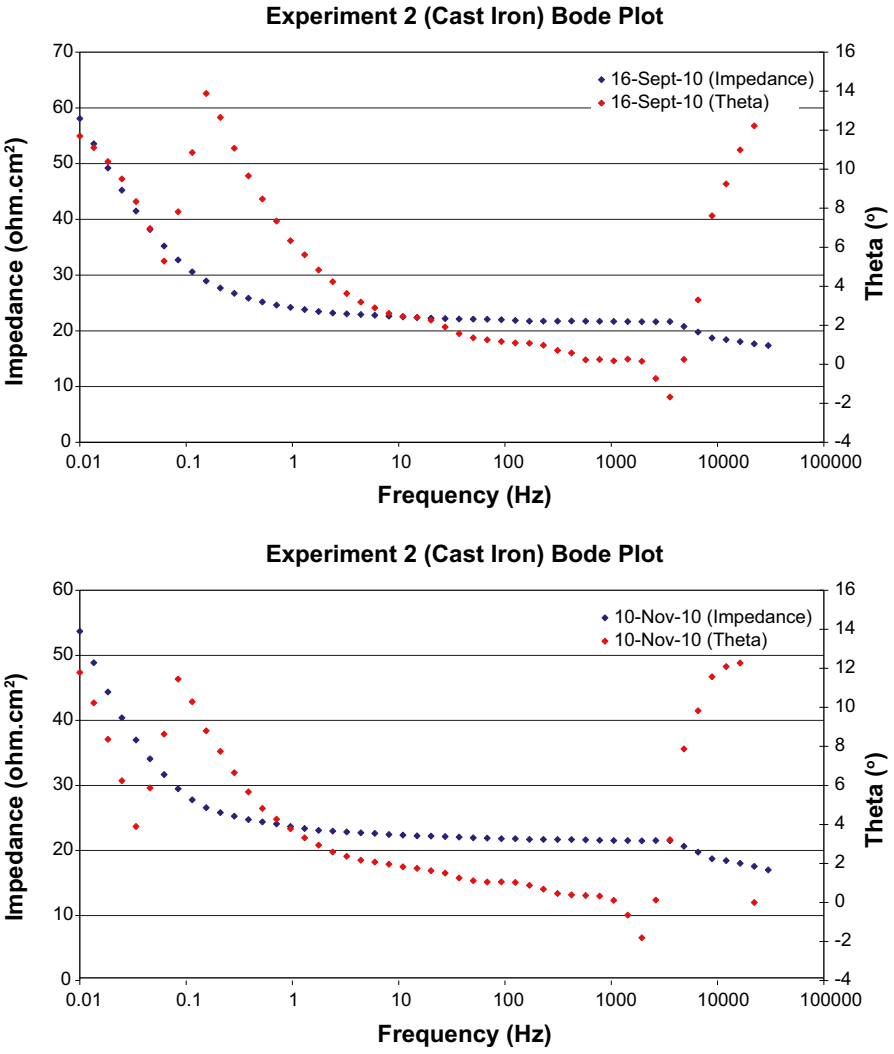

Figure A1-25. *Bode plots of cast iron in Experiment 2 (low density bentonite).*

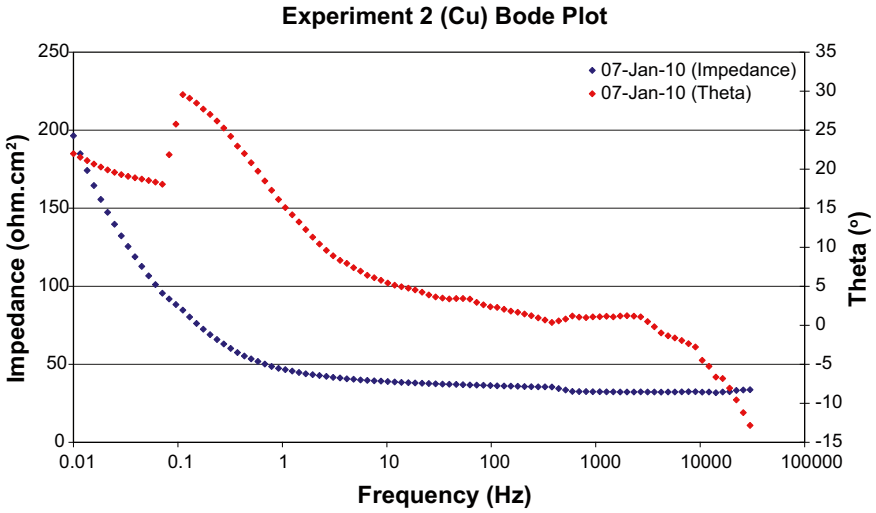

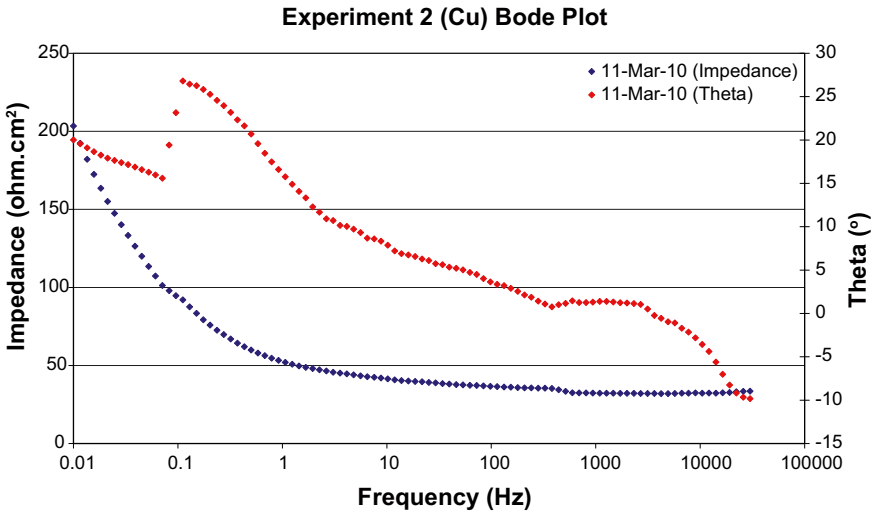

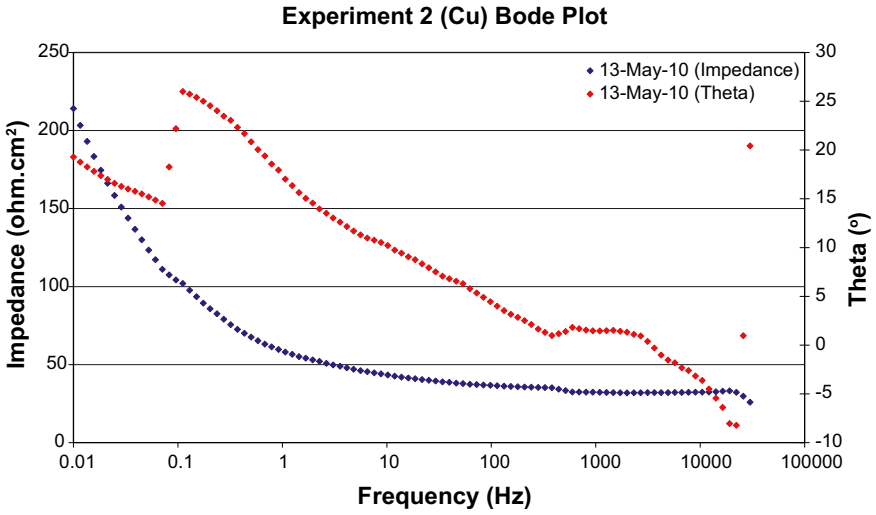

Figure A1-26. *Bode plots of copper in Experiment 2 (low density bentonite).*

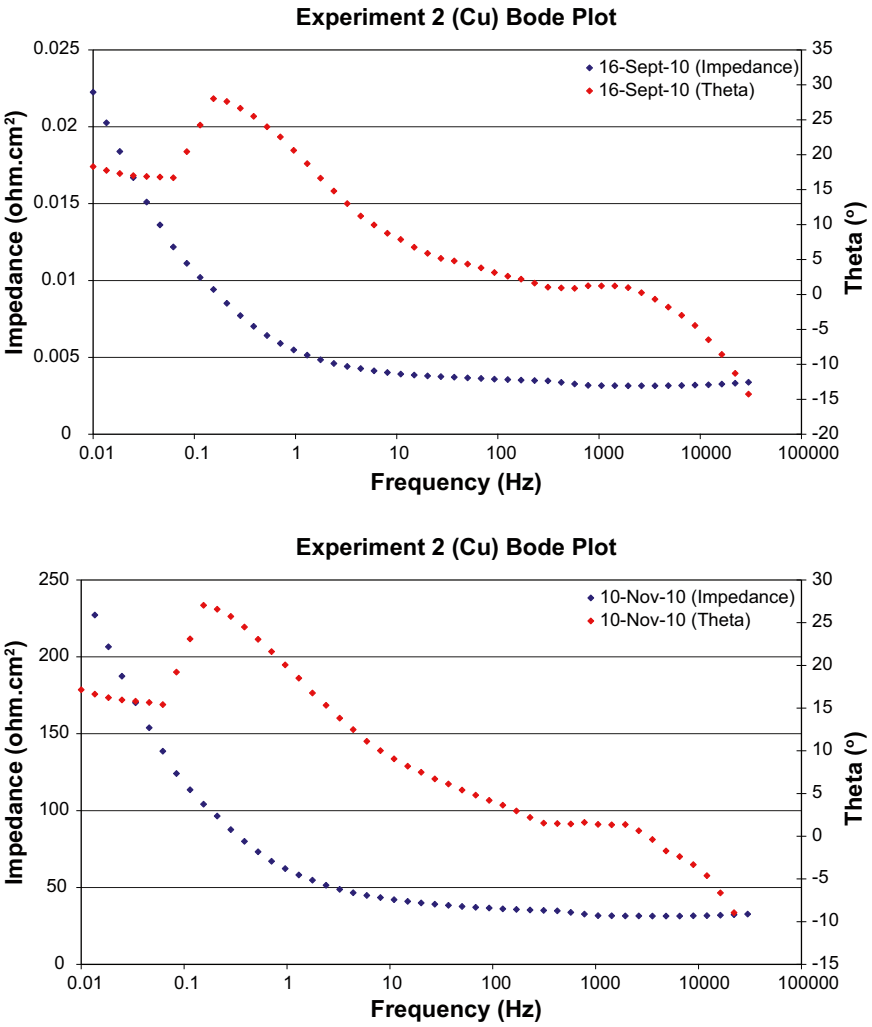

Figure A1-27. *Bode plots of copper in Experiment 2 (low density bentonite).*

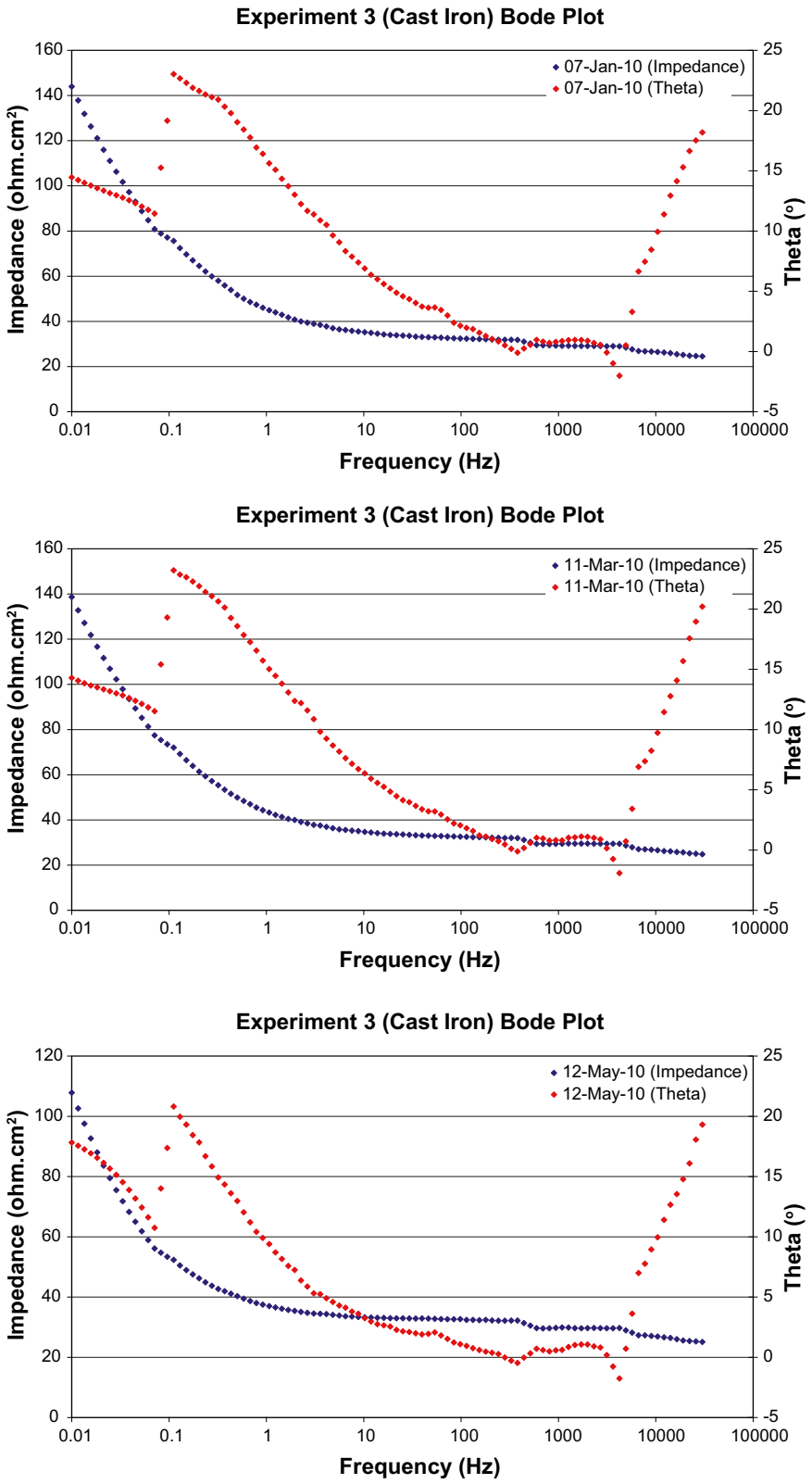

Figure A1-28. *Bode plots of cast iron in Experiment 3 (low density Bentonite).*

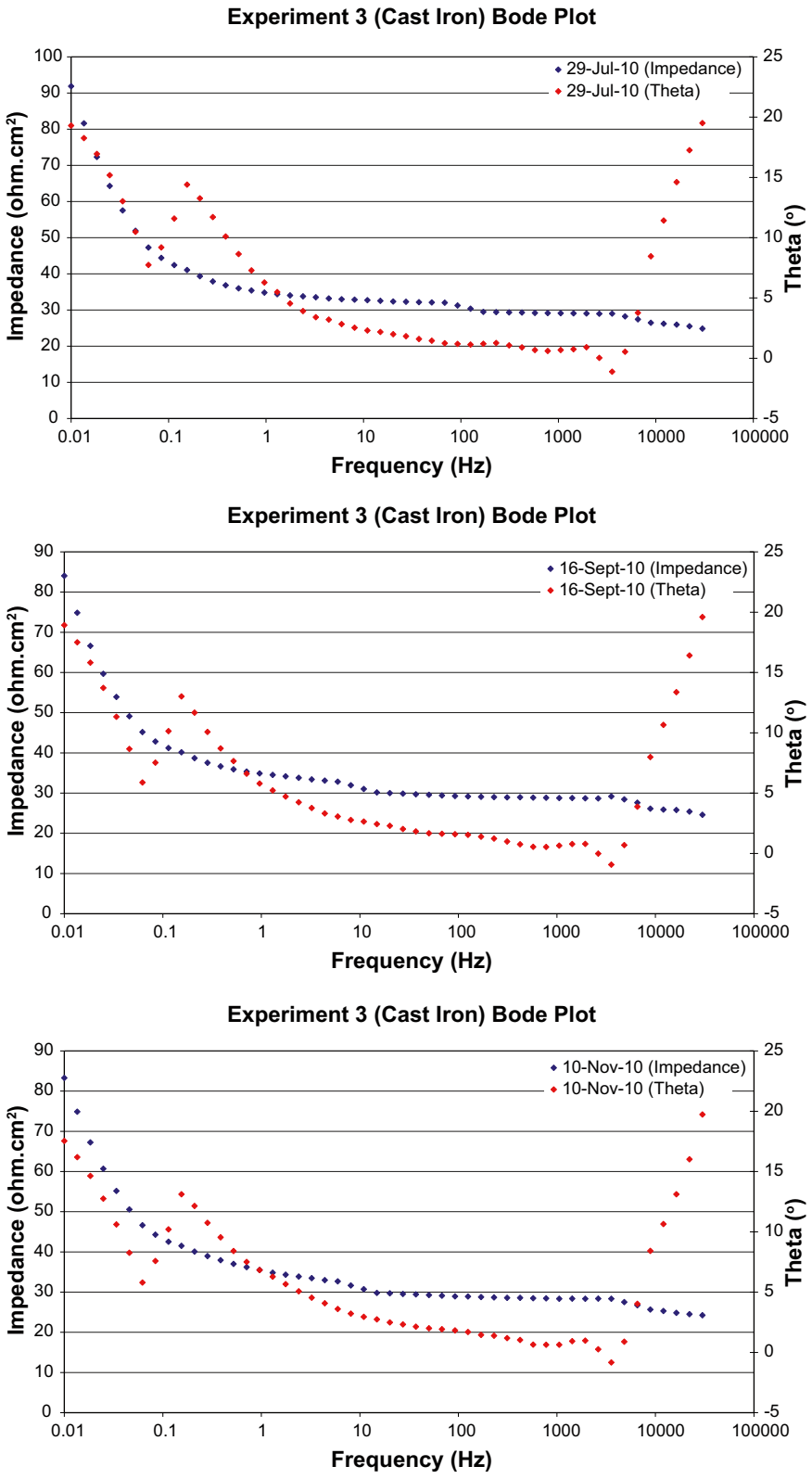

Figure A1-29. *Bode plots of cast iron in Experiment 3 (low density Bentonite).*

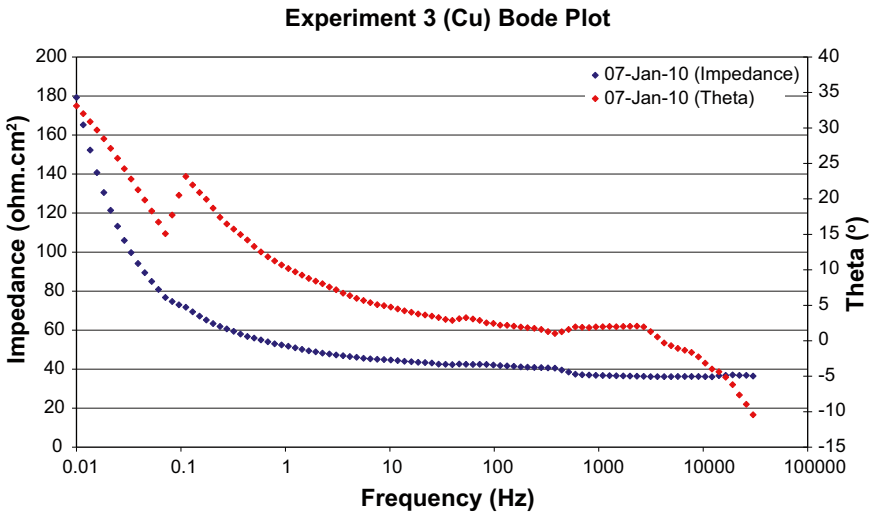

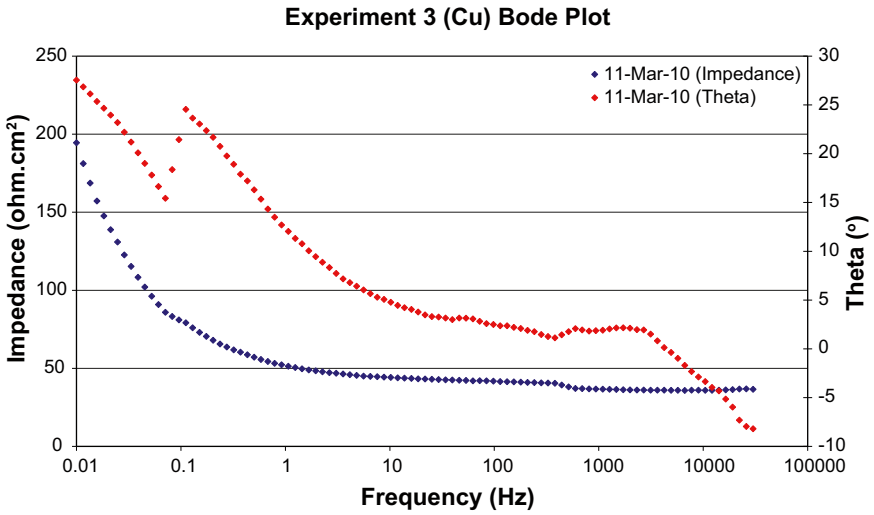

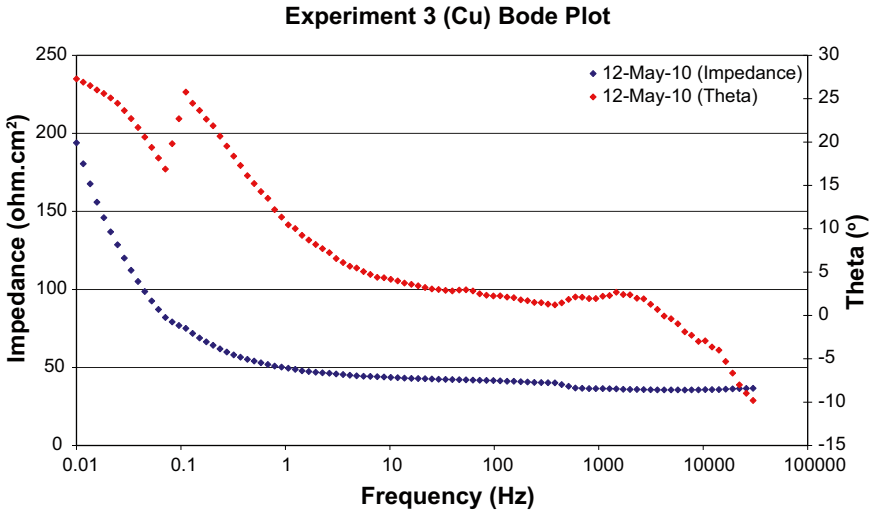

Figure A1-30. *Bode plots of copper in Experiment 3 (low density Bentonite).*

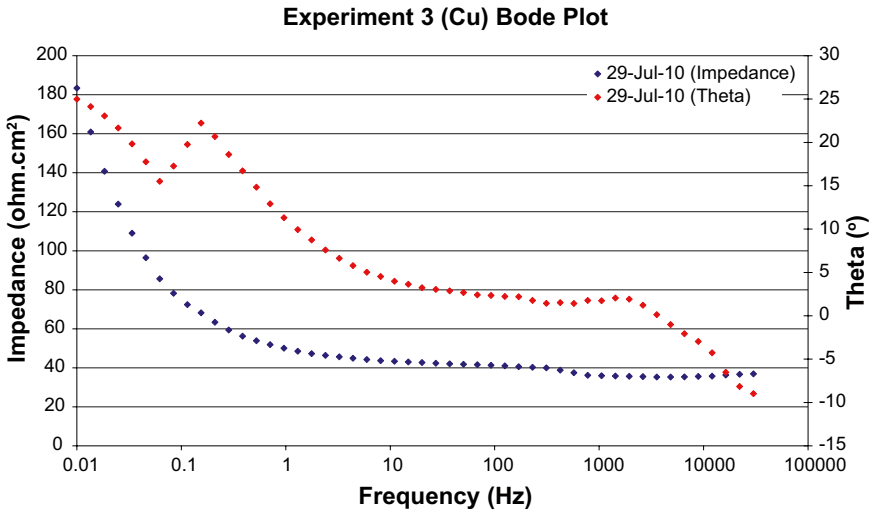

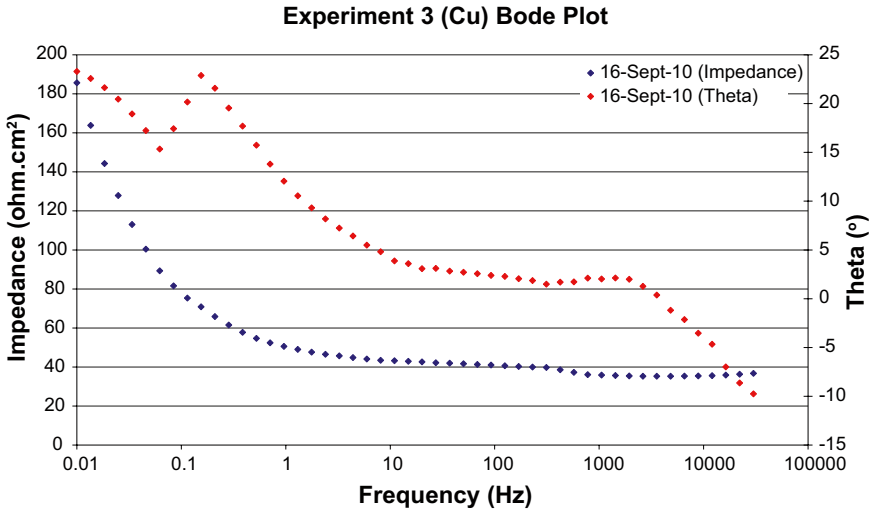

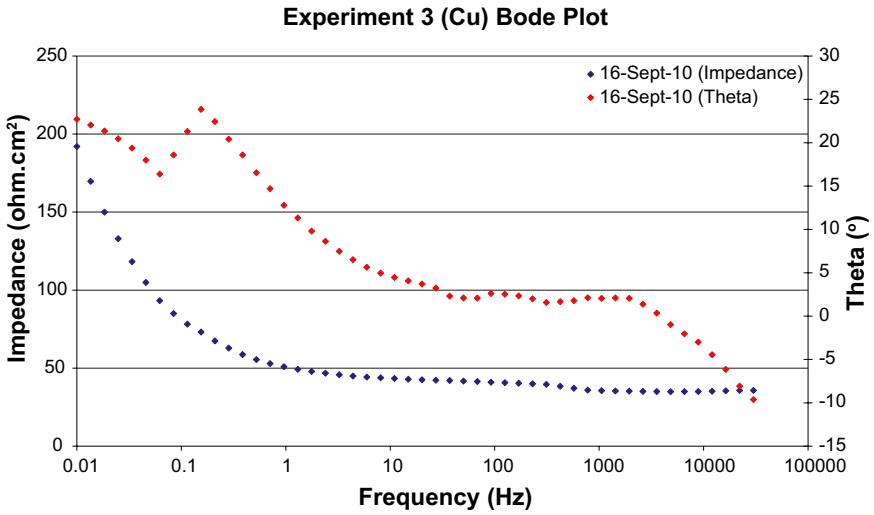

Figure A1-31. *Bode plots of copper in Experiment 3 (low density bentonite).*

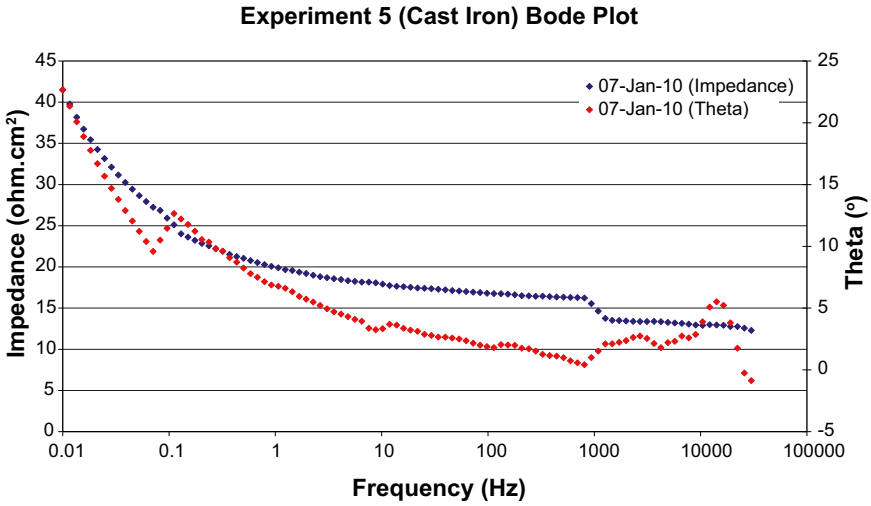

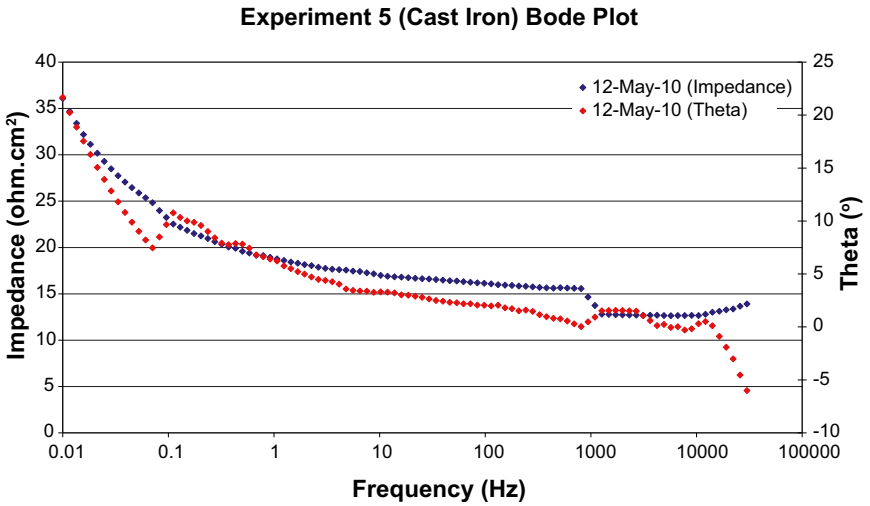

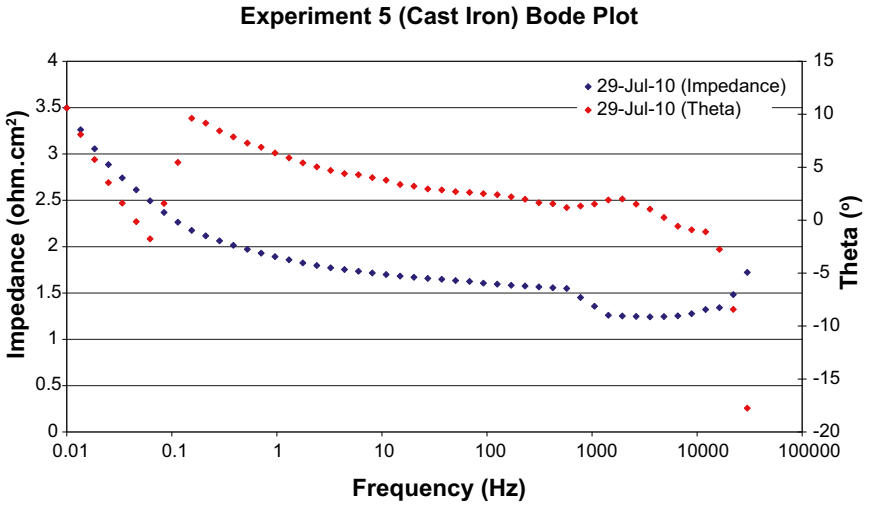

Figure A1-32. *Bode plots of cast iron in Experiment 5 (no Bentonite).*

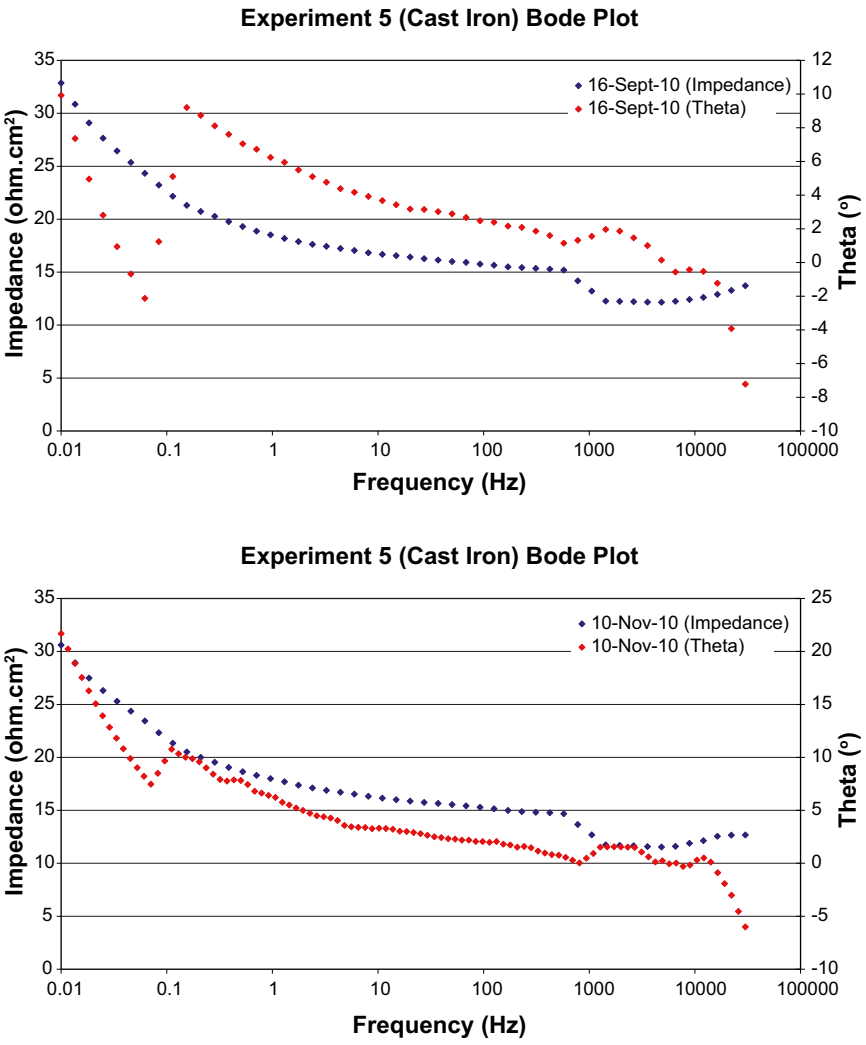

Figure A1-33. *Bode plots of cast iron in Experiment 5 (no bentonite).*

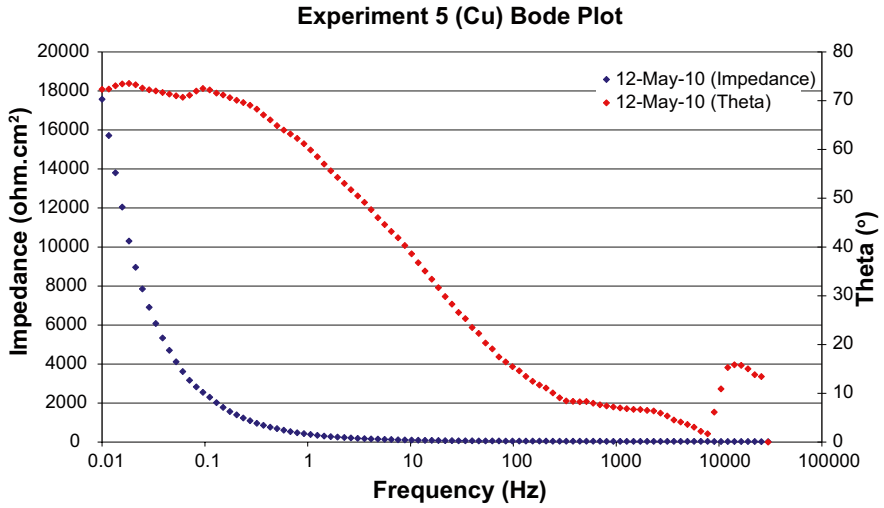

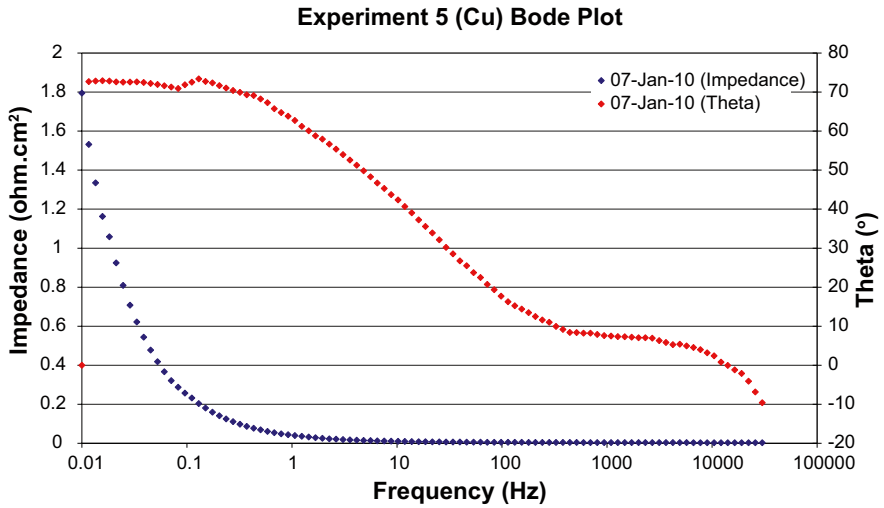

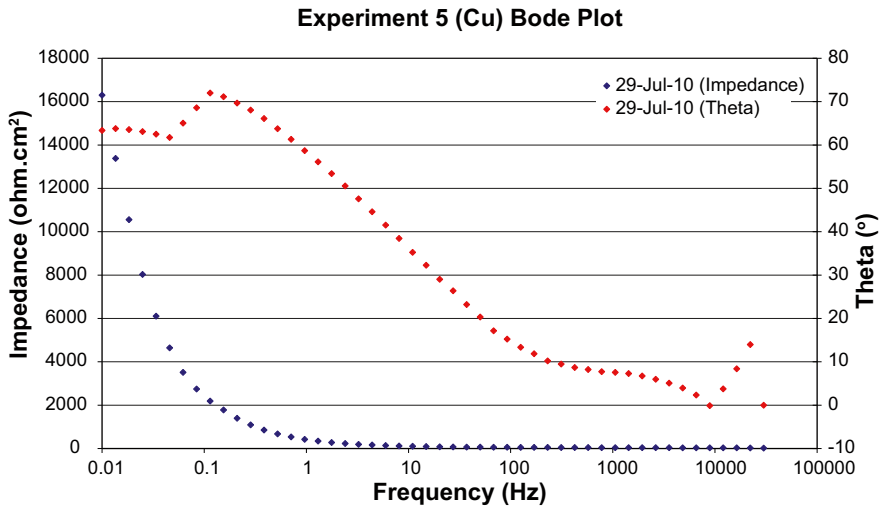

Figure A1-34. *Bode plots of copper in Experiment 5 (no bentonite).*

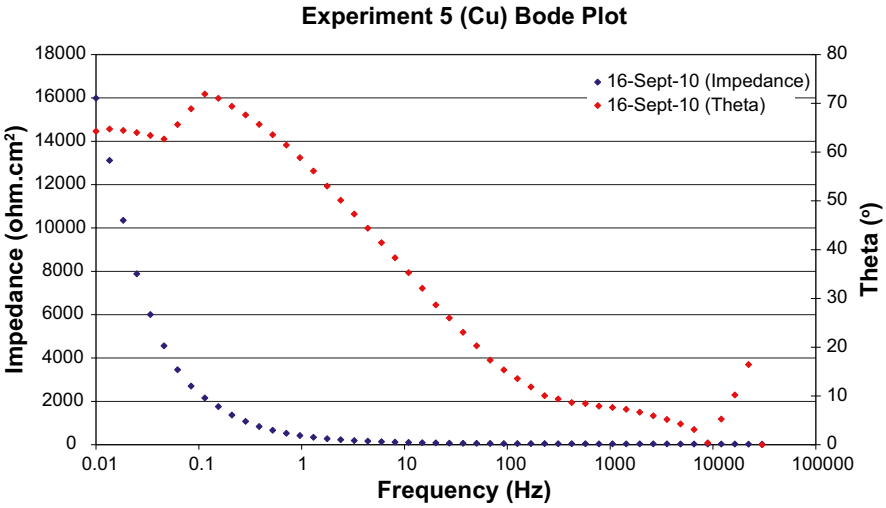

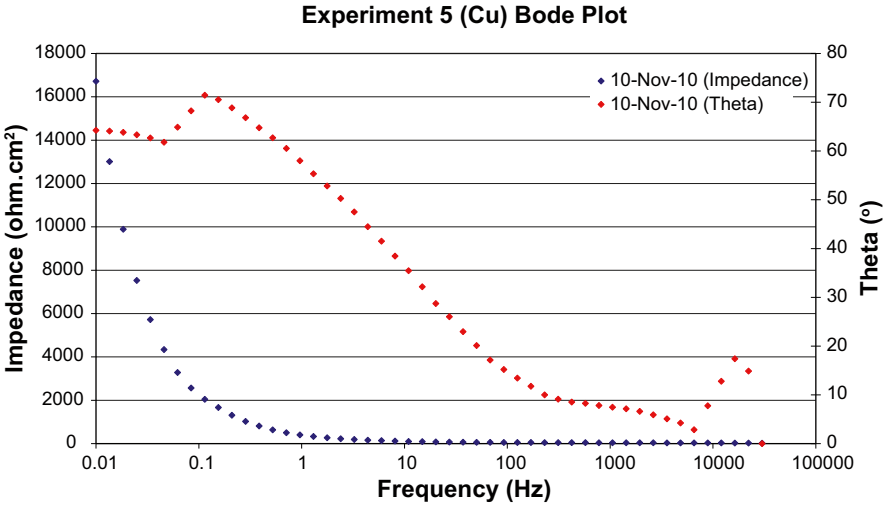

Figure A1-35. *Bode plots of copper in Experiment 5 (no bentonite).*

Appendix 2

Electrochemical corrosion rate measurements up to 2009

Please note that all potentials shown in the electrochemical measurements are with respect to the reference electrode (i.e. Ag/AgCl), not NHE.

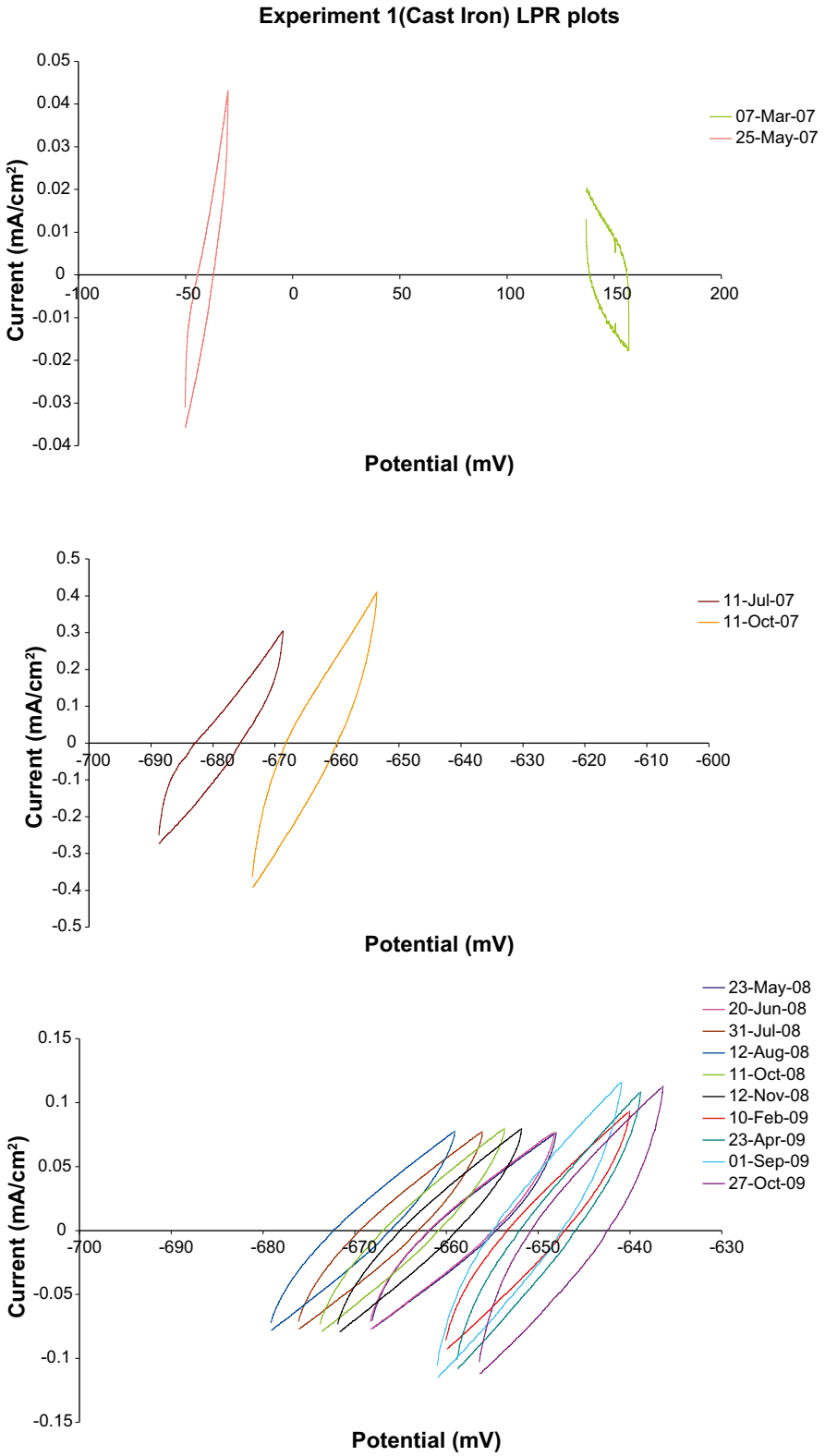

Figure A2-1. *LPR plots of cast iron in Experiment 1 (low density bentonite).*

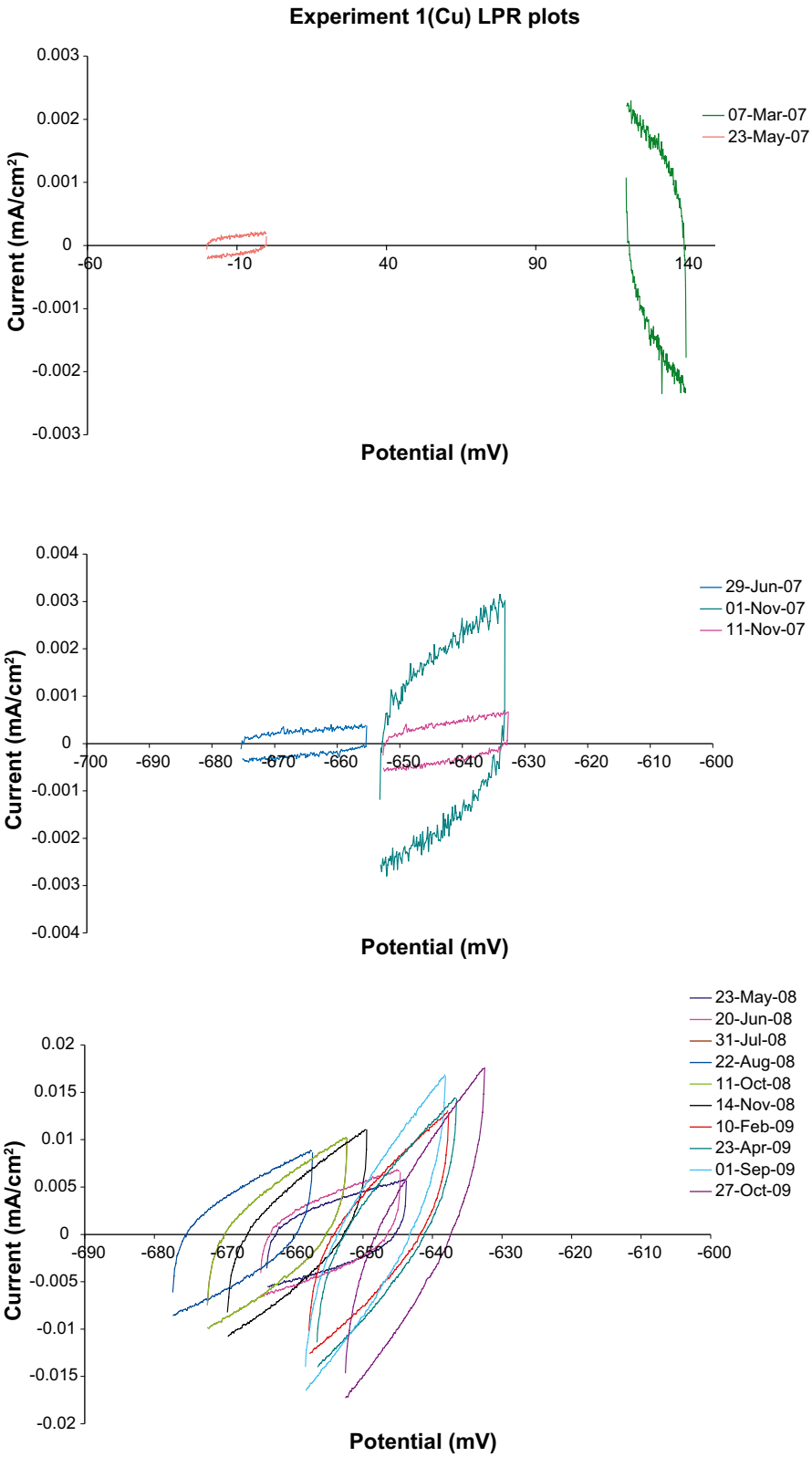

Figure A2-2. *LPR plots of copper in Experiment 1 (low density bentonite).*

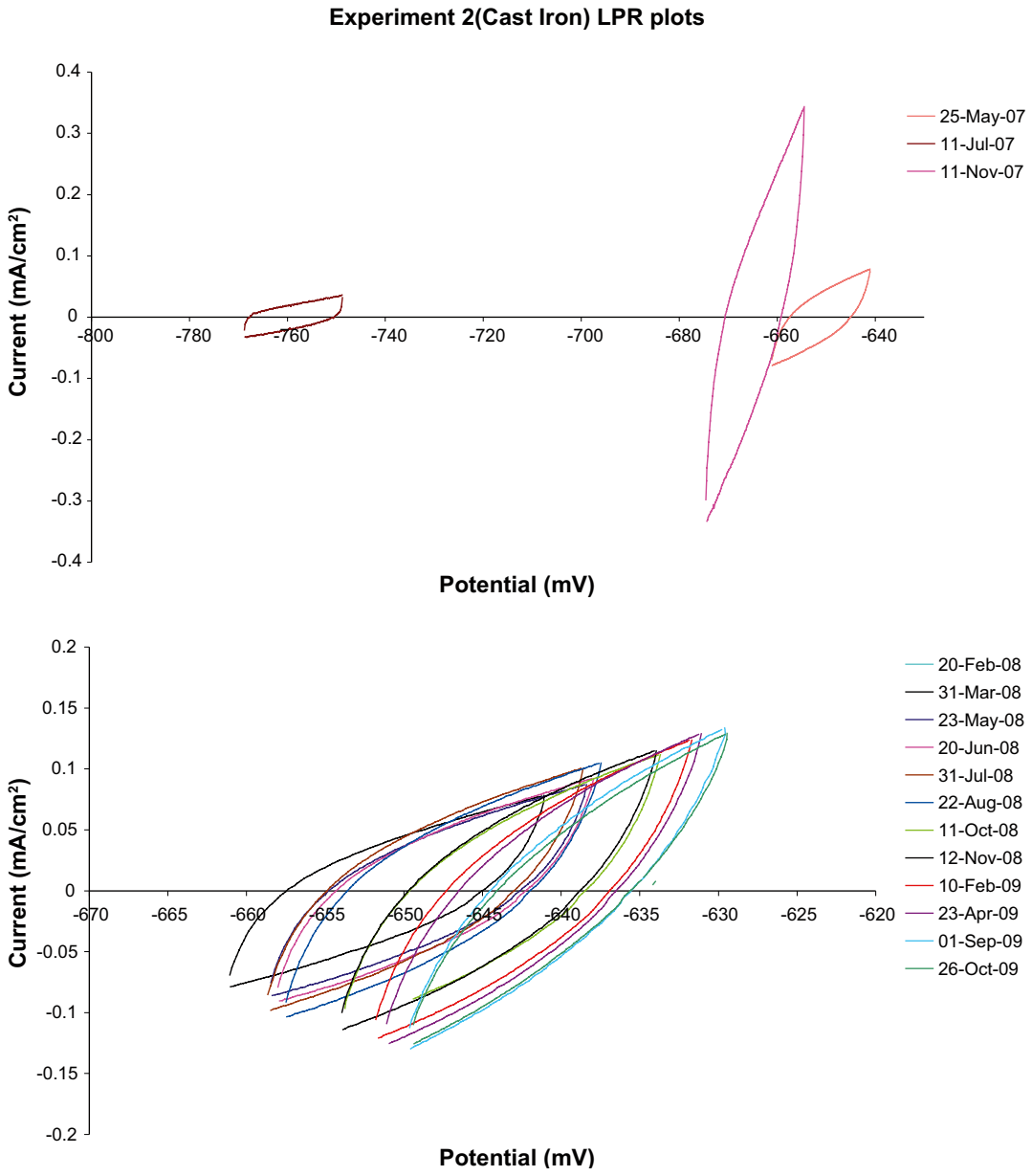

Figure A2-3. *LPR plots of cast iron in Experiment 2 (low density bentonite).*

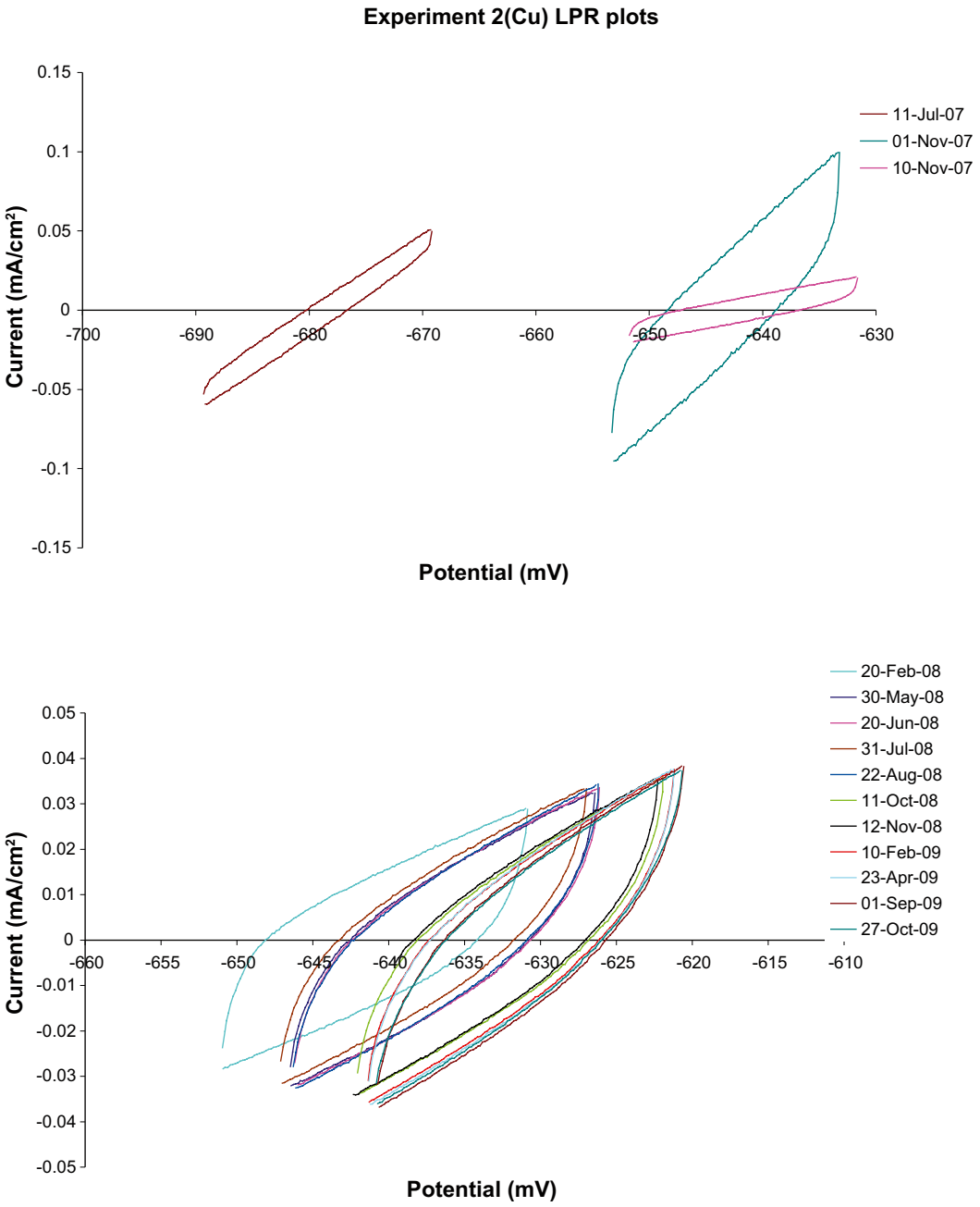

Figure A2-4. *LPR plots of copper in Experiment 2 (low density bentonite).*

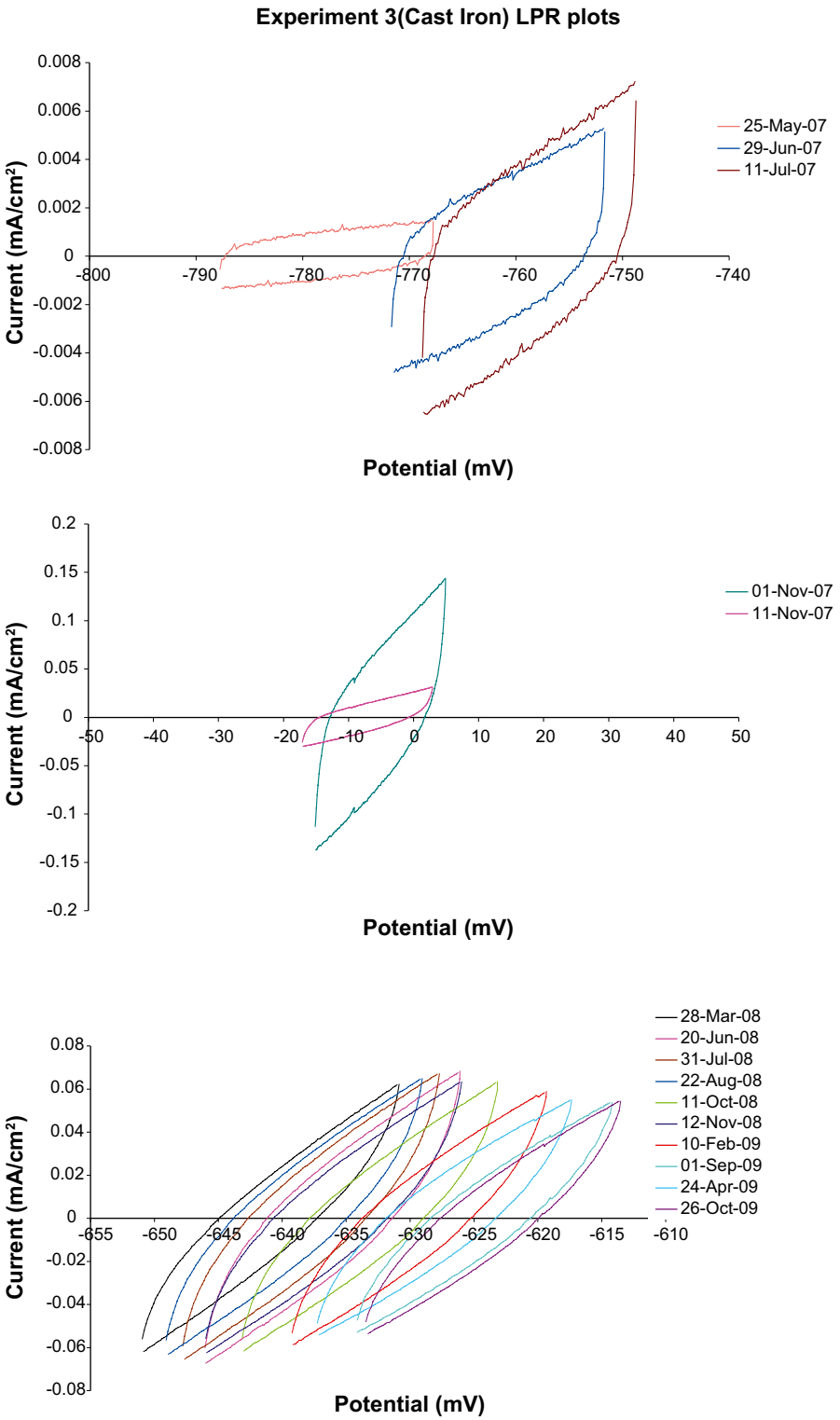

Figure A2-5. *LPR plots of cast iron in Experiment 3 (low density bentonite).*

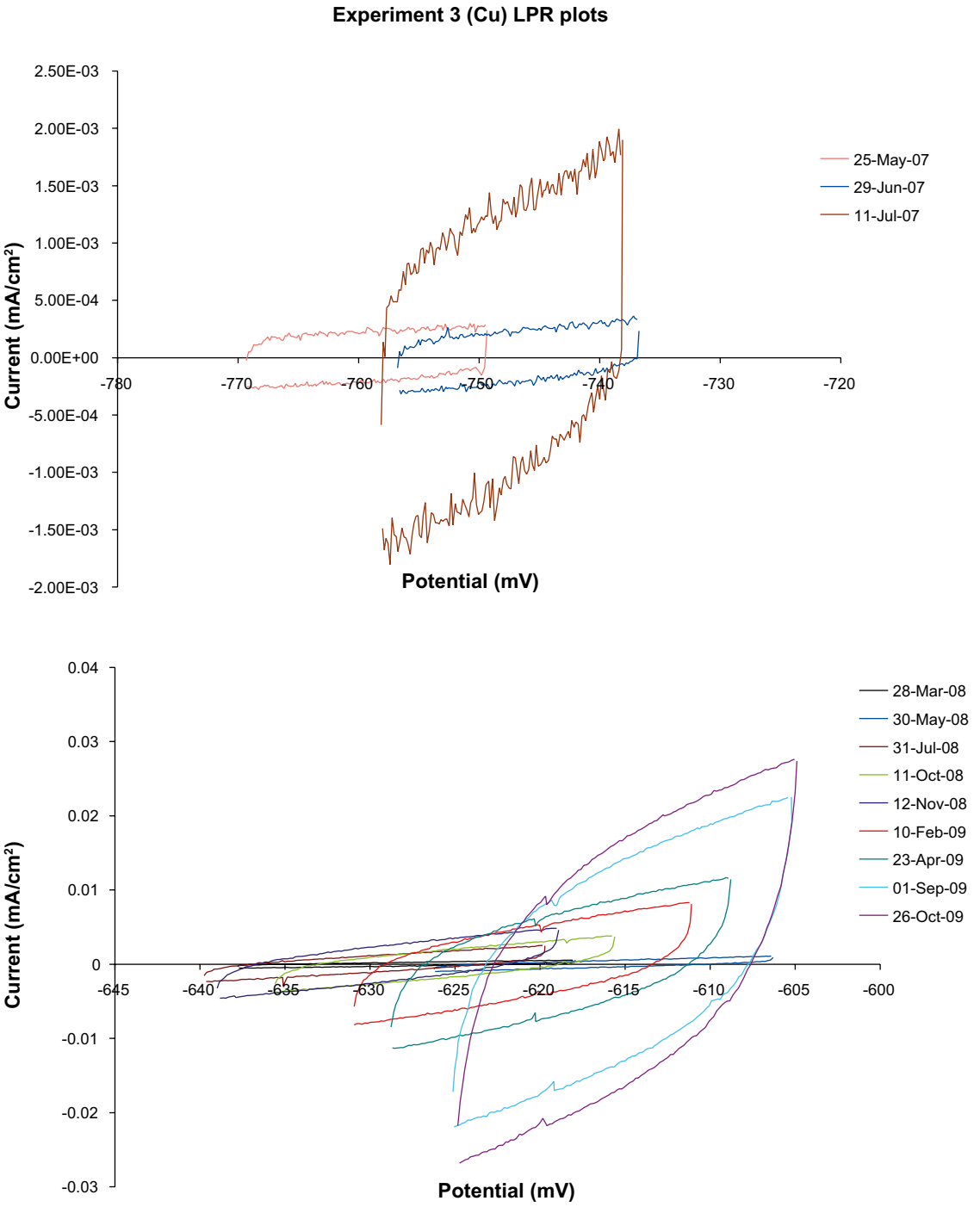

Figure A2-6. *LPR plots of copper in Experiment 3 (low density bentonite).*

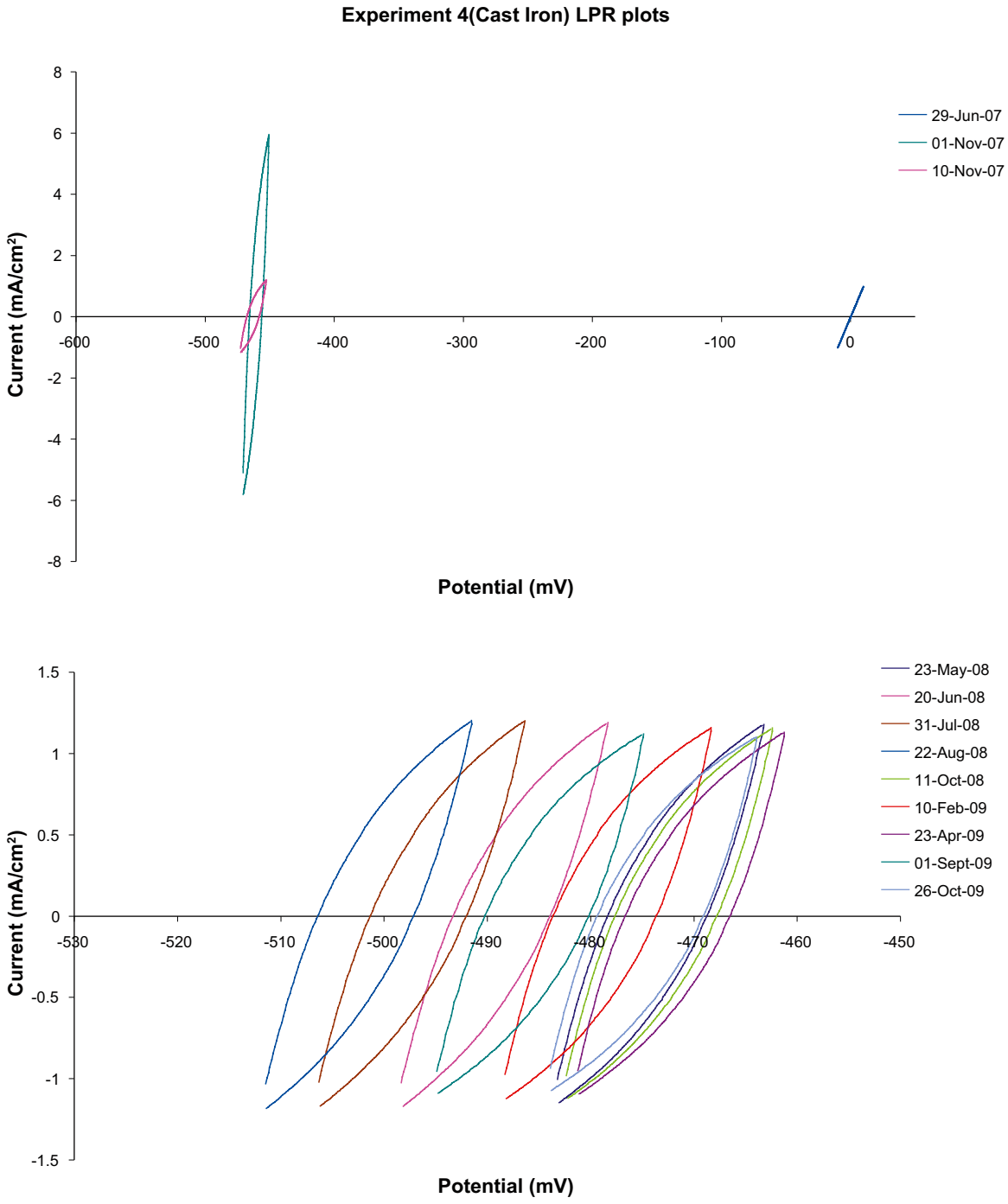

Figure A2-7. *LPR plots of cast iron in Experiment 4 (compacted bentonite) (Note: It is likely that the iron electrode was in contact with the stainless steel flange of the support cage for these measurements).*

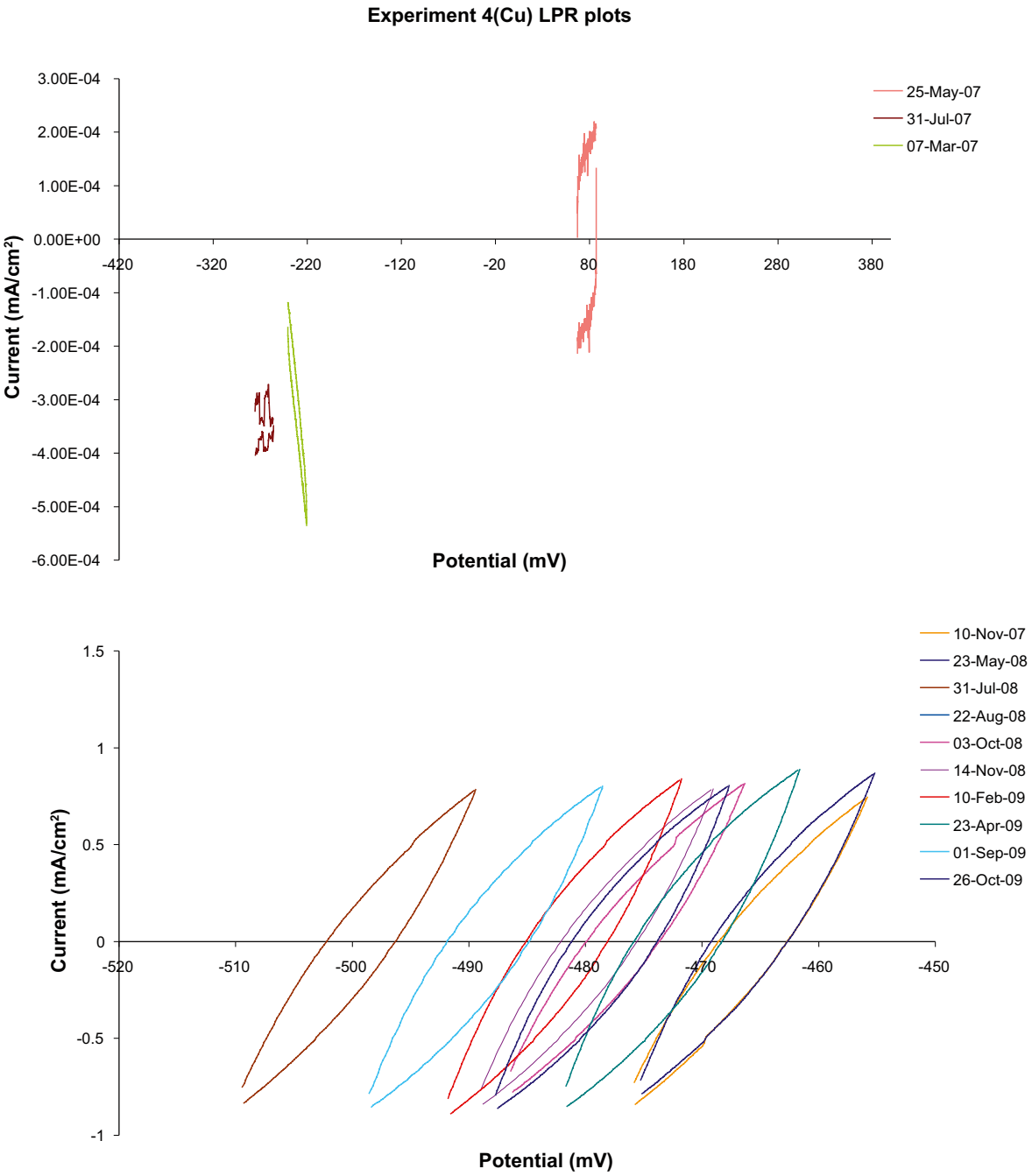

Figure A2-8. *LPR plots of copper in Experiment 4 (compacted bentonite).*

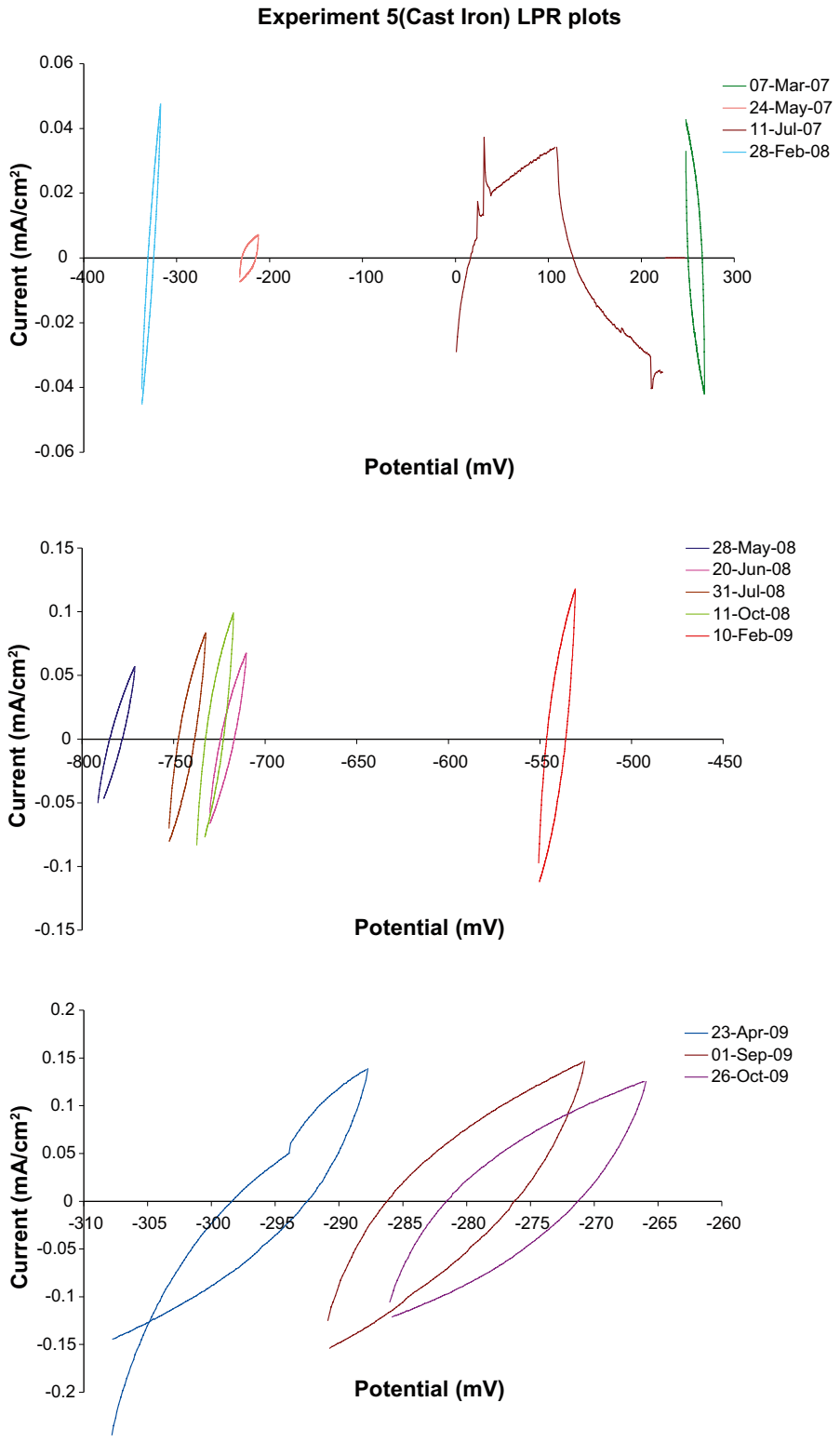

Figure A2-9. *LPR plots of cast iron in Experiment 5 (no bentonite).*

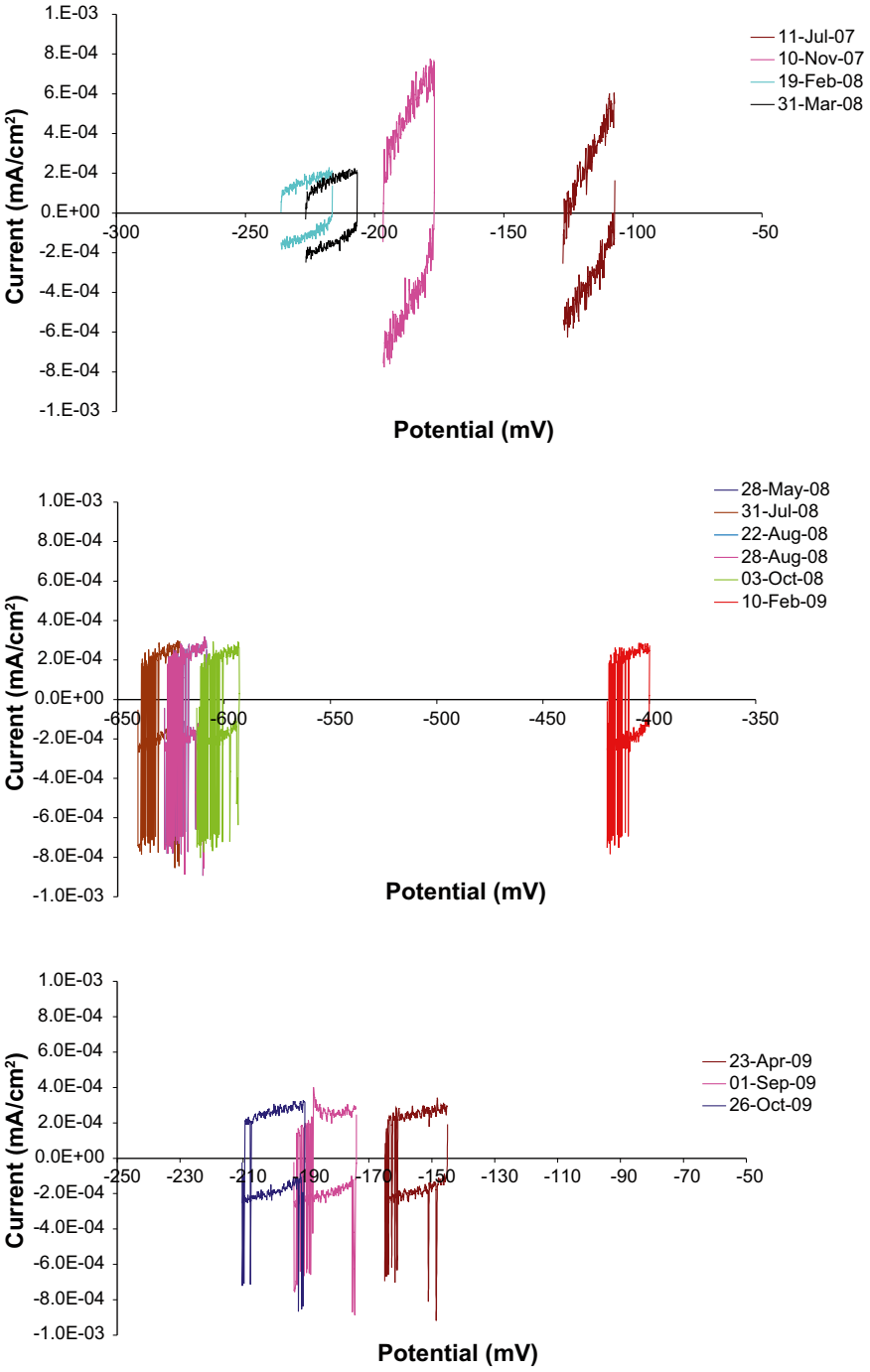

Figure A2-10. *LPR plots of Copper in Experiment 5 (no bentonite).*

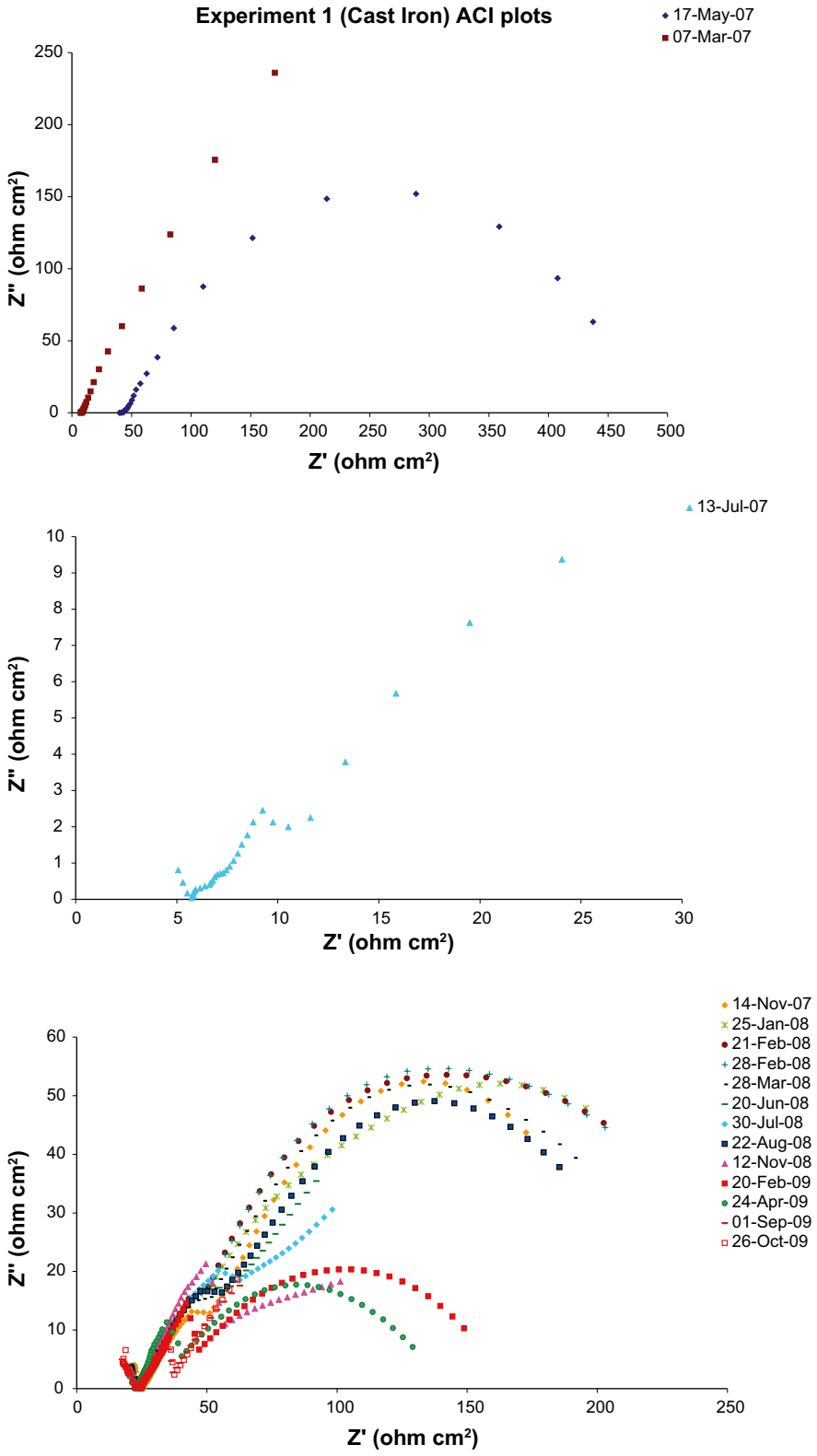

Figure A2-11. *ACI plots of cast iron in Experiment 1 (low density bentonite).*

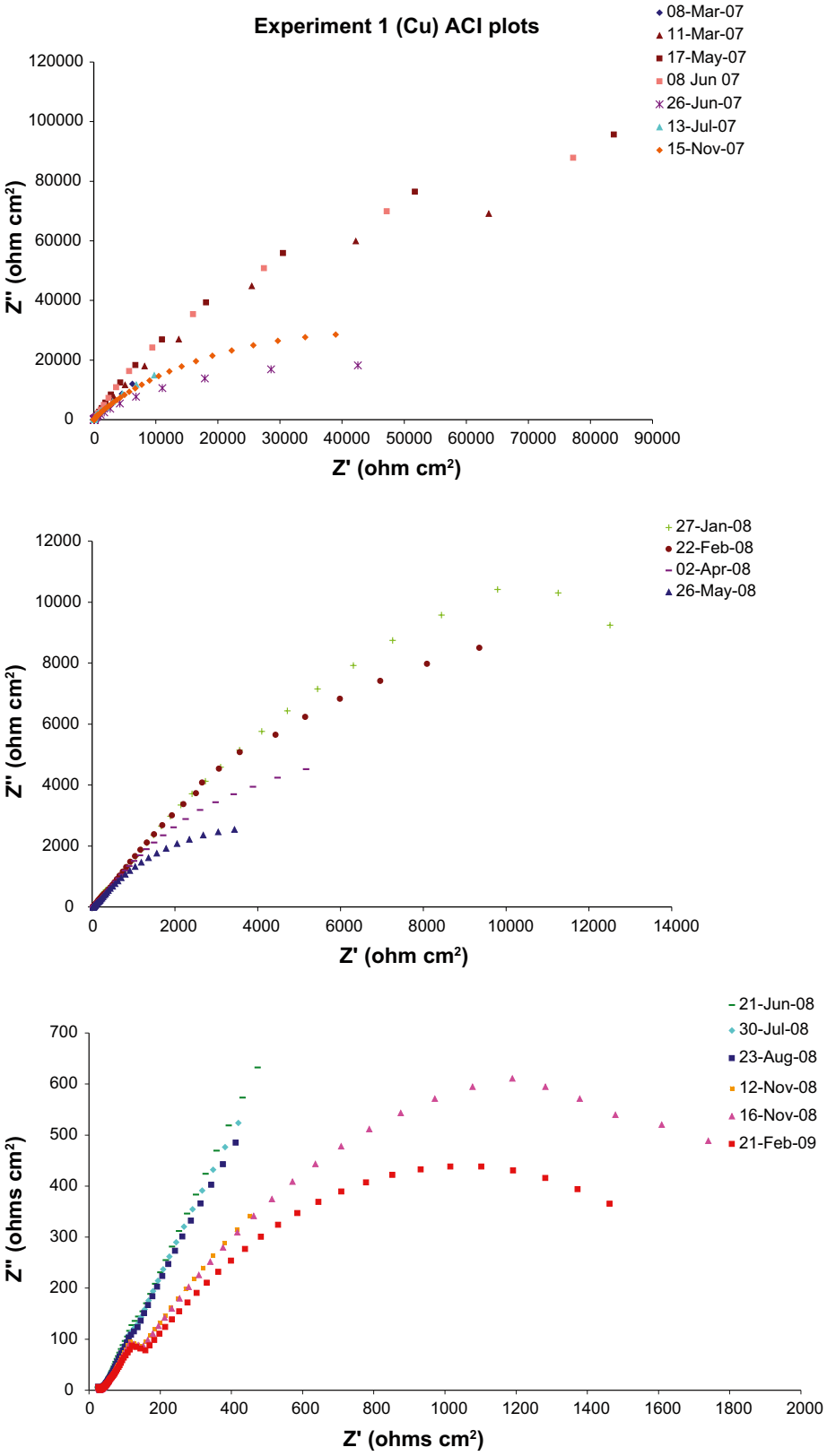

Figure A2-12. *ACI plots of copper in experiment 1 (low density bentonite).*

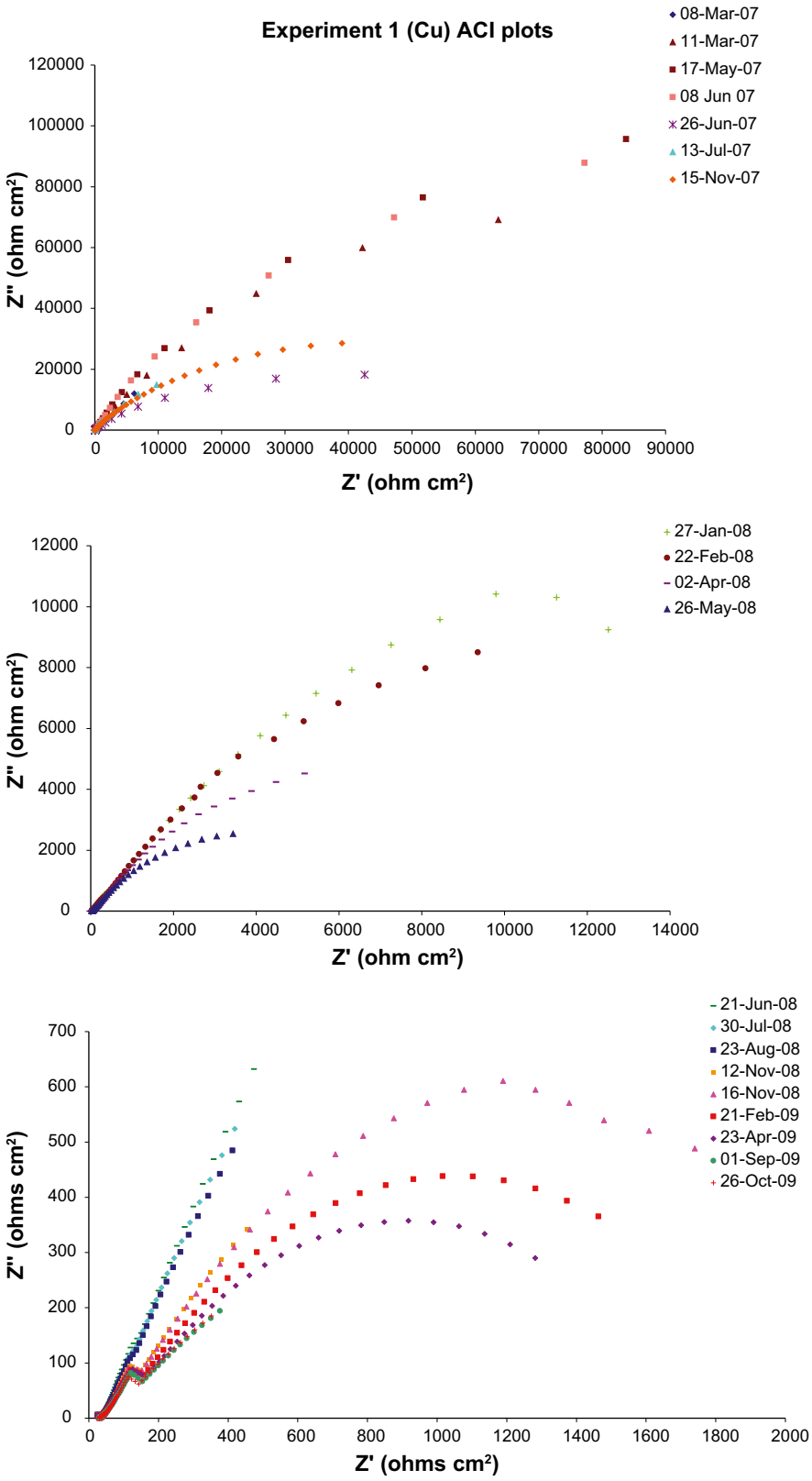

Figure A2-13. *ACI plots of copper in Experiment 1 (low density bentonite).*

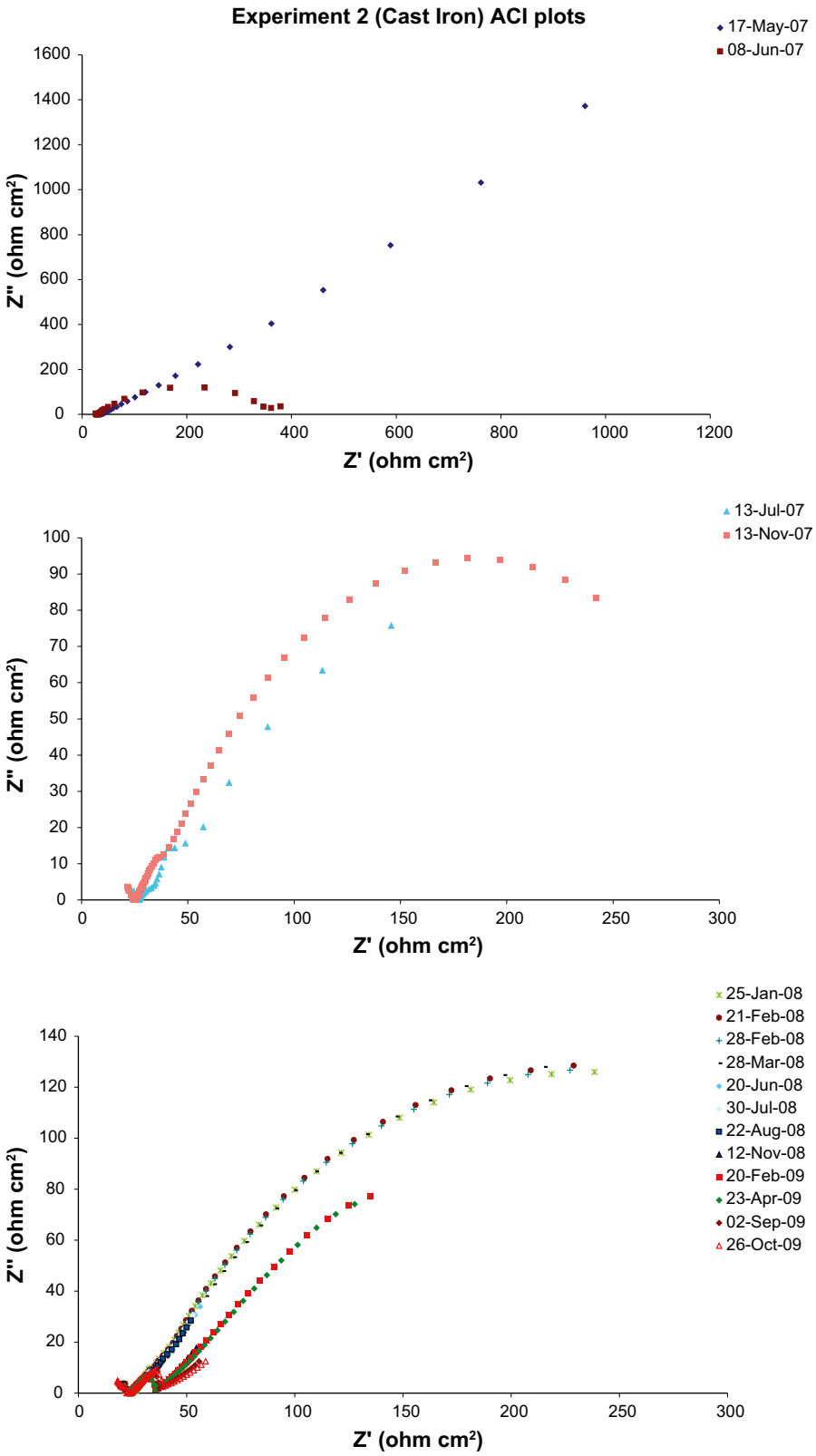

Figure A2-14. *ACI plots of cast iron in Experiment 2 (low density bentonite).*

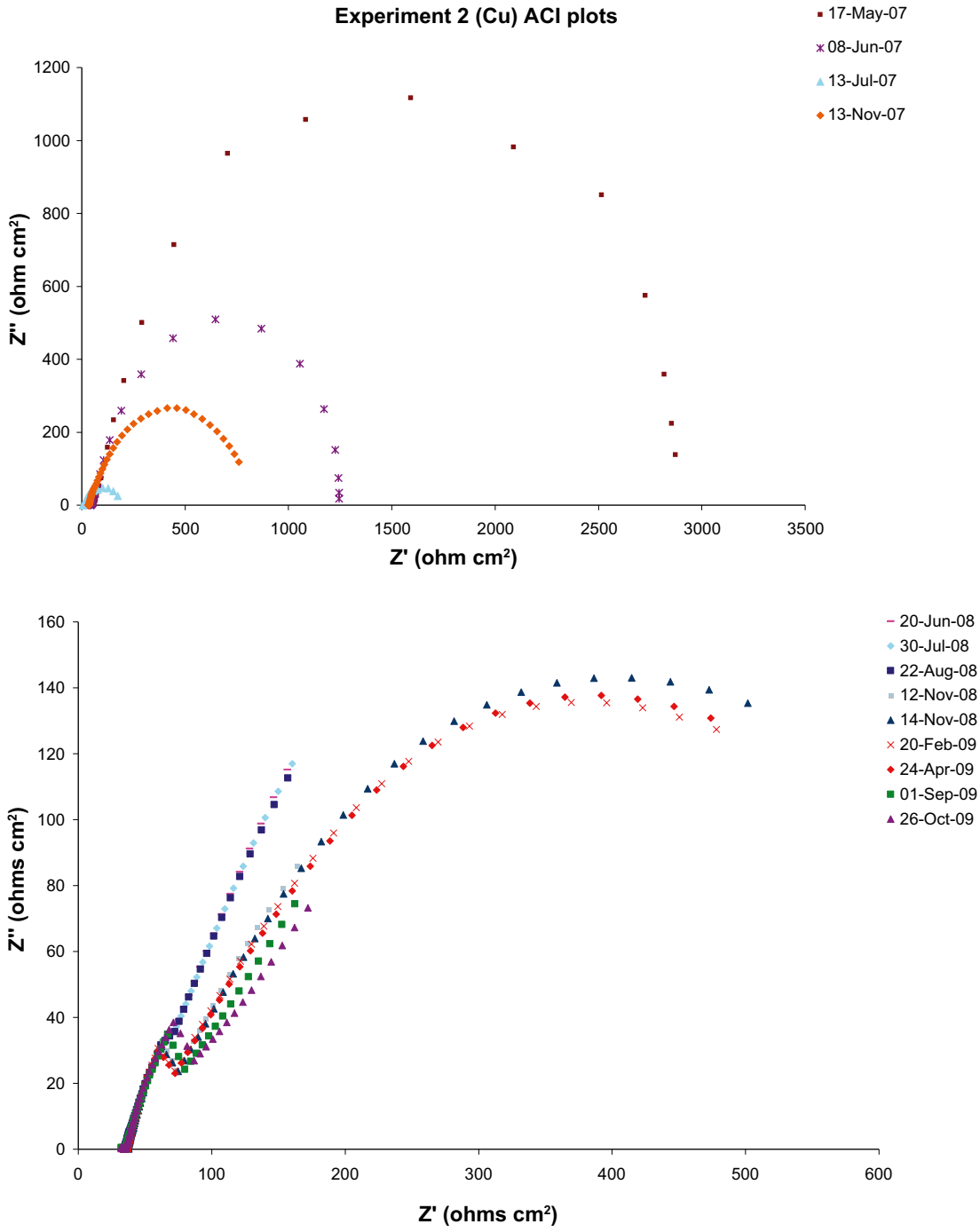

Figure A2-15. *ACI plots of copper in Experiment 2 (low density bentonite).*

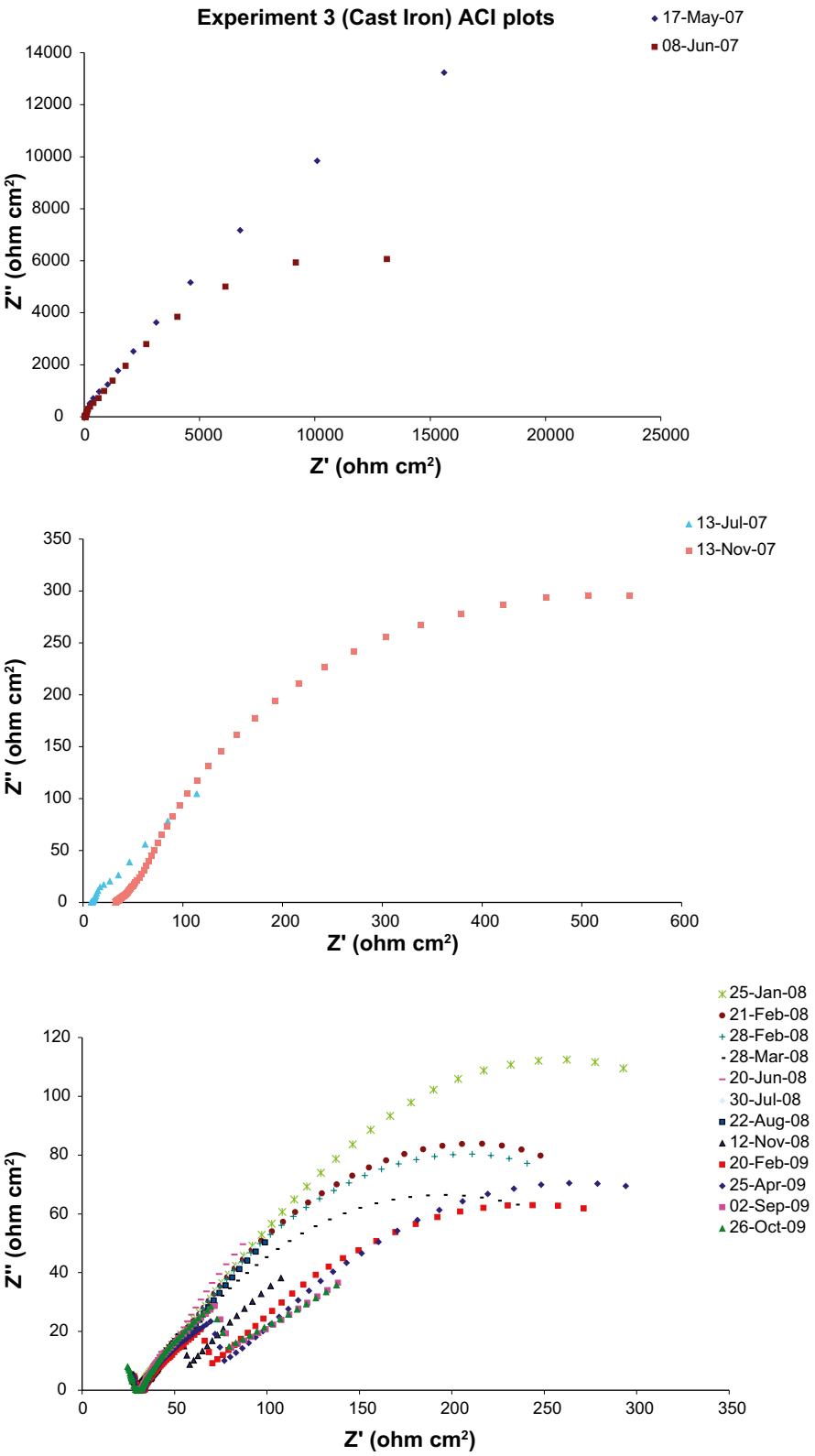

Figure A2-16. *ACI plots of cast iron in Experiment 3 (low density bentonite).*

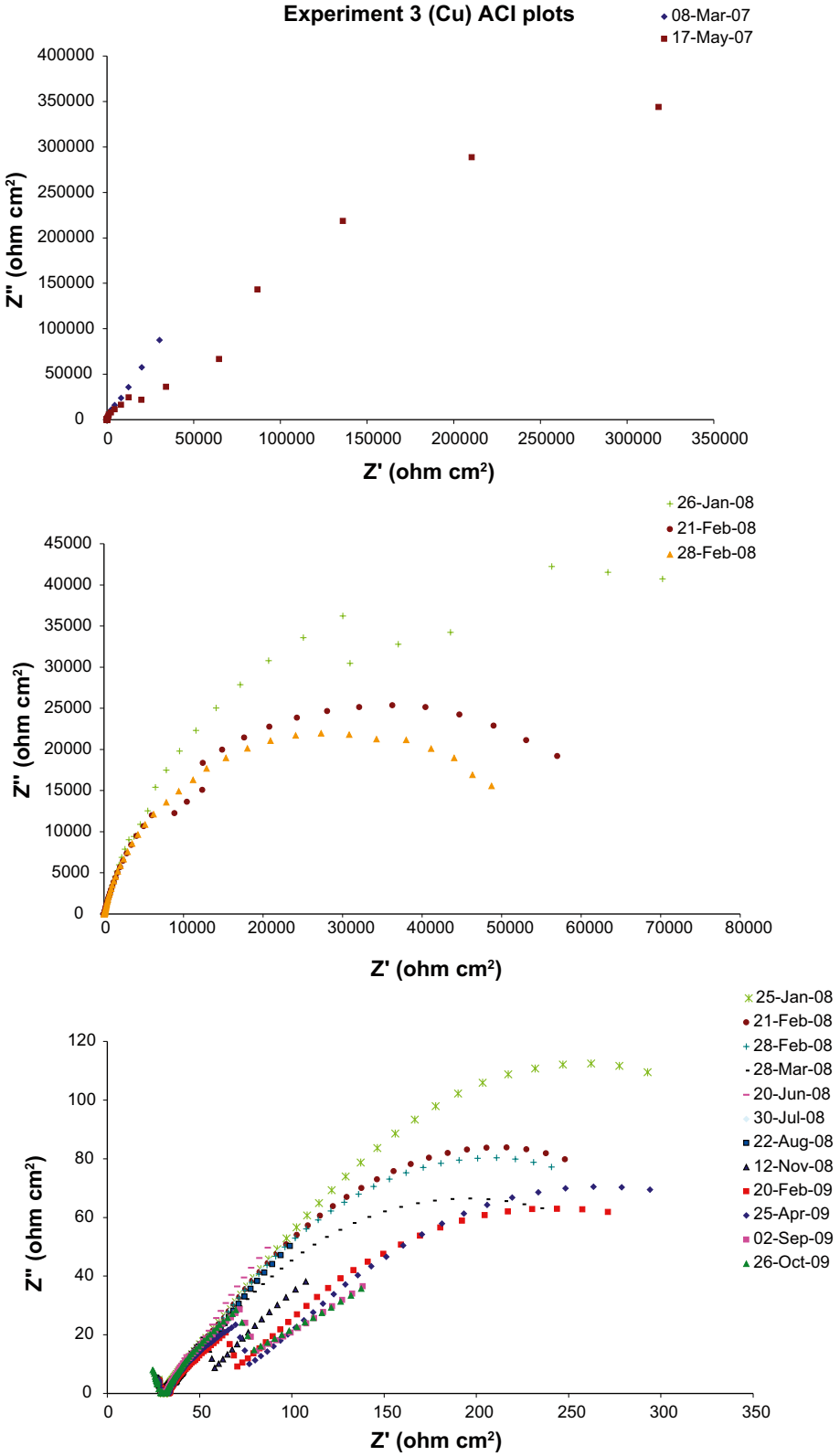

Figure A2-17. *ACI plots of copper in Experiment 3 (low density bentonite).*

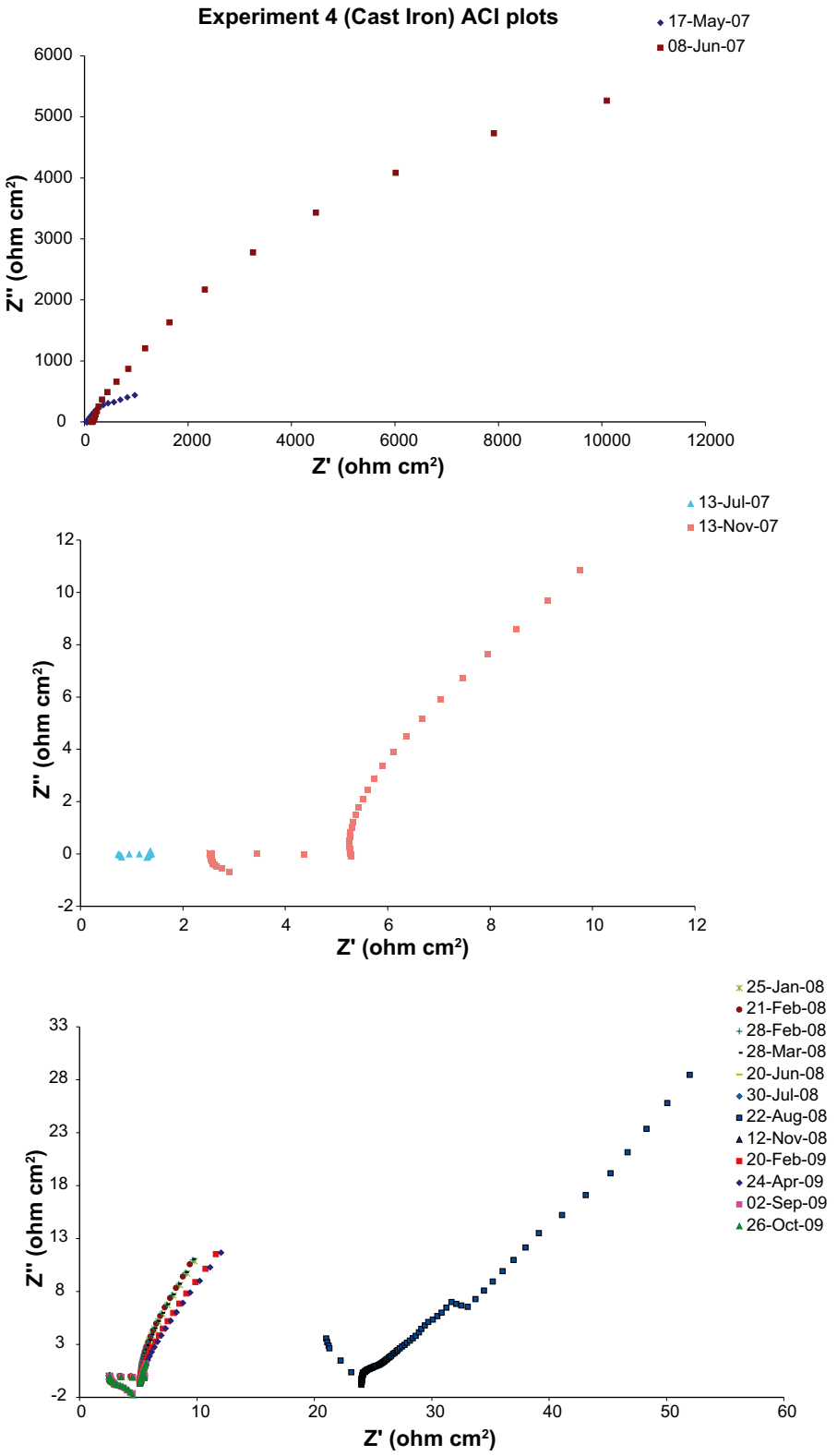

Figure A2-18. *ACI plots of cast iron in Experiment 4 (compacted bentonite). Note: It is likely that the iron electrode was in contact with the stainless steel flange of the support cage for these measurements).*

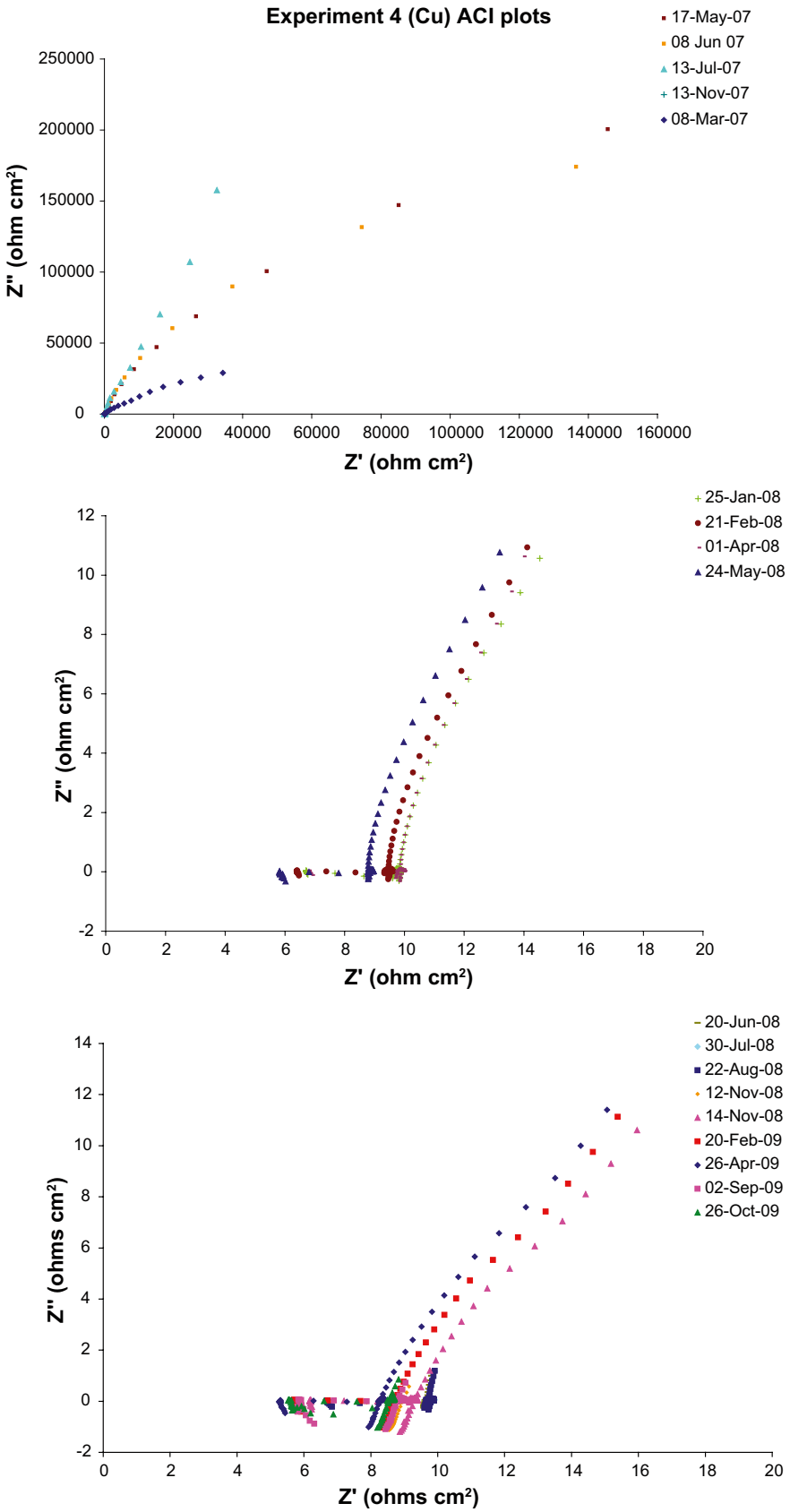

Figure A2-19. *ACI plots of copper in Experiment 4 (compacted bentonite).*

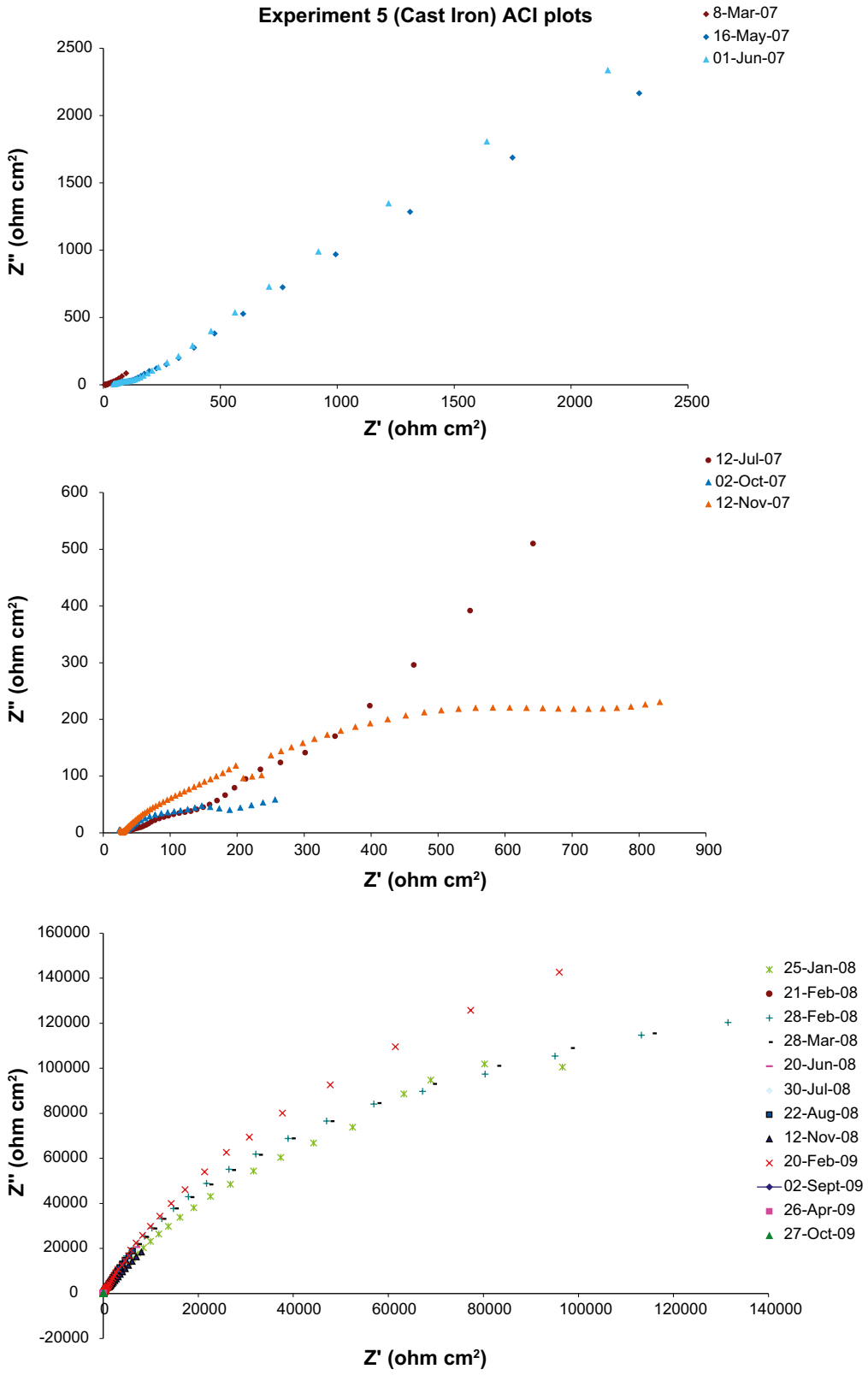

Figure A2-20. *ACI plots of cast iron in Experiment 5 (no bentonite).*

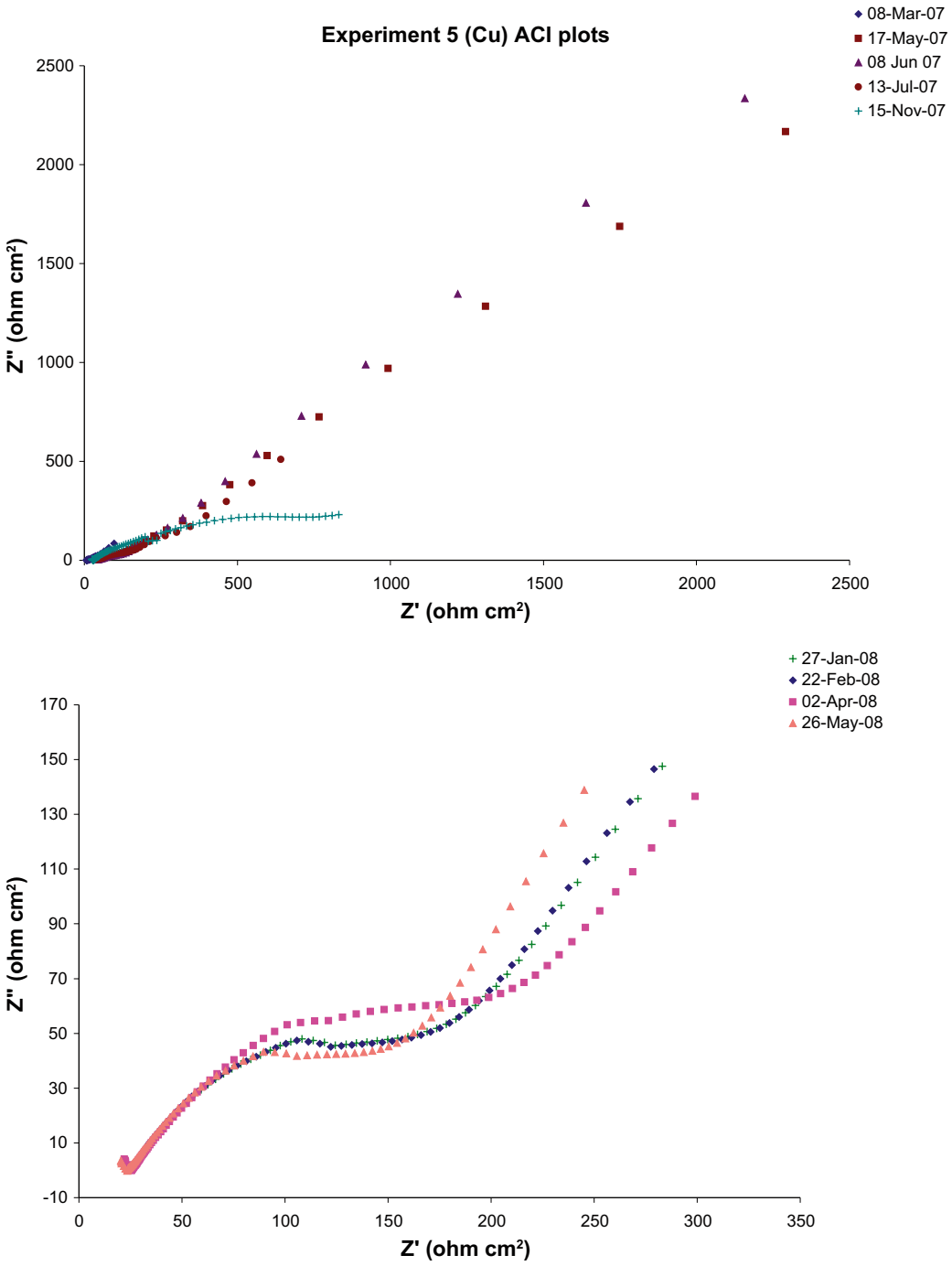

Figure A2-21. *ACI plots of copper in Experiment 5 (no bentonite).*

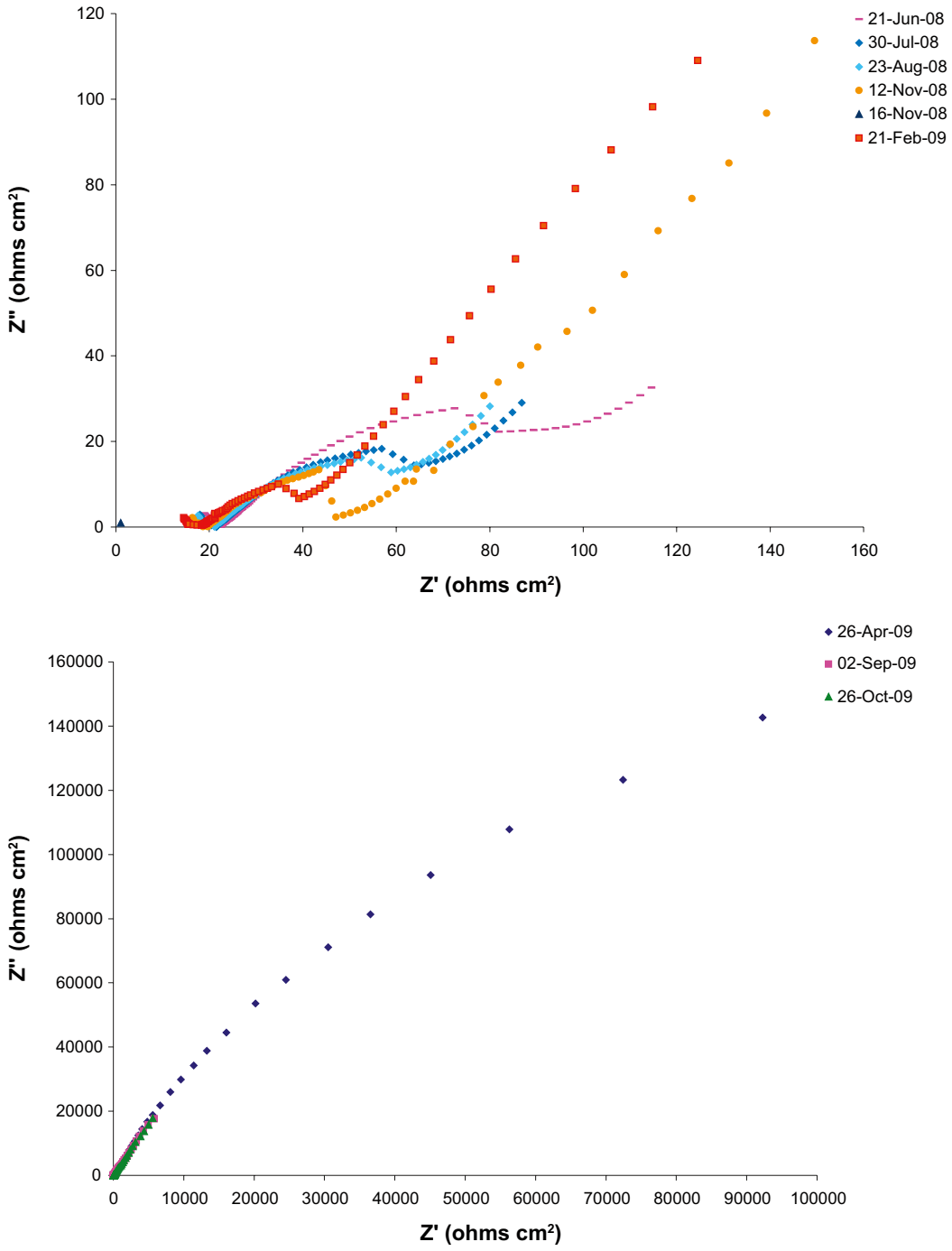

Figure A2-22. *ACI plots of copper in Experiment 5 (no bentonite).*

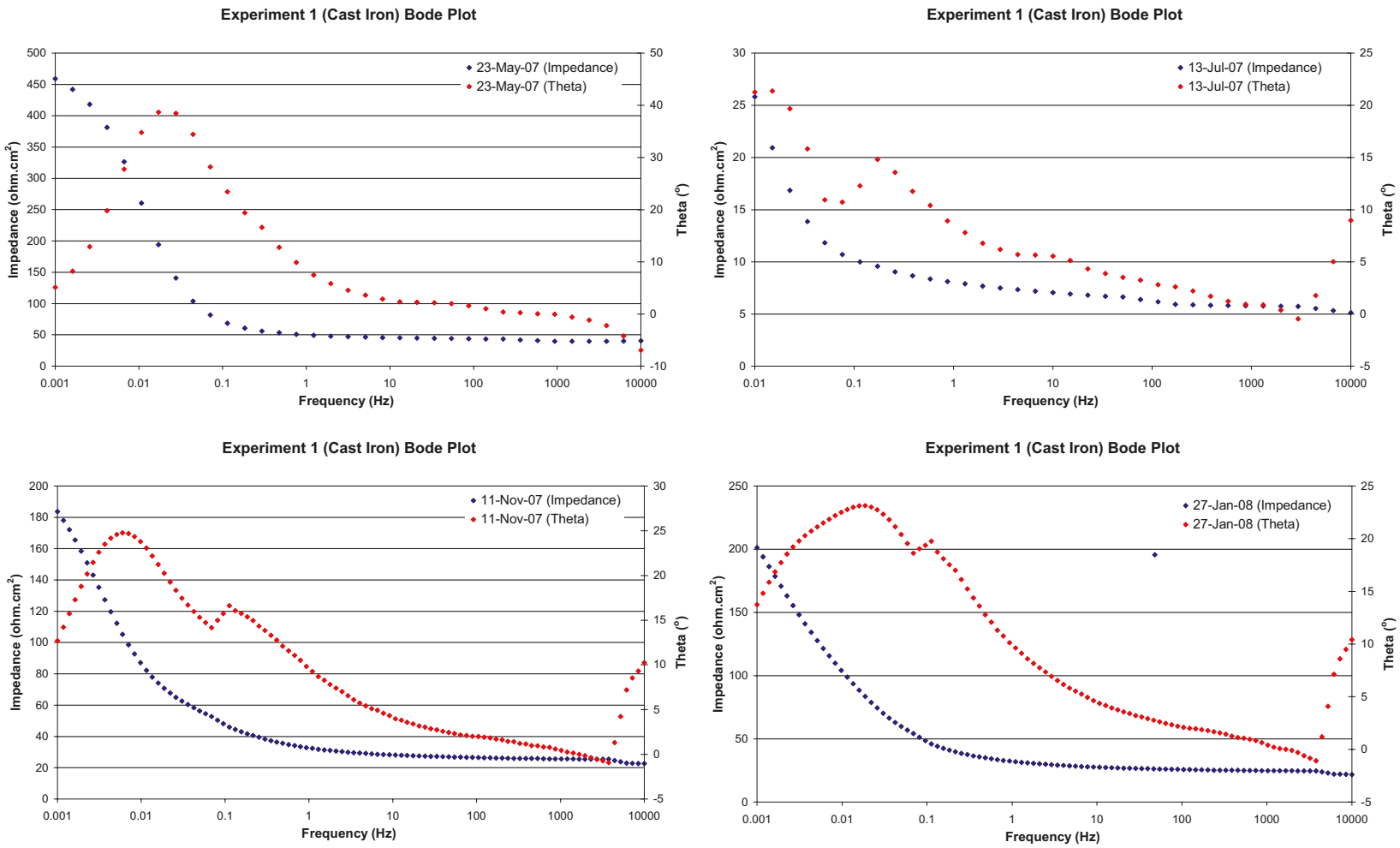

Figure A2-23. *Bode plots of cast iron in Experiment 1 (low density bentonite).*

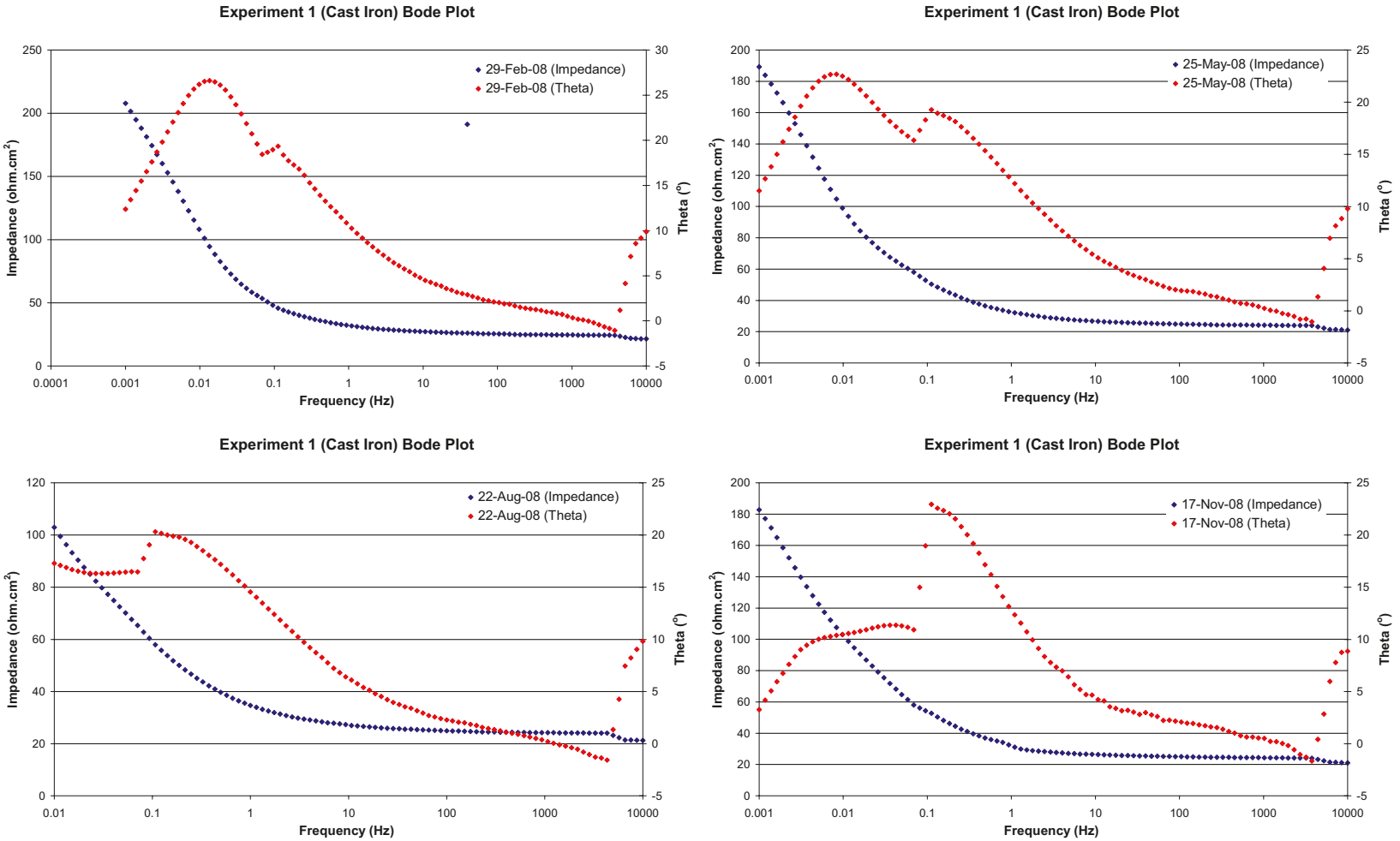

Figure A2-24. *Bode plots of cast iron in Experiment 1 (low density bentonite).*

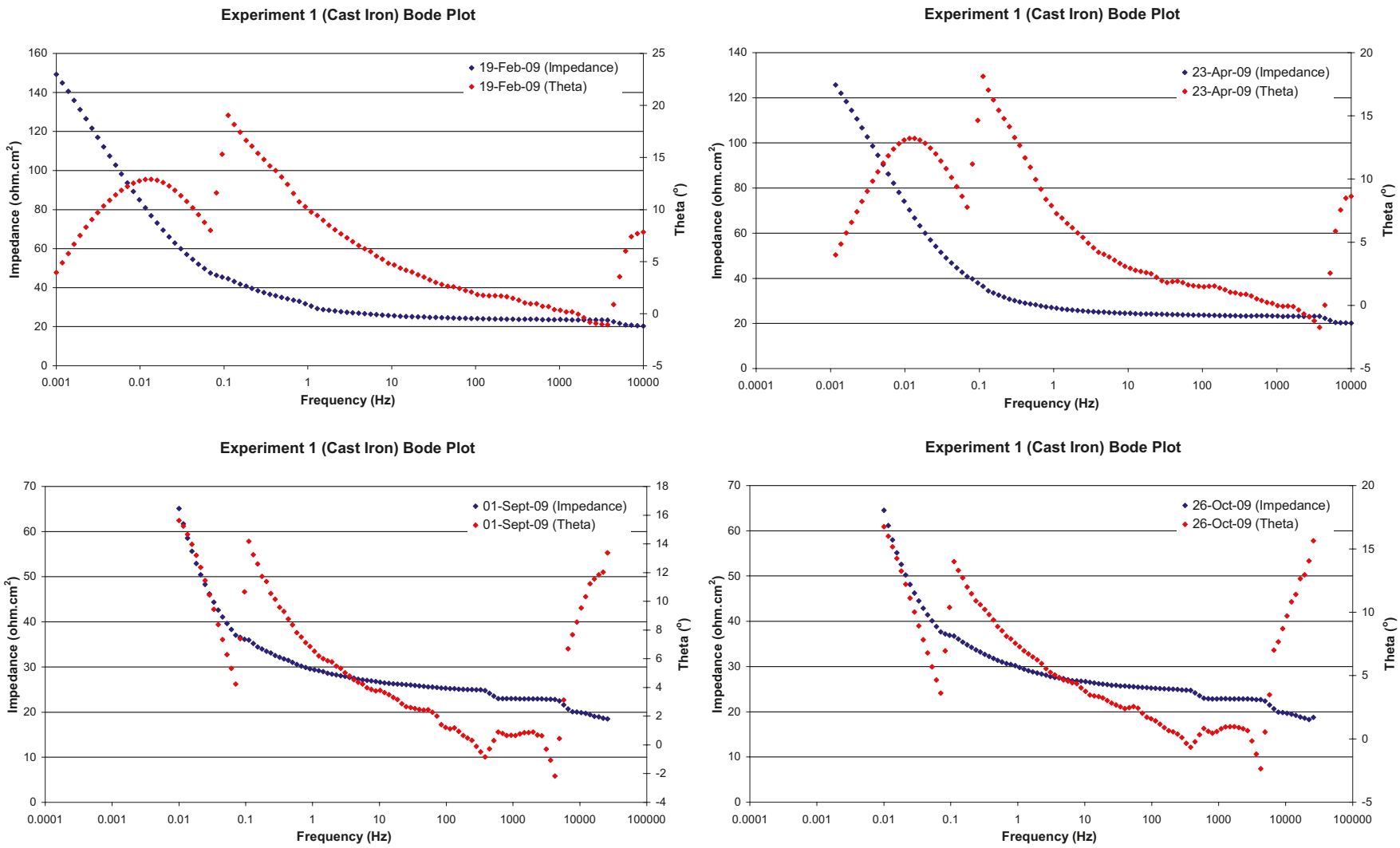

Figure A2-25. *Bode plots of cast iron in Experiment 1 (low density bentonite).*

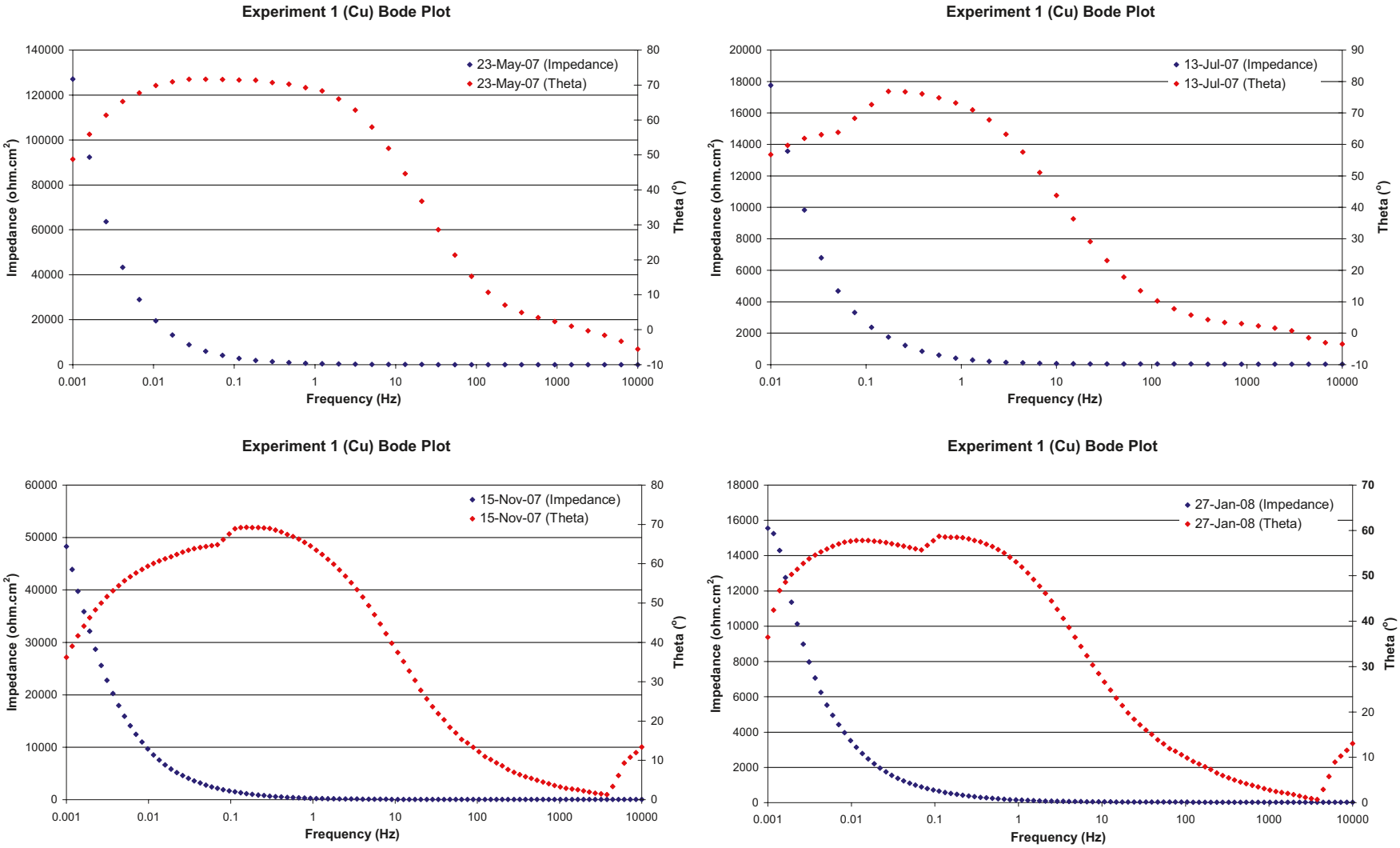

Figure A2-26. *Bode plots of copper in Experiment 1 (low density bentonite).*

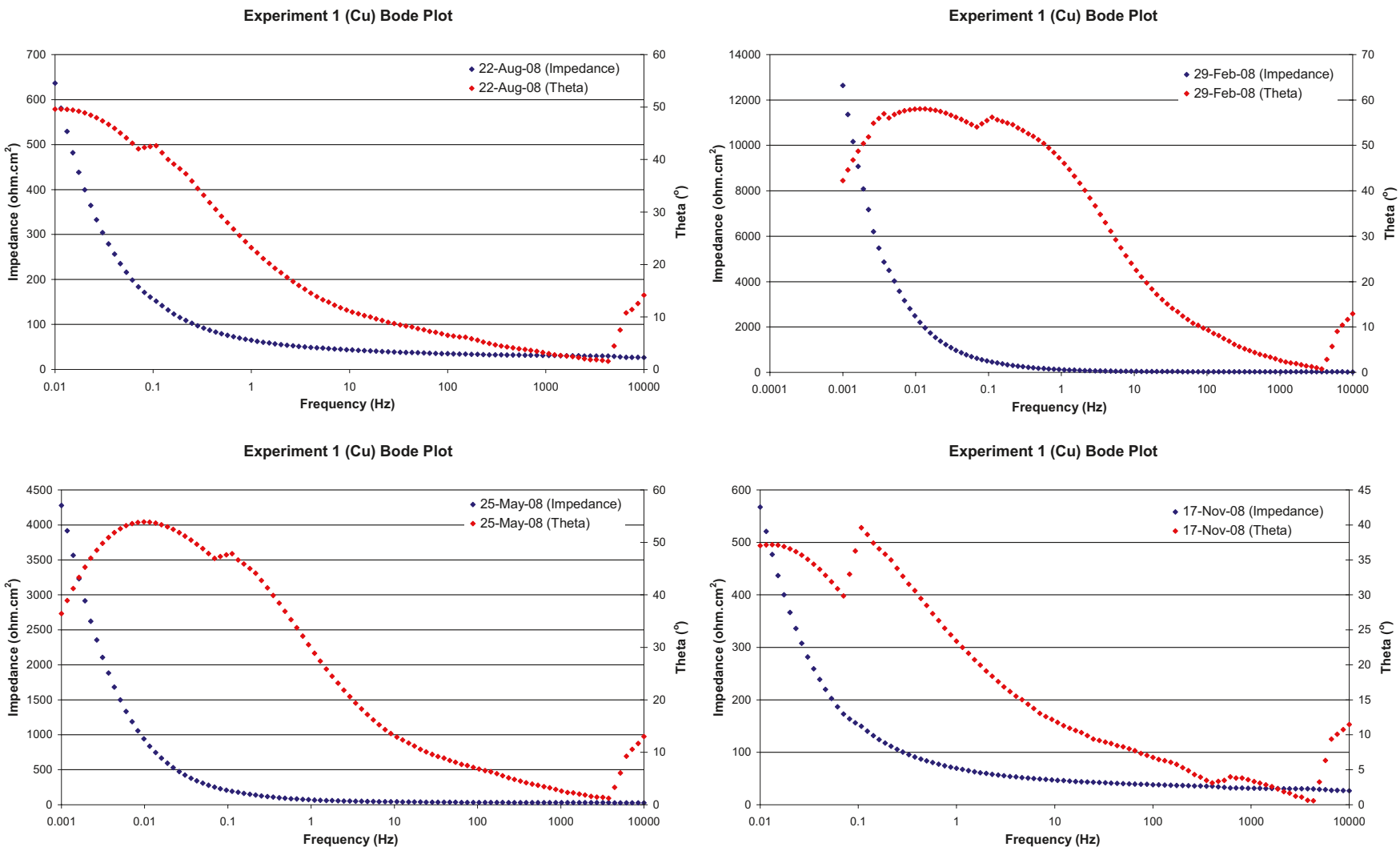

Figure A2-27. *Bode plots of copper in Experiment 1 (low density bentonite).*

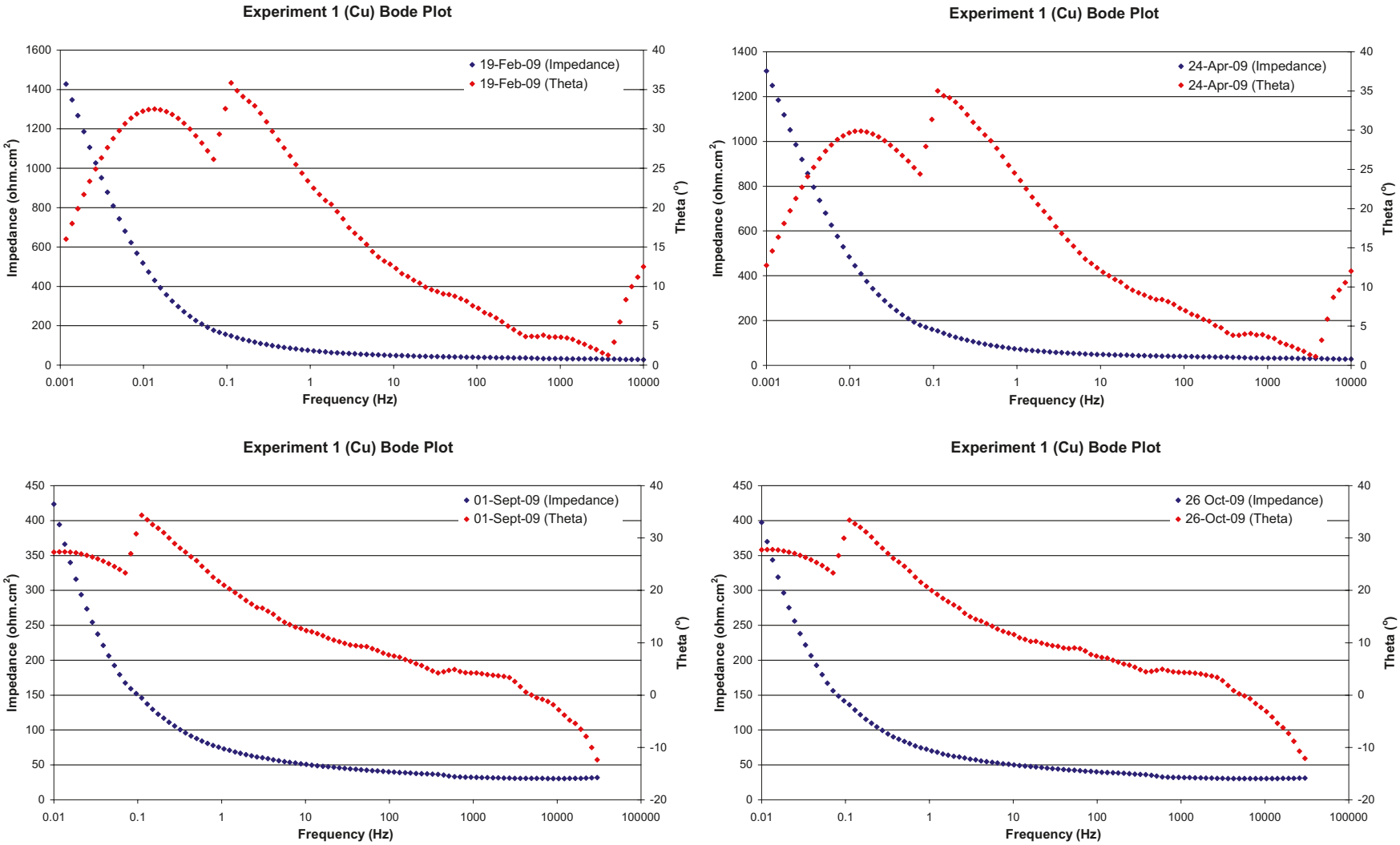

Figure A2-28. *Bode plots of copper in Experiment 1 (low density bentonite).*

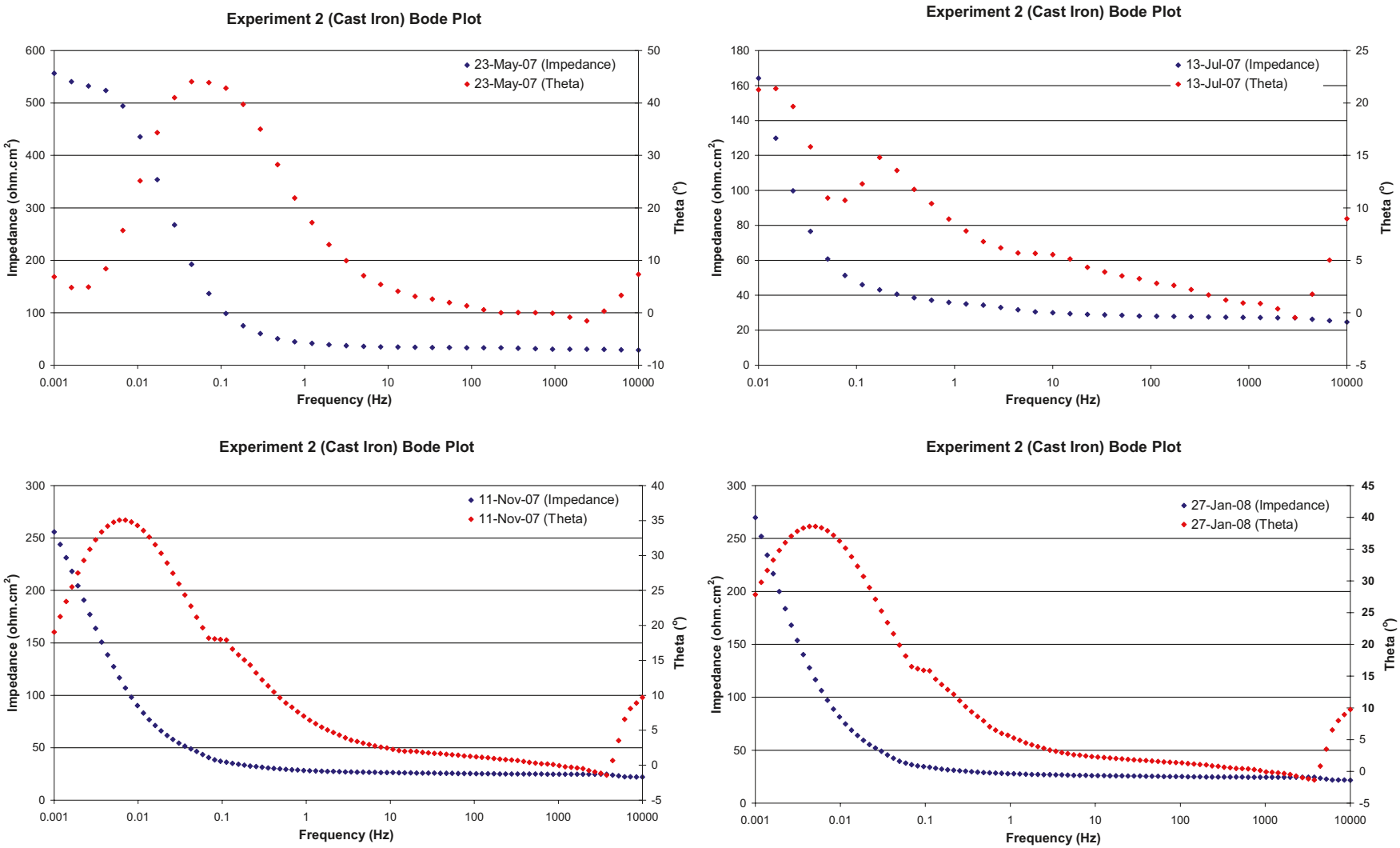

Figure A2-29. *Bode plots of Cast Iron in Experiment 2 (low density bentonite).*

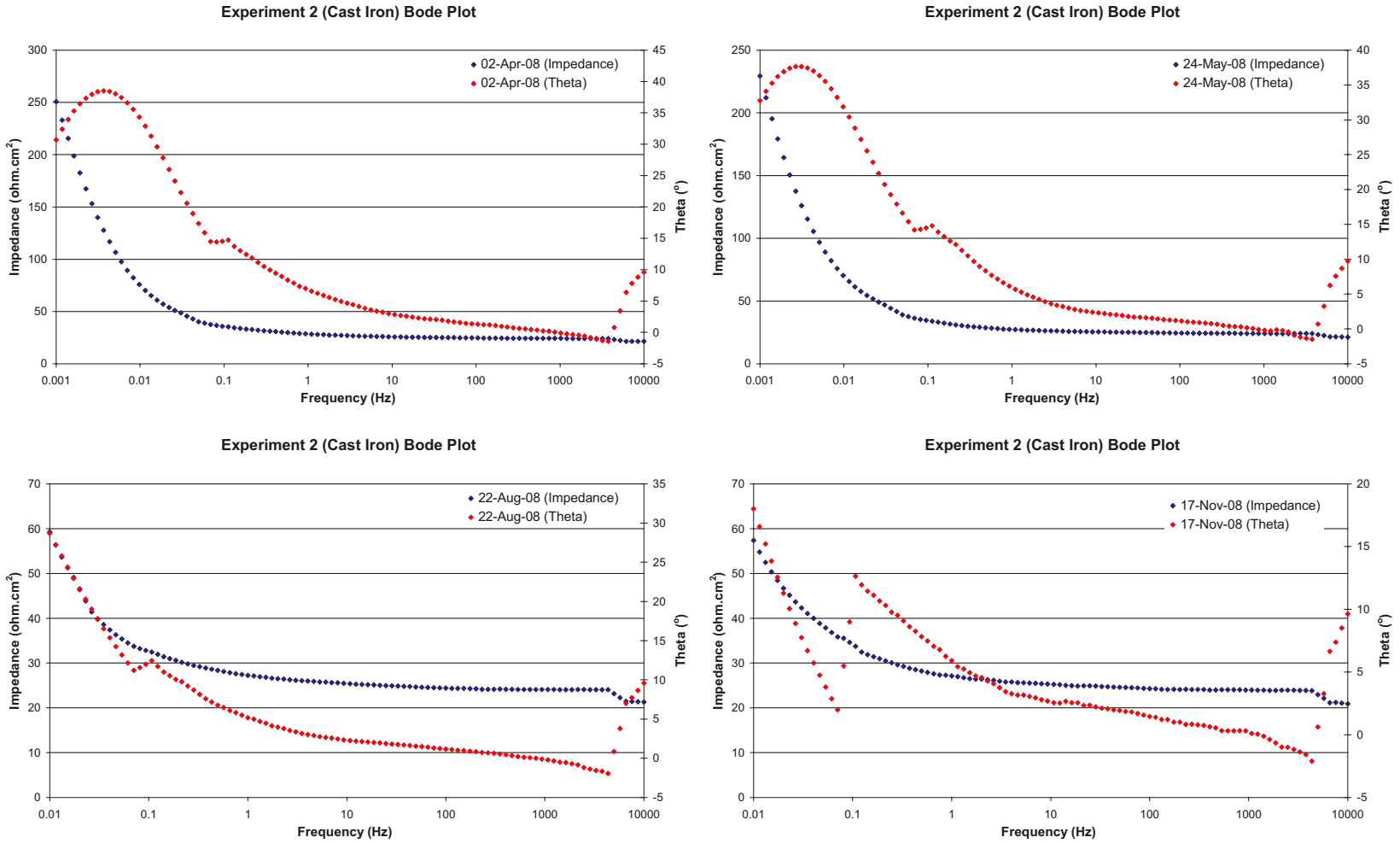

Figure A2-30. *Bode plots of Cast Iron in Experiment 2 (low density bentonite).*

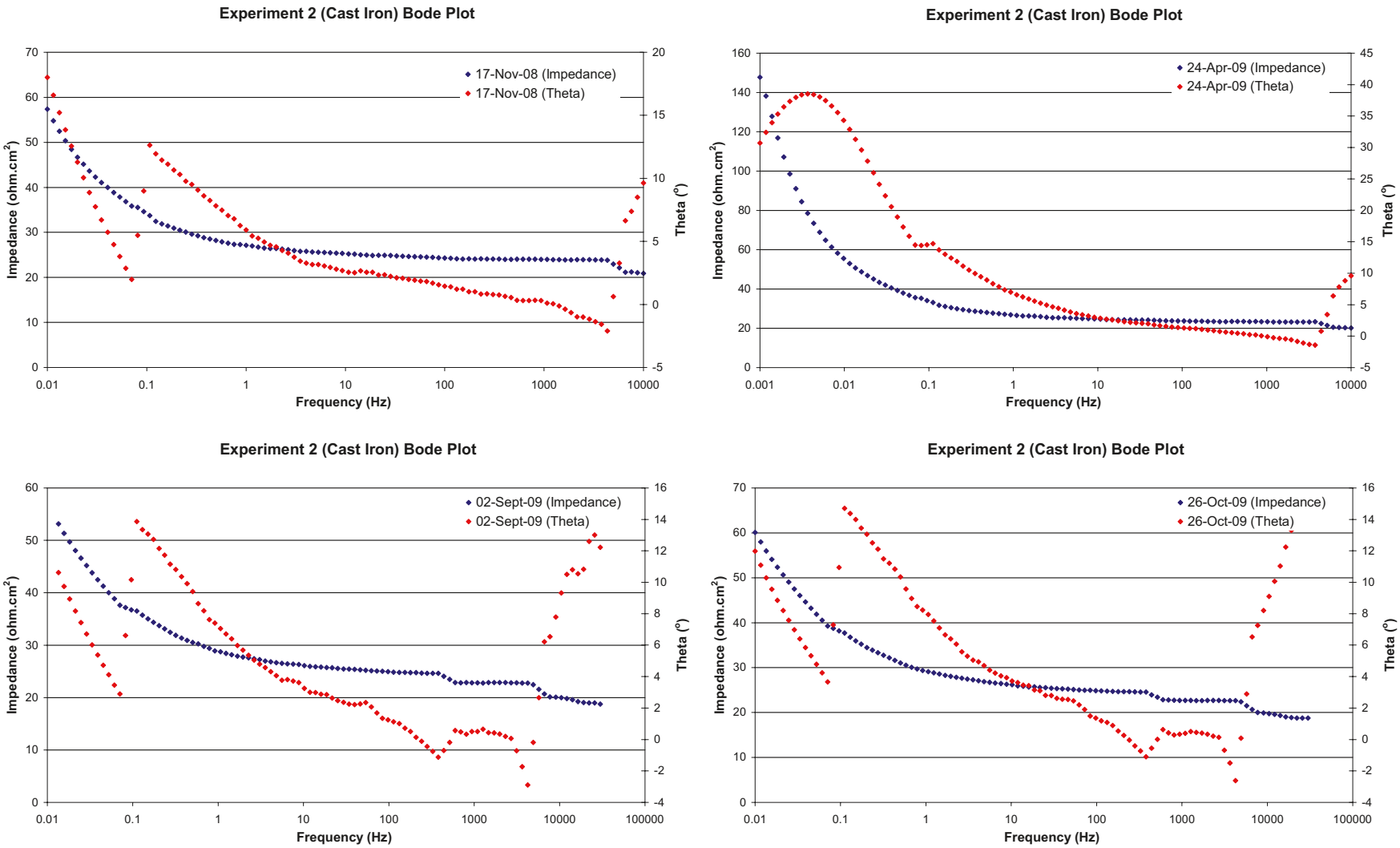

Figure A2-31. *Bode plots of Cast Iron in Experiment 2 (low density bentonite).*

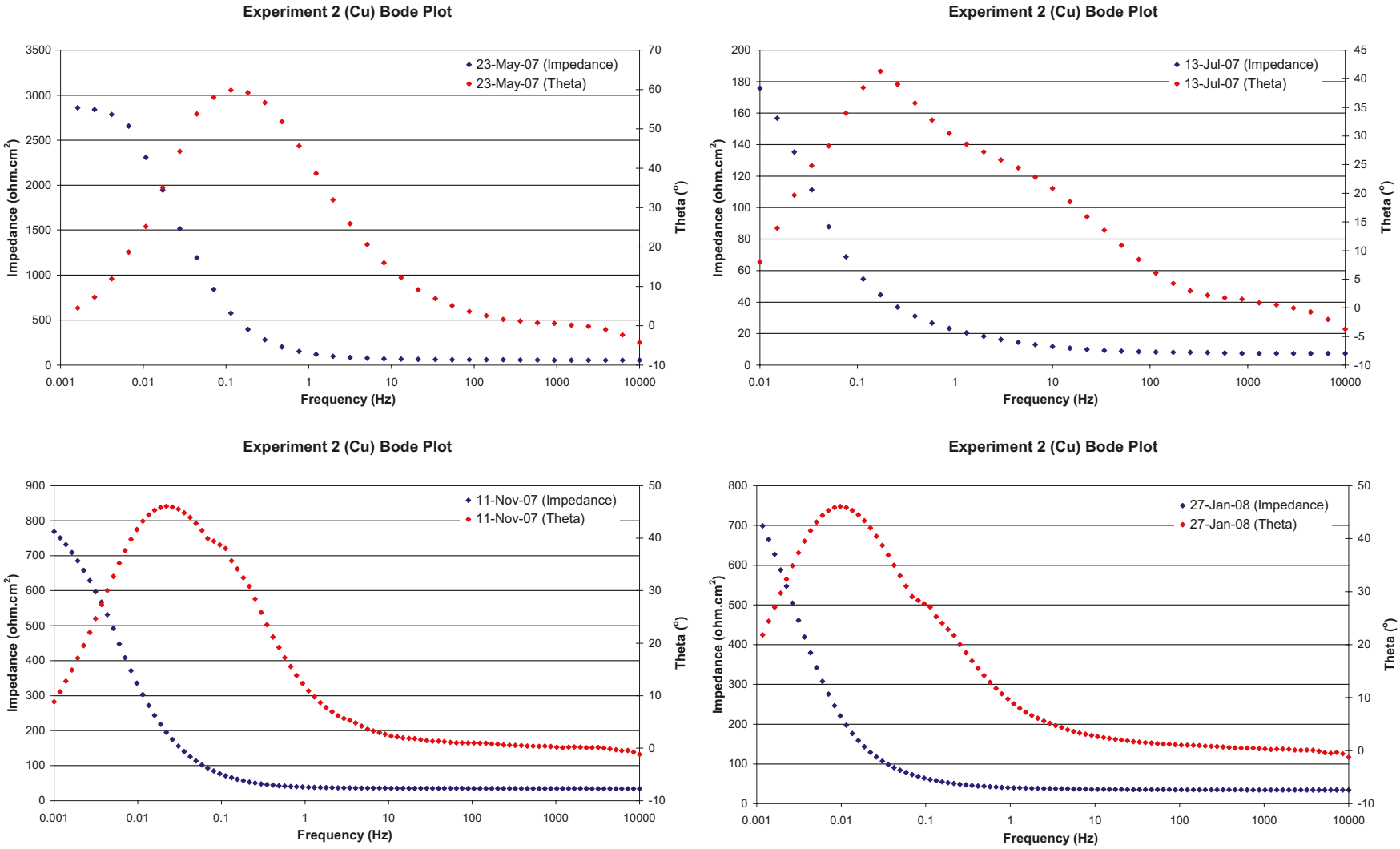

Figure A2-32. *Bode plots of copper in Experiment 2 (low density bentonite).*

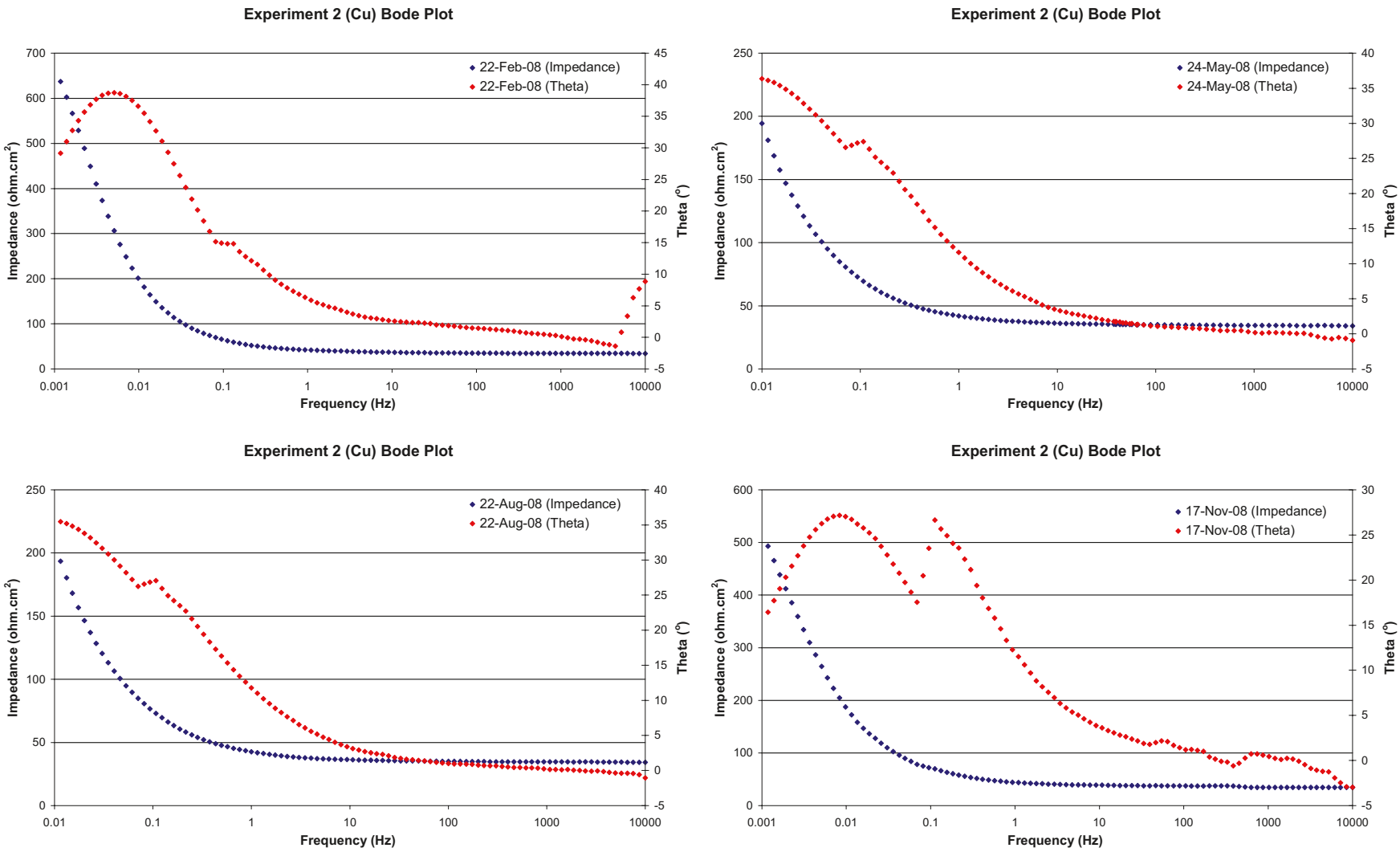

Figure A2-33. *Bode plots of copper in Experiment 2 (low density bentonite).*

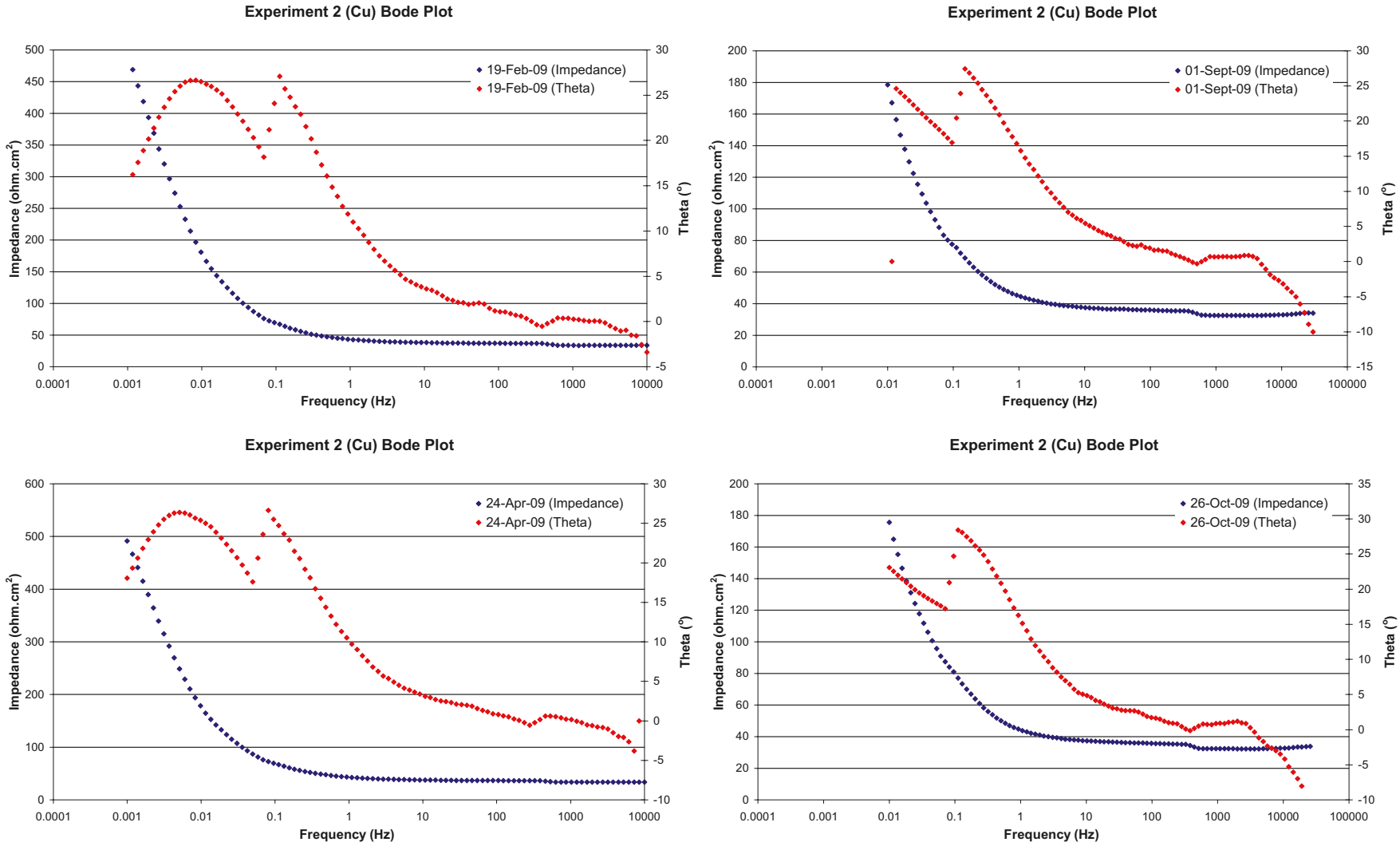

Figure A2-34. *Bode plots of copper in Experiment 2 (low density bentonite).*

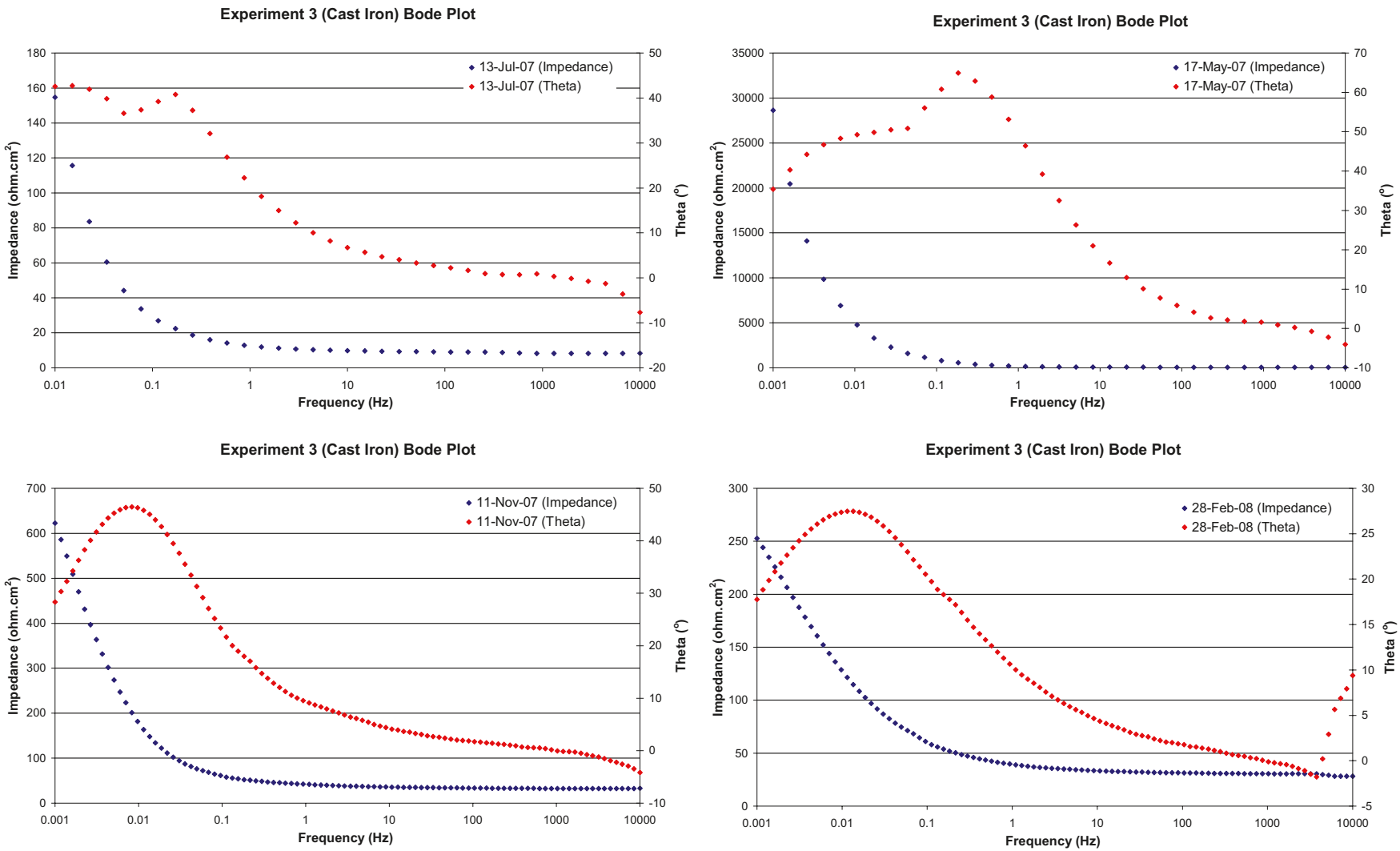

Figure A2-35. *Bode plots of cast iron in Experiment 3 (low density bentonite).*

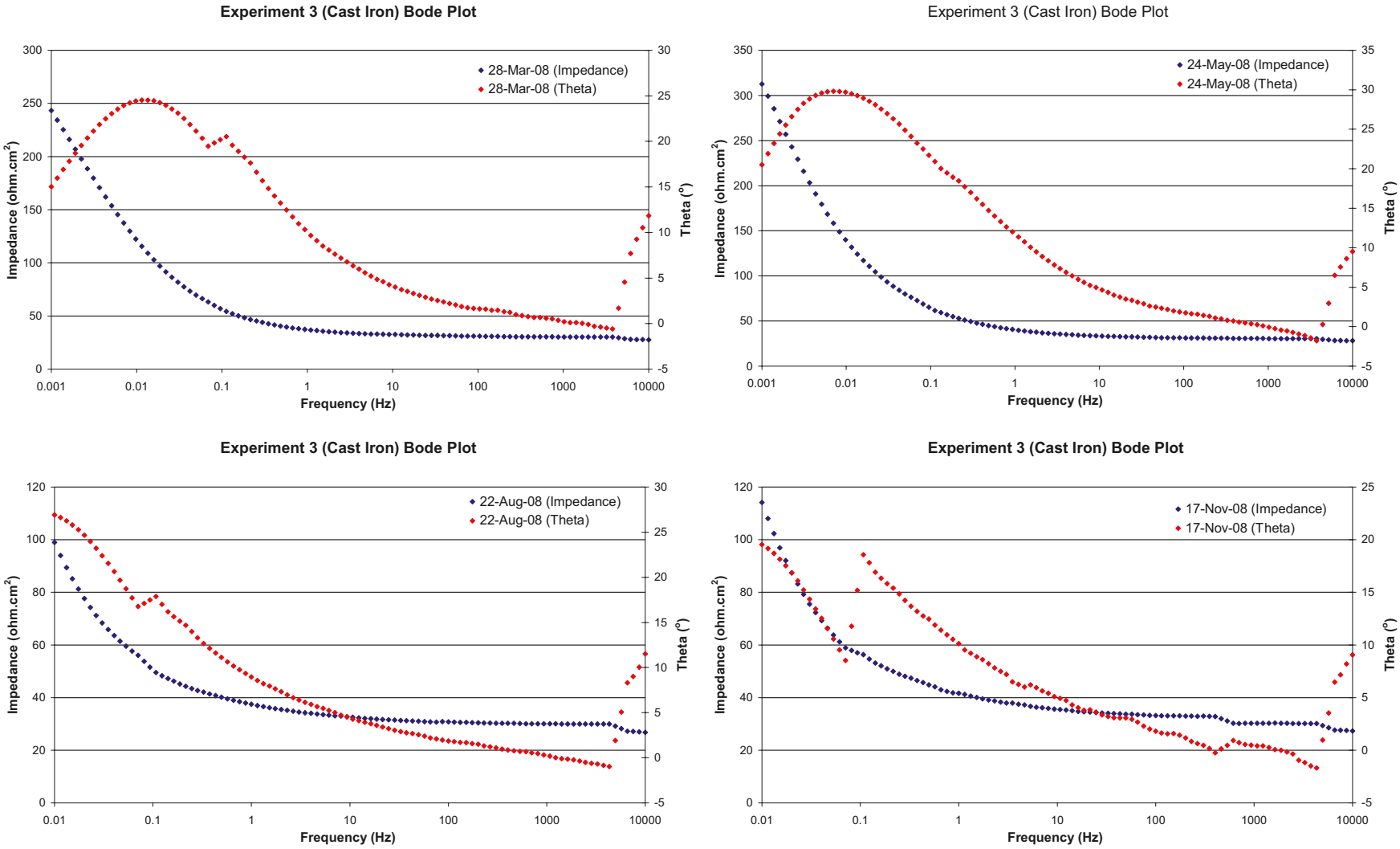

Figure A2-36. *Bode plots of cast iron in Experiment 3 (low density bentonite).*

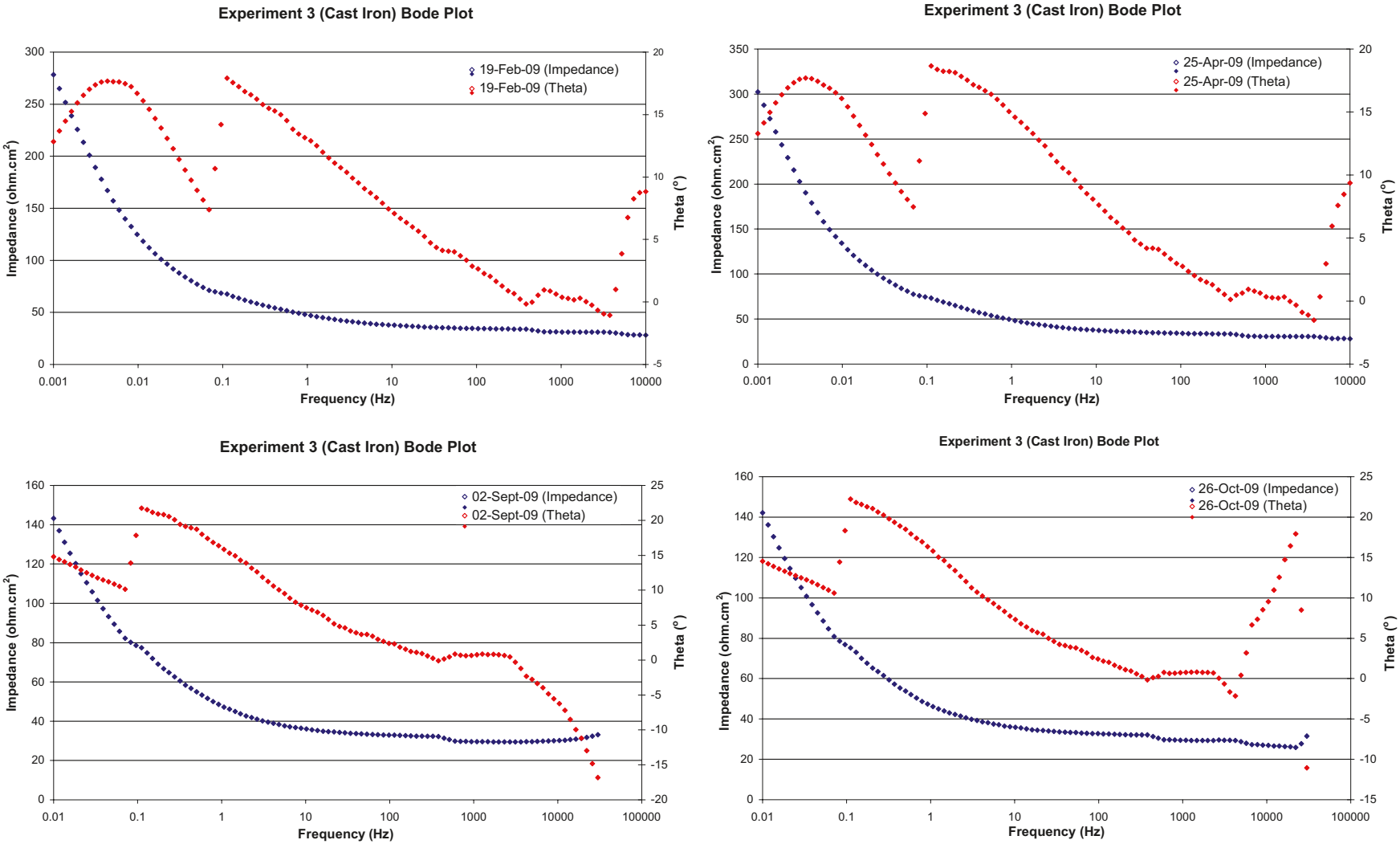

Figure A2-37. *Bode plots of cast iron in Experiment 3 (low density bentonite).*

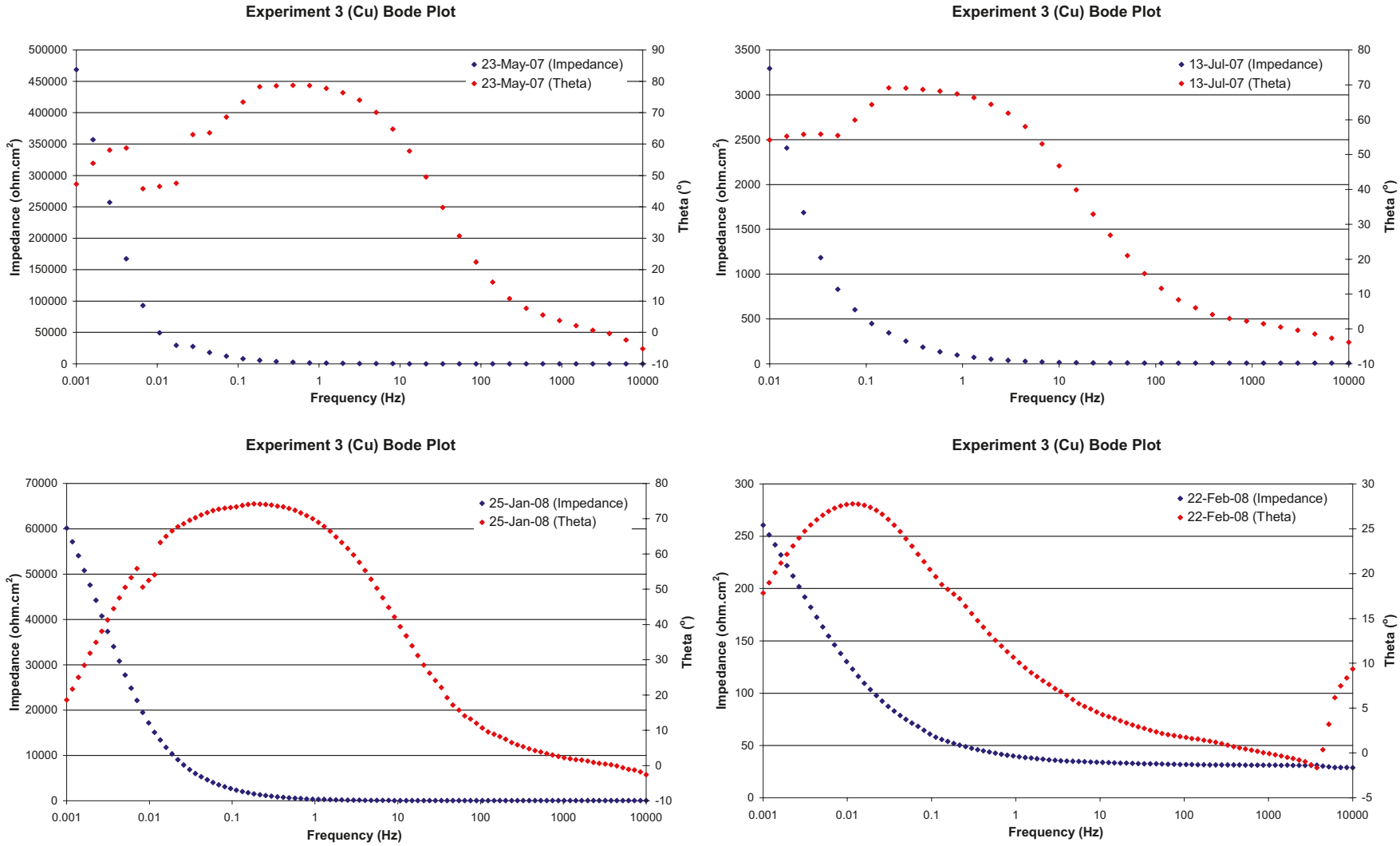

Figure A2-38. *Bode plots of copper in Experiment 3 (low density bentonite).*

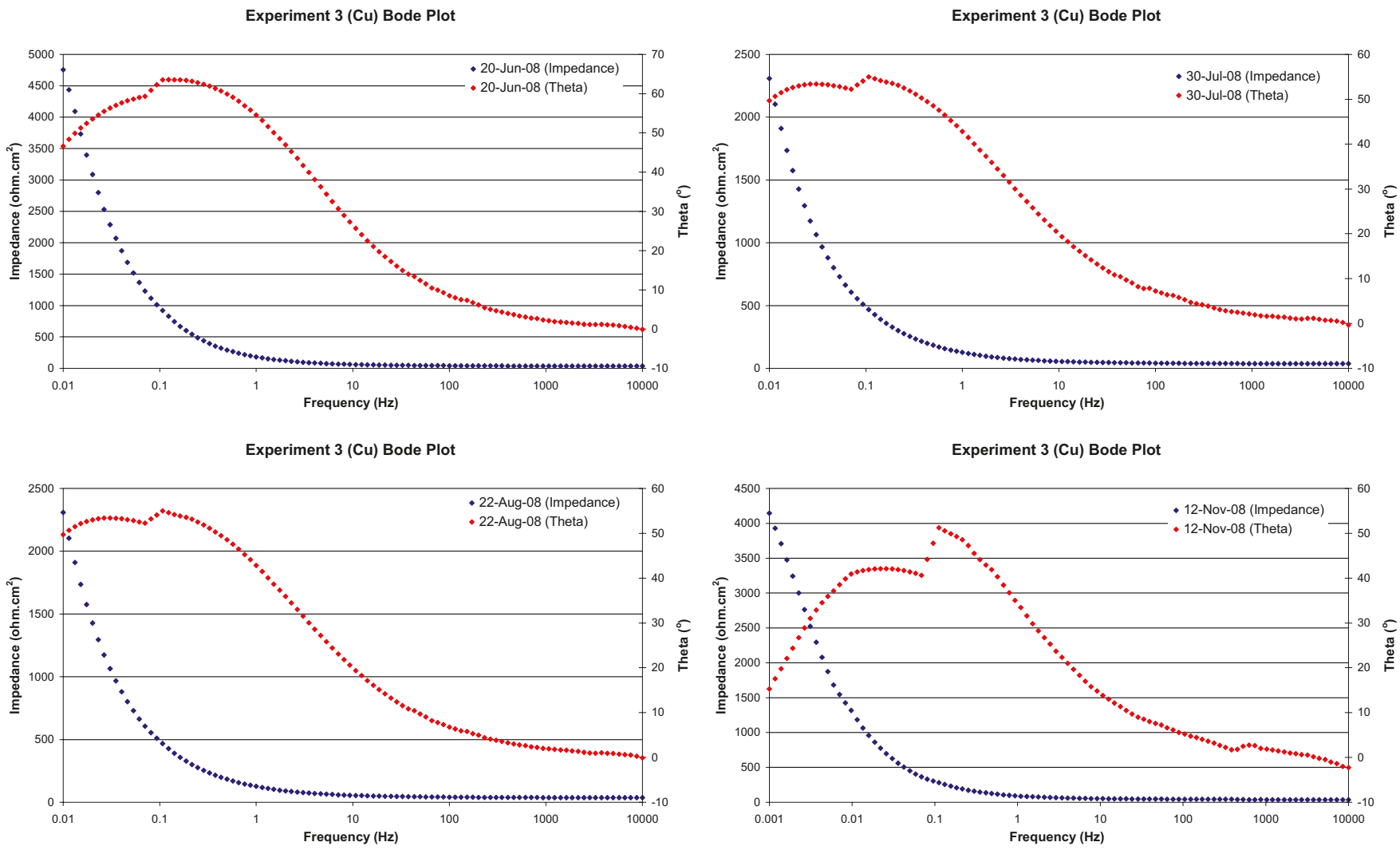

Figure A2-39. *Bode plots of copper in Experiment 3 (low density bentonite).*

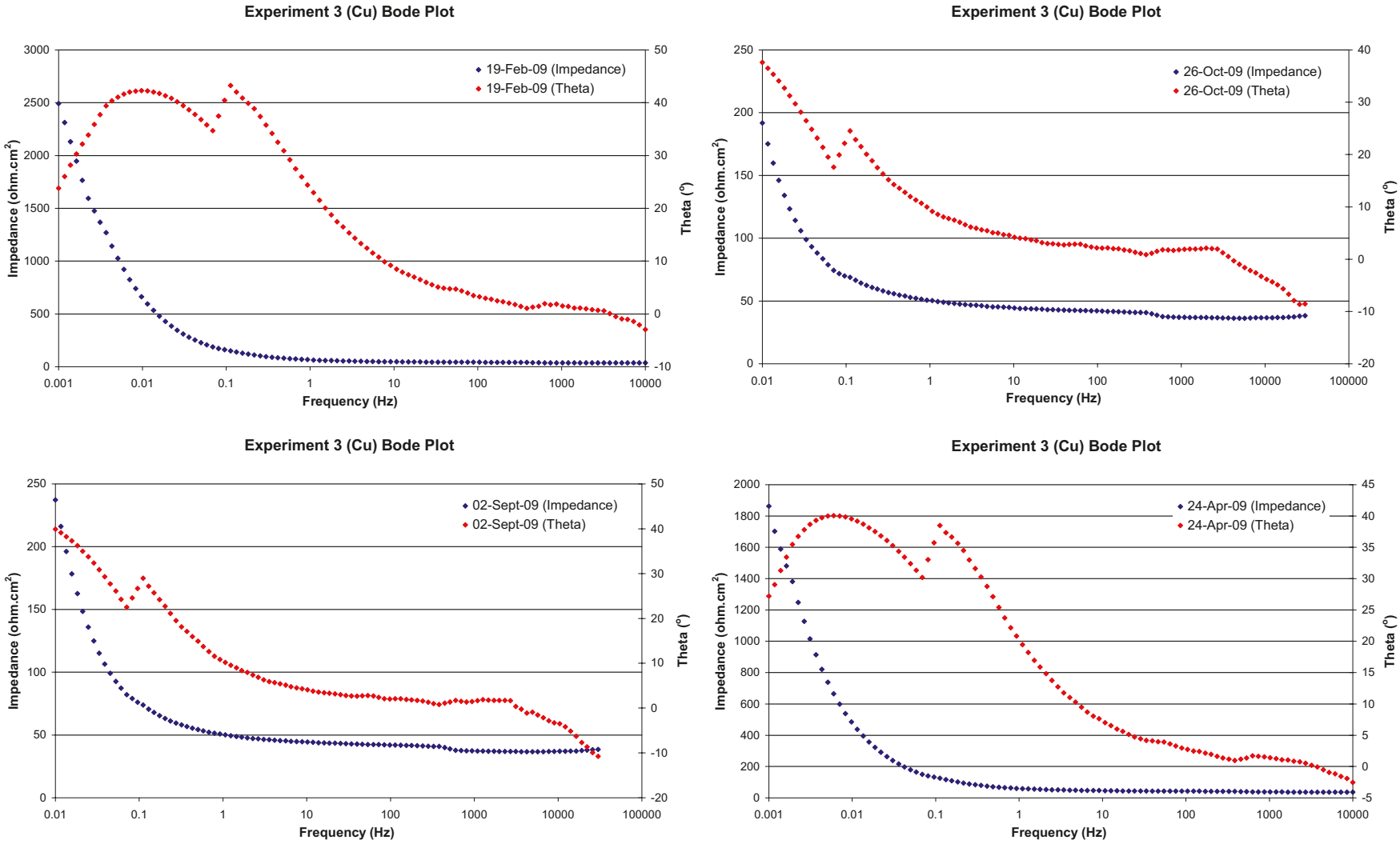

Figure A2-40. *Bode plots of copper in Experiment 3 (low density bentonite).*

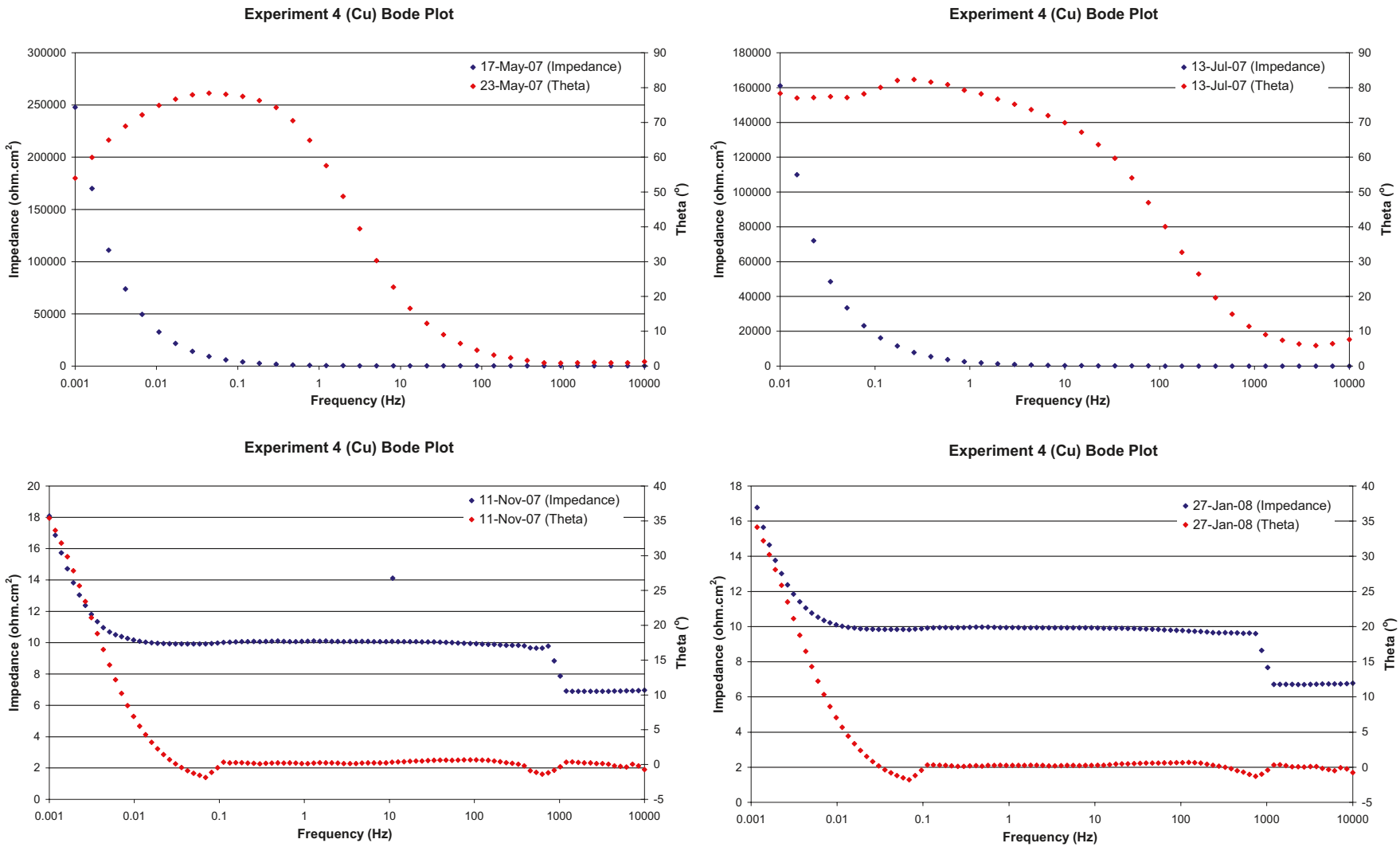

Figure A2-41. *Bode plots of copper in Experiment 4 (compacted bentonite).*

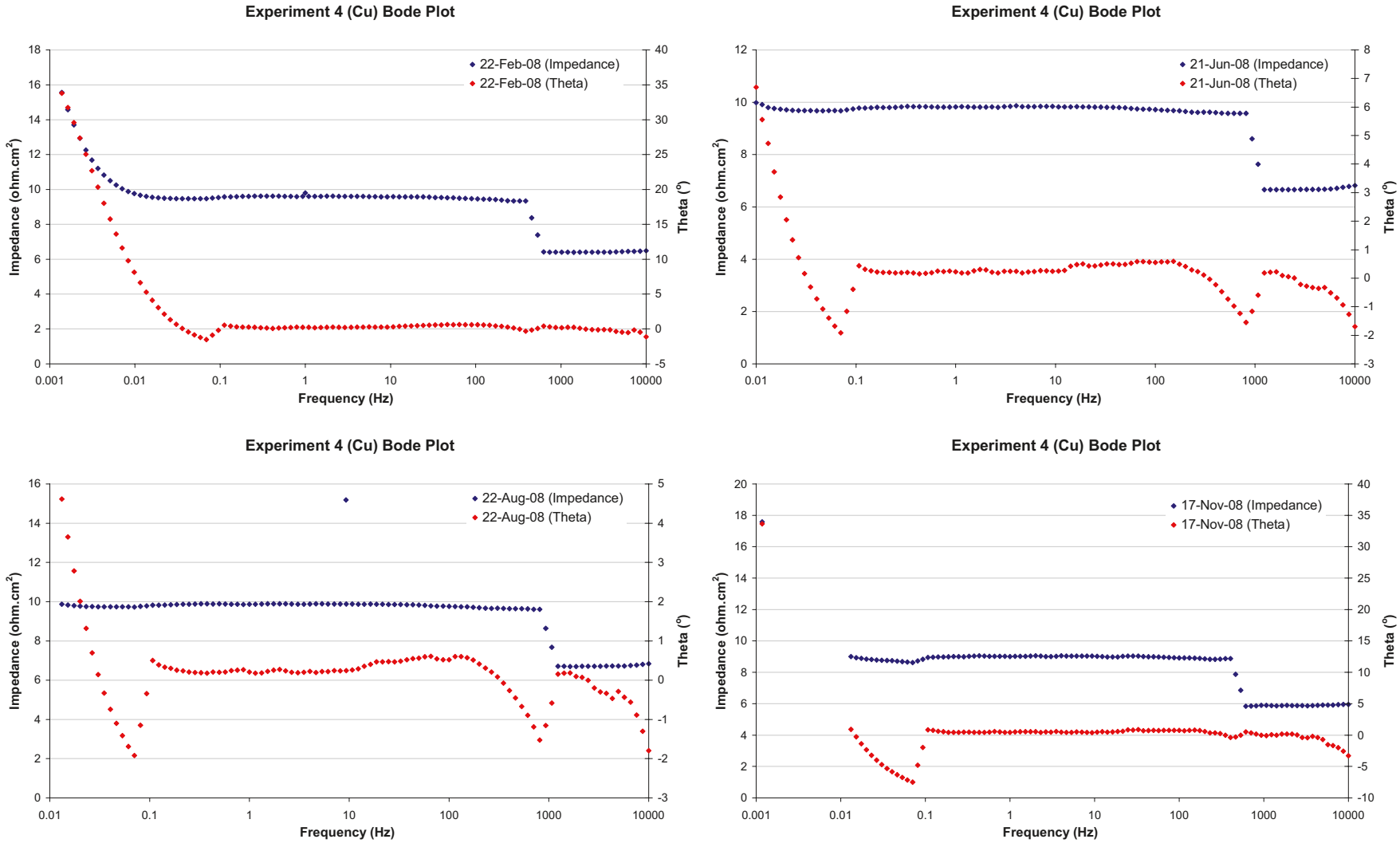

Figure A2-42. *Bode plots of copper in Experiment 4 (compacted bentonite).*

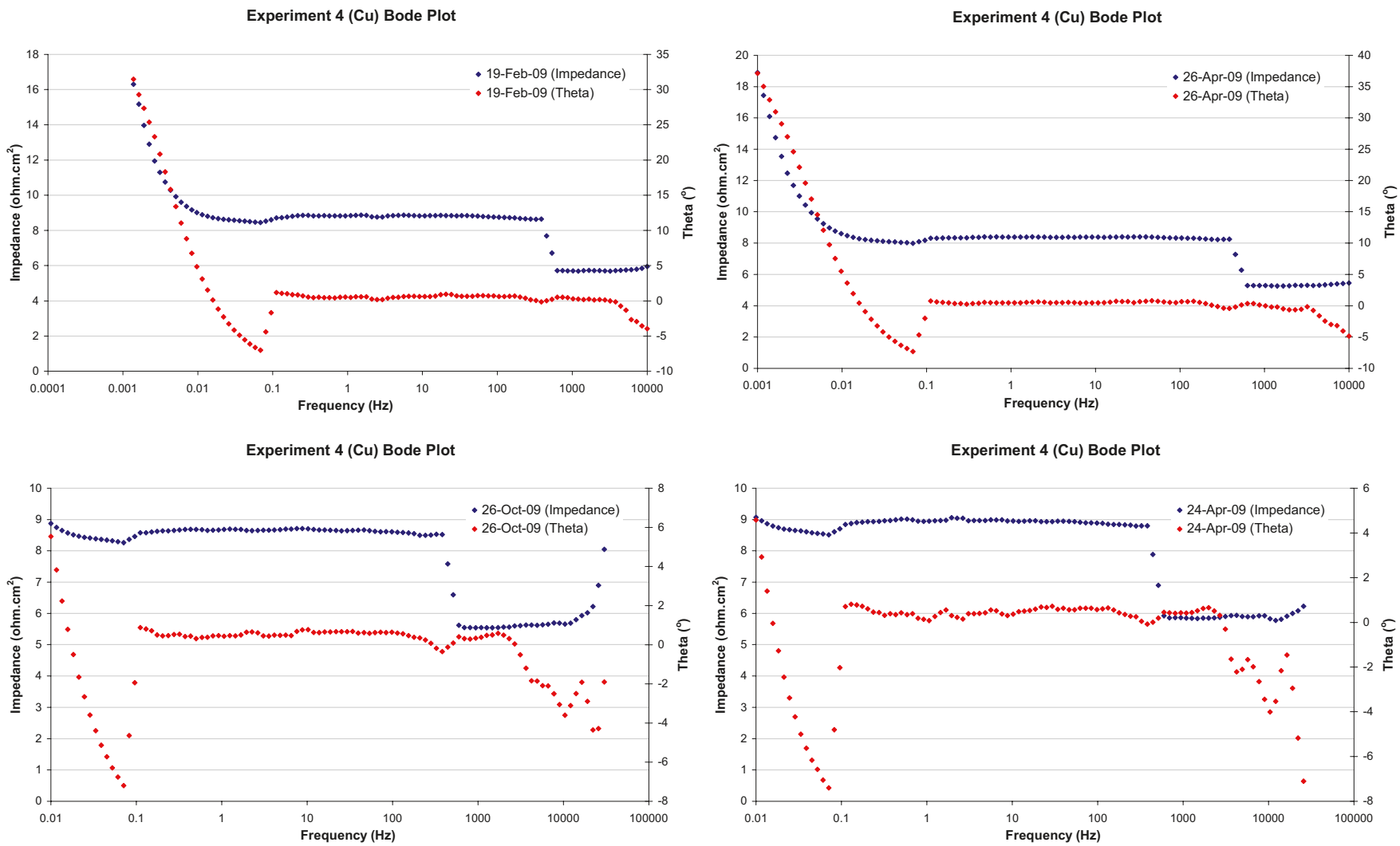

Figure A2-43. *Bode plots of copper in Experiment 4 (compacted bentonite).*

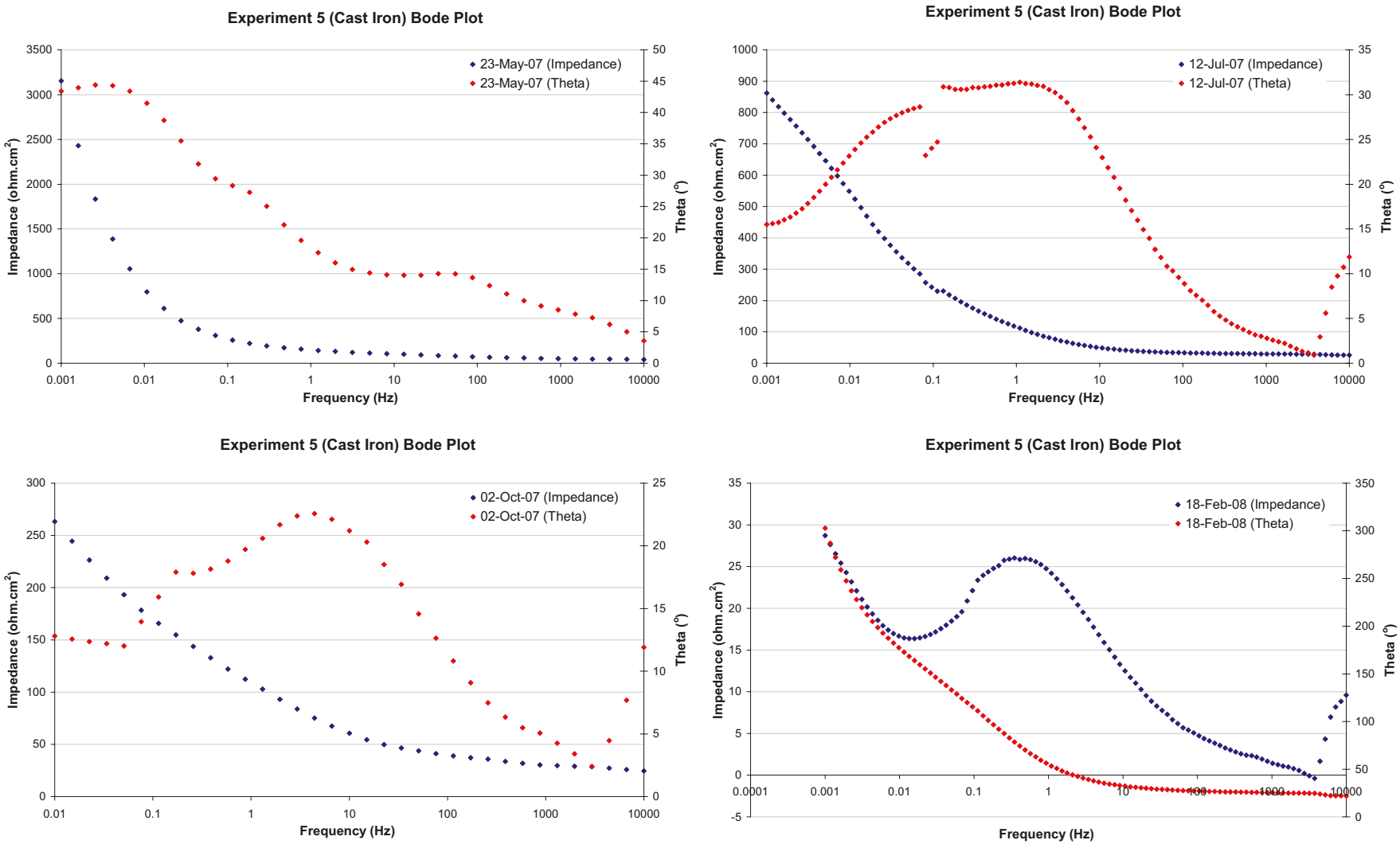

Figure A2-44. *Bode plots of cast iron in Experiment 5 (no bentonite).*

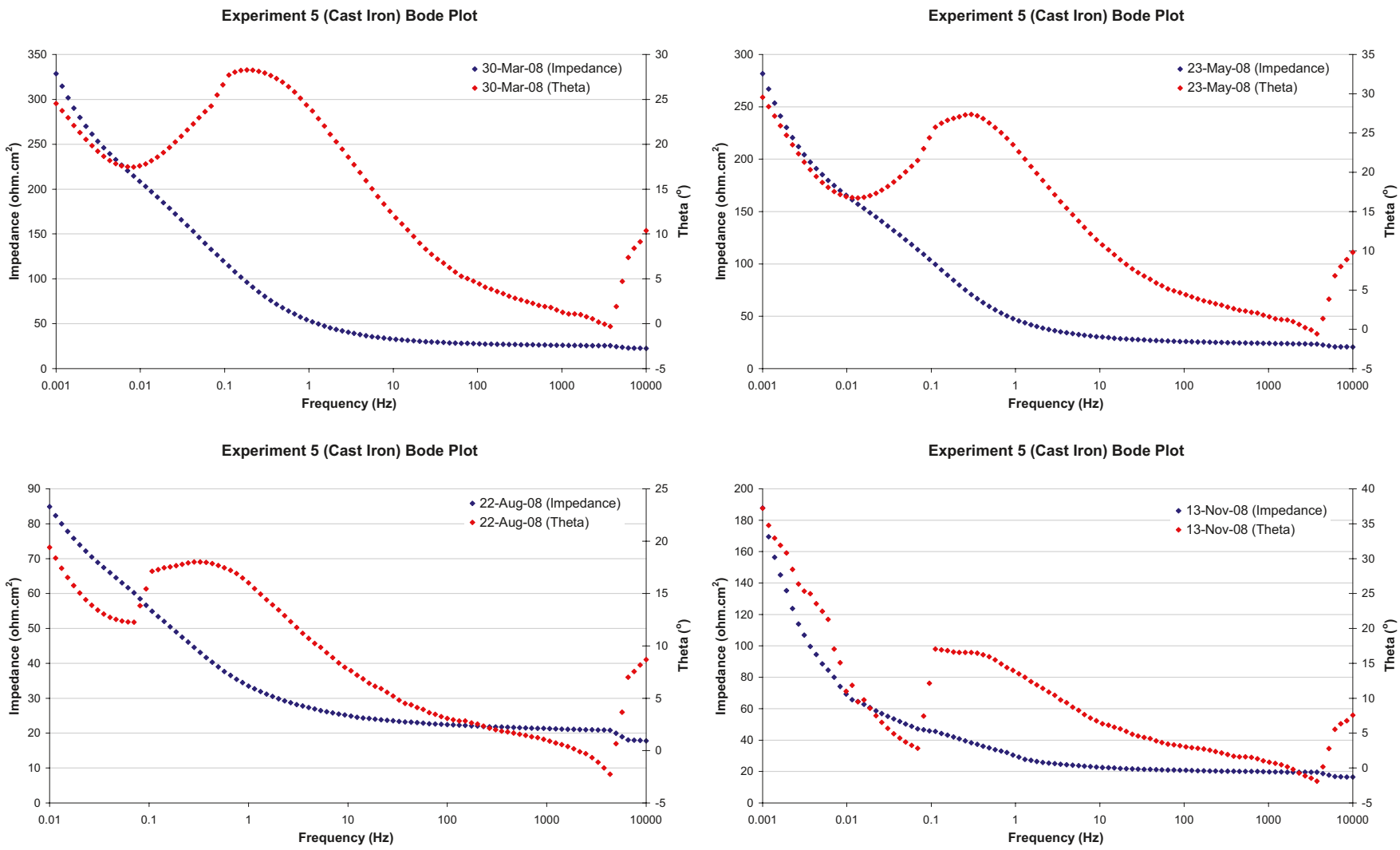

Figure A2-45. *Bode plots of cast iron in Experiment 5 (no bentonite).*

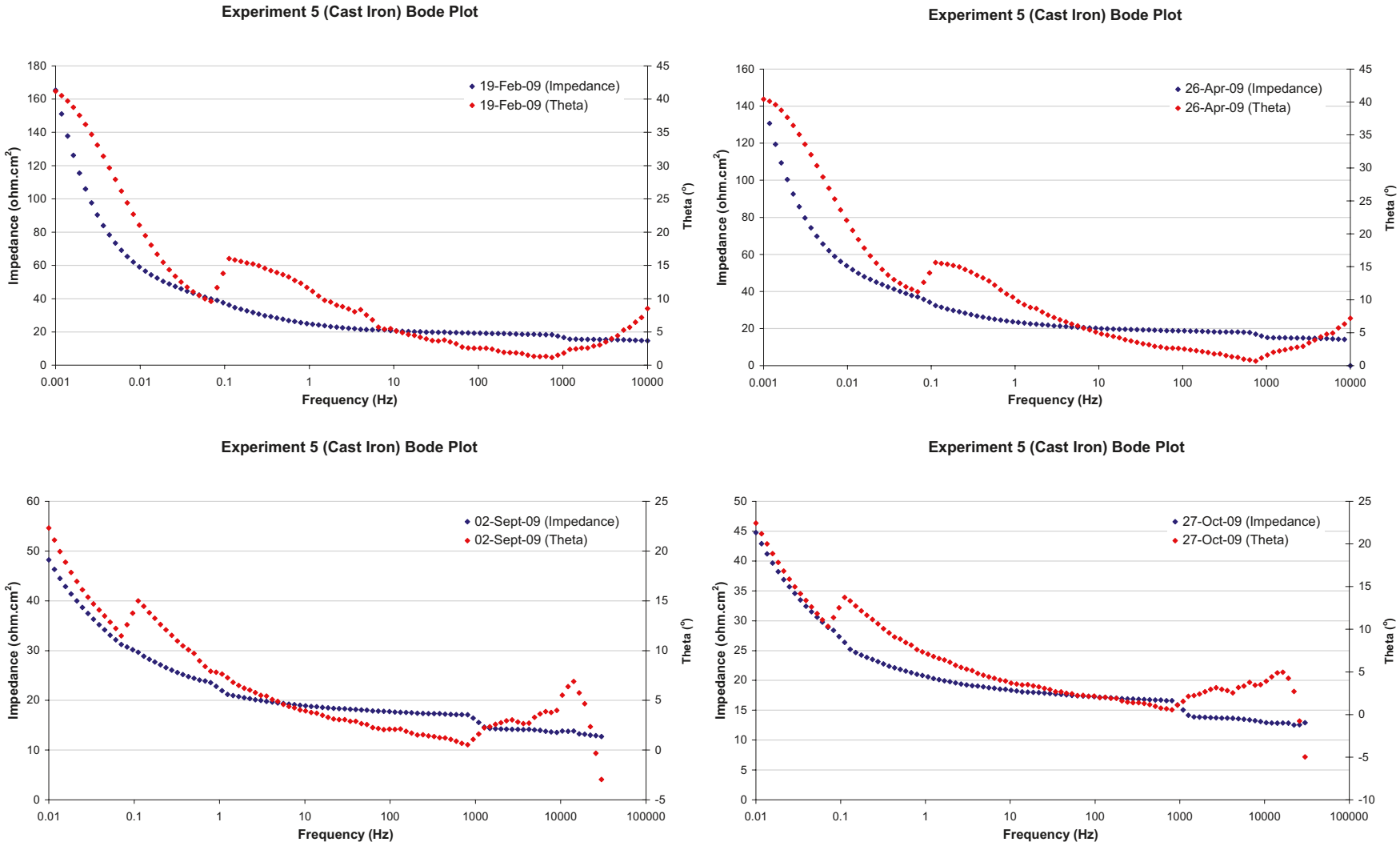

Figure A2-46. *Bode plots of cast iron in Experiment 5 (no bentonite).*

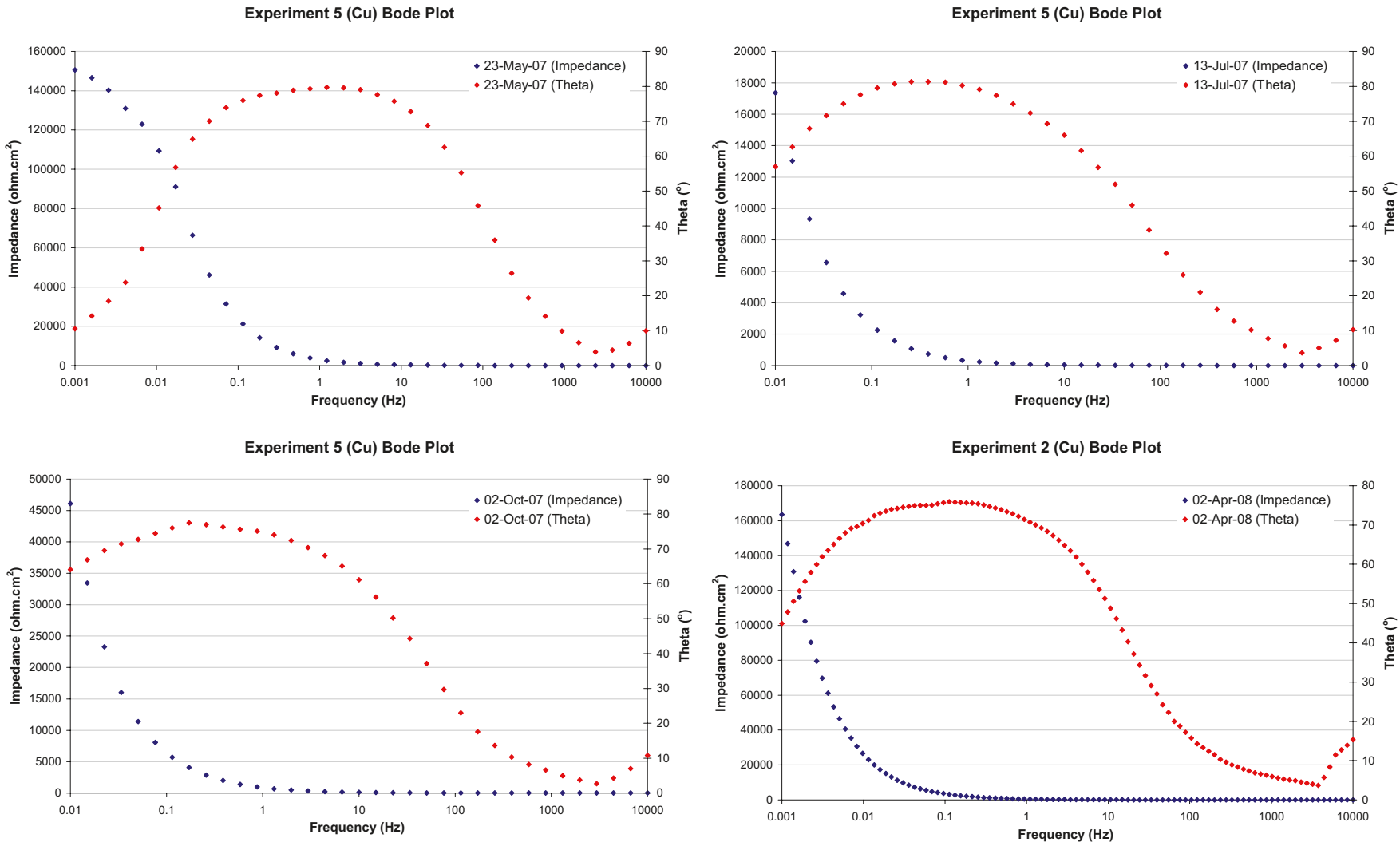

Figure A2-47. *Bode plots of copper in Experiment 5 (no bentonite).*

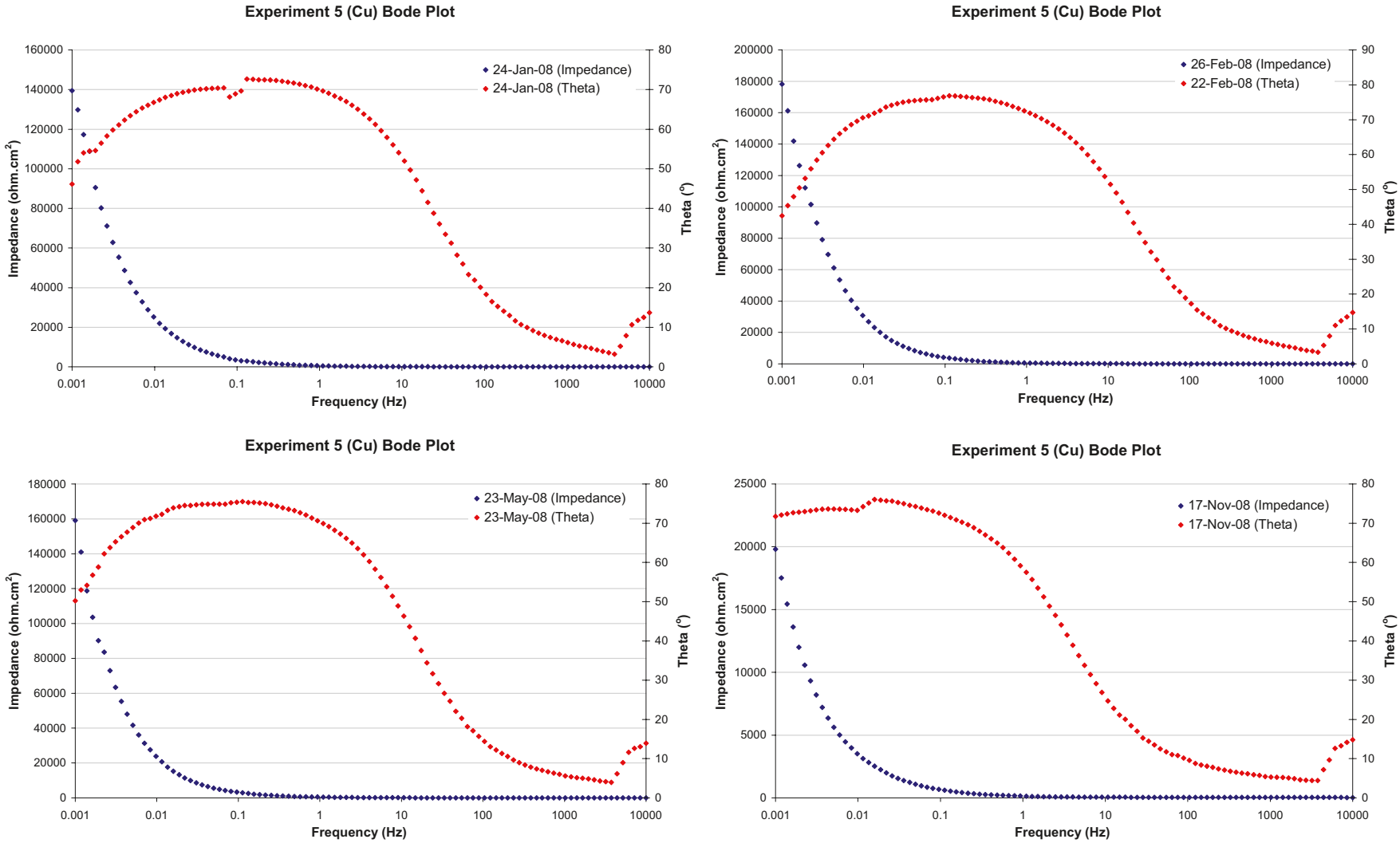

Figure A2-48. *Bode plots of copper in Experiment 5 (no bentonite).*

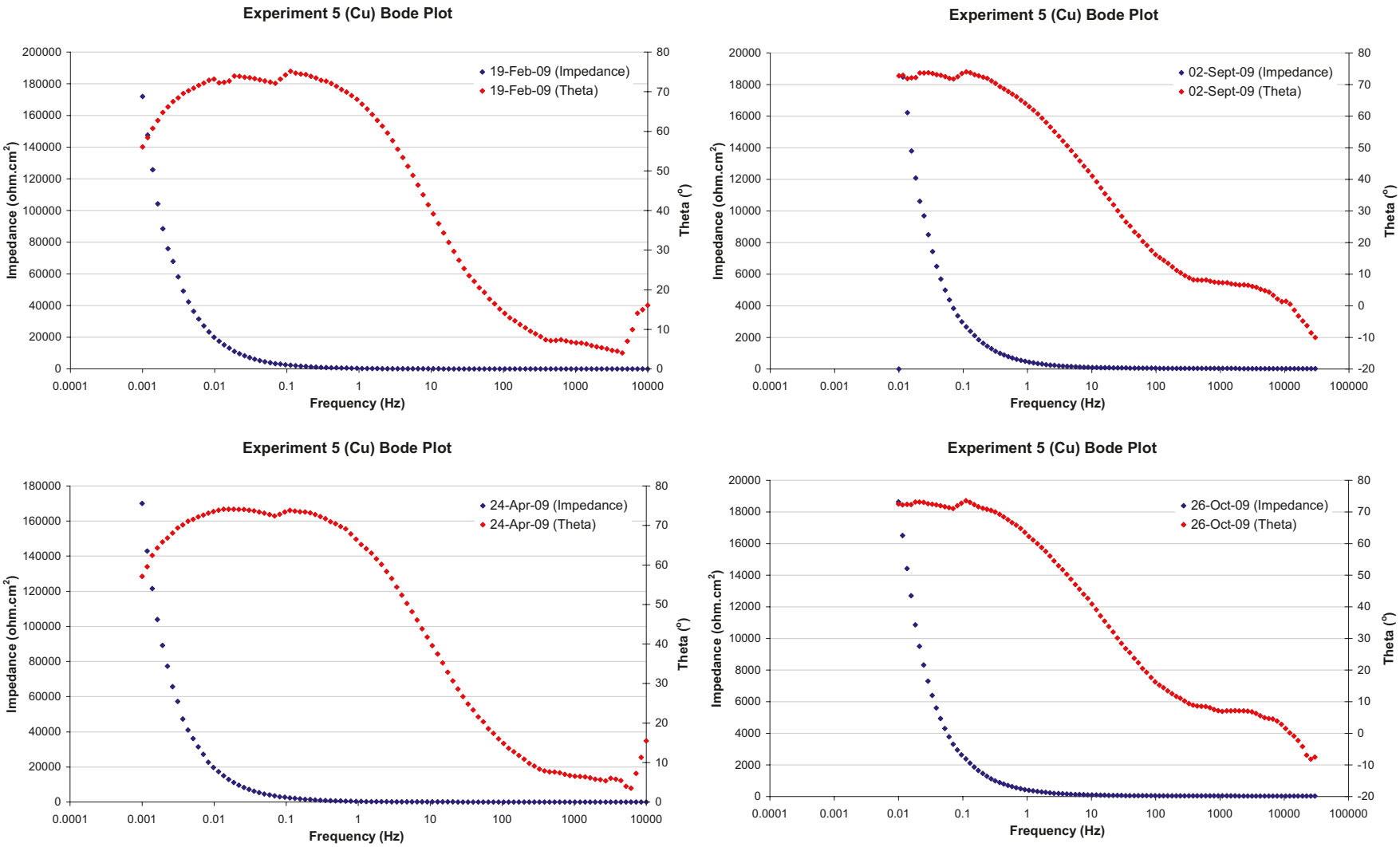

Figure A2-49. *Bode plots of copper in Experiment 5 (no bentonite).*

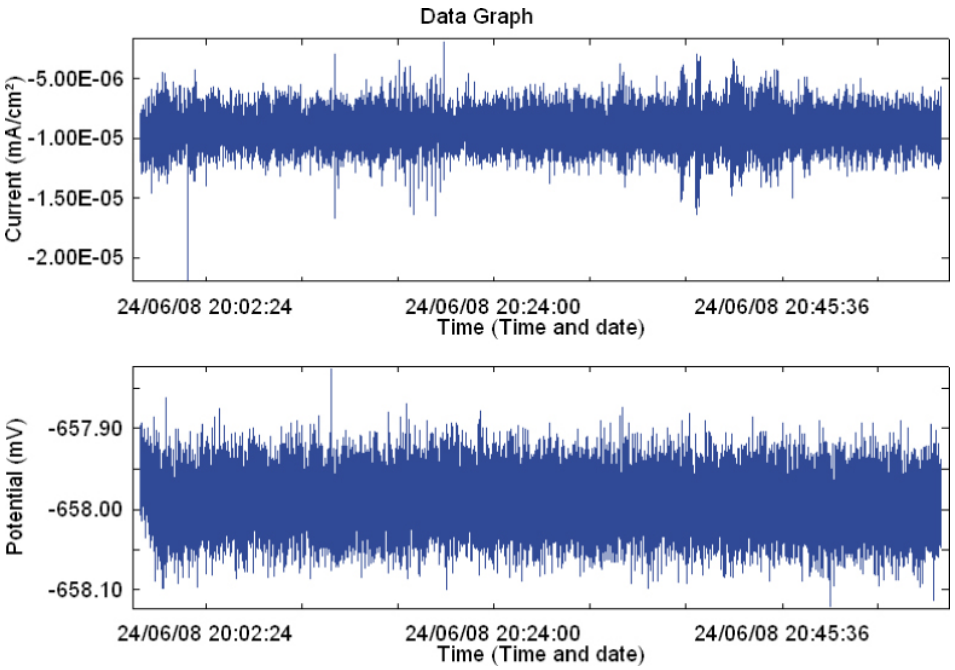

Figure A2-50. *Results from electrochemical noise measurements for cast iron in Experiment 1 (low density bentonite).*

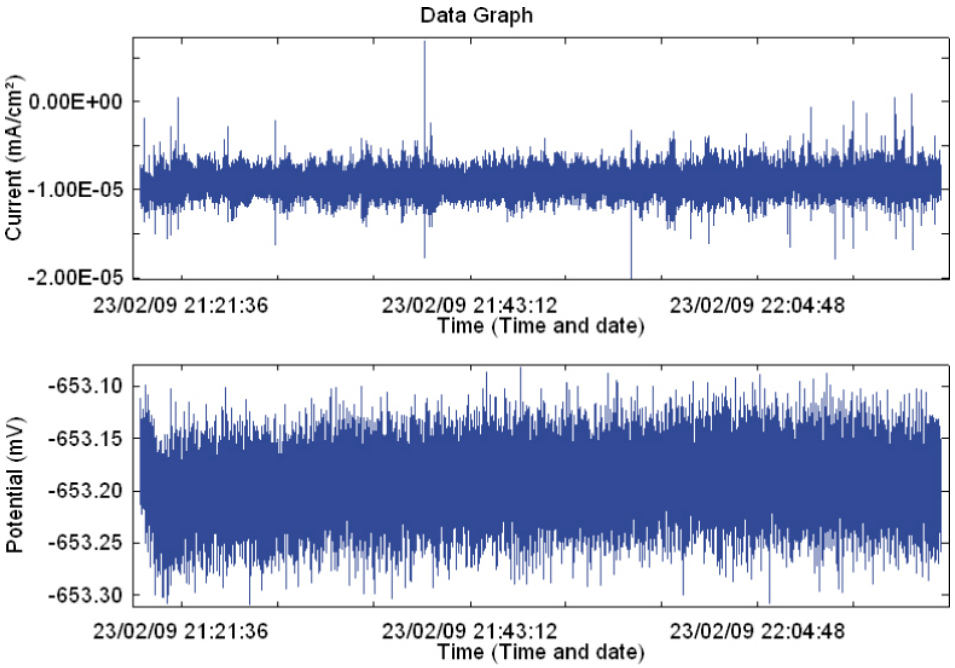

Figure A2-51. *Results from electrochemical noise measurements for cast iron in Experiment 1 (low density bentonite).*

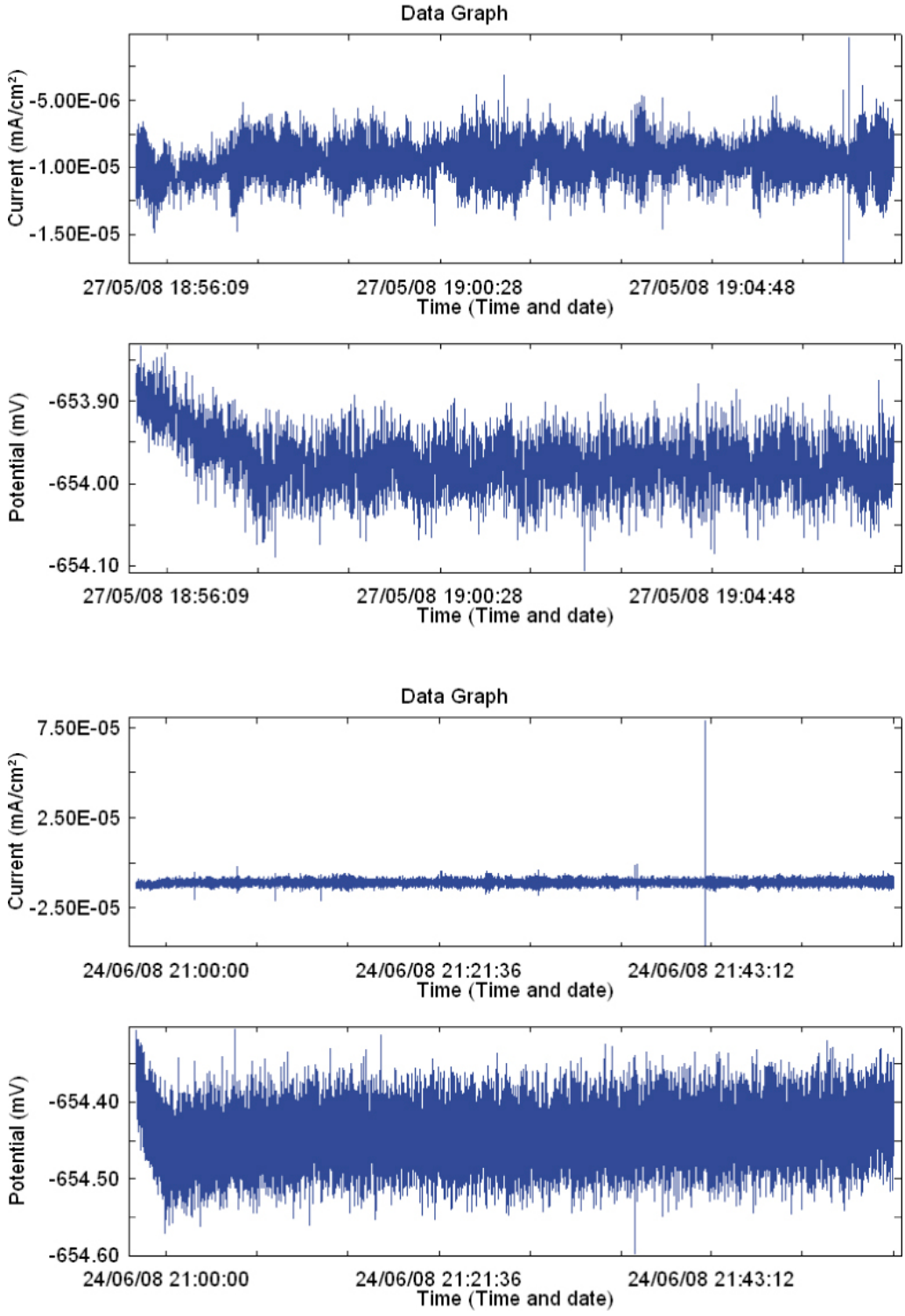

Figure A2-52. *Results from electrochemical noise measurements for copper electrode in Experiment 1 (low density bentonite).*

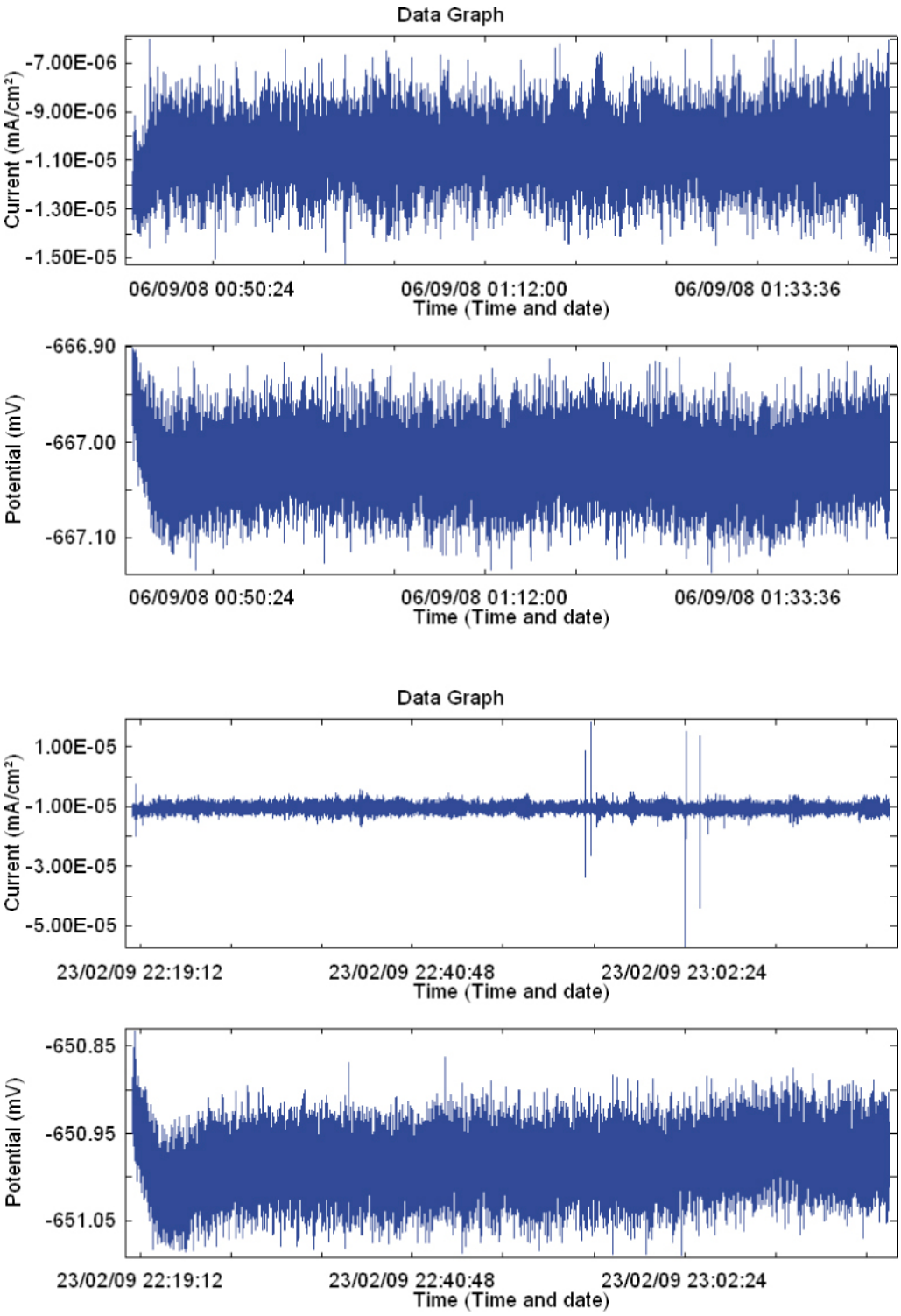

Figure A2-53. *Results from electrochemical noise measurements for copper electrode in Experiment 1 (low density bentonite).*

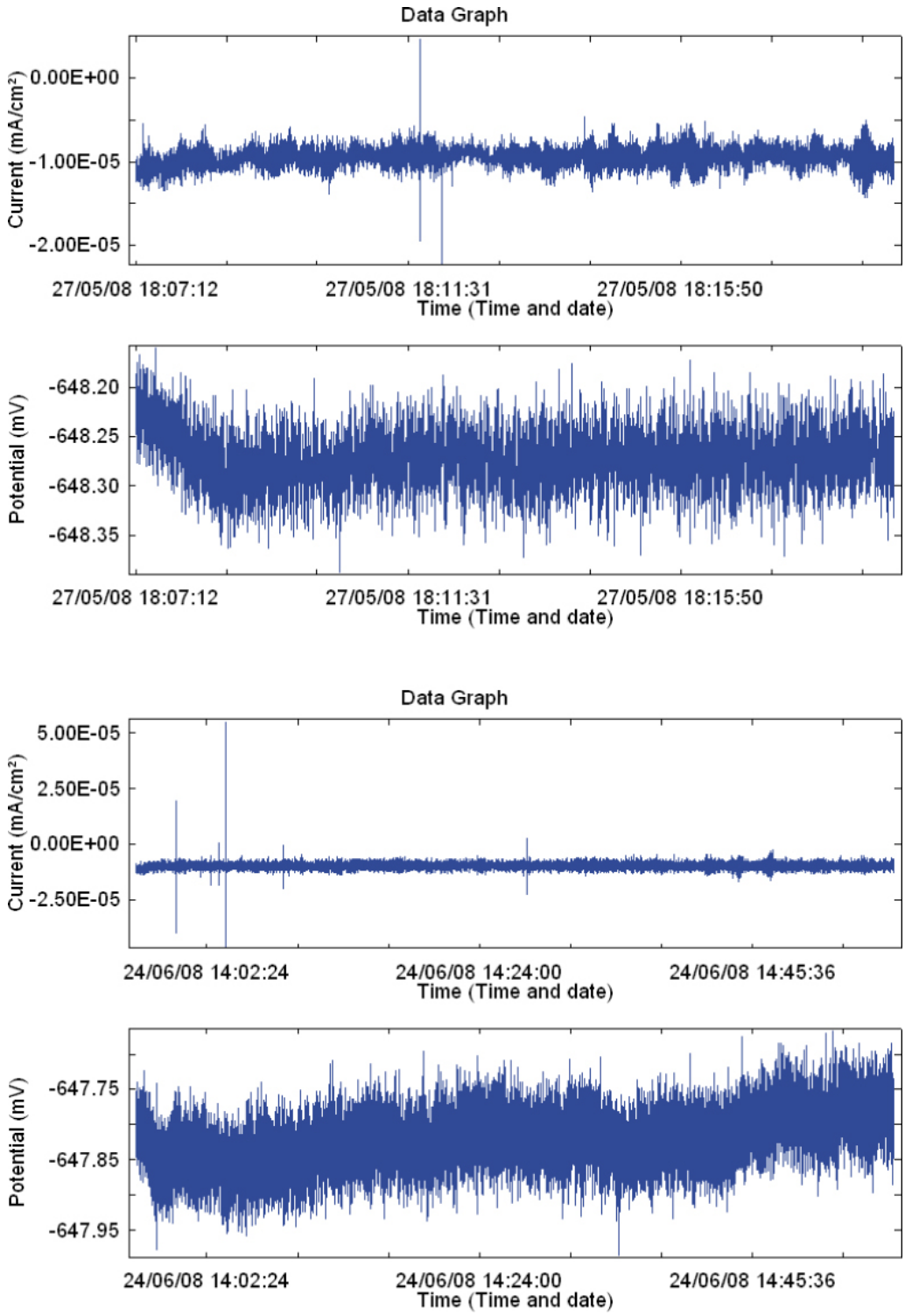

Figure A2-54. *Results from electrochemical noise measurements for cast iron electrode in Experiment 2 (low density bentonite).*

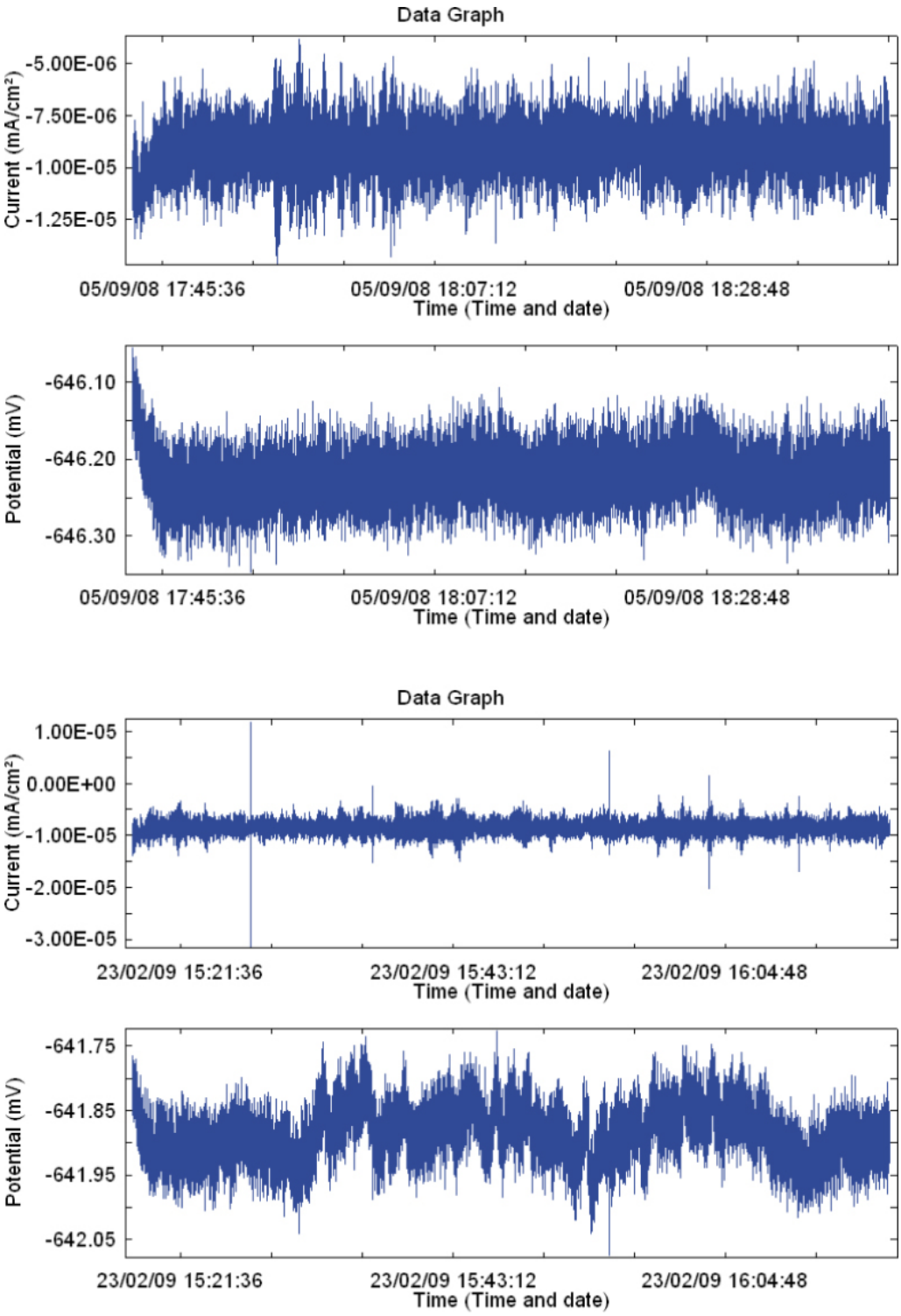

Figure A2-55. *Results from electrochemical noise measurements for cast iron electrode in Experiment 2 (low density bentonite).*

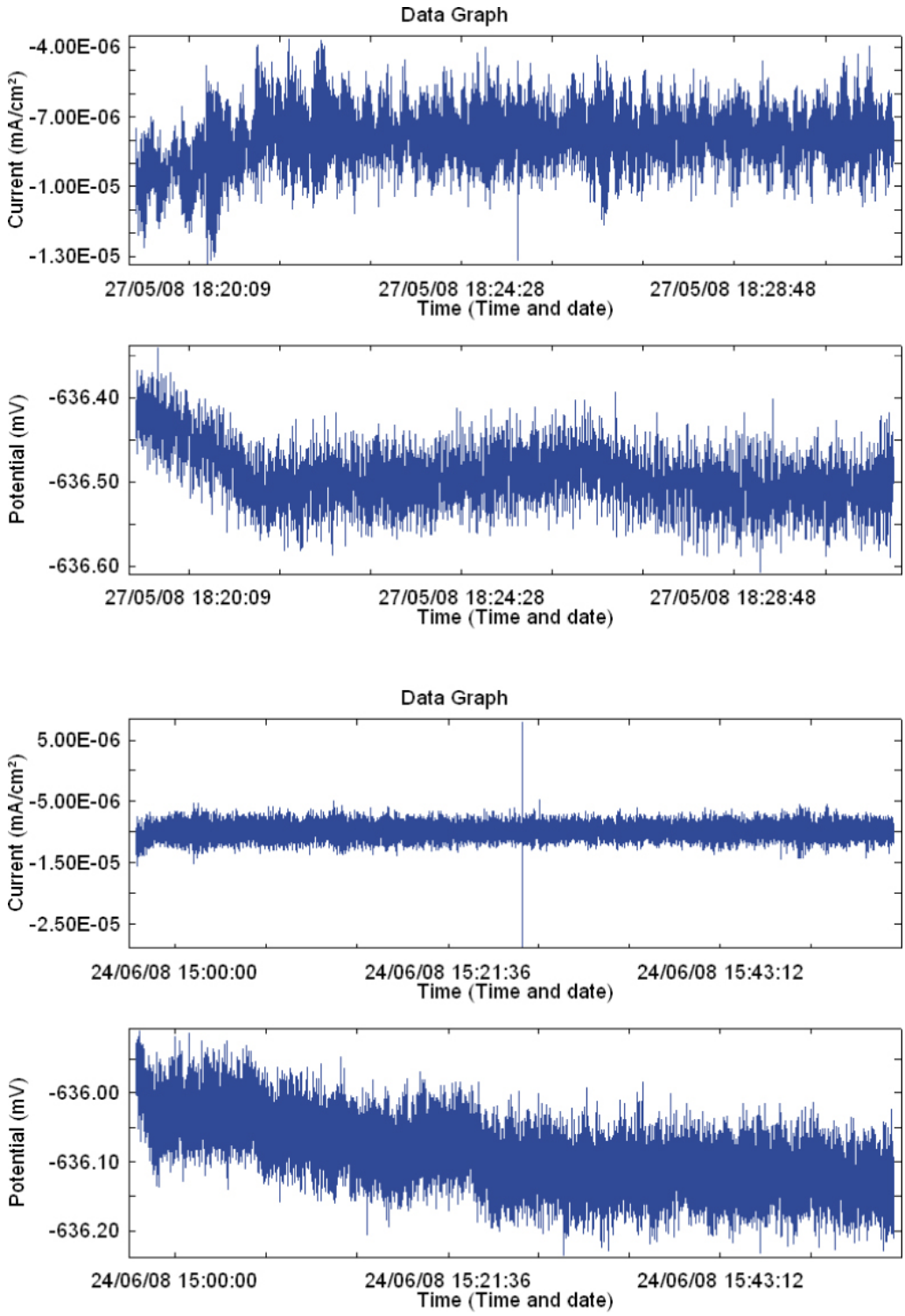

Figure A2-56. *Results from electrochemical noise measurements for copper electrode in Experiment 2 (low density bentonite).*

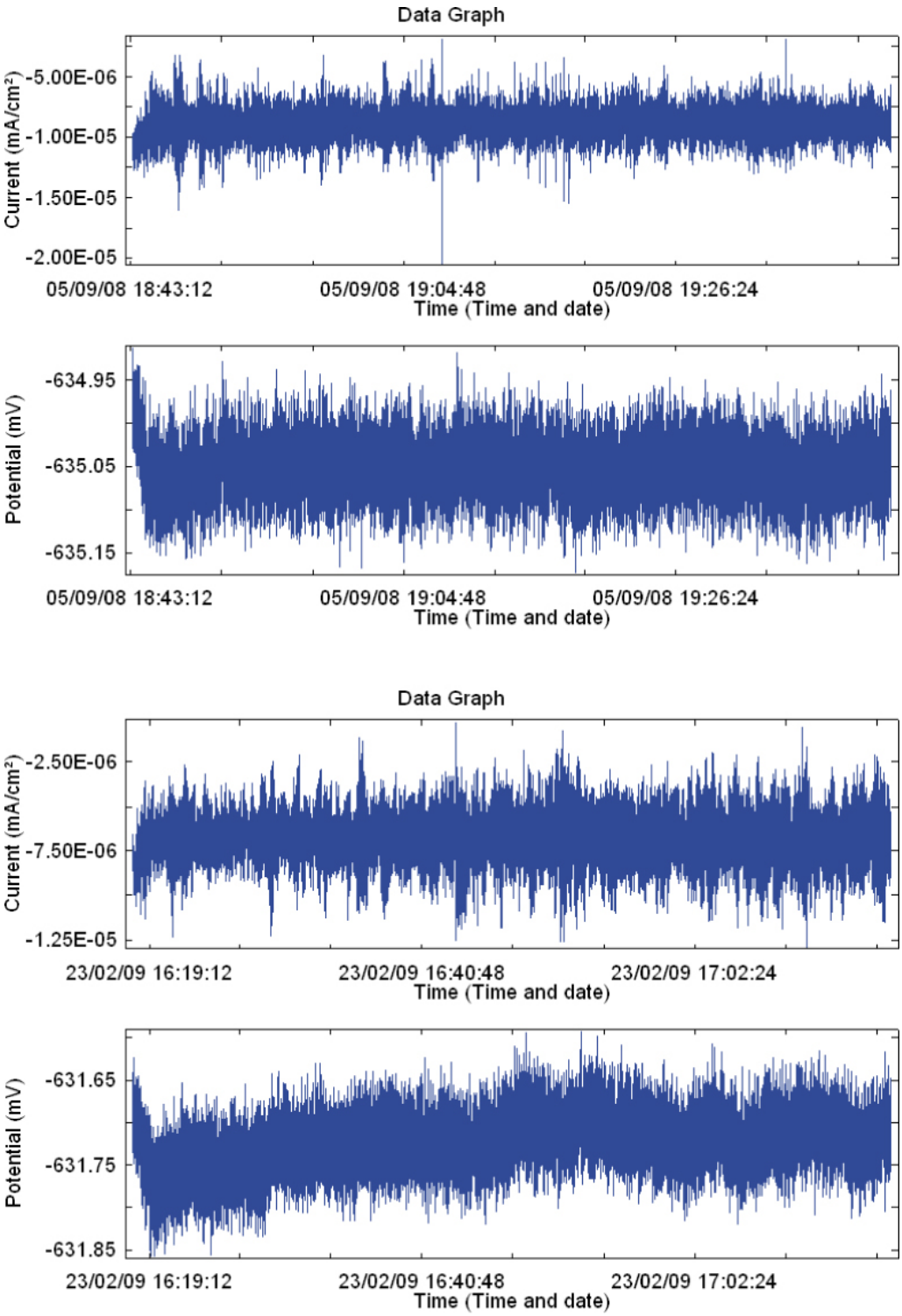

Figure A2-57. *Results from electrochemical noise measurements for copper electrode in Experiment 2 (low density bentonite).*

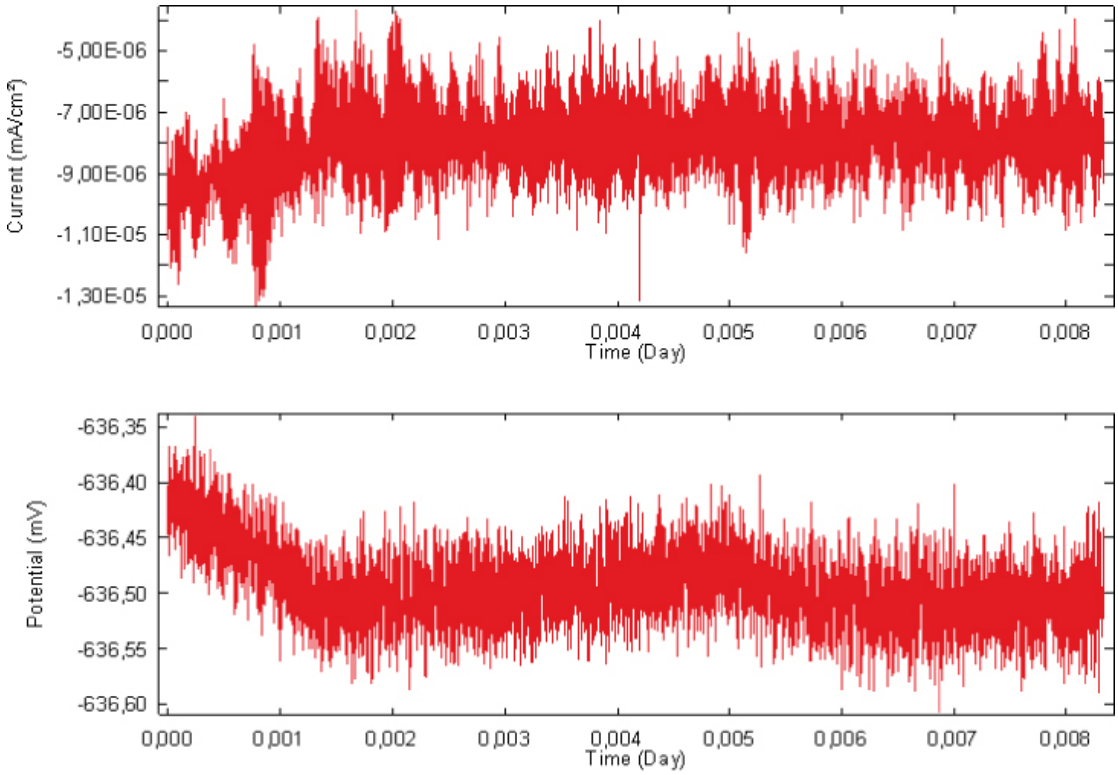

Figure A2-58. *Results from electrochemical noise measurements for a pair of copper electrodes in Experiment 2 (low density bentonite).*

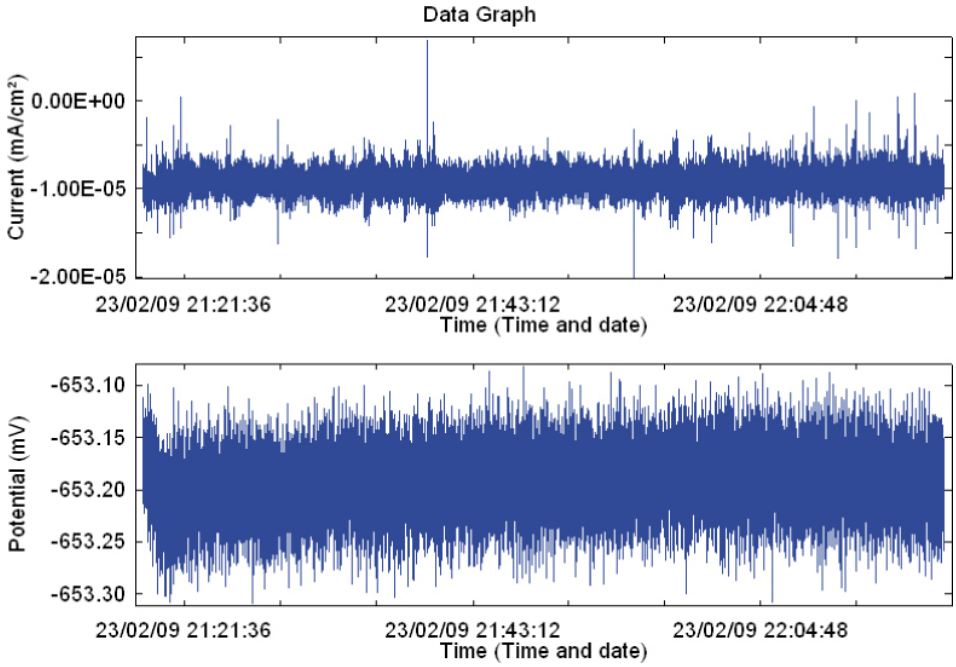

Figure A2-59a. *Results from electrochemical noise measurements for cast iron electrode in Experiment 3 (low density bentonite).*

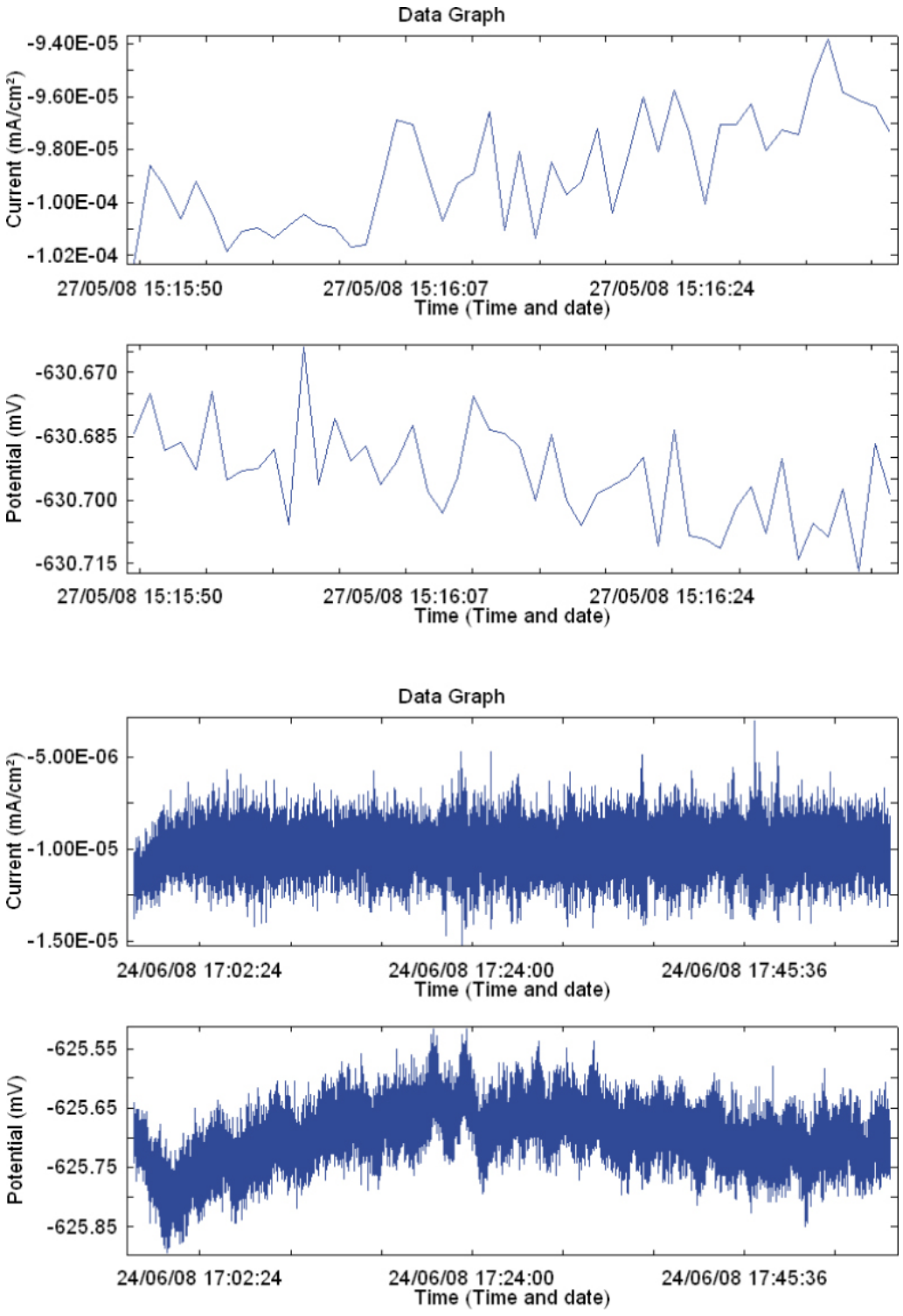

Figure A2-59b. *Results from electrochemical noise measurements for cast iron electrode in Experiment 3 (low density bentonite).*

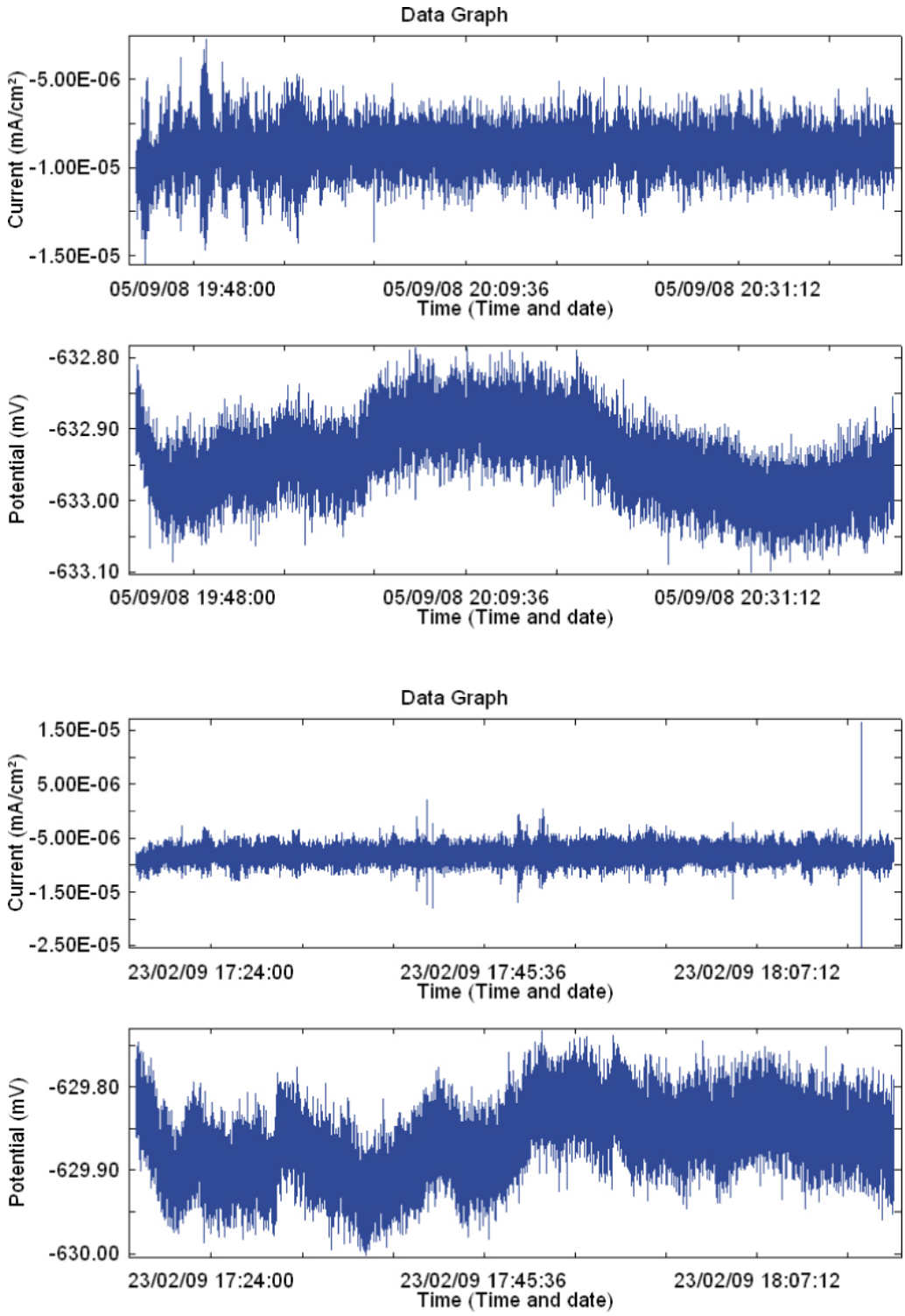

Figure A2-60. *Results from electrochemical noise measurements for cast iron electrode in Experiment 3 (low density bentonite).*

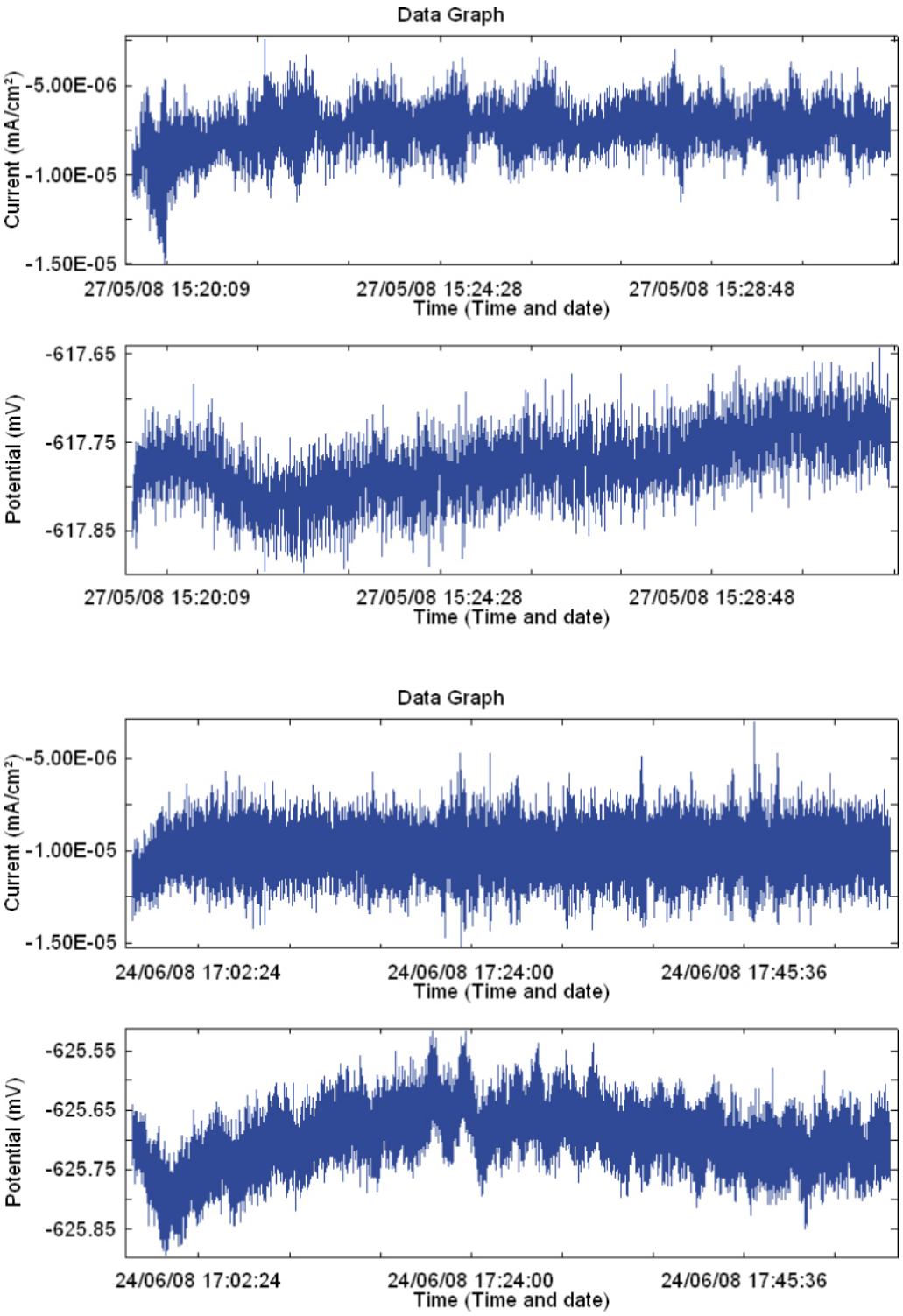

Figure A2-61. *Results from electrochemical noise measurements for copper electrode in Experiment 3 (low density bentonite).*

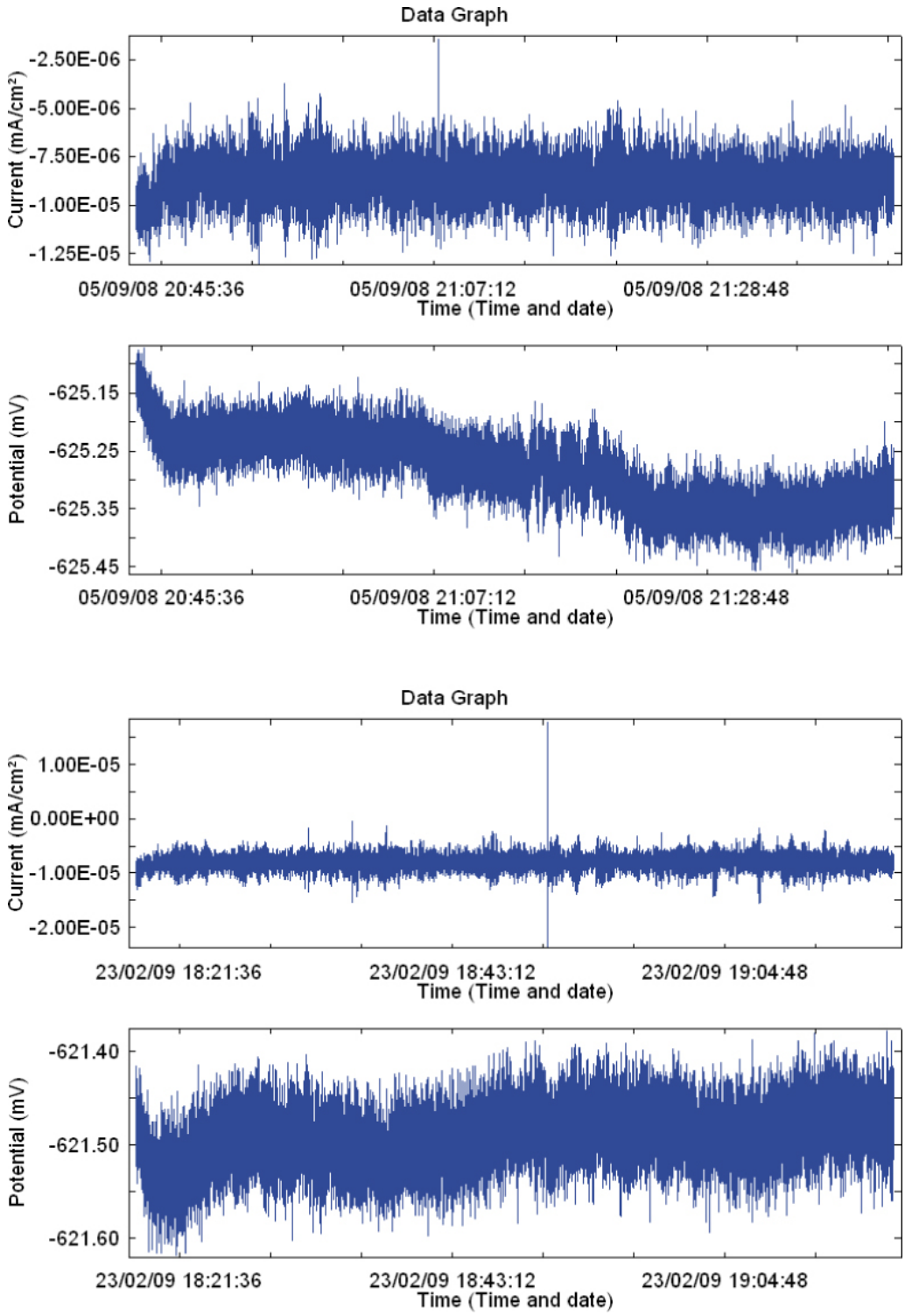

Figure A2-62. *Results from electrochemical noise measurements for copper electrode in Experiment 3 (low density bentonite).*

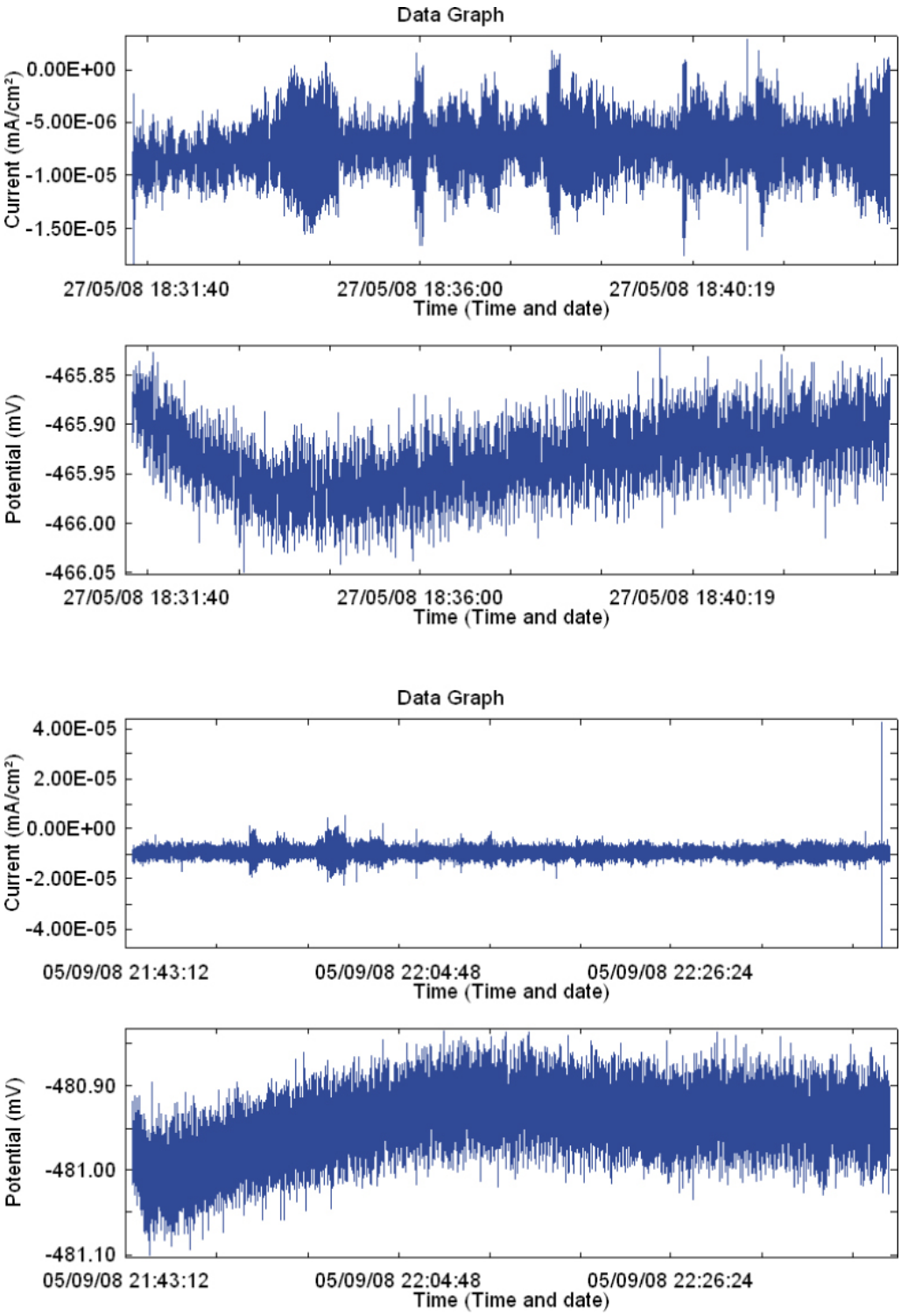

Figure A2-63. *Results from electrochemical noise measurements for cast iron electrode in Experiment 4 (compacted bentonite). Note: It is likely that the iron electrode was in contact with the stainless steel flange of the support cage for these measurements).*

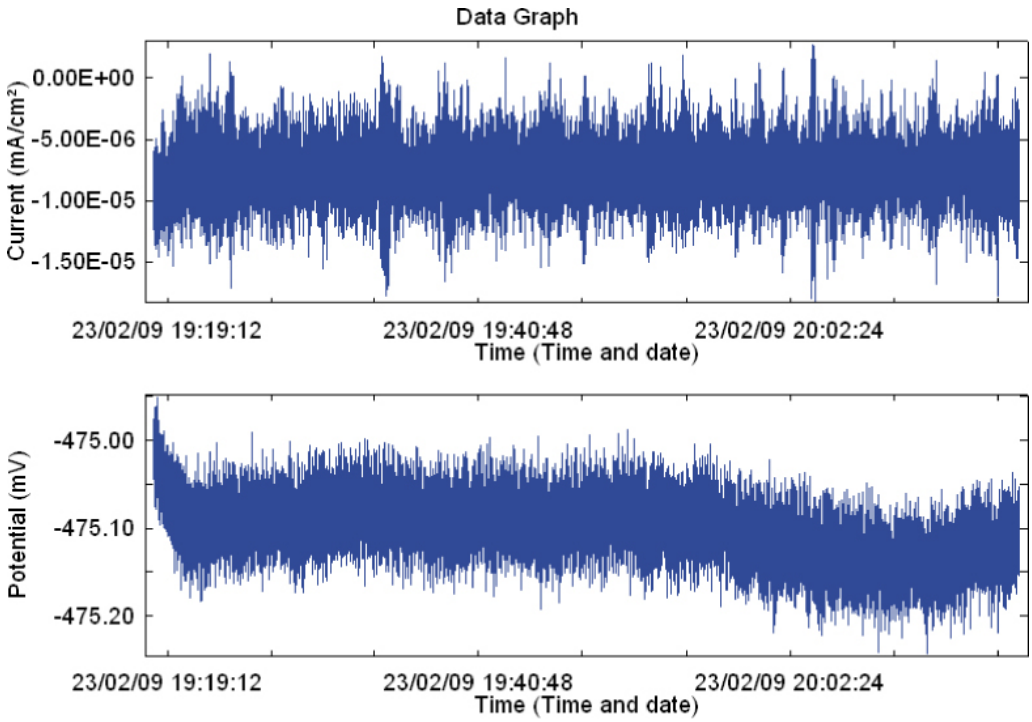

Figure A2-64. *Results from electrochemical noise measurements for cast iron electrode in Experiment 4 (compacted bentonite). Note: It is likely that the iron electrode was in contact with the stainless steel flange of the support cage for these measurements).*

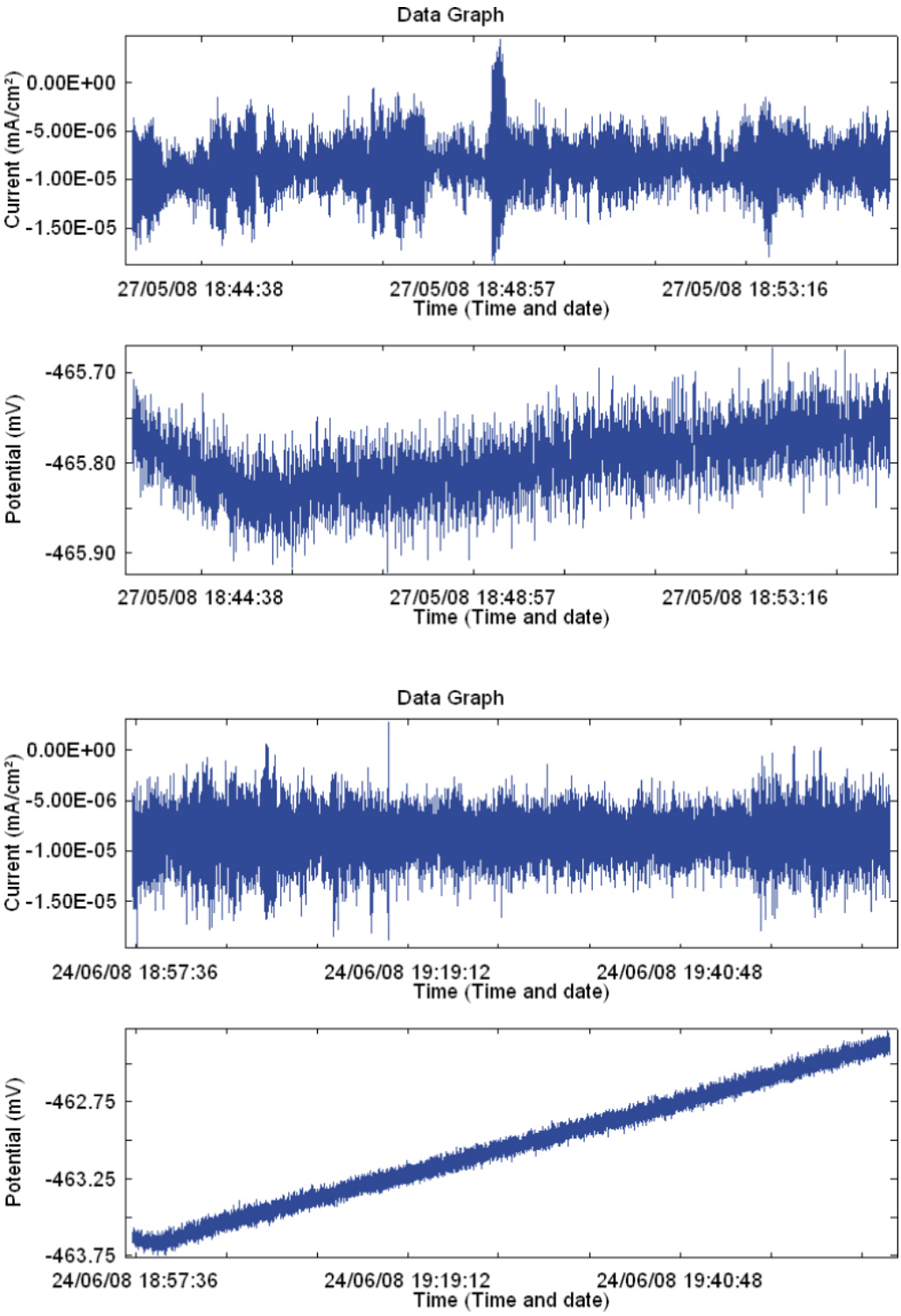

Figure A2-65. *Results from electrochemical noise measurements for copper electrode in Experiment 4 (compacted bentonite).*

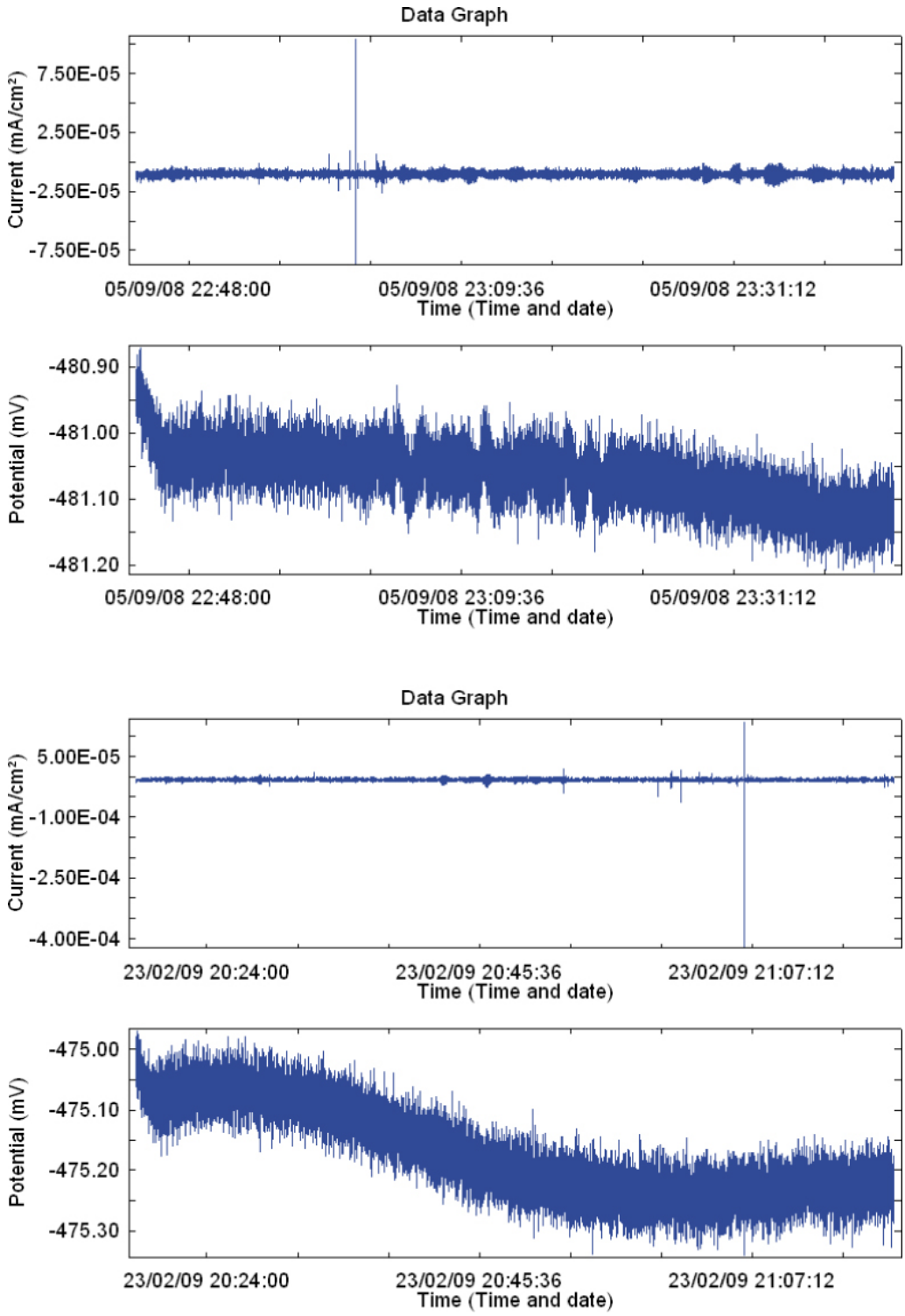

Figure A2-66. *Results from electrochemical noise measurements for copper electrode in Experiment 4 (compacted bentonite).*

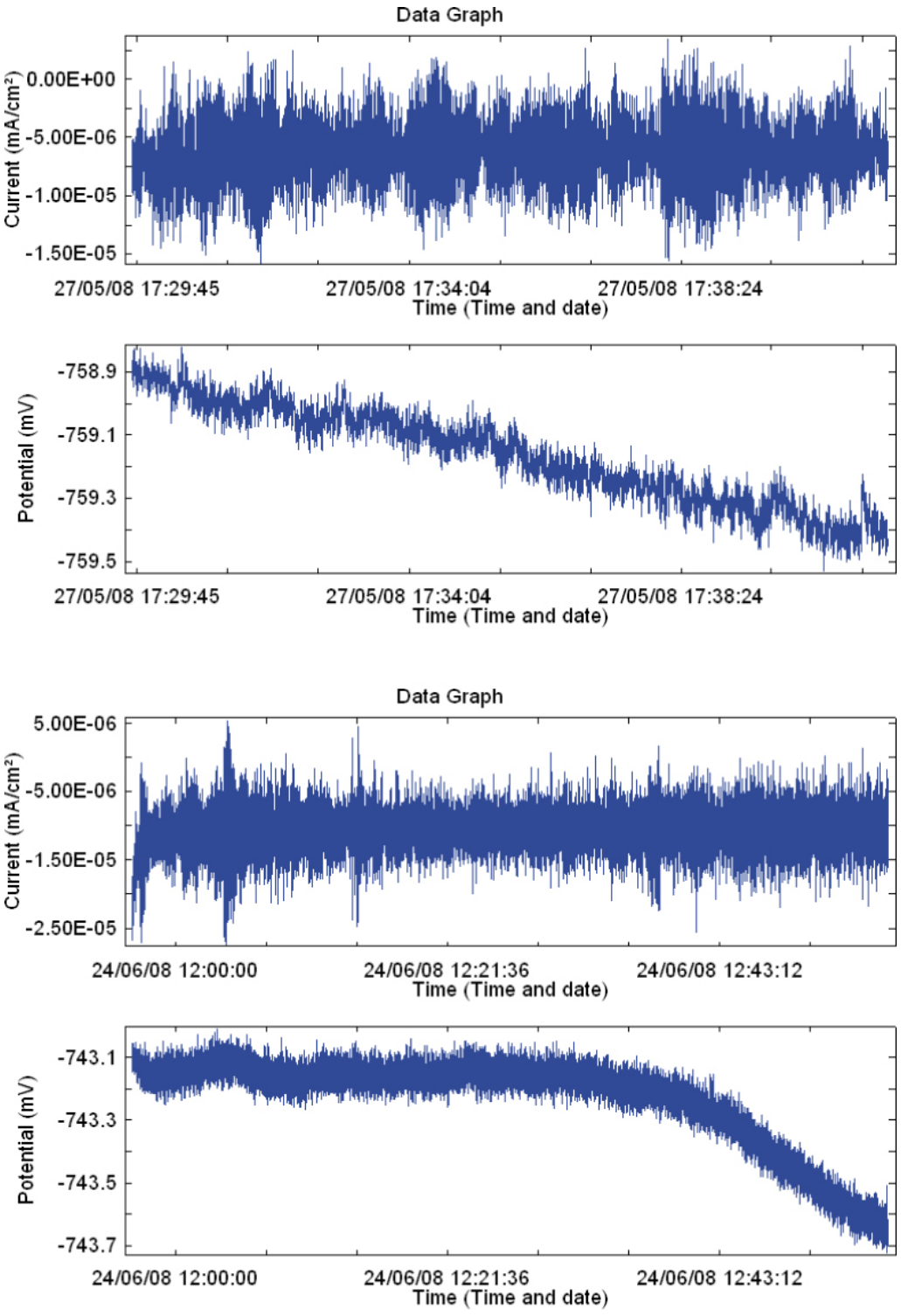

Figure A2-67. *Results from electrochemical noise measurements for cast iron electrode in Experiment 5 (no bentonite).*

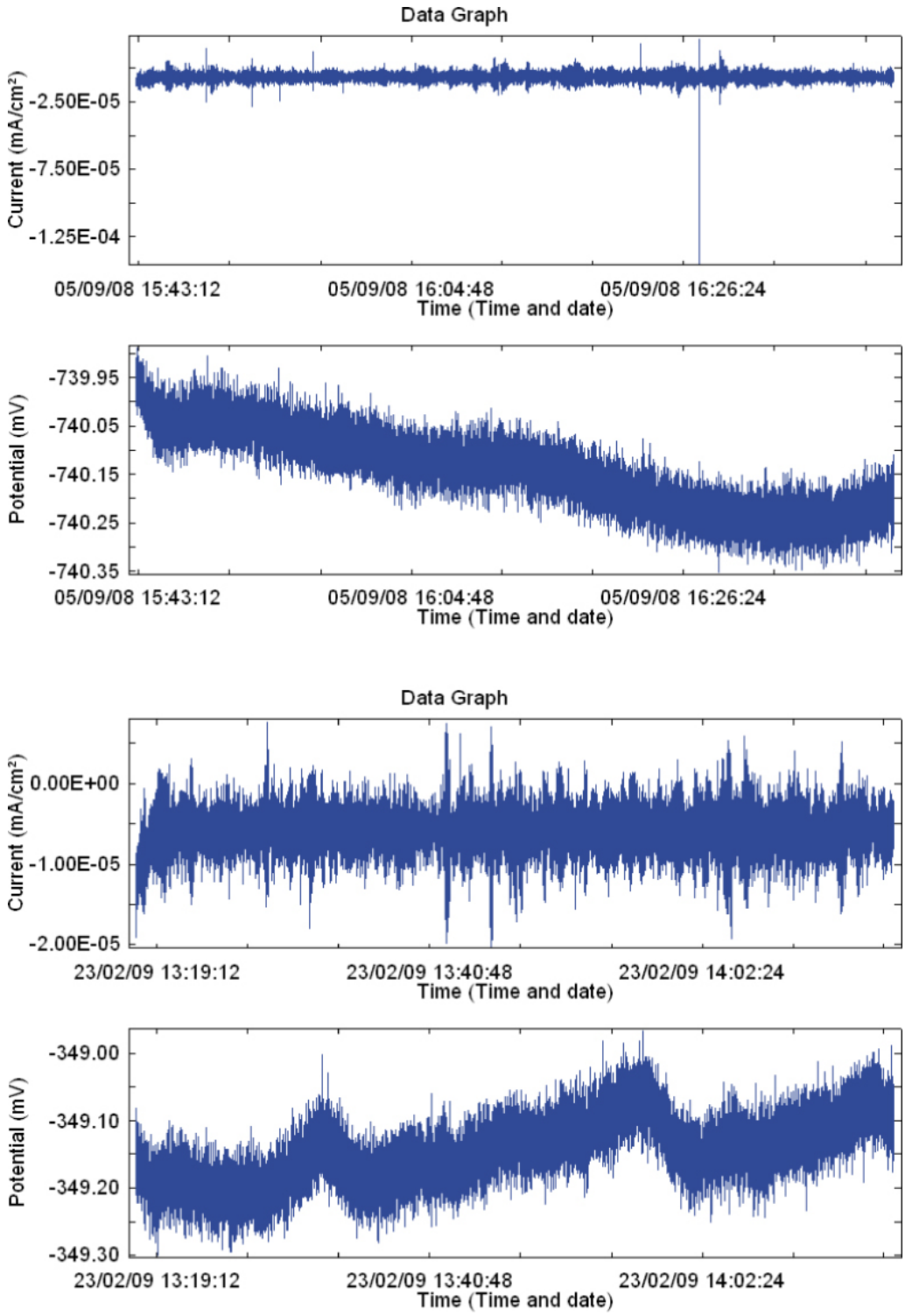

Figure A2-68. *Results from electrochemical noise measurements for cast iron electrode in Experiment 5 (no bentonite).*

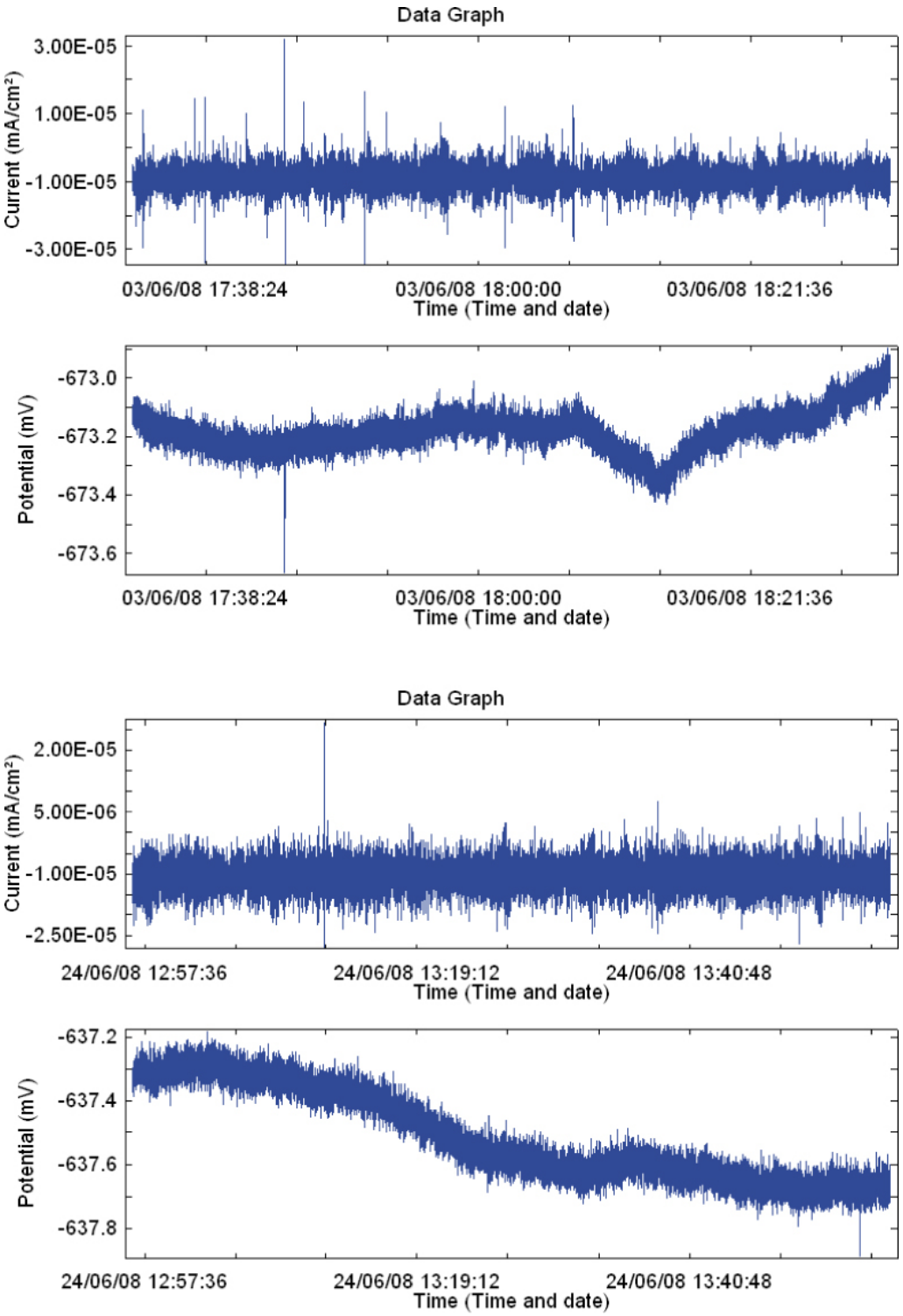

Figure A2-69. *Results from electrochemical noise measurements for copper electrode in Experiment 5 (no bentonite).*

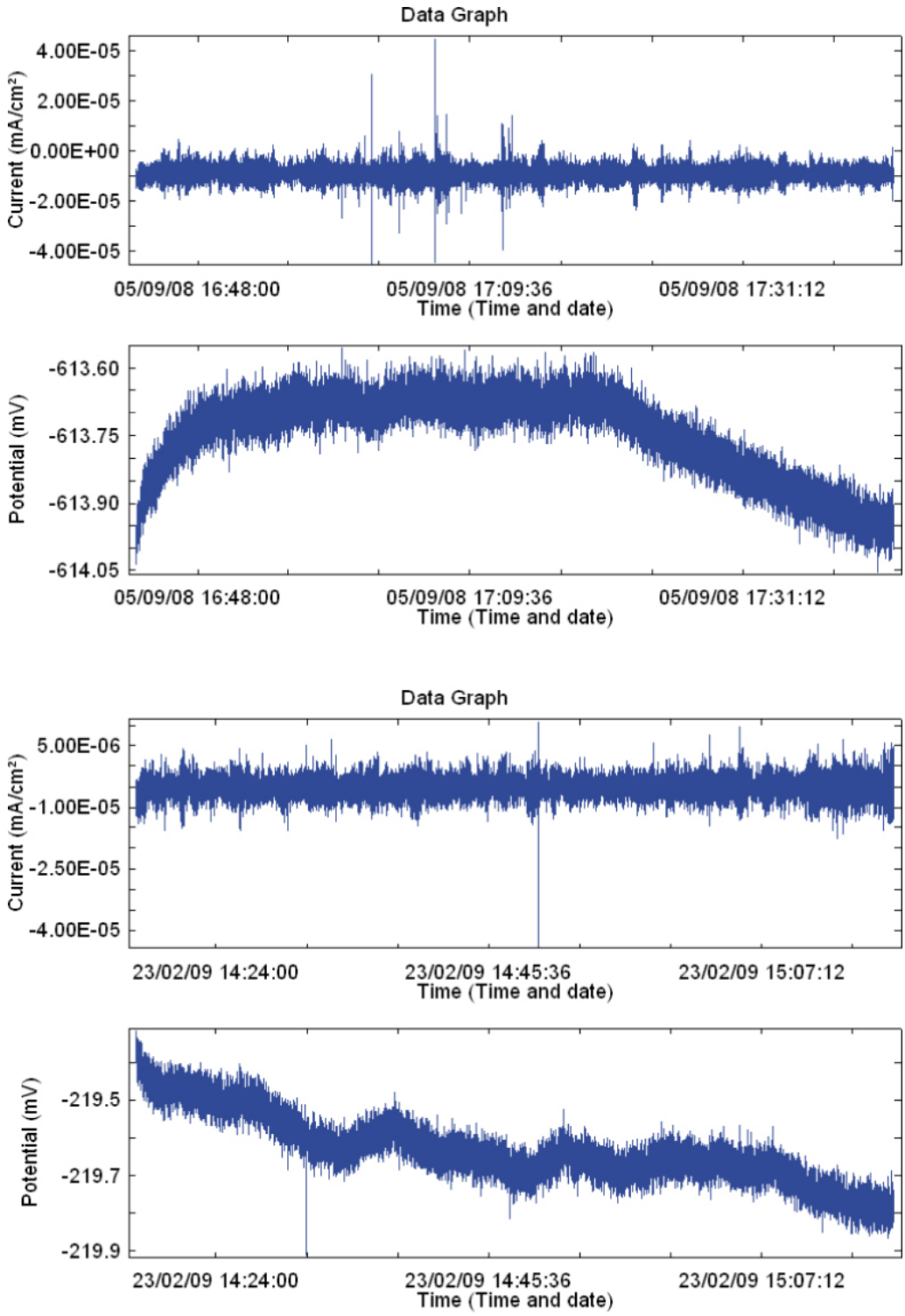

Figure A2-70. *Results from electrochemical noise measurements for copper electrode in Experiment 5 (no bentonite).*